University of Southampton

Faculty of Medicine

Cancer Sciences

Development and activity of a single chain CD70 dimer-of-trimer and its potential as a therapeutic immunostimulatory agent

Volume 1 of 1

by

Osman Dadas

Thesis for the degree of Doctor of Philosophy

September 2019

University of Southampton

Abstract

Faculty of Medicine

Cancer Sciences

Thesis for the degree of Doctor of Philosophy

Development and Activity of a single chain CD70 dimer-of-trimer and its potential as a therapeutic immunostimulatory agent

by

Osman Dadas

Clinically, cancer immunotherapy treatments which use monoclonal antibodies (mAbs) to augment adaptive immunity have largely focussed on blocking inhibitory receptors such as PD-1. To be fully activated, T cells need activating signals and recent evidence shows this to be lacking in a tumour environment. Tumour necrosis factor receptor superfamily (TNFRSF) members are key co-stimulators of T cells and require high level clustering for initiation of signalling. Agonist anti-TNFR mAbs have been used to improve the adaptive immune response but they require cross-linking by Fc gamma receptors (FcγR) to induce clustering of the target receptor. However, the availability of FcγRs in certain tissues can be limiting. CD27 is a co-stimulatory TNFRSF member expressed constitutively on T cells. We have sought to develop a multimeric CD27 ligand, CD70, to bypass the requirement for FcγRs. We developed a co-stimulatory recombinant protein consisting of three CD70 extracellular domains as a single chain, fused with the hinge, CH2 and CH3 domains of mouse IgG1 Fc to facilitate improved stability in circulation. This single chain mouse CD70-m1 (scmCD70-m1) protein was expressed stably in CHO-K1S cells. The protein was expressed as a dimer-of-trimer but additional oligomeric structures were noted. The homogeneous dimer-of-trimer form was isolated and shown to interact with recombinant mouse CD27. The protein also promoted in vitro T-cell activation and proliferation in combination with T cell receptor (TCR) stimulation, but not when given in the absence of the TCR signal. Similarly, when given in vivo with $OVA_{257-264}$ peptide, scmCD70-m1 significantly promoted the expansion of adoptively transferred OVA-specific T cells and contributed to memory T-cell differentiation. Importantly, and unlike anti-CD27 mAb, this expansion was independent of FcγRIIB. Despite these promising results however, scmCD70-m1 was rapidly cleared from the circulation due to the presence of high oligomannose-type glycans on the protein. Enzymatic removal of the oligomannose residues significantly improved the in vivo half-life and the ability of scmCD70-m1 to enhance in vivo expansion of antigen-specific T cells. Furthermore, a version of scmCD70-m1 lacking FcγR engagement, scmCD70-mm1, could stimulate in vivo expansion of antigen specific T cells purely based on dimer-of-trimeric interactions after enzymatic removal of oligomannose residues. However, the activity induced by scmCD70-m1 was higher than scmCD70-mm1 as scmCD70-m1 protein could receive FcγR engagement which further enhanced its activity. The enzyme-treated versions of both scmCD70-m1 and scmCD70-mm1 proteins were highly efficacious in the B-cell lymphoma model (BCL1). These data reveal that rationally-designed natural ligands can be more active than co-stimulatory mAbs and have the advantage of not requiring additional cross-linking by FcγRs.

Table of Contents

Table of Tables

Table of Figures

Research Thesis: Declaration of Authorship

Print name: Osman Dadas

Title of thesis: Development and Activity of a single chain CD70 dimer-of-trimer and its potential as a therapeutic immunostimulatory agent

I declare that this thesis and the work presented in it are my own and has been generated by me as the result of my own original research.

I confirm that:

1. This work was done wholly or mainly while in candidature for a research degree at this University;
2. Where any part of this thesis has previously been submitted for a degree or any other qualification at this University or any other institution, this has been clearly stated;
3. Where I have consulted the published work of others, this is always clearly attributed;
4. Where I have quoted from the work of others, the source is always given. With the exception of such quotations, this thesis is entirely my own work;
5. I have acknowledged all main sources of help;
6. Where the thesis is based on work done by myself jointly with others, I have made clear exactly what was done by others and what I have contributed myself;
7. None of this work has been published before submission.

Signature: Date:

Acknowledgements

I would like to thank my supervisors Prof Aymen Al-Shamkhani and Dr Sarah Buchan for their support and guidance throughout the project, helping to design experiments and take the project forward.

I would like to thank the past and present members of the Al-Shamkhani group, especially Dr Anne Rogel for her support in and out of the laboratory.

Thanks to members of the antibody and vaccine group, biomedical research facility and Dr Patrick Duriez for the technical support throughout the project.

I appreciate the help of Prof Max Crispin and Joel Allen for the analysis of samples during the project.

Big thanks to my family for their endless support, encouragement and understanding all the time.

Special thanks to my fiancée Ayse Ertay for always being by my side and her invaluable help and support during the whole PhD.

Abbreviations

ADCC	Antibody dependent cellular cytotoxicity
ADCP	Antibody dependent cellular phagocytosis
Ala	Alanine
Amp	Ampicillin
AP1	Activator protein 1
APC	Antigen presenting cell
Asn	Asparagine
BCG	Bacille Calmette-Guerin
BCL1	B-cell lymphoma 1
BCR	B-cell receptor
BM	Bone marrow
Ca^{2+}	Calcium
CAR	Chimeric antigen receptor
CDC	Complement dependent cytotoxicity
CDK	Cyclin-dependent kinases
CDR	Complementary determining regions
CHO-K1	Chinese hamster ovary K1 cells
CR	Complete response
CRAC	Ca^{2+} release activated Ca^{2+} channels
CRC	Colorectal cancer
CRD	Cysteine rich domain
CTL	Cytotoxic T lymphocyte
CTLA-4	Cytotoxic T-lymphocyte antigen-4
CV	Column volume
Cys	Cysteine
DAG	Diacylglycerol
DC	Dendritic cell
DcR1	Decoy receptor 1
DD	Death domain
dH_2O	Distilled H_2O
DM	Double mutant
DN	Double negative
DP	Double positive
EBV	Epstein-Barr virus
ELISA	Enzyme linked immunosorbent assay
Endo H	Endoglycosidase H
ER	Endoplasmic reticulum
ERAP-1	ER aminopeptidase-1
EtBr	Ethidium bromide
FcRn	Neonatal Fc receptor
FcγR	Fc gamma receptor
GABP	GA binding protein
GITR	Glucocorticoid-induced TNFR family related gene
GlcNAc	N-acetyl glucosamine
GM-CSF	Granulocyte-macrophage colony-stimulating factor
GMEM	Glasgow's modified eagle's medium
hCD27	Human CD27
HSC	Hematopoietic stem cell
i.v.	Intravenous
ICOS	Inducible co-stimulator
IFN-γ	Interferon-γ

Ig	Immunoglobulin
IgG	Immunoglobulin G
IL	Interleukin
Ins(1,4,5)P_3	Inositol 1,4,5-triphosphate
ITAM	Immunoreceptor tyrosine-based activation motif
ITIM	Immunoreceptor tyrosine-based inhibitory motif
KLRG1	Killer cell lectin like receptor G1
Lat	Linker of activated T cells
LN	Lymph node
mAb	Monoclonal antibody
MAPK	Mitogen activated protein kinase
Met	Methionine
MHC	Major histocompatibility complex
MPEC	Memory precursor effector cells
MSX	Methionine sulfoximine
NEB	New England Biolabs
NFAT	Nuclear factor of activated T cells
NF-κB	Nuclear factor kappa b
NK	Natural killer cell
NSCLC	Non-small cell lung cancer
OPG	Osteoprotegerin
OVA	Ovalbumin
OVAC	Ovarian cancer
PAMP	Pathogen associated molecular patterns
PAP	Prostatic acid phosphatase
PBS	Phosphate buffered saline
PD-1	Programmed death receptor-1
PI3K	Phosphatidyl inositol 3-kinase
PKC	Protein kinase C
PLCγ1	Phospholipase C gamma 1
PNGase F	Peptide N-glycosidase F
PR	Partial response
PRR	Pattern recognition receptors
PtdIns(4,5) P_2	Phosphatidylinositol 4, 5 biphosphate
PTK	Protein tyrosine kinase
RANK	receptor activator of NF-κB
RasGRP	Ras guanyl-nucleotide-releasing protein
RCC	Renal cell carcinoma
rmCD27-hFc	Recombinant mouse CD27 – human Fc
$S1P_1$	Sphingosine-1-phosphate receptor 1
sCD70	Soluble recombinant CD70
scmCD70-m1	Single chain mouse CD70 – mouse 1
scmCD70-mm1	Single chain mouse CD70 – mouse mutant 1
scTNF	Single chain TNF
SD	Stable disease
SDS-PAGE	Sodium dodecyl sulphate polyacrylamide gel electrophoresis
SEC	Size exclusion chromatography
SH2	Src-homology 2
SLEC	Short lived effector T cells
SLP76	SH-2 domain containing lymphocyte protein of 76000 MW
SM	Single mutant
SOC	Super optimal broth with catabolite repression
SP	Single positive
TAA	Tumour associated antigens
TAP	Transporter associated with antigen processing

T_{cm}	Central memory T cell
TCR	T-cell receptor
TEC	Thymic epithelial cells
T_{em}	Effector memory T cell
Tfh	Follicular helper T cells
Th	T helper cell
TIL	Tumour infiltrating lymphocyte
TNFR-1	TNF receptor 1
TNFRSF	Tumour necrosis factor receptor superfamily
TNFα	Tumour necrosis factor-α
T_{pm}	Peripheral memory T cells
TRAF	TNF receptor associated factor
Treg	Regulatory T cell
T_{rm}	Tissue resident memory T cell
TSP	Thymic seeding progenitor
UPLC	Ultra-high-performance liquid chromatography
Ver I	scmCD70-m1 Version I
Ver II	scmCD70-m1 Version II
WT	Wild type

Chapter 1 Introduction

1.1 The Immune System

The immune system is the defence mechanism of a host organism against infection. Its tight regulation is critical to prevent pathology since immunosuppression increases the likelihood of chronic infection and tumour development whereas aberrant immune cell activation can result in autoimmunity (1). There are two arms of the immune system. The innate arm is the first line of defence to be activated (1, 2). The second arm is the adaptive immune system which takes longer to become fully activated but has the capacity to adapt to an evolving infection and can develop immunological memory to enable a quicker response in the case of a secondary infection (1, 2).

1.2 Innate Immune system

The innate immune system includes cell types such as neutrophils, macrophages, dendritic cells (DC), mast cells, eosinophils and basophils. Cells of the innate immune system recognise pathogen associated molecular patterns (PAMPs) through germline encoded pattern recognition receptors (PRR) which leads to a series of activation events culminating in the development of an inflammatory response (3). Depending on the cell type, activation of PRRs can initiate phagocytosis (by e.g. macrophages) or promote antigen presentation (by e.g. DCs) (2). Antigen presenting cells (APCs) are key to the activation of adaptive immunity and include DCs, macrophages and B cells. The dominant APCs are DCs which, once loaded with antigen and suitably activated, migrate to secondary lymphoid organs (the spleen and lymph nodes (LN)) to interact with cells of the adaptive immune system (1, 4).

1.3 Adaptive Immune System

The adaptive immune system is also known as the acquired immune system and generates immunological memory which enables a rapid response during secondary encounter with the same pathogen (1, 2, 4). Cells of the adaptive immune system are either B or T lymphocytes. B and T cells possess cell surface receptors called the B cell receptor (BCR) and T cell receptor (TCR) respectively, which are specific for appropriately presented antigen or antigen-derived peptides. These receptors undergo gene rearrangement such

that each B and T cells express unique receptors thereby enabling the development of a broad resting B and T cell pool (1, 4).

1.4 T cell development and maturation

T cells develop from Hematopoietic stem cell (HSC) that differentiate in the bone marrow (BM) until the thymic-seeding progenitor (TSP) stage at which point the cell then exits the BM and travels to the thymus (5). TSPs develop into $CD4^+$ and $CD8^+$ T cells in the thymus and thus the term 'T'. Initially, progenitor cells differentiate into double negative (DN) thymocytes (Fig. 1.1) which lack both CD4 and CD8 molecules and are characterised by cell surface expression of CD25 and CD44 (6). Subsequent differentiation into early T cell progenitors, called DN1 cells, is associated with the profile $CD44^+CD25^-$. DN1 cells are found in the corticomedullary junction of the thymus and still have myeloid potential where they can differentiate into natural killer (NK) and DCs. DN1 cells migrate towards the subcapsular zone of the cortex and differentiate into DN2 cells ($CD44^+CD25^+$), subsequent to receiving stimulatory signals from fibroblasts and thymic epithelial cells (TEC) (5, 6). Gene rearrangement of the TCRβ chain starts in the DN2 stage but it is completed in the DN3 ($CD44^-CD25^+$) stage in the subcapsular zone where the cell becomes committed to developing into a T cell. In these early stages of differentiation, Notch signalling plays an important role in driving the T-cell lineage differentiation. At the DN3 stage, and after successful rearrangement of the TCRβ chain, a functional pre-TCR complex consisting of the TCRβ chain, CD3 chains and pre-Tα chain is formed and expressed on the cell surface (7). Signals through the pre-TCR complex, drive further differentiation whereas cells with no TCRβ expression are directed for apoptosis which is a process known as β-selection (Fig. 1.1) (6). At this DN4 ($CD44^-CD25^-$) stage, cells start migrating towards the medulla and upregulate CD8 and CD4 to become double positive (DP) cells. DP cells then rearrange their TCRα chain and a functional αβ TCR is formed. DP cells then undergo a positive selection process (Fig. 1.1) where self-antigenic peptide-MHC complexes are presented by the APCs in the thymus and only DP cells with intermediate or low avidity are selected to survive (5, 6). Cells with no recognition of peptide-MHC complexes die as they don't receive further stimulation to drive their development. The surviving cells migrate into the medulla by C-C chemokine receptor 7 (CCR7) driven chemokine trafficking and become single positive (SP) by downregulation of either CD4 or CD8 (6). The SP cells then undergo a negative selection process (Fig. 1.1) in which cells with high avidity for self-antigen-MHC complexes undergo apoptosis. This process prevents the generation of self-reactive T cells

(8). The surviving mature T cells then upregulate expression of sphingosine-1-phosphate receptor 1 ($S1P_1$) that is required for emigration from the thymus into the circulation (9).

Mature T cells can be divided into those expressing CD4 or CD8 on the cell surface. $CD4^+$ T cells recognise their antigen presented on major histocompatibility complex (MHC) II molecules presented largely by APCs whereas $CD8^+$ T cells recognise their antigen presented on MHC I molecules (detailed below).

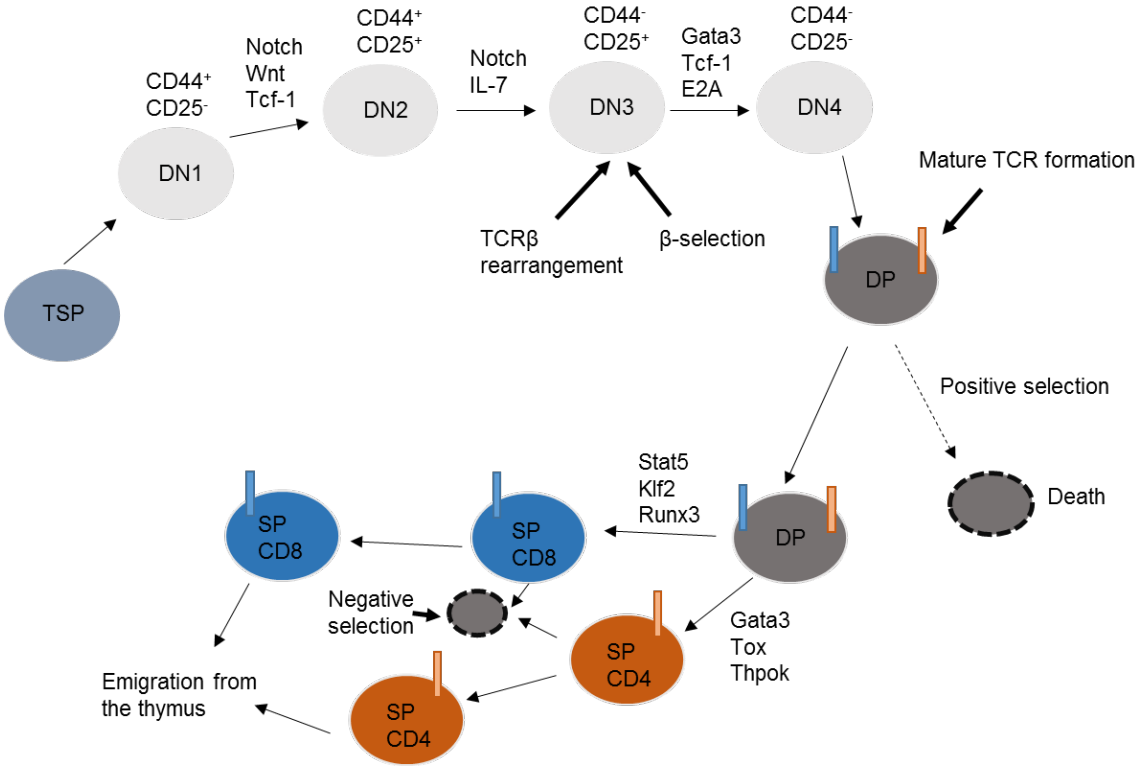

Figure 1.1. T-cell development in thymus. The stages from TSP to differentiation into single positive $CD4^+$ or $CD8^+$ T cells are illustrated. Some of the transcription factors involved in different stages of the development process are indicated. TSP; thymic-seeding progenitor, DN; double negative, DP; double positive, SP; single positive. Blue box; CD8 molecule, orange box; CD4 molecule. Figure adapted from (6).

1.4.1 CD4$^+$ T cells

Upon recognition of antigen and appropriate co-stimulation (see below), naive CD4$^+$ T cells can become activated and differentiate into effectors by clonal expansion. CD4$^+$ T cells can differentiate into different subsets mainly depending on their cytokine profile. CD4$^+$ T cell subtypes include T helper 1 (Th1), Th2, Th17, follicular helper T cells (Tfh) and regulatory T cells (Treg) (10). All the subtypes except Tregs are involved in the fight against infections whereas Tregs regulate the activity of effector cells in the periphery (10, 11).

Effector CD4$^+$ T cells are also known as 'helper' T cells and these can be important in the licensing of DCs by CD40-CD40L signalling. Licensed DCs are more potent at priming CD8$^+$ T cells and stimulation of CD8$^+$ T cells by licensed DCs contributes to both initial expansion of effector cytotoxic T lymphocytes (CTLs) and also effective formation of memory CTLs (12, 13).

1.4.2 CD8$^+$ T cells

Naïve CD8$^+$ T cells can differentiate into CTLs after recognition of antigen-MHC I complexes presented by APC and receiving optimal co-stimulatory interaction. CTLs can then initiate target cell killing on interaction with a target cell expressing the same peptide-MHC complex. Upon interaction, granules from CTLs fuse with the target cell membrane and release proteins such as perforin and granzymes that enter the target cell and initiate apoptosis (4). During prolonged stimulation such as in chronic infections and cancer, CD8$^+$ T cells can undergo a gradual loss of effector function and enter into a dysfunctional state known as exhaustion (14). Exhausted T cells upregulate the expression of inhibitory receptors such as programmed death receptor-1 (PD-1) and change their transcriptional state (14, 15).

1.4.3 Overview of T-cell activation and differentiation

The full activation of T cells (both CD4$^+$ and CD8$^+$) requires three different signals. Signal 1 follows the recognition of a peptide-MHC complex by the TCR. Signal 2 follows from co-stimulatory interactions between the T cell and an activated APC and signal 3 comes from cytokines in the local environment (16-18). Once all three signals have been received, T

cells undergo a rapid expansion phase contributing to generation of a large effector T-cell pool. Activation of T cells usually occurs in the lymphoid organs and after rapid expansion, $CD8^+$ T cells migrate into the periphery. Activated $CD8^+$ T cells differentiate into different effector populations, the majority being short lived effector T cells (SLEC) ($CD127^{low}KLRG1^{hi}$) and a small subpopulation of memory precursor effector cells (MPEC) ($CD127^{hi}KLRG1^{low}$) which are characterised by the expression of IL-7 receptor α (CD127) and killer cell lectin like receptor G1 (KLRG1) (19).

1.4.3.1 Peptide-MHC complex – TCR interaction: Signal 1

The first signal for T-cell activation comes from peptide-MHC interacting with a TCR. This requires the antigens to be processed and broken down into small peptide sequences before being presented with MHC on an APC cell surface. MHC molecules are highly polymorphic which enables them to bind a wide range of peptide sequences (20). Endogenous antigens can come from self-proteins, viruses or from neo-antigens generated by cancer cells and are largely processed via a large catalytic complex called the proteasome to generate peptides suitable for MHC I binding. Once peptides are generated, they are transferred into the endoplasmic reticulum (ER) from the cytoplasm by the transporter associated with antigen processing (TAP) (21). MHC I molecules bind to antigens that are 8-11 amino acids in length (20, 22). However the translocated peptides can be much longer and an aminopeptidase, ER aminopeptidase-1 (ERAP-1), present in the ER can further process the peptides to the appropriate lengths required for MHC I interaction (23). After a peptide has bound to an MHC I molecule with high affinity, the peptide-MHC I complex is transported from the ER to the cell surface (20).

In contrast, exogenous, endocytosed, antigens are usually cleaved by lysosomal proteases and preferentially bind MHC II (20). Antigens for MHC II binding can be internalized via various mechanisms such as endocytosis, micropinocytosis and phagocytosis. After internalization, the antigen is transferred into the endosome where it is processed and loaded onto MHC II molecules as a 13-17 amino acids long peptide (24). MHC II molecules are generated in the ER and transferred into the endosome. After antigen loading, the antigen-MHC II complex is trafficked onto the cell surface (20).

Some DCs have the ability to present peptides derived from exogenous antigens on MHC I molecules in a process known as cross-presentation. The internalized antigen can be processed either via the endosomal or proteasomal pathways. Cross-presentation can contribute to the generation of immune tolerance to self-antigens and also to the generation of an immune response towards pathogens (25, 26).

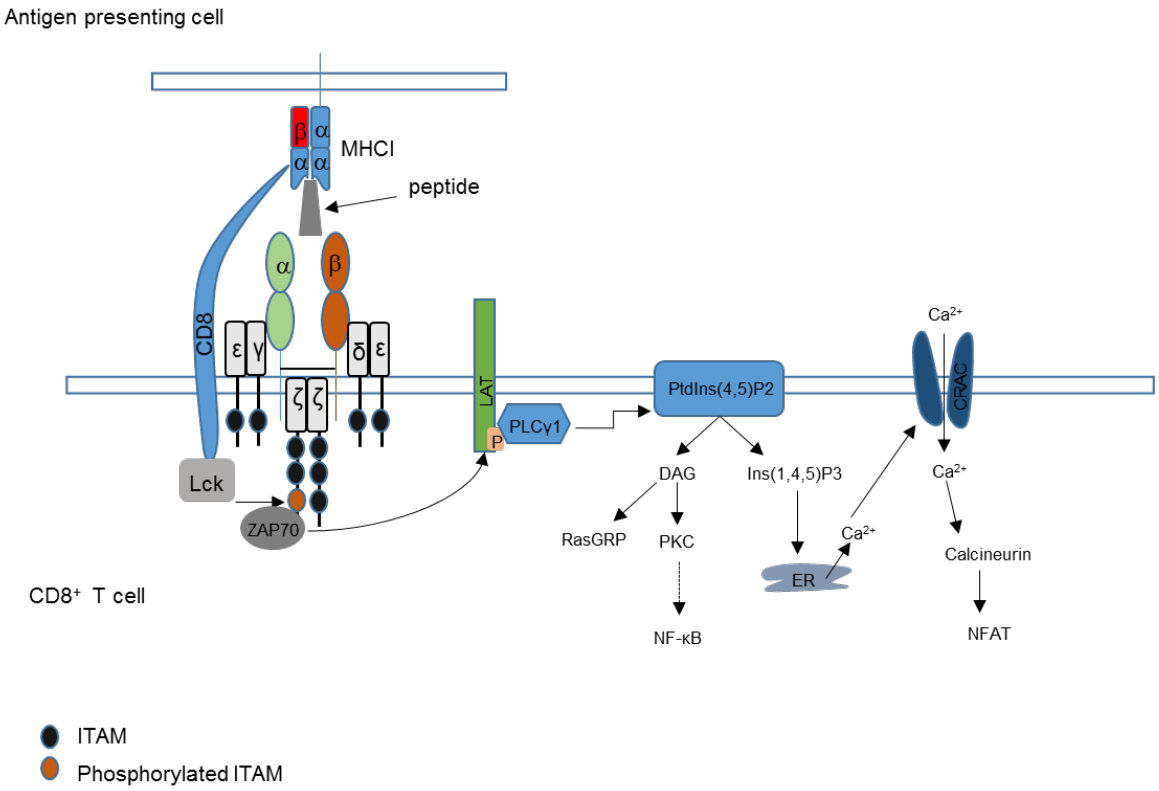

Figure 1.2. Representation of TCR complex interaction with peptide-MHC and downstream signalling. The structure of MHC I with the alpha chain comprising three domains (labelled α), linked to beta 2 microglobulin (shown by β) with bound peptide is presented. The canonical TCR is comprised of an alpha chain (α), a beta chain (β) and a CD3 complex comprising six chains (γ, ζ, δ, ε). Intracellular ITAM motifs on CD3 domains are indicated on the cytoplasmic tails. Position of the disulphide bond between the TCR α and β chains is also indicated (black line). The CD8 molecule interacts with Lck with its cytoplasmic domain and activates it. Activated Lck phosphorylates the ITAM motifs on CD3 chains leading to recruitment of ZAP70 which initiates a cascade of events (as illustrated on the figure and detailed in text) leading to activation of downstream pathways such as NF-κB and NFAT pathways.

Once a peptide-MHC complex reaches the cell surface, an appropriate T cell recognises the target antigen via its TCR. The TCR itself is a heterodimer made up of α and β subunits which are held together by a disulphide bond (Fig. 1.2) (27, 28). The peptide-MHC complex binding groove of the TCR consists of three complementary determining regions (CDR) that together determine specificity (29). In addition to the peptide-MHC recognition subunits, the TCR co-localises with the CD3 complex which consists of four subunits, γ, δ, ε and ζ, responsible for signal transduction (Fig. 1.2) (27). Once the TCR is triggered by peptide-MHC interaction, signalling is initiated by recruitment and activation of protein tyrosine kinases (PTK) of the Syk, Src and Tec families (27, 30, 31). The extracellular region of the CD4/CD8 co-receptor on the T-cell surface, interacts with the non-variable portion of the MHC molecule while the cytoplasmic domain binds and activates Lck, belonging to the Src family (32). Activated Lck, phosphorylates the immunoreceptor tyrosine-based activation motifs (ITAM) on CD3 subunits of the TCR complex (33). Upon phosphorylation of the ITAM motifs, ZAP70, a member of the Syk family, becomes able to bind to the phosphorylated domains via its Src-homology 2 (SH2) domain which then itself becomes phosphorylated on its ITAM motif leading to its activation (27). Activated ZAP70 further phosphorylates linker of activated T cells (LAT) and SH-2 domain containing lymphocyte protein of 76000 MW, (SLP76) (27, 34). These activated adapter molecules can act as scaffolds to recruit other proteins to the plasma membrane. For instance LAT recruits phospholipase C gamma 1 (PLCγ1) to the plasma membrane, and once activated, PLCγ1 cleaves phosphatidylinositol 4, 5 biphosphate (PtdIns(4,5)P_2) into inositol 1,4,5-triphosphate (Ins(1,4,5)P_3) and diacylglycerol (DAG) which are crucial secondary messenger molecules for T-cell activation (30, 33, 34). DAG can induce the activation of proteins such as Ras guanyl-nucleotide-releasing protein (RasGRP) and protein kinase C (PKC) (27, 33). As the other secondary messenger molecule, Ins(1,4,5)P_3 interacts with its receptors on the ER which leads to calcium (Ca^{2+}) release from the ER into the cytosol. The release of Ca^{2+} from the ER induces opening of Ca^{2+} release activated Ca^{2+} channels (CRAC) on the plasma membrane (Fig. 1.2) which leads to a Ca^{2+} influx from the extracellular environment (33, 35). Increased intracellular Ca^{2+} prevents the inhibitory activity of calmodulin and this induces the activation of calcineurin. Calcineurin is a phosphatase which activates the transcription factor nuclear factor of activated T cells (NFAT) by dephosphorylation (36) which is important for initiation of the transcription of genes such as interleukin-2 (IL-2), tumour necrosis factor-α (TNFα) and granulocyte-macrophage colony-stimulating factor (GM-CSF) (27, 33, 37).

IL-2 is an important cytokine for T-cell activation and proliferation. Another transcription factor activated during T-cell activation and which is also involved in IL-2 expression is nuclear factor kappa b (NF-κB) (38, 39). The adapter molecules activated by PTKs, such as LAT, recruit the phosphatidyl inositol 3-kinase (PI3K) to the plasma membrane where it becomes activated. Upon activation PI3K can activate the Akt/Protein kinase B pathway, leading to activation of NF-κB (27, 40).

1.4.3.2 Co-stimulatory interaction between APC and T cell: Signal 2

For effective generation of a T-cell response, co-stimulatory signalling is required in addition to TCR engagement with peptide-MHC (41). Stimulating T cells via the TCR in the absence of co-stimulation, generates unresponsive (anergic) T cells which are unable to proliferate, differentiate and secrete cytokines (42). Additionally, enforced co-stimulation of T cells with agonist mAb in the absence of TCR induction, does not cause T-cell activation (43, 44). This is important as it ensures that co-stimulation alone is insufficient to activate T cells in an antigen-independent manner. This also ensures that only T cells that are specific for a particular antigen are activated.

There are many co-stimulatory receptors on T cells and these can be largely classified into two sub-groups. The first group is the CD28 family that consists of receptors such as CD28 and inducible co-stimulator (ICOS). CD28 is the major co-stimulatory molecule expressed on T cells and it was one of the first to be identified. The early identification of co-stimulation came from the observation that simultaneous stimulation through the TCR and CD28 could drive dramatic increases in secretion of various cytokines including IL-2 (41, 45). Importantly, CD28 stimulation on its own did not cause any T-cell activation.

CD28 interacts with its ligands CD80 and CD86 expressed on the APC cell surface. Ligands of CD28 are expressed at low levels on APCs under physiological conditions and are rapidly up-regulated after activation (46). Upon ligation with its ligand, in presence of TCR stimulation, CD28 signalling initiates entry of naïve T cells into cell cycle. The cell cycle regulators such as cyclin D2 and cyclin-dependent kinases (CDK) 4/6 are activated to drive progression through cell cycle but simultaneously CD28 signalling blocks the effects of CDK inhibitors (47). CD28 possesses two motifs (YMNM and PYAP) in its cytoplasmic domain which are involved in binding and activating downstream effector molecules. Upon CD28

activation, YMNM motif interacts with PI3K which in turn activates Akt. The Akt pathway then triggers the activation of transcription factors such as NF-κB, NFAT and activator protein 1 (AP-1) which initiate activation of several genes including IL-2 (47, 48). Simultaneously, PYAP domain interacts with Lck and GRB2 which further enhance nuclear translocation of NFAT to increase induction of IL-2 production. As well as up-regulating IL-2 biosynthesis, CD28 signalling also up-regulates the expression of IL-2Rα chain to increase the responsiveness of the cells to IL-2. Activation of CD28 induces the up-regulation of glucose transporter; Glut 1 which increases glucose uptake into the cells to increase energy production required during rapid proliferation (47). In addition to driving signals required for activation and proliferation, CD28 signalling promotes the survival of activated T cells by up-regulation of anti-apoptotic proteins such as Bcl-XL which makes the cells resistant to apoptosis (47, 48).

The importance of CD28 in establishment of adaptive immunity has been studied in various pre-clinical studies. By using CD28 deficient mice, it has been shown that antigen specific T-cell response and T-cell differentiation were influenced. CD28 stimulation can promote the differentiation of $CD4^+$ T cells into Th2 phenotype and this was impaired in CD28 deficient mice. Additionally, Th2 $CD4^+$ T cells are required for providing help for B cells to form germinal centres and this was also defective in CD28 deficient mice (17). In a study investigating $CD4^+$ and $CD8^+$ responses to influenza virus, blocking CD28 signalling impaired both $CD4^+$ and $CD8^+$ T-cell response with reduced expansion of virus specific CTLs (49). Cytotoxic activity of $CD8^+$ T cells was also impaired. Similar results were observed in CD28 deficient mice where virus specific CTLs were reduced in response to influenza infection (50) indicating the importance of CD28 mediated co-stimulation in generating optimal T-cell responses.

The second family of co-stimulators is the TNFRSF described in more detail in section 1.6 below (p. 13).

1.4.3.3 Cytokine Stimulation: Signal 3

Cytokines are also important to maximise T-cell activation. IL-2 was one of the first cytokines to be identified and its involvement in T-cell proliferation and maintenance are well established (47, 51). In addition to IL-2, inflammatory cytokine signalling can also enable T cells to undergo successful clonal expansion and differentiation (16, 18, 52). The first evidence for the requirement of inflammatory cytokines as a third signal came from an in vitro study showing that the ability of immobilized MHC peptide/protein complexes on microspheres and co-stimulation to enhance the activation of T cells was significantly improved by inclusion of IL-1, for $CD4^+$ T cells, or IL-12, for $CD8^+$ T cells (18).

1.5 Effector mechanisms of activated $CD8^+$ T cells

Once activated and differentiated into an effector phenotype, $CD8^+$ T cells change their cell surface expression of molecules that regulate their trafficking. The expression of CD62L (L-selectin) and CCR7 are downregulated and other molecules such as; P-selectin ligand, E-selectin ligand, CXCR3 and CCR5 are upregulated (53). These molecules direct the migration of effector $CD8^+$ T cells into sites of infection after the $CD8^+$ T cells migrate out of the lymph nodes by interaction between S1P1 and its ligand, S1P (53).

After encountering a target cell, CTLs mainly induce target cell killing by two main mechanisms by maintaining cell to cell contact with the target. The first mechanism is the release of granules from the CTL to the target cell. Once the CTL recognises the peptide-MHC I complex on the target cell, cellular contact is initiated and the granules secreted from the CTL fuse with the target cell membrane releasing contents which include molecules such as perforin and granzymes A and B (54). Perforin opens pores on the target cell membrane which allows the release of CTL granule contents into the target cell. Granzymes A and B are serine proteases which can activate caspase dependent and independent mechanisms to trigger apoptosis in the target cell. Granzyme B mainly induces apoptosis by cleaving caspases which leads to rapid cell death by apoptosis (55). Granzyme A activates mechanisms which are slower than Granzyme B triggered apoptosis. Granzyme A triggers a caspase-independent pathway by inducing a mechanism that leads to generation of single-stranded DNA nicks which forces the cell into apoptosis (55, 56).

The second mechanism of triggering apoptosis in the target cell is mediated by the interaction between Fas ligand (FasL) on a CTL and its receptor, Fas, on the target cell. FasL is upregulated on the CTL cell surface after recognition of the peptide-MHC I complex by TCR. The Fas pathway activates caspases and cytochrome c release from mitochondria which drive apoptosis in the target cell (57). Additionally, CTLs release TNF-α and interferon-γ (IFN-γ) to mediate their effector functions. TNF-α functions as a pro-inflammatory cytokine and can initiate apoptotic signalling (58). IFN-γ functions to activate other effector cells of the immune system such as neutrophils and macrophages and can also metabolically suppress the infected target cells (58).

1.5.1 Memory CD8$^+$ T cells

After pathogen elimination, a dramatic contraction phase takes place where approximately 95% of the generated CD8$^+$ T cells are eliminated via apoptosis (59). The surviving pathogen-specific T cells differentiate into memory T cells that provide long term protection against subsequent pathogen challenge. The memory T-cell population can form a pool of antigen specific T cells which can be ~1000 fold higher than the frequency of naïve antigen specific T cells (60).

The higher frequency and other features such as being present at multiple tissues around the body and being able to rapidly express effector molecules, enables the memory T cells to act quicker than the naïve population in the case of secondary antigen encounter (59). Memory cells can also start the cell division process earlier than naïve T cells. When naïve and memory CD8$^+$ T cells were compared in vivo, the memory population showed an increase in cell size at 8 hrs and cell division started about 12 hrs post-immunisation. In contrast, the size of the majority of naïve cells remained unchanged up to 48 hrs and the first cell division was detected around 27 hrs post-immunisation (61, 62). Another study from the same group also demonstrated that memory CD8$^+$ T cells had high levels of CDK 6 activity and low level expression of the cell cycle inhibitor p27Kip1 which renders the memory CD8$^+$ T cells in a pre-activated state and facilitates rapid activation after antigen encounter (63). Although memory cells do not require antigen exposure or TCR stimulation for maintenance, cytokines such as IL-7 and IL-15 are required for long term persistence and homeostatic turnover (59).

The memory T-cell pool is formed by different populations which have distinct properties in their tissue distribution, self-renewal and recall capacity for effector functions. The initial two subsets of memory $CD8^+$ T cells identified were central memory T cells (T_{cm}) and effector memory T cells (T_{em}) which were classified based on their expression of CD62L (L-selectin) and CCR7 which are both required for homing into LNs (59, 64). T_{cm} cells ($CD62L^+ CCR7^+$) are largely localized in the LNs and spleen but T_{em} cells ($CD62L^- CCR7^-$) are largely localized in the non-lymphoid organs. During secondary stimulation, T_{em} cells have the ability to provide immediate effector function with high cytotoxicity against the target whereas T_{cm} cells lack immediate action but have proliferative capacity, can differentiate into $CCR7^-$ effector cells and can produce high levels of IL-2 (64, 65).

Recently a new population of memory T cells has been identified based on the expression of CX3CR1. Expression of CX3CR1 at high levels was found to be another characteristic of T_{em} cells whereas T_{cm} cells lacked CX3CR1 expression. Another population with intermediate level of CX3CR1 however, was found to be distinct from both populations, being present in lymphoid tissues and these were classified as peripheral memory T cells (T_{pm}) (66). The T_{pm} population can migrate between tissues, lymphatics and blood circulation. They can also self-renew and give rise to T_{cm} cells in the absence of antigen and upon antigen encounter, they can differentiate into T_{em} cells (66). The other memory T-cell population is tissue resident memory cells (T_{rm}) which are found in certain tissues such as brain, skin, gut and lungs. These cells do not re-circulate in the body and their phenotypic profile includes expression of CD103 and CD69 (67, 68). These cells provide the first line of defence against pathogen invasion.

1.6 TNFRSF members

In addition to members of the CD28 family (see section 1.4.3.2 above), TNFRSF members are important in providing co-stimulation (signal 2) for activation of T cells. TNFRSF receptors are type I transmembrane proteins with extracellular domains that are composed of a variable number of cysteine rich domains (CRDs) that form the ligand binding region (Fig. 1.3) (69). The family includes 30 members which can be classified into three different groups; decoy receptors (e.g. osteoprotegerin (OPG) and decoy receptor 1 (DcR1)), death domain (DD) containing receptors (e.g. Fas and TNF receptor 1 (TNFR-1)) and TNF receptor associated factor (TRAF) binding receptors (70-72).

The TRAF binding receptors include CD40, OX40, 4-1BB, CD27, glucocorticoid-induced TNFR family related gene (GITR) and receptor activator of NF-κB (RANK) (70, 71). Many of the TNFRSF members on T cells are transiently expressed only after activation through the TCR e.g. 4-1BB is expressed after 12 to 24 hrs after stimulation of adoptively transferred T cells in vivo (73); in contrast other members of the family are constitutively expressed on resting T cells e.g. CD27 (74). The majority of TNFSF ligands are expressed as trimers on the cell surface of immune cells but soluble forms resulting from proteolytic cleavage can also be found (75, 76). TNFRSF receptors become activated upon multimerisation after engaging with specific ligands which are usually absent in health but are upregulated in response to inflammatory factors. This interaction can activate different signalling pathways resulting in survival, proliferation, apoptosis or differentiation (77). Signalling pathways are not identical downstream of all TNFRSF members but signals are often conferred following TRAF recruitment leading to JNK and NF-κB pathway activation (Fig. 1.4) (78). 4-1BB, OX40, GITR and CD27 are several members of the TNFRSF expressed on T cells that have been targeted in research studies and clinical trials (79-82). All of these receptors can contribute to the T-cell response during the primary activation. However, side-by-side comparisons of these receptors revealed that CD27 activation is more potent than other receptors in the primary activation of antigen specific $CD8^+$ T-cells (83, 84). My PhD project focussed on targeting CD27 and therefore a more detailed description of CD27 follows.

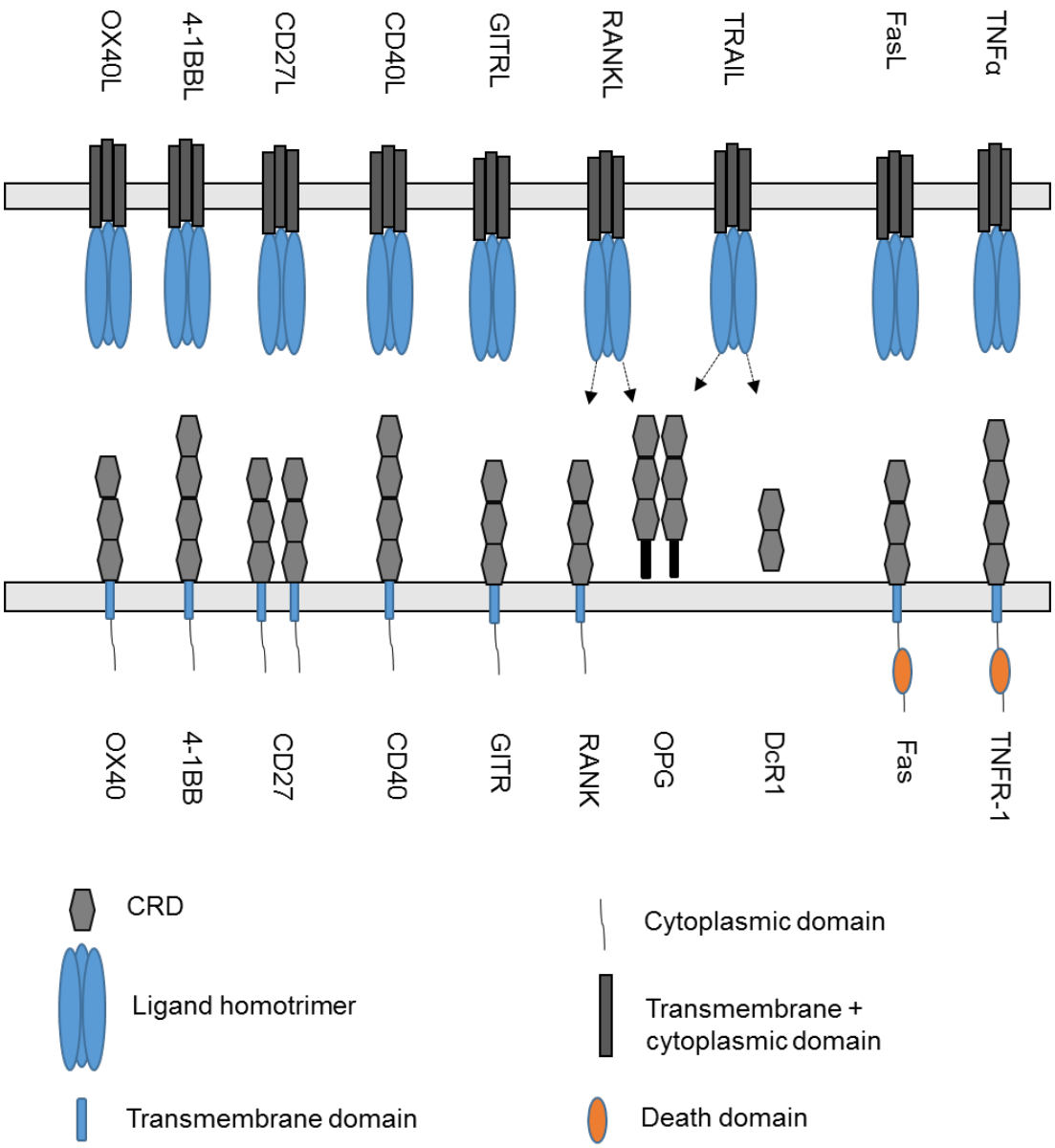

Figure 1.3. Structures of selected TNFRSF members and their ligands. Selected members of the TNFRSF and their ligands are depicted. The ligands of the TNFSF are illustrated as homotrimers. The number of CRDs in the extracellular domains of TNFRSF receptors are indicated.

1.6.1 CD27

CD27 is a disulphide-linked homodimer on T cells, NK cells and at a low level on subsets of B cells (85, 86). Although the majority of TNFRSF members are expressed only after immune cell activation, CD27 is unusual as it is expressed constitutively on T cells (79) and the expression level is upregulated after activation. The ligand for CD27, CD70, is expressed at low levels under physiological conditions but is elevated after immune cell activation on DC, B cells, T cells and NK cells (79, 87). CD27 interacts with TRAF2 and TRAF5 via an amino acid motif; PIQEDYR, leading to activation of TRAFs and downstream JNK and NF-κB signalling pathways (Fig. 1.4) (88).

Stimulation of CD27 supports the clonal expansion of T cells. Signalling through CD27 contributes to increased expression of anti-apoptotic protein Bcl-XL, reduced levels of FasL on $CD4^+$ cells and reduced sensitivity of $CD8^+$ T cells to FasL-stimulated apoptosis (89, 90). CD27 signalling also leads to upregulation of cytokine receptors such as IL-2Rα and IL-12Rβ which increases sensitivity of the cells to cytokines (70, 91). Additionally, transcription factors AP-1, ERK, mitogen activated protein kinase (MAPK) and NFAT are activated, leading to production of cytokines including IL-2, IL-4, IL-5, IL-12 and IFN-γ (70, 91). Apart from supporting anti-apoptotic pathways and inducing cytokine production, CD27 activation has effects on metabolic pathways by improving the expression of Pim-1, a serine threonine kinase, which supports enhanced protein translation and aerobic glycolysis during the rapid expansion of activated T cells (79, 89, 92). Additionally, expression of chemokines such as XCL1 and CXCL10 (93) are induced, promoting the communication of T cells with APCs during priming which improves effector T-cell differentiation.

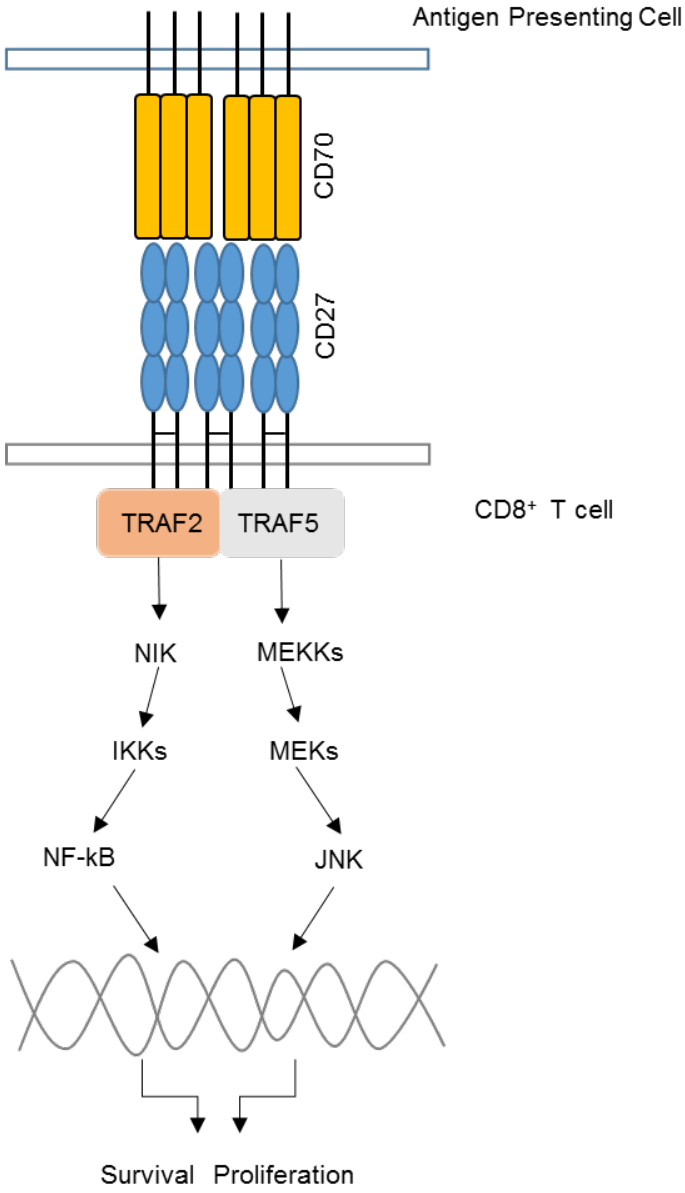

Figure 1.4. Interaction of CD27 with CD70 and downstream signal transduction. Trimeric cell surface CD70 (indicated in yellow) interacts with disulphide linked (black lines) dimeric cell surface CD27 (indicated in blue) which leads to initiation of signal transduction by recruitment of TRAF2/TRAF5 (indicated in orange and grey respectively). TRAF2/TRAF5 activation initiates activation of downstream molecules leading to activation of NF-κB and JNK pathways as illustrated. NF-κB and JNK pathways induce expression of genes involved in survival and proliferation.

The CD27-CD70 pathway induces the differentiation of $CD4^+$ T cells into a Th1 type phenotype and $CD8^+$ T cells into CTLs (79). The activation of naïve $CD8^+$ T cells by activated DCs requires CD70. Additionally, the anti-tumour response generated by antigen and anti-CD40 immunisation requires CD70 and the activity achieved by anti-CD40 mAb can be recapitulated by anti-CD27 activity (94, 95). These data indicate that activation of naïve $CD8^+$ T cells by CD40-licensed DCs, requires the presence of CD27 on $CD8^+$ T cells.

Supporting this phenomenon, blocking CD27 signalling or using CD27-/- mice led to reduced expansion of $CD8^+$ T cells during the primary response (96). The effector functions of CTLs are enhanced by CD27 signalling and secretion of IFNγ and cytotoxic capacity are improved. Expression of the transcription factor Eomesodermin (97) and cytokine IL-2 (98) are upregulated after CD27 stimulation. These in turn can stimulate increased production of IFNγ which is important for CTL activity (99). IL-2 is also important for the survival of activated $CD8^+$ T cells in the periphery (98). Furthermore, CD27 signalling can enable T cells with low affinity TCR-antigen engagement to undergo clonal expansion and this leads to a broadened TCR repertoire of responsive T cells (100).

Apart from the effects on effector functions, CD27 signalling is required for the establishment and secondary induction of memory T cells. Generation of memory T cells after infection with influenza requires CD27 (83). Generation of memory $CD8^+$ T cell subsets is impaired in the absence of CD27 during the initial priming phase (101, 102). Preventing CD27 signalling in CTLs during the initial priming, impairs their capacity to expand during secondary stimulation and they become more prone to TRAIL-mediated apoptosis on secondary stimulation which resembles TRAIL-mediated activation induced cell death where CTLs are primed without the presence of helper T cells (96). During the secondary response, boosting mice with antigen and a soluble recombinant form of the CD27 ligand (sCD70), resulted in improved expansion and survival of the memory $CD8^+$ T cells (87). Stimulation of memory $CD8^+$ T cells with anti-CD40 mAb requires additional co-stimulatory signalling, especially through CD27/CD70 pathway. On the other hand, stimulation with antigen and CD27 alone can drive the expansion and survival of memory $CD8^+$ T cells (87) suggesting that CD27/CD70 pathway can be sufficient for the secondary activation of antigen specific cells.

CD27 co-stimulation during the priming of $CD8^+$ T cells is critical for the expression of IL-7Rα on effector $CD8^+$ T cells which is important for the generation and the frequency of the memory pool (103, 104). After initial activation of TCR signalling, $CD8^+$ T cells downregulate IL-7Rα expression but stimulation with CD27 induces re-expression of IL-7Rα which increases the memory precursor pool. Transcription of IL-7Rα is promoted by the transcription factor GA binding protein α (GABPα). Stimulation of $CD8^+$ T cells with CD27 leads to increased levels of GABPα which suggests that transcription of IL-7Rα is increased as a downstream consequence of CD27 stimulation (104).

In addition to driving expansion of memory cells, CD27 signalling activates pathways leading to protection from apoptosis, mirroring its effects on primed T cells. Stimulation of the memory pool with antigen alone or antigen in combination with sCD70, showed that the cells stimulated with sCD70 had lower levels of apoptotic markers such as Annexin V compared to the antigen only stimulated population (87). The pro-survival mechanisms activated by CD27 signalling during initial priming (detailed above) might also be activated during the expansion of the memory $CD8^+$ T cells. Studies in which CD27 is manipulated to improve tumour therapy are discussed in a later section (section 1.10.6).

1.6.1.1 CD27-CD70 deficiency

It has been shown that deficiency in expression of CD27 can make individuals prone to development of Epstein-Barr virus (EBV)-driven lymphoproliferative disorders. Initially two individuals with CD27 deficiency were identified with persistent symptomatic EBV viremia and hypogammaglobulinemia (105). Detailed analysis of one of the individuals revealed inefficient $CD8^+$ T-cell function and disturbed T-cell dependent B-cell responses. Although CD27 deficiency did not affect the differentiation and maturation of the $CD8^+$ T cells and EBV-specific memory $CD8^+$ T cells could be identified in the patient, the ability of those cells to produce IL-2 was impaired (105). CTLs are considered to be the main regulators of clearance of EBV-viral infections and IL-2 production capacity is critical for their functionality (105-107). Thus, this suggests that impaired IL-2 production by virus specific $CD8^+$ T cells in CD27 deficient individuals is an important factor in the development of EBV-related complications. Subsequent studies also identified another 15 individuals with CD27 deficiency who had EBV-driven lymphoproliferative disorders including EBV-positive B-cell malignancies (108, 109).

Similarly, deficiency in CD70 (six individuals identified to date) contributes to EBV-related disorders including immunodeficiency and B-cell malignancies (110-112). In a detailed analysis of a CD70 deficient patient, EBV-specific T cells showed impaired expansion when stimulated with B-cells with CD70 deficiency. However, stimulation with B cells expressing CD70 could restore the expansion of virus specific T cells (110).

The importance of the CD27-CD70 pathway in priming and memory differentiation of T cells has been extensively characterised in pre-clinical models (see section 1.6.1). The clinical data from individuals with CD27/CD70 deficiency further highlight the importance of this pathway in protection against EBV-related complications.

In addition to the importance of CD27 pathway in clearing cancer-inducing viruses, activation of CD27 can also regulate the immune response to produce a strong anti-tumour immunity to tumours irrespective of viral origin. For this reason, an overview of cancer, immunotherapy and manipulation of CD27 in the context of cancer immunotherapy are described below.

1.7 Overview of Cancer

Cancer is the second major cause of death worldwide and is characterised by abnormal growth of transformed cells with new characteristics (113). Tumour development is a multistep process and during the development stage, tumour cells acquire properties which enable their survival, termed as the hallmarks of cancer. Initially, six hallmarks were identified and these include; limitless replicative potential, resistance to apoptosis, avoidance of inhibitory signalling, sustained growth signalling, angiogenesis and metastasis (114, 115). In addition to these, changed cellular metabolism and evading destruction by immunity have recently been identified as the new emerging hallmarks. Tumour cell characteristics develop over time and the major contributors are considered to be a permissive local tumour microenvironment due to tumour promoting inflammation during development and genomic instability of the tumour cells enabling accumulation of mutations (114).

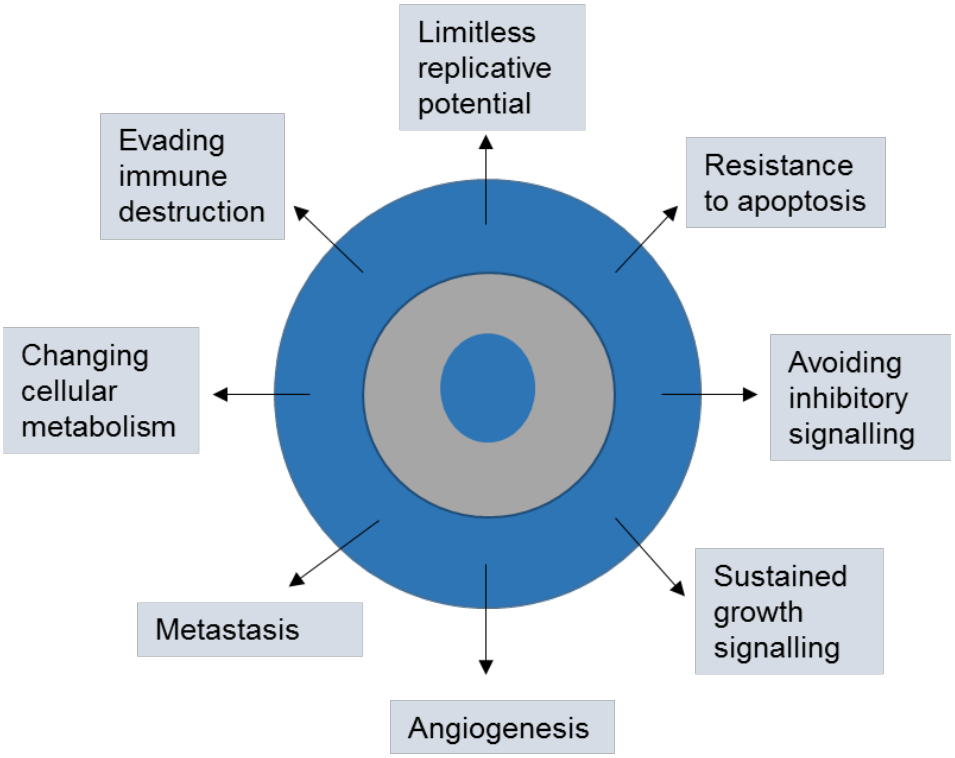

Figure 1.5. Hallmarks of cancer. The characteristics gained by cancer cells during tumour development are illustrated as the hallmarks of cancer. The initially identified characteristics were; limitless replicative potential, resistance to apoptosis, avoiding inhibitory signalling, sustained growth signalling, angiogenesis and metastasis. The more recently identified characteristics include evading immune destruction and changed cellular metabolism.

1.8 Cancer Immune Surveillance

In addition to defence against pathogenic agents, the immune system also contributes to the elimination of transformed cells from the body in a process called cancer immune surveillance (116, 117) as evidenced by patients or mice with primary or secondary immunodeficiency which show increased risk of cancer development. For instance RAG-2 is required for formation of mature lymphocytes and without RAG-2, mice have no B or T cells, and also quicker and increased tumour development compared to wild-type mice (118). Also, when the cytotoxic ability of lymphocytes was disrupted via various mechanisms, this led to increased tumour development in mouse models (116). Similarly in perforin deficient mice, lymphoma development with age was observed. However, when those tumours were transplanted into WT animals, they were rejected confirming the importance of fully functional immune cells for tumour immunosurveillance (117, 119).

Patients with common variable immunodeficiency disease are prone to elevated levels of various epithelial cancers and lymphomas (120, 121). Additionally, suppressing the immune system causes increased risk of cancer development in large cohort studies of patients undergoing immunosuppression for organ transplantation (120).

Tumour cells can aberrantly over-express normal proteins and these are known as tumour associated antigens (TAA). Additionally, tumour cells can express neo-antigens which are tumour specific antigens generated by mutations in proteins. Cells of the immune system are capable of identifying and eliminating transformed host cells via the recognition of both TAA and neo-antigens (122-124). Indeed the frequency of tumour infiltrating lymphocytes (TILs) is associated with a good prognosis in cancers such as breast cancer, oesophageal cancer, ovarian cancer and colon cancer (125-128).

1.9 Cancer immunotherapies

Although immune cells can contribute to tumour rejection, tumours still develop in immune competent individuals. Specifically for T-cell responses, the absence of sufficient co-stimulatory interactions and immunosuppressive environment (e.g. presence of inhibitory checkpoint receptors PD-1 and cytotoxic T-lymphocyte antigen-4 (CTLA-4) or inhibitory cytokines such as TGF-β and IL-10) can limit their activity in tumour rejection (129, 130). For these reasons, various cancer immunotherapy approaches have been developed to increase the magnitude and efficiency of the anti-tumour immune response. These treatment strategies include cell based, vaccine based and monoclonal antibody based approaches which are discussed below.

1.9.1 Cell based cancer immunotherapy

Extraction of immune cells from a patient, expansion ex vivo and transfer back to the patient is an approach used to increase the frequency of tumour specific immune cells and thus improve the strength of the anti-tumour immune response. Sipuleucel-T is a patient specific treatment licenced for the treatment of castration-resistant prostate cancer. Treatment involves the extraction of DCs from the patient, activation of the cells with a recombinant protein consisting of prostatic acid phosphatase (PAP) conjugated to granulocyte macrophage colony stimulating factor (GM-CSF) and transfer back into the patient.

Activated DCs are then able to initiate a cytotoxic response by stimulating T lymphocytes. This therapy was found to significantly improve the median survival of patients by 4.1 months compared to a placebo treated control group (131).

Another cell based approach in immunotherapy is adoptive T-cell transfer. T lymphocytes that are specific against the tumour can be isolated from the peripheral blood or tumour and expanded ex vivo. Activatory cytokines are used to expand cell number and the expanded T-cell pool is transferred to the patient (122). Treatment of metastatic melanoma patients with autologous TIL expanded and transferred in conjunction with IL-2, resulted in complete regression in 22% of patients who were previously refractory to standard treatments (132).

Similar to adoptive T-cell transfer, autologous T cells from a patient can be isolated and genetically modified to express chimeric antigen receptors (CAR) on cell surface which are targeted against an antigen overexpressed on tumour cells (133). The genetically modified CAR T cells are expanded in laboratory before being infused back into the patient. This approach can help to overcome the lack of T-cell activation in the body and can generate an effective T-cell response against tumours. The CAR has a domain for antigen specificity and also an intracellular co-stimulatory domain that improves the effectiveness of the CAR T cell by overcoming the lack of co-stimulatory signalling in tumour microenvironment (133, 134). The infused CAR T cells can persist for a long time (6 months or longer) in circulation providing long term activity and this therapy has been shown to be particularly effective against B-cell malignancies where CAR T cells targeting CD19 (a B-cell antigen) are used for treatment (135-137).

Although adoptive cell therapy is a promising field, the procedure is specific for individual patients and can be labour intensive (138). Thus, alternative approaches such as vaccine treatments may be more practical to activate the immune system in vivo.

1.9.2 Vaccine based cancer immunotherapy

Vaccine based approaches seek to expand the immune system in vivo rather than in vitro. One approach is to use patient-derived tumour cells which are irradiated and transferred back to the patient in combination with an immune-stimulatory adjuvant such as Bacille Calmette-Guerin (BCG) (139, 140). Although this can contribute to effective stimulation of the immune system, the number of tumour cells can be a limiting factor (140). In order to overcome this, tumour cell lines with an immune-stimulatory adjuvant (e.g. BCG) can be used (141). In order to improve the diversity of antigens delivered and make the vaccination more practical, several cell lines of a particular tumour type can be combined to generate a vaccine (140). Canvaxin™ is a melanoma cancer cell vaccine consisting of three different melanoma cell lines delivered with BCG. Treatment of stage III melanoma patients with Canvaxin™ as postoperative adjuvant therapy, significantly improved survival rates by 25 months (142).

1.9.3 Antibody based cancer immunotherapy

Another approach is to use monoclonal antibodies (mAbs) which can either be used to directly target tumour cells to initiate target cell killing or as immunomodulatory agents to harness the immune system to generate a strong anti-tumour response. Direct targeting and immunomodulatory mAbs work by different mechanisms which are detailed below.

1.9.3.1 Direct targeting mAbs

Direct targeting mAbs can target specific receptors expressed on tumour cells. For instance rituximab is directed against the B-cell marker CD20 and has been used for the treatment of B-cell malignancies as a component of standard of care (143-145). Rituximab has high affinity for CD20 and binds with high specificity. By engaging with CD20, rituximab can initiate direct effects such as inducing apoptosis of the tumour cell or can initiate antibody dependent cellular cytotoxicity (ADCC), antibody dependent cellular phagocytosis (ADCP) or complement dependent cytotoxicity (CDC) which lead to target cell death (143, 145). Rituximab is a well-tolerated drug and improves overall response rate (ORR) and complete response (CR) rate in various B-cell malignancies with minimal toxicity. Adverse events such as cytokine release syndrome, hypotension, infections and cardiovascular problems have been observed but the majority of the events were low-grade, mild and tolerable (145).

1.9.3.2 Immunomodulatory mAbs

In addition to direct targeting approaches, mAbs can be used to actively engage the immune system. Clinically this approach has focussed largely on blocking receptors which confer inhibitory signals to T cells, such as CTLA-4 or PD-1 (or its major ligand PD-L1) (146). Ipilimumab, which targets CTLA-4, has contributed to significantly improved overall survival of metastatic melanoma patients (147). Comparing the efficacy of a vaccine only (136 patients), ipilimumab only (137 patients) or vaccine and ipilimumab combination (403 patients) in pre-treated (cytokine or chemotherapy) advanced stage metastatic melanoma patients, showed that ipilimumab alone or in combination with a vaccine significantly improved the overall survival compared to vaccine only treatment. Adverse events included some severe effects which were manageable but the majority were low grade with diarrhoea being the most common adverse event (147).

Similarly for PD-1, blocking the interaction of PD-1 with its ligands using an anti-PD-1 mAb, Nivolumab, induced clinical activity in several cancer types including Hodgkin's Lymphoma (148), non-small cell lung cancer (NSCLC) (149) and renal cell carcinoma (RCC) (150, 151). 23 patients with refractory or relapsed Hodgkin's Lymphoma who had previous chemotherapy treatment, showed significant responses to Nivolumab where a partial response (PR) in 16, CR in 4 and stable disease (SD) in 3 patients were observed. The majority of the adverse events observed with Nivolumab treatment were low grade and the most common events were rash and reduced platelet count with no life threating toxicity (148). Also, Pembrolizumab is another mAb targeting PD-1 and in NSCLC, it can improve the survival of patients especially against PD-L1 positive tumours (152, 153). Additionally, the combination of Ipilimumab and Nivolumab has been tested in patients with melanoma and this approach was found to improve response rates compared with either monotherapy (154-156). Although a higher percentage of patients had immune-related adverse events and more severe conditions were observed with combination treatment, these were manageable (155, 156).

Despite the success of inhibitory checkpoint blockers, the frequency of responders remains low and there is need to further improve the anti-tumour immune response. More recently there has been interest in using mAbs as agonists of co-stimulatory receptors on the surface of immune cells to boost the anti-tumour immune response. This approach has also been shown to synergise with inhibitory checkpoint blockade to generate a strong anti-tumour

immunity. The approaches targeting the co-stimulatory receptors will be described in more detail below.

1.10 Targeting TNFRSF for immunotherapy

As described in section 1.6 above, TNFRSF members are important co-stimulators of T cells. Several members of the family have been targeted using either recombinant ligands or agonist mAbs in pre-clinical models to improve tumour therapy. Although agonistic mAbs targeting several members of the TNFRSF can initiate anti-tumour responses in mice (80, 157), their activity is reliant, not only on the antigen-specific Fab region but also the Fc region (Fig. 1.6.B). It has become apparent in recent years that choosing the optimal antibody isotype and ensuring the availability of FcγR which mediate cross-linking of mAb by engagement with the Fc domain, are critical. As FcγR engagement of mAb Fc domain is critical for their activity, a summary of FcγR biology is included in this section.

1.10.1 FcγRs

FcγRs are classified into type I (FcγRI, FcγRIIB, FcγRIII and FcγRIV in mouse, FcγRI, FcγRIIA, FcγRIIB, FcγRIIC, FcγRIIIA and FcγRIIIB in human (Fig. 1.6.A)) and type II receptors (DC-SIGN and CD23) based on the binding stoichiometry and the domain they bind on antibody Fc region (158). Type I receptors belong to the immunoglobulin superfamily and type II receptors are members of the C-type lectin receptor family. Type I FcγRs interact with the immunoglobulin G (IgG) molecule at a 1:1 stoichiometry with the loop region of FcγR (between the Ig-like domains) interacting with the hinge-CH2 interface of IgG Fc (Fig. 1.6.B). In contrast, type II receptors interact with the IgG at a 2:1 stoichiometry (receptor:IgG) and they bind to the CH2-CH3 domain of the Fc region (158). Type I receptors are heavily characterised to be involved in influencing the outcome of mAb activity and a brief overview of these receptors follows.

Type I receptors are sub-classified into activatory and inhibitory receptors based on the signalling motif on their cytoplasmic domain. Their extracellular domains consists of two or three Ig-like domains and intracellular domains can have an ITAM (activatory) or immunoreceptor tyrosine based inhibitory (ITIM) motif (Fig. 1.6.A) (158, 159). FcγRI, FcγRIII

and FcγRIV in mouse, and FcγRI and FcγRIIIA in human require the FcRγ subunit to be expressed at the cell surface together with the α subunit whereas the other receptors only have the α subunit. The ITAM motif of the receptors with α and γ subunits, is expressed on the γ chain whereas the other receptors express the ITAM or ITIM motif on the α chain (160). Activatory FcγRs include FcγRI, FcγRIII and FcγRIV in mouse, and FcγRI, FcγRIIA, FcγRIIC and FcγRIIIA in human. The only inhibitory receptor is FcγRIIB in both mouse and human. FcγRIIIB in humans has no intracellular domain and is expressed as a GPI-anchored protein. Hence, it is not characterised as an activatory or inhibitory receptor (160).

In mouse, FcγRI exhibits high affinity to monomeric IgG (IgG2a) and FcγRIV exhibits high affinity to IgG2a and IgG2b. FcγRIIB and FcγRIII have low affinity towards monomeric IgG and they interact with multimeric IgG. In humans, FcγRI is the only receptor with high affinity to monomeric IgG and other FcγRs have low affinity. When activatory receptors are engaged with IgG and clustered, this triggers phosphorylation of the ITAM motifs which leads to activation of cytoplasmic Syk and Src family of kinases and pro-inflammatory signalling pathways (158, 160). The stimulation of the activatory FcγRs can drive various outcomes such as ADCC or ADCP and secretion of cytokines, depending on the cell type they are expressed on. Distinct from the activating receptors, SHIP phosphatases are recruited to the phosphorylated ITIM motif of the inhibitory FcγRIIB upon receptor clustering. The outcome of FcγRIIB triggering can lead to blocking Src family kinase activation and counteracting the pro-inflammatory signals initiated by activatory FcγRs (160).

Type I FcγRs can be expressed on different immune cells and several FcγRs can be expressed on the same cell. In mouse, FcγRI is expressed on monocytes, macrophages and DCs, FcγRIIB is expressed on B cells, monocytes, macrophages, neutrophils, DCs, basophils, mast cells and eosinophils, FcγRIII is expressed on NK cells, monocytes, macrophages, neutrophils, DCs, basophils, mast cells and eosinophils and FcγRIV is expressed on monocytes, macrophages and neutrophils (159, 161)

In humans, FcγRI is constitutively expressed on monocytes and macrophages but expression can be induced on other immune cells such as neutrophils, eosinophils and DCs as a consequence of pro-inflammatory environment (162). FcγRIIA is expressed on monocytes, macrophages, neutrophils, eosinophils and DCs, FcγRIIB is expressed on

macrophages, neutrophils, eosinophils, DCs and B cells, FcγRIIC is expressed on NK cells, FcγRIIIA is constitutively expressed on monocytes, macrophages and NK cells and expression can be induced on DCs. FcγRIIIB is constitutively expressed on neutrophils and expression can be induced on eosinophils. In both mouse and human, apart from B cells which only have FcγRIIB expression and NK cells which only have activatory FcγR expression, the outcome of FcγR clustering on the other immune cells depends on a balance between the downstream signals initiated by inhibitory and activating receptors (158, 160).

Mice have four IgG subclasses; IgG1, IgG2a, IgG2b and IgG3. Similarly, humans also have four IgG subclasses; IgG1, IgG2, IgG3 and IgG4 (158). Mouse IgGs have more distinct profiles in the interaction with FcγRs. IgG1 binds only to FcγRIIB and FcγRIII, IgG2a and IgG2b bind to all of the FcγRs with higher affinity towards the activating FcγRI and FcγRIV. IgG3 shows minimal or negligible binding to FcγRs. In humans, IgG1 and IgG3 bind to all FcγRs with higher affinity towards activatory FcγRs (mainly FcγRI) whereas IgG2 and IgG4 show more preferential interaction with FcγRs mainly in the form of immune complexes (159, 163, 164).

Interaction with activatory or inhibitory FcγR can elicit different outcomes for the activity of the IgG mAb. For agonistic activity, it has been established for several members of the TNFRSF that FcγRIIB is required to enable cross-linking of the mAb and thus clustering of the target receptor. However, mAbs that exert their activity through deleting target cells, binding to activatory FcγRs is more advantageous (163). Correspondingly, mAbs which have a higher affinity for FcγRIIB (e.g. IgG1 isotype in mice) are better at agonistic activity whereas mAbs with higher affinity for the activatory receptors (e.g. IgG2a isotype in mouse) are better at depleting target cells. Here, an overview of some key studies with mAbs targeting different members of the TNFRSF follows.

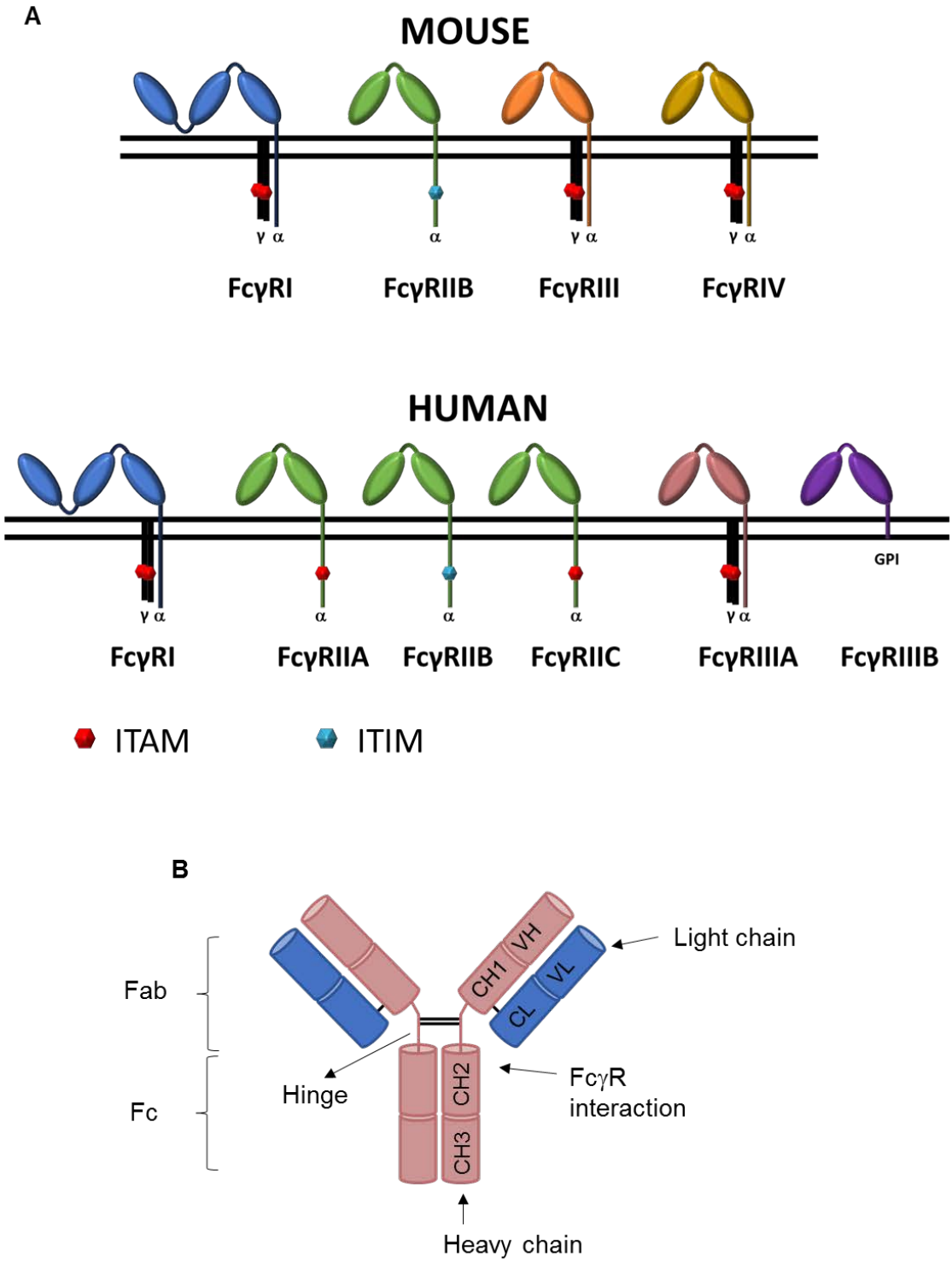

Figure 1.6. Schematic representation of FcγRs and IgG. (A) Mouse and human FcγRs are illustrated. There are four receptors for mouse and six receptors for human. The receptors consist of Ig-like extracellular domains and indicated α and γ chains as the intracellular subunits. (B) IgG mAb consists of two identical heavy and light chains which are linked by disulphide bonds (indicated as black lines between the chains). The Fab domain interacts with the antigen whereas the Fc domain interacts with the FcγRs. The hinge-CH2 interface where the FcγRs bind is indicated. Figure adapted from (159).

1.10.2 Therapeutic targeting of CD40

CD40 is predominantly expressed on APCs such as B cells and DCs, and agonistic mAbs against CD40 improve anti-tumour responses by activating and licensing APC (80, 165). Targeting CD40 in mouse models has shown promising results in tumour types including lymphoma (80). However, despite anti-tumour efficacy being shown in multiple pre-clinical models, the clinical activity of agonistic anti-CD40 agents have been limited, inducing tumour shrinkage in approximately 20% of patients at best (80, 166). Additionally, the strongest agonist of CD40, CP-870,893, was limited by toxicity with a maximum tolerated dose of 0.2 mg/kg which is likely to limit the efficacy of the antibody by not allowing saturation of the receptor (80).

It has been well established in pre-clinical models that agonistic anti-CD40 mAbs require FcγRIIB induced cross-linking for their optimal activity (167). The therapeutic efficacy of anti-CD40 mAbs was dependent on antibody isotype with the antibodies (mIgG1 or rIgG2a) being engaged by FcγRIIB with high affinity, showing anti-tumour efficacy whereas mIgG2 isotype, which has a low affinity towards FcγRIIB and does not get efficiently cross-linked, not showing any anti-tumour efficacy in a murine BCL1 model (168).

The translation from pre-clinical models to clinic is limited in this context since there is no human antibody with high affinity for FcγRIIB to favour the interaction to achieve high levels of cross-linking for agonistic activity. The anti-CD40 mAbs (e.g. ChiLob 7/4) with human IgG2 isotype can show agonistic activity without FcγR engagement. It has been shown that a unique configuration in the disulphide bonds in the hinge and CH1 domains can impact on the structure of the antibody (169). The hIgG2 antibodies can exist in h2A or h2B forms which have differences in the structure of their disulphide bonds and specifically, the h2B form can elicit activation of CD40 without requiring cross-linking. The “B” form has two disulphide bonds; one between the light chain constant domain and hinge region and another one between heavy chain CH1 domain and the hinge region. These disulphide bonds are proposed to give a more compact, less flexible conformation to the antibody which in turn might be able to interact with receptors in a more rigid structure to initiate activation (169). The human IgG2 isotype CP-870,893 antibody can also drive agonistic activity without requiring FcγR mediated cross-linking (169). Although it can induce FcγR independent activity, recent evidence suggests that, by Fc engineering to improve affinity

to FcγRIIB, the activity of this antibody can be further enhanced by FcγR mediated cross-linking indicating that for maximal activity, FcγR engagement is still required (170).

1.10.3 Therapeutic targeting of 4-1BB

Agonistic agents against 4-1BB showed treatment responses in several murine tumour models such as lymphoma (171), floor of mouth squamous cell cancer (172) and liver cancer (173). The therapeutic effect of a 4-1BB agonist in a lymphoma model was further improved by combination treatment with Treg depletion (171). In that study, the Treg cells were selectively depleted using the anti-folate receptor 4 mAb and the therapeutic efficacy of the agonistic anti-4-1BB was improved from 40% to 100% of responders (171).

As well as activated T cells, 4-1BB is also expressed on Tregs and a recent study demonstrated that by using the appropriate mAb isotype (mIgG2a), Tregs could be depleted by anti-4-1BB and this provided anti-tumour efficacy in solid tumour models (174). Although, agonistic targeting of anti-4-1BB (mIgG1) could also provide efficacy, the response generated was lower than the mIgG2a isotype in the murine tumour models tested. Additionally, when the two isotypes were used sequentially by first depleting Tregs and then inducing agonism, mainly on $CD8^+$ T cells, the effect was better than both monotherapies and the sequence of administration was important, as when given concurrently, the combination effect was lost (174). Similar to agonistic anti-CD40 mAb, the agonistic activity of anti-4-1BB mAbs relied on availability of FcγRIIB cross-linking whereas being cross-linked by activatory FcγRs could convert an agonistic mAb into a depleting antibody (174).

Currently there are two anti-4-1BB mAbs in clinical development (Table 1.1). Both antibodies have shown to be safe in patients and were tolerated up to 10 mg/kg. Antibodies caused adverse events in 15% or less of patients including dizziness, rash, diarrhoea and increased liver enzymes (175, 176), although a strong anti-tumour response was not generated. The anti-4-1BB mAb Utomilumab induced PR or CR in 13% of patients with Merkel cell carcinoma and stable disease in 24.5% patients with advanced solid tumours (176).

1.10.4 Therapeutic targeting of OX40

Similar to 4-1BB, OX40 is transiently expressed on activated T cells and constitutively expressed on Tregs. Targeting OX40 with an agonistic mAb proved to be efficacious in generating anti-tumour immunity in several tumour models such as murine mammary cancer, melanoma, colon carcinoma and renal carcinoma (177, 178). Treating mice with murine mammary cancer with a soluble form of OX40L also contributed to improved survival (25% response compared to 3.5% in the control group) and generation of long-term protective immunity (178).

Agonistic OX40 mAbs can also generate anti-tumour immune responses by inducing the selective deletion of Tregs. Although, mAb isotype is important in this context and direct targeting antibodies such as mIgG2a induce better deletion, there is evidence suggesting that agonistic anti-OX40 mAbs (mouse IgG1 isotype) can function by inducing effector T-cell expansion and Treg depletion at the same time to generate effective anti-tumour immunity (81, 179). The FcγR requirement of agonistic anti-OX40 mAbs has not been directly investigated. However, the requirements identified for other anti-TNFRSF mAbs would be expected to apply for anti-OX40 mAbs too. In a study in which different Fc engineering mutations were used to enhance the affinity of human IgG1 anti-OX40 mAb to FcγRIIB, the agonistic activity of the mAb was also improved confirming that FcγR mediated cross-linking enhances the activity of anti-OX40 mAbs (180).

The first anti-OX40 mAb to enter clinical trials was a murine IgG1 (clone 9B12, now known as humanized IgG1 Tavolimab) which generated immune-stimulating effects such as increased effector T-cell activation and proliferation. The antibody failed to generate strong anti-tumour immunity although regression of one or more metastatic lesions was observed in 30% of patients (181, 182). The antibody was well tolerated with mild to moderate adverse events including fatigue, mild rashes, fever/chills and a brief period of lymphopenia. Currently, there are several clinical trials being carried out with OX40 agonists and the results are yet to be published.

1.10.5 Therapeutic targeting of GITR

GITR is another member of the TNFRSF that is up-regulated on effector T cells after activation but is constitutively expressed on Tregs. Similar to 4-1BB and OX40, targeting GITR has been shown to induce anti-tumour immunity in many pre-clinical models and the action could either be through agonism on effector T cells or depletion of Tregs (183). The requirement for FcγR availability for the anti-tumour efficacy of anti-GITR antibody has also been illustrated. The depletion of Tregs was dependent on availability of activatory FcγRs (184) and considering the data on other anti-TNFRSF mAbs, agonistic activity of anti-GITR mAb would be expected to rely on availability of FcγRIIB.

A humanized IgG1 anti-GITR agonist mAb, MK-4166, was tested alone or in combination with anti-PD1 (Pembrolizumab). The MK-4166 mAb was well tolerated in patients as a mono or combination therapy, with main adverse events including fatigue, nausea and abdominal pain. Only 5.3% of patients had treatment related grade 3 or above adverse events. As a combination therapy, 4 complete response and 5 partial responses were observed in 13 melanoma patients who had no previous treatment.

Overall, outcomes from the clinical trials targeting TNFRSF members indicate that these agents are safe and can achieve biological and clinical responses in patients and a summary of anti-TNFRSF mAbs in clinic (185) can be seen in Table 1.1.

My PhD focuses on targeting CD27 and a more detailed overview of pre-clinical and clinical targeting of CD27 therefore follows.

Table 1.1. Summary of agonistic anti-TNFRSF mAbs in clinical trials targeting CD40, 4-1BB, OX40, GITR and CD27.

Target antigen	*Drug name*	*Isotype*
CD40	CDX1140	Human IgG2
	CP-870,893	Human IgG2
	ChiLob 7/4	Mouse/human chimera IgG1
	APX005M	Human IgG1
	SEA-CD40	Human IgG1 (Non-fucosylated)
	JNJ-64457107	Human IgG1
4-1BB	Urelumab	Human IgG4
	Utomilumab	Human IgG2
OX40	PF-04518600	Human IgG2
	MOXR-0916	Human IgG1
	BMS-986178	Human IgG1
	Tavolimab	Human IgG1
	INCAGN01949	Human IgG1
	GSK-3174998	Human IgG1
GITR	TRX-518	Human IgG1
	AMG-228	Human IgG1
	MK-4166	Human IgG1
	GWN-323	Human IgG1
	MK-1248	Human IgG4
	BMS-986156	Human IgG1
	INCAGN01876	Human IgG1
CD27	Varlilumab	Human IgG1

1.10.6 Therapeutic targeting of CD27

As described in section 1.6.1, CD27 is important for promoting T-cell priming, memory formation, survival and secondary stimulation of the memory T-cell pool. Importantly, CD27 co-stimulation also provides anti-viral and anti-tumour responses that are mediated by T-cell activity. A previous study from our lab has shown that while stimulation of CD40 with an agonistic mAb could clear established murine BCL1 lymphoma tumours, this activity was dependent on CD70 (95). In addition, agonistic anti-CD27 mAb was sufficient to generate anti-tumour immunity against BCL1 and A31 murine lymphoma (95) and delayed tumour growth in murine melanoma models with significantly reduced metastatic spread (186). Other groups have shown using a CD70 transgenic mouse model in which CD70 was constitutively expressed on B cells, that CD70 enhances the antigen specific response of T cells and confers protection from a lethal dose of EL4 lymphoma tumour challenge (187). In a separate study, CD70 was constitutively expressed on DCs in CD27-/- mice; adoptive transfer of WT OT-1 $CD8^+$ T cells into these mice and challenge with OVA, contributed to rejection in a murine melanoma model with OVA expression (B16-OVA) and long term survival whereas transferring CD27-/- OT-1 T cells did not generate protective immunity (188). These data clearly show that stimulation of CD27/CD70 pathway can generate strong anti-tumour immunity.

In line with the effects of CD27 agonism on tumour protection in mice, targeting CD27 was found to improve the effector functions of $CD8^+$ T cells infiltrating a tumour site and reduced the expression of the inhibitory receptor PD-1 (186). Additionally, data from our lab show that when agonistic anti-CD27 mAb and anti-PD-L1 are combined, they synergise to restore the functions of quiescent $CD8^+$ T cells and reduce the expression of genes related to quiescence and anergy (189). Others have also shown that the combination of CD27 agonism and PD-1 blockade can provide strong anti-tumour immunity in the absence of $CD4^+$ T cell help (190). In our group, stimulation of antigen specific $CD8^+$ T cells in vivo with antibodies targeting different members of the TNFRSF including CD27, OX40, GITR and 4-1BB, showed that agonistic anti-CD27 contributed to significantly higher expansion compared to stimulation through other members (84). In the same study, anti-CD27 combined with PD-1 blockade significantly improved anti-tumour immunity. The combination therapy showed synergy for the enhanced expansion and effector activity of $CD8^+$ T cells (84). In another study in which a direct targeting antibody (anti-CD20) was combined with agonistic antibodies targeting TNFRSF such as OX40, GITR and CD27, the anti-CD20 and anti-CD27 combination showed significantly better activity and synergy

compared to others (191). Agonistic anti-CD27 stimulation could activate T cells and NK cells which released inflammatory cytokines leading to enhanced recruitment and activation of the myeloid cells, which in turn increased tumour clearance initiated by the anti-CD20 mAb (191).

With regards to the influence of agonist anti-CD27 on human T cells, an anti-human CD27 mAb (1F5) as IgG1 isotype was developed and tested in vivo in a human CD27 (hCD27) transgenic mouse model. The antibody could enhance the activation and frequency of antigen specific T cells when mice were immunised with ovalbumin (OVA) protein. Further characterisation using hCD27 mice revealed that 1F5 could induce a strong anti-tumour immune response against several murine tumour models including BCL1, CT26 colon carcinoma and EG-7 thymoma. In addition to induced survival benefit, the surviving mice showed resistance to a secondary tumour re-challenge indicating the establishment of protective long term immunity (43). However, the activity observed with 1F5 was completely dependent on FcγR interaction and eliminating the interaction with FcγRs eliminated the anti-tumour efficacy of 1F5. As 1F5 is of hIgG1 isotype and this isotype can initiate depletion of the target cells, results in another study showed that, in immune-deficient mice (where B and T lymphocytes are absent), 1F5 could initiate depletion of human lymphoma cells (44). As these cells express very high levels of CD27, the outcome was possibly the result of depletion of those cells due to high CD27 expression levels on the cell surface; presumably the lower levels of CD27 expressed on T cells mean that these are not so susceptible to depletion. This concept of TNFRSF expression level influencing the likely outcome of exposure to anti-TNFRSF mAb has also been shown using anti-4-1BB mAbs, in which high expressors are more susceptible to depletion (174).

In addition to effector T cells, CD27 is also expressed on Tregs. In a recent study in which different isotypes of anti-CD27 mAb were compared in vivo, mIgG2a and hIgG1 (but not mIgG1) isotypes were found to induce anti-tumour effects by mainly targeting the depletion of Tregs (157). This is in line with the FcγR engagement of these mAbs (engaging with activatory FcγRs) and also it might be a reflection of the higher level of CD27 expressed on Tregs compared to effector T cell populations. The mIgG2a isotype has high affinity for the activatory FcγRs and induced a stronger depletion of Tregs compared to the hIgG1. Human IgG1 isotype binds to all FcγRs and it could generate agonism as well as Treg depletion whereas the agonistic activity of mIgG2a was minimal. In contrast, mIgG1 induced strong agonistic activity and no Treg depletion. The activities of the antibodies were also found to

be dependent on the tumour model. In a BCL1 model where the tumour localises into the spleen, mIgG1 isotype induced strong anti-tumour immunity and hIgG1 induced moderate response with mIgG2a being inactive (157). In several other solid tumour models however, the mIgG2a showed the strongest activity, mainly by depleting the Tregs, with hIgG1 showing moderate activity again whereas the activity of mIgG1 was minimal (157).

Following on from these pre-clinical results, an anti-human CD27 mAb has been taken forward for testing in clinical trials. The hIgG1 mAb (CDX1127, also known as Varlilumab, Table 1.1) is tolerated up to 10 mg/kg dose and shows biological and clinical activity against melanoma, RCC, solid and hematologic malignancies contributing to tumour shrinkage (192, 193). Stimulation with Varlilumab induced secretion of chemokines, increase in activated T-cell numbers and also stimulated depletion of Tregs. This observation was in line with the pre-clinical activity of anti-CD27 mAb with hIgG1 isotype which showed both activation of effector T cells and depletion of Tregs. A Phase I/II clinical trial to assess the safety of anti-CD27 and PD-1 blockade as a combination therapy (run by Celldex Therapeutics and Bristol-Myers Squibb; clinical trial NCT02335918) in colorectal cancer (CRC) and ovarian cancer (OVAC) has proved the combination to be safe with no additive toxicities and could generate SD (17% in CRC and 39% in OVAC) or PR (5% in CRC and 10% in OVAC) in patients (194). Additionally, combination of anti-CD27 and PD-1 blockade will be tested in a Phase II study in patients with advanced B-cell non-Hodgkin lymphoma (run by National Cancer Institute; clinical trial NCT03038672) (195). Also, a clinical trial to initially test the safety and activity of combining anti-CD20 and anti-CD27 antibodies in patients with relapsed or refractory B-cell malignancies has been designed and will be starting in the near future (run by University Hospital Southampton NHS Foundation Trust, University Hospital Plymouth NHS Trust, The Christie NHS Foundation Trust, Oxford University Hospitals NHS Trust, Celldex Therapeutics and Cancer Research UK; clinical trial NCT03307746) (196).

1.11 Mechanism of action of TNFRSF targeting mAbs and TNFSF ligands

In addition to mAbs (197, 198), soluble recombinant ligands (199, 200), aptamers (201), transfection of dendritic/tumour cells (202, 203) and recombinant viruses (204) have been used to target members of the TNFRSF. However the major mechanism to target the TNFRSF is agonistic mAbs.

As described above (section 1.10), agonist anti-TNFRSF mAbs achieve optimal activity via cross-linking provided by interaction with the inhibitory FcγRIIB receptor (167, 170, 205). The agonist anti-human CD27 mAb, 1F5, contributed to generation of strong anti-tumour immunity in mice which was completely reliant on FcγR interaction (43). In a pre-clinical study where mouse models with human CD40 and human FcγR expression (lacking both mouse CD40 and mouse FcγR) were used, the activity of anti-human CD40 mAbs were dependent on FcγR availability. By trying Fc engineering approaches to increase affinity to FcγRIIB but not activatory receptors, it has been shown that the agonistic activity of the mAbs could be improved, highlighting the difficulty in using anti-human mAbs for agonistic activity in patients (170). Additionally, FcγRs can show variation in availability and might be limiting in the tumour microenvironment (206, 207). Polymorphisms in FcγRIIB has been shown to contribute to reduced level of FcγRIIB expressed on B cells and macrophages in mice which were prone to development of autoimmunity (208). Consistent with the pre-clinical observations, data have been reported in systemic lupus erythematosus autoimmune condition where individuals have reduced level of FcγRIIB expression on B cells (209). It has also been shown in vivo that the level of FcγRIIB expression is critical for agonist mAbs. A two-fold decrease in expression can completely eliminate the agonistic activity (210). Overall these confirm that the availability of FcγRIIB can vary between individuals and this can influence on the activity of the agonistic mAb.

To overcome these potential limitations, it may be possible to use the soluble ligand as an agonist in a way that is independent of the requirement for FcγRs. Trimeric cell surface TNFSF ligands bind to multiple receptors in a multi-molecular structure and the activity of soluble trimer ligands can be potentiated via additional ligand cross-linking (211-213). The improved function of soluble TNFSF ligands via cross-linking has been demonstrated for CD27L, OX40L and CD40L (214, 215).

In order to avoid the requirement for additional agents to cross-link trimeric TNFSF ligands, forms of soluble TNFSF ligands were previously developed as oligomers of trimers. TNFSF ligand fusion proteins comprising ligand and either the Fc region of IgG or fragment of lung surfactant protein D, were generated and found to form soluble hexameric and dodecameric structures, respectively (214, 216). The idea that this strategy can generate more robust agonism was illustrated by the finding that these multimeric proteins were significantly more active than the trimeric forms (214). Testing the Fc-fusion proteins in vivo showed that the proteins were active and stimulated the expansion of $CD8^+$ T cells (87, 200). Active Fc-TNFSF proteins were made up of 3 Fc domains at the N-terminus and 2 ligand trimers at the C-terminus with 50 to 80% of products being the active hexameric structure, depending on the ligand (217).

1.12 Background to the project

Previously in our laboratory, a soluble recombinant Fc-CD70 (sCD70) fusion protein was developed with the hinge, CH2 and CH3 domains of human IgG1 Fc being fused to the N-terminus of a single mouse CD70 extracellular domain (200). The active protein was comprising 2 ligand trimers and 3 dimeric Fc regions (see Fig. 3.1) and activated cells in both in vitro and in vivo assays. In conjunction with $OVA_{257-264}$ peptide, sCD70 enhanced cytokine production by T cells, significantly improved the in vivo expansion of adoptively transferred OT-1 T cells and improved the cytotoxic capacity of CTLs (200).

While these data were encouraging, the product was not homogeneous and comprised different sizes of oligomers with short in vivo half-life (217), likely due to the prevention of interaction with the neonatal Fc receptor (FcRn), responsible for recycling of mAbs through interaction with the Fc domains (218), because of steric hindrance in the oligomer structures. The aim of this project is therefore to develop a new generation soluble CD70 fusion protein which can be generated as a homogeneous product and acts independent of FcγRs. To achieve this, three CD70 extracellular domains will be expressed as a single chain, fused with the hinge, CH2 and CH3 domains of mouse IgG1 such that the end product will be a dimer-of-trimer (scmCD70-m1), incorporating a single Fc domain. Dimerisation of the CH3 domains and the hinge region will form the hexameric ligand structure required for receptor activation (200, 214).

1.13 Hypothesis

TNFRSF members interact with ligands in a multimeric structure to fully activate T cells. Agonistic mAb achieve receptor multimerisation by FcγR cross-linking but FcγR availability can be limiting. We hypothesise that recombinant new generation soluble CD70 fusion protein will activate T cells in an FcγR independent manner.

1.14 Project aims

The aim of this project is to develop a recombinant CD70 protein that stimulates anti-tumour T cell immune responses independent of FcγR cross-linking. Specifically I aim to generate a product which 1) is more homogeneous than the original sCD70; the dimer-of-trimer will consist of one intact Fc domain and higher oligomeric structure formation should be minimal. In contrast, the original sCD70 was produced by fusing one Fc domain to one CD70 domain and protein with hexameric ligand domain also possessed three intact Fc domains which potentially increased oligomer formation due to interaction and disulphide bond formation between multiple Fc domains. 2) Exhibits a longer half-life; the single Fc domain should be able to sufficiently interact with FcRn for recycling and improved half-life. In the previous generation, multiple Fc domains and oligomeric structure may have hindered FcRn interactions. 3) Exhibits activity independent of FcγR cross-linking due to its hexameric ligand structure.

Specifically;

- The dimer-of-trimer protein will be generated and compared to a trimeric CD70 ligand in vitro, looking at T-cell responses.

- The dimer-of-trimer protein will be directly compared to an agonistic anti-CD27 mAb in detailed in vitro and in vivo assays investigating effects on T-cell responses and pre-clinical tumour models. By producing different forms of the ligand, studies will be conducted to examine FcγR requirement of the dimer-of-trimer ligands and anti-CD27 mAb in in vivo T-cell responses.

- As CD27 is expressed as a dimer on cell surface and is therefore partially oligomerised, mutant forms of CD27 to eliminate disulphide linked dimerisation will

be generated to investigate the importance of this post-translational modification on CD27 signal transduction.

1.14.1 Chapter Summaries

In chapter 3, the dimer-of-trimer scmCD70-m1 was generated and characterised for its structure, binding to CD27 and inducing in vitro T-cell proliferation. The protein was compared to trimeric CD70 and agonistic anti-CD27 mAb in in vitro T-cell proliferation assays.

In chapter 4, the dimer-of-trimer scmCD70-m1 was compared to the agonistic anti-CD27 mAb in in vivo adoptive T-cell transfer and murine BCL1 model. A version of scmCD70-m1 lacking FcγR engagement was also generated and compared to the protein capable of receiving FcγR cross-linking and agonistic anti-CD27 mAb. The in vivo serum stability of the ligand forms and mAb were investigated and assays to increase the in vivo stability of ligand forms were developed.

In chapter 5, a mutant version of CD27 lacking disulphide linked dimerisation was generated and compared to the WT CD27 to investigate effects on cell surface expression and signal transduction through CD27.

Chapter 2 Materials and Methods

2.1 Cloning

2.1.1 Cloning scmCD70-m1 into pEE14 expression vector

The new generation scmCD70-m1 insert was designed (by Prof Aymen Al-Shamkhani) and ordered from GeneArt to be supplied in pcDNA3.1 (+). The plasmid comprised of a HindIII restriction site upstream of a Kozak sequence, start codon and sequence encoding scmCD70-m1 followed by an EcoRI restriction site. Plasmid was dissolved at 250ng/µl concentration in TE buffer (Qiagen, Hilden, Germany), 12.5 ng was transformed into a vial of OneShot TOP10 cells (Invitrogen, California, United States) and large scale plasmid DNA was isolated by using commercial kits with a yield of 791.2 ng/µl. The insert was then cloned into the pEE14 (Lonza, Basel, Switzerland) expression vector as follows.

For restriction digestion, 7.6 µl of pcDNA3.1 (+) at 791.2 ng/µl concentration was incubated with 2 µl of HindIII and 2 µl of EcoRI (both Promega, Wisconsin, United States, concentrations 10 U/µl and 12 U/µl respectively) in the presence of 5 µl Buffer E (10X stock, Promega) in a final volume of 50 µl made up with autoclaved distilled H_2O (dH_2O). Digestion was allowed to proceed for 2 hrs at 37 °C. Digestion products were then run on a 1% (w/v) agarose gel and the insert of interest was extracted and cleaned by using Qiagen kit according to manufacturers' instructions.

In parallel, the pEE14 vector was digested by sequential digestion with EcoRI and HindIII. First EcoRI digestion was performed with 7 µl of DNA at 595 ng/µl concentration, 1.2 µl of EcoRI and 3 µl of Buffer H (Promega) made up to 30 µl. Reaction was allowed to proceed for 2.5 hr at 37 °C. After digestion, DNA was isolated and cleaned by using the gel extraction kit. DNA was eluted in 30 µl and the whole amount was incubated with 1.5 µl of HindIII and 5 µl of Buffer E made up to 50 µl with clean water. Digestion was allowed for 2 hr at 37 °C. Digestion products were then run on a 0.7% agarose gel and the vector of interest was extracted and cleaned by using QIAquick gel extraction kit (Qiagen) according to manufacturers' instructions.

To incorporate scmCD70-m1 into cut pEE14, a 15 µl ligation reaction based on molar ratio was set up based on the following equation; (kb of insert (2.3) / kb of vector (9.4)) x amount of vector (20 ng) = amount of insert (4.89 ng for a 1:1 molar ratio). A 3:1 insert to vector ratio was used comprising vector, insert, 3 units of T4 DNA ligase (Promega), T4 DNA ligase buffer (Promega, 1 µl of a 10X stock) to a final volume of 15 µl in autoclaved dH_2O. The reaction was carried out for 3 hrs at room temperature (RT) and 2 µl of ligation reaction transformed into OneShot TOP10 bacterial cells. In brief, 2 µl of the reaction was incubated with one vial of TOP10 bacteria on ice for 30 mins, then 45 seconds in water bath at 42 °C followed by 2 mins on ice. Cells were then supplemented with 250 µl of super optimal broth with catabolite repression (SOC) (nutrient rich growth medium for bacteria, Invitrogen, California, USA) and incubated at 37 °C for 1 hr in a shaking incubator. Bacteria (10 µl of bacterial culture + 90 µl of SOC medium) were then streaked onto pre-prepared LB-agar plates supplemented with 100 µg/ml ampicillin (amp, Melford Laboratories, Ipswich, UK) and bacteria allowed to grow overnight (~ 17 hrs) at 37 °C. Six single colonies were then selected and grown in 5 ml LB supplemented with 100 µg/ml amp overnight (~ 17 hrs) at 37 °C. DNA was then isolated from individual colonies using the QiaPrep Spin MiniPrep Kit (Qiagen) according to manufacturers' instructions. To confirm the presence of the insert and vector of interest, extracted DNA was digested with EcoRI and HindIII. For this, 400 ng of product was incubated with 0.2 µl of each enzyme for 1.5 hr at 37 °C. Incorporation of the insert into the pEE14 vector was visualised by running the digestion products on a 1% agarose gel.

2.1.2 Cloning Ver II insert into pcDNA3.1 (+) expression vector

The DNA sequence with the cysteine (Cys) to alanine (Ala) mutations in the hinge region of the Fc domain was ordered from GeneArt to be flanked with XbaI and EcoRI restriction sites and supplied in a commercial plasmid. The insert was supplied in PMA-T plasmid DNA and was first dissolved in TE buffer at 250ng/µl and transformed into OneShot TOP10 cells to produce large scale DNA as described in detail above. For restriction digestion, 3 µg of plasmid DNA was digested with XbaI (Promega) and EcoRI with 15 units of each enzyme in a 50 µl reaction containing buffer E and autoclaved dH_2O. Digestion was carried out for 2 hrs at 37 °C and the products were run on a 1% agarose gel. The insert was extracted from the gel and cleaned by using Qiagen kit according to manufacturers' instructions.

Simultaneously, the pEE14 vector containing the scmCD70-m1 insert was digested with XbaI and EcoRI restriction enzymes. For digestion, 3 µg of plasmid DNA was digested for 2 hrs at 37 °C with 15 units of each enzyme in a 50 µl reaction containing 5 µl buffer E and autoclaved dH_2O. The products were also run on a 1% agarose gel and the cut vector was extracted from the gel as described above. The Ver II insert was then ligated into the pEE14 vector in a 15 µl ligation reaction. The calculations were based on the equation described in section 2.1.1 and 3.9 ng of insert and 20 ng of vector was used to set up 3:1 insert to vector Molar ratio. The ligation was allowed to proceed for 3 hrs at RT in presence of 3 units of T4 DNA ligase and 1X T4 DNA ligase buffer. The ligation products were transformed into OneShot TOP10 cells as described above and six single colonies were then grown in 5 ml LB (supplemented with amp) for 17 hrs to extract the plasmid DNA by using Qiagen mini-prep kit. The extracted plasmid DNA from each colony was analysed by digesting 400 ng with 2 units of XbaI and 2 units of EcoRI for 2 hrs at 37 °C. 200 ng of digested sample was then visualised on a 1% agarose gel to confirm the ligation.

In order to clone the scmCD70-m1 Ver II insert into pcDNA3.1 (+) vector, 3 µg of pEE14-scmCD70-m1 Ver II plasmid was digested with HindIII and EcoRI restriction enzymes with 15 units of each enzyme for 2 hrs at 37 °C in a 50 µl reaction in presence of 5 µl buffer E and autoclaved dH_2O. The products of digestion were run on a 1% agarose gel and the scmCD70-m1 Ver II insert was extracted from the gel. In parallel, 4 µg of pcDNA3.1 (+) scmCD70-m1 Ver I plasmid DNA was digested with 15 units of EcoRI in a 30 µl reaction containing 3 µl buffer H (10X stock, Promega) and autoclaved dH_2O. The digestion was carried out for 2 hrs at 37 °C and the digested plasmid DNA was isolated from the enzymes by using Qiagen gel extraction kit. The isolated DNA (~3.2 µg) was then digested with 15 units of HindIII in a 50 µl reaction in presence of 5 µl buffer E for 2 hrs at 37 °C. The products were run on a 1% agarose gel and the digested vector was extracted and cleaned by using the Qiagen kit.

The scmCD70-m1 Ver II insert was then ligated into pcDNA3.1 (+) vector in a 15 µl reaction. The reaction was set up as 3:1 insert to vector Molar ratio, using 25.56 ng of insert and 20 ng of vector, calculated by using the equation described in section 2.1.1. The ligation was carried out for 3 hrs at RT in presence of T4 DNA ligase and T4 DNA ligase buffer. The ligated products were then transformed into OneShot TOP10 cells as described above and four single colonies were grown in 5 ml LB (supplemented with amp) cultures for ~17 hrs to extract the DNA by using Qiagen mini-prep kit. The extracted plasmid DNA from each

colony was analysed by digesting 400 ng with 2 units of XbaI and 2 units of EcoRI for 2 hrs at 37 °C. 200 ng of digested sample was then visualised on a 1% agarose gel to confirm the ligation.

2.1.3 Cloning the Fc domain with D265A mutation into scmCD70-m1 Ver I

The Fc domain with the D265A mutation was commercially ordered from GeneArt and was supplied in PMA-T plasmid DNA. The pEE14 vector with the scmCD70-m1 Ver I was previously digested to remove the Fc domain with XbaI and EcoRI digestion (described in section 2.1.2). In order to clone into the pEE14 vector, PMA-T with D265A insert was digested with XbaI and EcoRI restriction enzymes. 3 µg of plasmid DNA was digested with 15 units of each enzyme at 37 °C for 2hrs in presence of buffer E and autoclaved dH_2O. The products were run on a 1% agarose gel and the insert was extracted and cleaned using Qiagen gel extraction kit. Then the insert was ligated into the cut pEE14 – scmCD70-m1 vector in a ligation reaction with 3:1 insert to vector Molar ratio. For this, 3.9 ng of insert and 20 ng of vector were incubated in a 15 µl reaction in the presence of T4 DNA ligase and the T4 DNA ligase buffer. The reaction was allowed to proceed for 3 hrs at RT before being transformed into OneShot TOP10 cells as described above. From the single colonies, six were grown in 5 ml LB (supplemented with amp) for ~17 hrs and plasmid DNA isolated using Qiagen mini-prep kit. The extracted plasmid DNA from each colony was analysed by digesting 400 ng with 2 units of XbaI and 2 units of EcoRI for 2 hrs at 37 °C. 200 ng of digested sample was then visualised on a 1% agarose gel to confirm the ligation.

2.1.4 Agarose gel

Agarose gels were prepared by dissolving agarose powder (Invitrogen) in 1X TBE buffer (90 mM Tris, 90 mM Boric acid, 2mM EDTA) with 50 ng/ml concentration of ethidium bromide (EtBr) (Sigma, Missouri, USA). The plasmid DNA samples were prepared with 1X orange loading dye (stock supplied at 6X; Thermo Fisher) and run next to a 1 kb DNA ladder (Thermo Fisher O'GeneRuler) in the running buffer 1X TBE containing 50 ng/ml concentration of EtBr for 1 hr at 80 mA. The bands in the gels were visualised using GelDoc XR imager (Bio-Rad, California, USA) using Quantity One software (Bio-Rad).

2.2 Large scale plasmid DNA production

To generate larger amounts of plasmid DNA, bacterial OneShot TOP10 cells were transformed (via heat shock) with the plasmid DNA as described in section 2.1.1 and plated on LB/agar plates with 100 µg/ml amp. A single colony was chosen after ~17 hrs incubation and cultured in 5 ml LB supplemented with amp for 6-7 hr before 1 ml of the pre-culture was transferred into a bigger culture (250 ml LB supplemented with 1 µg/ml amp) and grown for ~17 hrs prior to extraction of plasmid DNA using Hi-Speed plasmid maxi kit (Qiagen) according to the manufacturers' guidelines. Final DNA concentration was measured via spectrophotometry (NanoDrop 1000) to determine absorbance at 260 nm. Quality of the DNA was confirmed by 260/280 ratio where 1.8-2.0 was accepted as high purity yield.

2.3 Cell Culture

Suspension 293F cells (human embryonic kidney origin) (Thermo Fisher) were cultured in Freestyle 293 expression medium (Gibco, Massachusetts, USA) with no additional supplements. Cells were split every 3-4 days and maintained in a shaking incubator at 37 °C and 8% CO_2. Adherent 293T cells (human embryonic kidney origin) (obtained by Prof Aymen Al-Shamkhani from Department of Biochemistry, University of Oxford) were grown in Dulbecco's Modified Eagle's Medium (Gibco) supplemented with 10% (v/v) fetal calf serum (FCS) (Sigma), 2 mM glutamine (Gibco),1 mM pyruvate (Gibco), 100 µg/ml streptomycin (Gibco) and 100 units/ml penicillin (Gibco) split every 3-4 days by addition of trypsin-EDTA (Sigma) to detach the cells from the flask. Cells were maintained at 37 °C and 5% CO_2. Adherent CHO-K1 cells (Chinese hamster ovary cells) (ATCC) were grown in Glasgow's Modified Eagle's Medium (GMEM) (Firstlink, UK) supplemented with additional 2 mM glutamine and 1 mM pyruvate. Cells were split by scraping and maintained at 37 °C and 5% CO_2. CHO-K1S suspension cells (adapted from adherent CHO-K1) were grown in FortiCHO (Gibco) growth medium supplemented with 2 mM glutamine and 10ml/L HT supplement (50X stock, Gibco). Cells were split every 3-4 days and maintained in a shaking incubator at 37 °C and 8% CO_2. Jurkat-NF-κB-GFP cells (Systems Biosciences, California, USA) were grown in suspension in RPMI 1640 medium (Gibco) supplemented with 10% FCS, 2 mM glutamine, 1 mM pyruvate and 1 mg/ml geneticin (Gibco). Cells were split every 3-4 days and maintained at 37 °C and 5% CO_2. Cell concentration was determined by using a coulter counter (Beckman Coulter, California, USA).

2.4 Transfection of mammalian cells

2.4.1 Transient transfection of 293F cells for protein expression

For transient transfection, 293F cells were kept at low density and split to 0.6-0.8 x 10^6/ml on the day before transfection. For transfection, 6 x 10^8 293F cells were collected by centrifugation at 491 x g for 5 mins and re-suspended in 200 ml fresh medium at 3 x 10^6/ml. 800 µg of DNA was diluted to 0.5 µg/µl with medium and added to the cells in Erlenmeyer flasks (Corning, New York, USA) compatible with shaking incubators. Flasks were then incubated for 5 mins in a shaking incubator and 2.4 mg of Polyethylenimine (25 kDa linear, Polysciences, Germany) at 0.5 µg/µl concentration (diluted in fresh medium) was added. Cells were incubated overnight and 200 ml fresh medium and valproic acid sodium salt (Sigma; final concentration of 2.2 mM) were added to cells the following day. Cells were incubated for 7 days and supernatant harvested on day 7 by centrifugation at 3488 x g for 20 mins.

2.4.2 Stable transfection of CHO-K1S cells

CHO-K1S cells were grown until sufficient confluency (~ 1.5 x 10^6/ml) on the day of transfection. DNA and GenePorter transfection reagent (Genlantis, San Diego, USA) were diluted in OPTIMEM medium (Invitrogen) as per manufacturers' instructions and diluted DNA was added to the diluted GenePorter solution. For 6 well plate transfection, 2 µg DNA/well and 16 µl GenePorter/well were used, each being diluted in 500 µl OPTIMEM. The mixture was incubated at RT for 30 mins before being added to the cells. During the incubation, cells were harvested and 2 x 10^6 cells were plated per well in fresh medium. The DNA – GenePorter solution was added to the cells and mixed by gentle pipetting. Cells were incubated at 37 °C for 5 hrs and supplemented with 1ml fresh complete medium. After 72 hrs, cells were harvested, re-suspended in selection medium (GMEM supplemented with 10% dialysed FCS, 50 µM Methionine Sulfoximine (MSX) (Sigma) and 1X glutamine synthetase supplement (Sigma)) and plated into 96 well plates by two fold dilutions across the plates, starting with different cell densities. Cells were grown for 2-3 weeks and clones were tested for protein secretion by ELISA (detailed below).

2.4.3 Transient transfection of 293T cells

Three days prior to transfection, 1x 10^5 cells were plated per well of a 6-well plate. The cells were supplemented with 4 ml fresh complete growth medium and incubated at 37 °C. On day 3, cells were transfected with plasmid DNA and FuGene HD transfection reagent (Promega) using a 3:1, FuGene to DNA ratio. 15 µl of FuGene reagent and 5 µg of plasmid DNA were used per well. The FuGene reagent is stored at 4 °C and it was allowed to come to RT before being used. A master mix of medium, plasmid DNA and FuGene reagent was prepared to have a final volume of 150 µl to be added per well. The mixture was incubated for 15 mins at RT and in the meantime, media was removed from the cells and they were washed with 1.5 ml of phosphate buffered saline (PBS)/well. The cells were supplemented with 3 ml antibiotic free growth medium and the FuGene-DNA mix was added as 150 µl per well. Cells were incubated at 37 °C for 72 hrs before assessing expression of the transfected receptor. After 72 hrs, the medium was removed, cells were washed with PBS and 1.5 ml of 1 mM EDTA-PBS solution was added per well to detach the cells by putting the plates on a rotator for approximately 15 mins. Once the cells were detached, they were harvested, counted by coulter counter and expression of the receptor was assessed by flow cytometry or western blot using the required number of cells.

2.4.4 Stable transfection of Jurkat-NF-κB-GFP cells

To generate stable clones expressing CD27, cells were transfected in 24-well plates. 4 x 10^5 cells were plated in antibiotic free growth medium in 500 µl per well and 6 wells were used for each plasmid DNA with 1 µg of DNA and 2 µl of lipofectamine 2000 (Invitrogen) used per well. For 6 wells, 6 µg of DNA was diluted in 300 µl OPTIMEM medium. Simultaneously, 12 µl of lipofectamine was diluted in 300 µl OPTIMEM medium and solutions were incubated at RT for 5 min. Then the DNA solution was added to the lipofectamine solution and incubated for 20 min at RT. The DNA-lipofectamine mixture was then added to the cells, 100 µl/well, and cells were incubated at 37 °C for 72 hrs. After the incubation, cells from 6 wells were pooled and then split again into 6 wells. Two wells were transferred into 2 wells of a 6-well plate and supplemented with 3 ml selection medium (RPMI supplemented with 10% FCS, 2 mM glutamine, 1 mM pyruvate and 1 mg/ml geneticin) while each of the other 4 wells were diluted in 10 ml selection medium and 100 µl/well was distributed to have 5000 to 10000 cells per well in 96-well plates (flat bottom) depending on the cell counts. The wells were supplemented with an extra 100 µl fresh medium to give a 200 µl final volume and cells were incubated for 2-3 weeks until single

colonies were grown. Once single clones were detected, the cells were re-suspended and 40 µl was taken to stain with anti-CD27 mAb to detect the expression of CD27 (detailed below).

2.5 Enzyme linked immunosorbent assay (ELISA)

2.5.1 Detection of scmCD70-m1 or scmCD70-mm1 in stable CHO-K1S clone supernatants.

For the detection of scmCD70-m1 from cell culture supernatants, 96 well plates (maxisorp – nunc-immuno plates, Thermo Fisher) were coated overnight at 4 °C with goat anti-mouse IgG antibody (Sigma – M0284) at 5 µg/ml in ELISA coating buffer (15 mM Na_2CO_3 and 35 mM $NaHCO_3$, pH 9.6). Plates were washed four times with ELISA wash buffer (PBS/0.05% (v/v) Tween 20) and blocked with 1% (w/v) Bovine Serum Albumin (BSA)/PBS solution for 1 hr at RT. Plates were then washed a further four times (200 µl/well) before adding experimental samples or standards (recombinant mouse TIGIT-Fc (R & D Systems) in 50 µl, which were then incubated at RT for 1.5 hrs. Standards and experimental samples were diluted in CHO-K1S growth medium. Then plates were washed a further four times and goat anti-mouse-Fc HRP antibody (Sigma – A0168) was diluted 1 in 5000 in 1% BSA/PBS solution and 100 µl was added per well. After 1.5 hrs incubation, plates were washed four times and 50 µl/well substrate was added. Substrate comprised of 1 o-Phenylenediamine dihydrochloride tablet (Sigma) dissolved in 25 ml citrate buffer (100 mM stock) to which was added 25 ml phosphate buffer (200 mM stock), 50 ml dH_2O and 20 µl hydrogen peroxide (Merck, Germany). Plates were incubated in the dark until sufficient colour development was observed. The reaction was stopped using 50 µl/well 2.5 M H_2SO_4 and the colour change was quantified by measuring absorbance at 490 nm using a plate reader (Epoch - BioTek, Vermont, USA).

2.5.2 Detection of scmCD70-m1, scmCD70-mm1 or anti-CD27 in mouse serum

The same protocol described for detection of scmCD70-m1 in supernatants was used for detection of scmCD70-m1, scmCD70-mm1 and anti-CD27 (AT124-1, mIgG1) in mouse serum but with different coating and detection antibodies as listed in Table 2.1. Blood samples were allowed to clot and centrifuged at 15700 x g at 4 °C for 30 mins. Serum samples were collected and stored at -20 °C until being used. Samples and standards

(purified versions of the proteins to be detected) were prepared in 1%BSA/PBS and added to the plates in 50 µl which were pre-coated in the appropriate proteins (Table 2.1) overnight at 4 °C. The samples were incubated in the plate for 1.5 hrs at RT and the plates were washed four times with ELISA wash buffer (PBS/0.05% Tween 20). Then the detection antibodies (Table 2.1) were added in 100 µl 1%BSA/PBS and incubated for 1.5 hr at RT. The plates were again washed four times and incubated with the substrate prepared as described above. The signal was detected as explained in section 2.5.1.

Table 2.1. Reagents used for detection of scmCD70-m1, scmCD70-mm1 and AT124-1 by ELISA.

Coating	To be detected	Detecting Antibody
TAN 1-7 (anti-CD70 mAb, in-house) at 5 µg/ml	scmCD70-m1 or scmCD70-mm1	Rat anti-mouse HRP (Jackson Immunoresearch, 415-035-166) at 1/5000 dilution
Recombinant mouse CD27-hFc (R&D Systems) at 0.5 µg/ml	AT124-1 mIgG1	Goat anti-mouse HRP (Sigma A0168) at 1/5000 dilution

2.6 Protein purification

2.6.1 Protein A purification of scmCD70-m1 or scmCD70-mm1

For the purification of scmCD70-m1, supernatants from scmCD70-m1 secreting cells were harvested by centrifuging at 3488 x g at 20 mins at 4 °C and concentrated using Vivaflow 200 concentration system (Sartorius, Göttingen, Germany). Supernatants were then filtered through either 0.2 µM (TPP vacuum filtration) or 0.45 µM (Millipore vacuum filtration) filters and supplemented with 1/5 volume of 5X TRIS/NaCl buffer (200 mM TRIS, 1M NaCl, 10 mM EDTA). Supernatants were then passed over pre-prepared protein A columns (in house or MabSelect SuRe, GE Healthcare, Illinois, USA) at a flow rate of 4 ml/min, prior to washing the column with 1X TRIS/NaCl buffer. Protein was then eluted using Glycine-HCl pH 3.0 (100 mM Glycine, 1 mM EDTA) buffer which was rapidly neutralized by addition of 5X TRIS/NaCl buffer. Elution products were concentrated and dialysed against endotoxin low PBS (dialysis cassettes; Thermo Fisher Slide-A-lyzer) or further purified via size exclusion chromatography (Fig. 2.1). The same protocol was followed for the purification of scmCD70-mm1.

2.6.2 Size Exclusion Chromatography (SEC) for fractionation of scmCD70-m1 or scmCD70-mm1

Protein A purified samples of scmCD70-m1 or scmCD70-mm1 were concentrated and approximately 7.5 ml of sample was injected for fractionation through a Superdex 200 26/950 column (in-house) using a flow rate of 3 ml/min (Fig. 2.1). Selected fractions were pooled together and concentrated to approximately 2 mg/ml concentration before dialysis against endotoxin low PBS. Samples were filter sterilised (0.2 µM filter, GE Healthcare) and stored at -20 °C as aliquots. For analytical SEC, 10 µg of protein was run on a Superdex 200 5/150 GL (GE Healthcare) column with 0.3 ml/min flow rate.

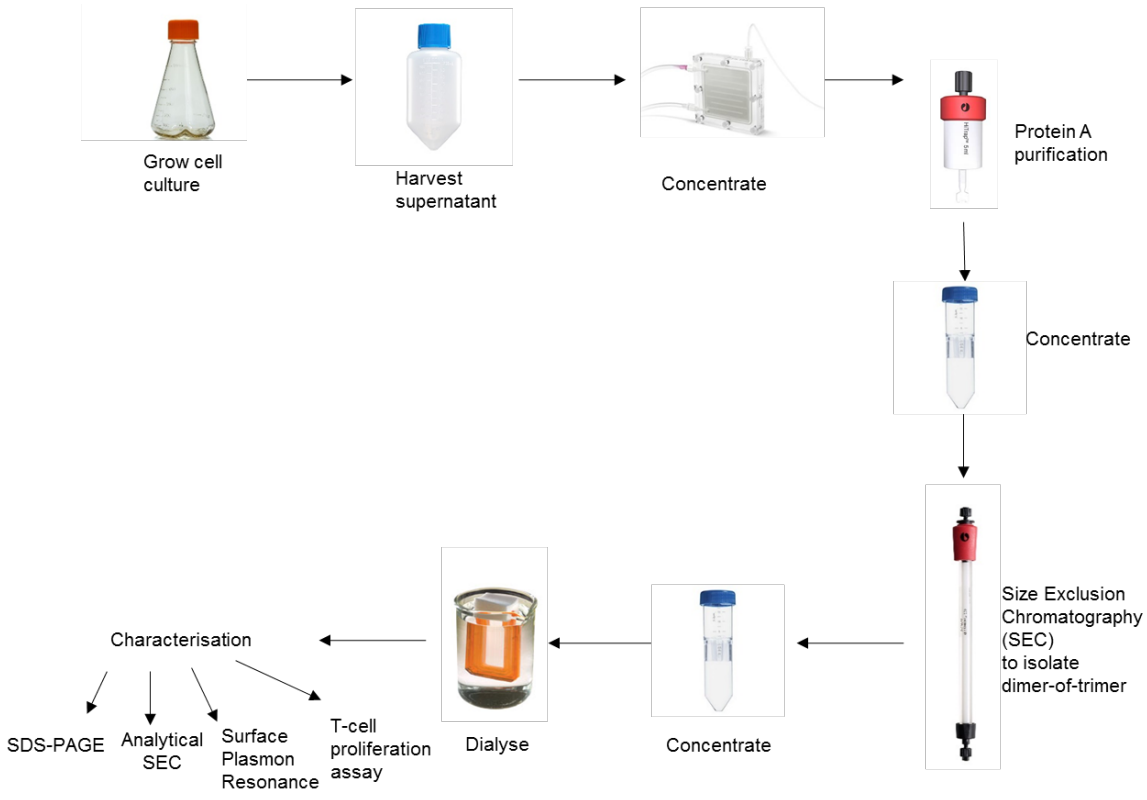

Figure 2.1. Process of expression, purification and characterisation of scmCD70-m1. Once CHO-K1S clones were generated, a single clone was expanded for the appropriate time period in a shaking incubator. Then supernatant was harvested, concentrated down to a small volume (~150 ml) and scmCD70-m1 protein was purified using protein A chromatography. The purified samples were concentrated and fractionated by using SEC to isolate dimer-of-trimer fraction. The dimer-of-trimer fractions from multiple SEC runs were combined and concentrated down to ~2mg/ml and dialysed into PBS before further characterisation which included SDS-PAGE and analytical SEC to confirm purity, surface plasmon resonance to confirm binding to CD27 and in vivo T-cell proliferation assay to confirm activity.

2.6.3 YTA 3.1.2 column for purification of mCD4-CD70 trimer

To purify the mCD4-CD70 trimer (produced in 293F cells), 16 mgs of YTA 3.1.2 (anti-mCD4 mAb, in-house) in PBS was dialysed against 0.2 M citrate pH 6.5 and coupled with 1 gr of cyanogen bromide (CnBr) activated sepharose 4B beads (GE Healthcare). To activate the beads, 1 gr of beads were added to 200 ml 10 mM HCl for 20 mins at RT, poured into a sintered glass filter and washed with 500 ml of 10 mM HCl and 500 ml of 0.2 M citrate. Beads were collected and mixed with the antibody solution (YTA 3.1.2) and left on a rotator for 4 hrs at RT. The solution then passed through the sintered glass filter and beads were collected to be mixed with 15 ml of 1M ethanolamine pH 9.5 for 1 hr on a rotator at RT. The solution was then passed on to a sintered glass filter and beads washed with 100 mM Tris, glycine pH 3.0 and 100 mM Tris solution again (250 ml each). Beads were then collected into a tube and stored in 100 mM Tris solution at 4 °C. To set up a column, a 20 ml syringe tube was used. First, glass wool was inserted, followed by a filter paper, then the coupled bead solution and filter paper again. After attaching the tubing, the column was washed with 100 mM Tris, 30 mM Tris, glycine pH 3.0 and 30 mM Tris solution again before use.

The supernatant from cells secreting mCD4-CD70 was applied to the column at 0.5 ml/min flow rate. After running the supernatant through the column, the column was washed with 10X column volume (CV) low salt solution (150 mM NaCl, 30 mM Tris, 1.5 mM EDTA), 10X CV high salt solution (500 mM NaCl, 100 mM Tris, 5 mM EDTA) and 10X CV low salt solution again. The bound protein was then eluted by running a glycine solution pH 3.0 through the column. Once the acid solution started coming off the column (detected by pH indicator paper), 40 x 1 ml fractions were collected and neutralised by addition of 100 µl 2M Tris pH 8.0. The absorbance at 280 nm of each fraction was measured via a NanoDrop spectrophotometer to identify fractions containing protein; these were then pooled and concentrated. Samples were concentrated using a 10 kDa membrane concentrator tube (Sartorius) and centrifuging at 1962 xg at 4 °C.

2.7 Sodium dodecyl sulphate polyacrylamide gel electrophoresis (SDS-PAGE)

To visualise protein products and ensure proteins were of the expected size, 10 µg of protein was loaded/lane into Nu-PAGE or Bolt Bis-Tris gels (Thermo Fisher). Samples were run under reducing and non-reducing conditions with dithiothreitol (DTT, Thermo Fisher) at a final concentration of 50 - 62.5 mM used as the reducing agent. Reaction mixtures diluted

in 4X laemmli buffer (62.5 mM Tris pH 6.8, 2% SDS, 10% glycerol, 0.04% bromophenol blue) were prepared, boiled at 95 °C for 5 min, cooled and loaded into the gels. Gels were run in 3-(N-morpholino) propane sulfonic (MOPS) buffer at 100 - 150 V for 1 – 1.5 hr using Novex sharp pre-stained protein standard (Thermo Fisher) as a size marker. Gels were then fixed for 15 mins in gel fixative solution (25% isopropanol, 10% acetic acid in dH_2O), stained with Coomassie brilliant blue solution (10% acetic acid, 0.006% Coomassie brilliant blue (Sigma) in dH_2O) for 30 mins and destained with 10% acetic acid in dH_2O before imaging using a GelDoc XR imager and Quantity One software.

2.8 Western Blot

293T cells were transiently transfected with the appropriate plasmid DNA (see section 2.4.3). After 72 hrs, cells were harvested by removing the supernatant, washing with PBS and detaching the cells with 1mM EDTA-PBS solution (as described in section 2.4.3). The cells were then centrifuged at 1520 xg for 5 mins to discard the supernatant containing EDTA. Another PBS wash was performed and supernatant was discarded before re-suspending cells in 1X RIPA (50 mM Tris pH 8.0, 150 mM NaCl, 1% NP-40, 0.5% sodium deoxycholate, 0.1% SDS) buffer (supplemented with 1X protease inhibitors (Roche, Basel, Switzerland) and 1X phosphatase inhibitors (Roche)) at a ratio of 1×10^6 cells in 10 µl buffer. The cells were incubated on ice for 30 mins and mixed by vortexing every 10 mins. Cell lysates were then centrifuged at 15700 xg for 5 min at 4 °C and supernatants collected and stored at -20 °C. In order to perform the western blot, samples were prepared under reduced (appropriate volume of lysate, 50 mM final DTT concentration, 7.5 µl 4X laemmli buffer and PBS to a final volume of 30 µl) and non-reduced conditions (as reduced but without DTT), boiled at 95 °C for 5 mins and loaded onto a 10% Nu-PAGE Bis-Tris gel. The gel was run at 100-120 V for 1.5 hrs in MOPS running buffer. The gel was then removed from the cassette and transferred into transfer buffer (1X Nu-PAGE transfer buffer (20X stock, Thermo Fisher) with 10% final methanol concentration in dH_2O) and left on rotor for 20 min. In parallel, a transfer membrane (immobilon-P, Merck) was activated in pure ethanol for 15 sec, washed with dH_2O for 10 mins and transferred into transfer buffer for another 10 mins on a rotor at RT. The transfer apparatus was then assembled appropriately to enable proteins to be transferred from the gel to the activated membrane. Membrane and gel were incubated together in transfer buffer by running at 100 V for 1 hr in a cooled environment. The membrane was removed and washed with 20 ml wash buffer (10 mM TRIS, 150 mM NaCl, 0.1% Tween20, pH 7.6-8.0) for 5 mins before being blocked with wash buffer containing 5% milk for 1 hr at RT. After blocking, the membrane was washed again for 5

mins with wash buffer and primary antibody solution (AT124-1 rIgG2a, in-house) was added in wash buffer/5% milk at 5 µg/ml and allowed to incubate overnight (~ 17 hrs) at 4 °C, prior to being washed 3 times for 10 mins with 20 ml wash buffer each. The membrane was then incubated with anti-rat secondary antibody (GE Healthcare NA935V, 1/5000 dilution) in wash buffer/5% milk for 1 hr at RT. Finally the membrane was washed 3 times and incubated with ECL substrate (Thermo Fisher) according to manufacturer's instructions for 5 min in the dark before being transferred into a cassette to be overlaid with a film (Amersham hyperfilm ECL, GE Healthcare). The film was developed using a Compact X4 (Xograph, Stonehouse, UK) film processor according to manufacturers' instructions.

2.9 Surface Plasmon Resonance (SPR)

2.9.1 Determining binding of scmCD70-m1 to CD27

To confirm binding between scmCD70-m1 and recombinant mouse CD27, SPR analysis was performed (using Biacore T100; GE Healthcare). First an anti-human Fc chip was prepared by amine coupling of anti-human IgG into a CM5 sensor chip (GE healthcare) following manufacturers' instructions. scmCD70-m1 solutions were prepared at 10 µg/ml and first passed through the flow cell to confirm minimal background binding to the anti-human Fc bound chip. Recombinant mCD27-hFc (R&D systems, Minnesota, USA) was then passed through the anti-human Fc chip for binding, which was followed by the injection of the scmCD70-m1 for binding to the rmCD27-hFc (Fig. 2.2.A). All samples were prepared in HBS-EP+ running buffer (GE Healthcare) and every injection was performed for 5mins at 10 µl/min flow rate. The chip was regenerated with 3M $MgCl_2$ for 30 sec at 10 µl/min flow rate. Binding was detected using Biacore Bioevaluation software (Biacore). The same protocol was followed for determining binding of purified mCD4-CD70 to CD27 and also when supernatants from clones were tested.

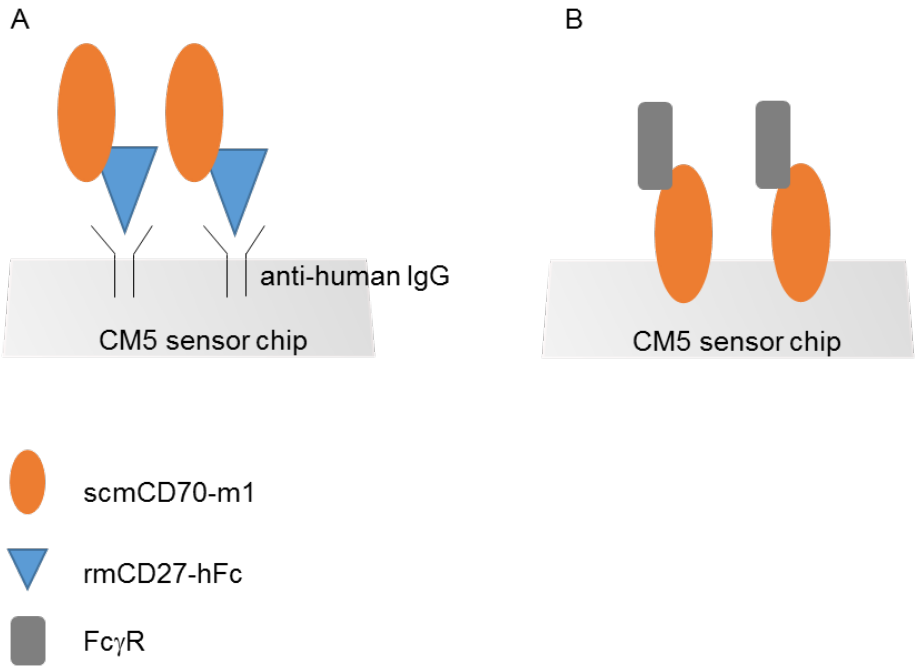

Figure 2.2. Schematic of SPR analysis examining scmCD70-m1 binding to CD27 or FcγR. (A) An anti-human IgG chip was used to capture rmCD27-hFc and then scmCD70-m1 was injected to determine binding to rmCD27-hFc captured on the chip. (B) scmCD70-m1 was directly immobilized onto the CM5 sensor chip and FcγR solutions were injected to determine binding to scmCD70-m1.

2.9.2 Determining binding of proteins to FcγR

To determine binding to FcγRs, scmCD70-m1 and control antibodies were immobilized onto a CM5 sensor chip via amine coupling according to manufacturers' instructions and approximately 2000-3000 response units (RU) was reached. Recombinant mouse FcγRs (R&D Systems) were then injected (Fig. 2.2.B) at appropriate concentrations with 5 mins association, 30 µl/min, and 10 mins dissociation rates. The outcome was detected via the Biacore Bioevaluation software.

2.9.3 Determining binding of proteins to FcRn

To examine the binding of scmCD70-m1 to FcRn and compare to binding of anti-CD27 mAb to FcRn, scmCD70-m1 or anti-CD27 proteins were immobilized onto the flow cells of a CM5 sensor chip via amine coupling according to manufacturers' instructions and approximately 2000 RU was reached. FcRn interacts with target proteins at acidic pH (pH 6.0) (219) and SPR running buffer, HBS-EP+, was therefore prepared at pH 6.0. Different concentrations of recombinant mouse FcRn (R&D systems) were prepared in the pH 6.0 buffer and injected

onto the chip with 3 mins association and 5 mins dissociation time at 30 µl/min flow rate. After every injection, HBS-EP+ buffer at pH 7.4 was used as the regeneration buffer. The outcome was detected via the Biacore Bioevaluation software.

2.10 Glycosylation analysis by ultra-high-performance liquid chromatography (UPLC)

Glycosylation analysis of proteins was performed in collaboration with Prof Max Crispin's laboratory (University of Southampton) where PhD student Joel Allen performed the analysis. To analyse the relative amounts of each oligomannose-type glycan for the total population of N-linked glycans expressed on a given protein, 20 µg of each sample was initially subjected to SDS-PAGE. Then the band corresponding to the protein of interest was excised and washed with 100% acetonitrile (1 ml) followed by a wash in ultra-pure H_2O (1 ml) which was repeated three times. Then the gel sample was incubated with 5 µg of Peptide N-glycosidase F (PNGase F) (New England Biolabs (NEB), Massachusetts, USA) in 100 µl PBS solution for 16 hrs at 37 °C to digest the N-linked glycans expressed on the protein of interest. The released glycans were then labelled with the fluorescent label procainamide (Abcam, Cambridge, UK) in 100 µl labelling solution (110 mg/ml procainamide, 60 mg/ml sodium cyanoborohydride in 30% DMSO, 70% acetic acid) for 4 hrs at 65 °C. The labelled glycans were then purified using Spe-ed Amide cartridges (Applied Separations) and an aliquot was kept to be analysed. Simultaneously, in order to determine the relative abundance of oligomannose-type glycans, an aliquot of fluorescently labelled glycans was subjected to digestion with Endoglycosidase H (Endo H) (NEB) for 16 hrs at 37 °C. The Endo H was then removed using a polyvinylflouridine membrane (Merck) and the resultant glycans were analysed. Glycans were analysed on a Waters Acquity H-Class UPLC instrument with a Glycan BEH Amide column (2.1 mm x 100 mm, 1.7 µM, Waters, Manchester, UK) and the following gradient: time (t) = 0: 22 % A, 78 % B (flow rate = 0.5 ml/min); t = 38.5: 44.1 % A, 55.9 % B (0.5 ml/min); t = 39.5: 100 % A, 0 % B (0.25 ml/min); t = 44.5: 100 % A, 0 % B (0.25 ml/min); t = 46.5: 22 % A, 78 % B (0.5 ml/min), where solvent A was 50 mM ammonium formate (pH 4.4) and B was acetonitrile. Fluorescence was measured at an excitation wavelength of 310 nm and an emission wavelength of 370 nm. Data were processed using Empower 3 software (Waters).

2.10.1 Endo H treatment

2.10.1.1 Non-denaturing

For analytical digestion of proteins with Endo H, 10 µg of protein (in PBS) was diluted in 0.1M NaOAc (sodium acetate) pH 5.2 and enzyme (amount indicated in figures and legends) was added in 20 µl total reaction volume. The reaction was incubated at 37 °C for 1 or 3 hrs. Then samples were topped up with 7.5 µl of 4X laemmli buffer, an appropriate volume of DTT to a final concentration of 50 mM and dH_2O to a final volume of 30 µl. Samples were then boiled at 95 °C for 5 min and half (5 µg of protein) of the sample was loaded into a 10% Bolt Bis-Tris Plus gel. The gel was run in MOPS running buffer at 100-130 V for ~ 2 hrs and stained with Coomassie brilliant blue.

For large scale digestion, the required amount of proteins (10-20 mgs) were dialysed into 0.1M NaOAc pH 5.2 solution by performing 5 x 1L dialysis over 3-4 hrs. Then the solution was rescued from the dialysis cassette (using a cassette with a 10 kDa cut-off) and 5 units of Endo H per µg of protein was added. The reaction was incubated at 37 °C for approximately 4 hrs. Then the solution was dialysed against 5L PBS with 5 x 1L dialysis over 20 hrs. The enzyme activity was confirmed by running 10 µg of protein on a gel under reduced conditions next to an untreated sample to confirm the shift in band size (as described above).

2.10.1.2 Denaturing

For denaturation, 10 µg of protein (in PBS), 1 µl of glycoprotein denaturing buffer (10X stock, 5% SDS, 400 mM DTT, NEB) and dH_2O were combined to make a 10 µl reaction volume. The reaction was incubated at 100 °C for 10 mins and then placed on ice. The sample was briefly centrifuged and 2 µl of glycobuffer 3 (10X stock, 500 mM sodium acetate) an appropriate volume of dH_2O and an appropriate volume of Endo H for the required amount of enzyme was added to make a 20 µl final volume. The reaction was incubated at 37 °C for 1 or 3 hrs and results were analysed by SDS-PAGE under reduced conditions. For this, 7.5 µl of 4X laemmli buffer, an appropriate volume of DTT to have a final concentration of 50 mM and dH_2O to a final volume of 30 µl were added to the sample. The mix was boiled at 95 °C for 5 mins and half (5 µg of protein) of the sample was loaded

into a 10% Bolt Bis-Tris Plus gel. The gel was run in MOPS running buffer at 100-130 V for ~2 hrs and stained with Coomassie brilliant blue.

2.10.2 PNGase F treatment

2.10.2.1 Non-Denaturing

In order to assess PNGase F activity against the native form of the scmCD70-m1 protein, 10 µg of protein was incubated with 100 or 1000 units of enzyme in a 20 µl reaction which included 1X glycobuffer 2 (10X stock, 500 mM sodium phosphate, NEB) and dH_2O. The reactions were carried out for 4 or 24 hrs at 37 °C for comparison. To visualise the products, 7.5 µl of 4X laemmli buffer, an appropriate volume of reducing agent (DTT) to a final concentration of 50 mM and dH_2O were added to the samples to a final volume of 30 µl. The samples were then boiled at 95 °C for 5 mins and half (5 µg of protein) of the sample was loaded into a 10% Bolt Bis-Tris Plus gel. The gel was run in MOPS running buffer at 100-130 V for ~2 hrs and stained with Coomassie brilliant blue.

2.10.2.2 Denaturing

For denaturation, 10 µg of protein (in PBS), 1 µl of glycoprotein denaturing buffer and dH_2O were combined to make a total of 10 µl reaction volume. The reaction was incubated at 100 °C for 10 mins and then placed on ice. The sample was briefly centrifuged and 2 µl of glycobuffer 2, 2 µl of 10% NP-40, 6 µl dH_2O and appropriate volume of PNGase F for the required amount of enzyme was added. The reaction was incubated at 37 °C for 3 hrs and results were analysed by running SDS-PAGE under reduced conditions. 7.5 µl of 4X laemmli buffer, an appropriate volume of DTT to a final concentration of 50 mM and dH_2O to a final volume of 30 µl were added to the sample. The sample was then boiled at 95 °C for 5 mins and half (5 µg of protein) of the sample was loaded into a 10% Bolt Bis-Tris Plus gel. The gel was run in MOPS running buffer at 100-130 V for ~2 hrs and stained with Coomassie brilliant blue.

2.11 Stable Jurkat clone screening

Once single clones were apparent in 96-well plates, ¼ of the cells were harvested (by gentle pipetting) and washed with 1 ml 0.1% (w/v) BSA/PBS. Then cells were re-suspended in 100 µl 0.1% BSA/PBS and anti-CD27 primary antibody directly added to the solution. Primary antibodies used were either AT124-1 (in-house, mIgG1) at 10 µg/ml or commercial LG.3A10 antibody (directly labelled with PE, BD Biosciences, New Jersey, USA) at 2 µg/ml. The cells were incubated with the primary antibody for 30 mins at 4 °C and washed 2 times with 1 ml 0.1% BSA/PBS (cells incubated with AT124-1) or PBS (cells incubated with LG.3A10) by centrifuging at 491 xg for 5 mins. The cells incubated with LG.3A10 were analysed by flow cytometry at this point. The cells stained with AT124-1 were further incubated with the anti-mouse secondary antibody (Jackson Immunoresearch 115-136-071, 1/200 dilution) for 30 mins at 4 °C in 100 µl 0.1% BSA/PBS solution. The cells were then washed 2 times with 1 ml PBS and analysed via flow cytometry. The samples were analysed by using BD FACSCanto II (BD Biosciences).

2.12 Sorting of Jurkat-NF-κB-GFP cells stably transfected with CD27

Jurkat-NF-κB-GFP cells were harvested and centrifuged at 491 x g for 5 mins to discard the supernatant. The cells were transferred into sterile polystyrene round bottom tubes (Corning) and washed 2 times with 0.1% BSA/PBS solution (3 ml each) by centrifuging at 491 x g for 5 min. Then the cells were re-suspended in the appropriate volume of 0.1% BSA-PBS solution containing the directly conjugated anti-CD27 antibody. The cells were re-suspended at a density of 1 x 10^7 cells/ml with 1 µg/ml antibody concentration. Cells were incubated with the antibody for 30 mins at 4 °C and washed 3 times with 1% FCS/PBS solution (3 ml each). Cells were finally re-suspended at a density of 1 x 10^7 cells/ml in 1% FCS/PBS solution to be used for sorting. Collection tubes were prepared by using pure FCS solution (100 µl/tube) to prevent the cells drying and rupturing when collected during sorting. Cell sorting was carried out by a trained user at the faculty of medicine flow cytometry facility (University of Southampton) using BD FACSAria cell sorter (BD Biosciences). Approximately 70000 cells were collected after sorting which were then washed 2 times with growth medium and were plated into a well of a 6-well plate with selection antibiotic to recover.

2.13 Stimulation and activation of CD27 transfected Jurkat-NF-κB-GFP cells

To investigate the activation of Jurkat-NF-κB-GFP cells stably transfected with CD27 (see section 2.4.4), cells were re-suspended in fresh growth medium at the required density (indicated in the figure legends) and added into the wells of 96-well plates (U bottom). In parallel, control or CD27 targeting proteins were prepared separately in growth medium at the required concentrations (indicated in figure legends) and added to the wells. Cells were incubated for 6 hrs at 37 °C. Then the plate was centrifuged at 1363 xg for 2 min to pellet the cells and the supernatant was discarded. Cells were then washed with 200 µl/well PBS again by centrifuging and finally cells were re-suspended in 80 µl PBS to be analysed by flow cytometry using the expression of GFP as the outcome of activation.

To co-culture the Jurkat-NF-κB-GFP transfectants with CHO-K1 cells expressing FcγRIIB, Jurkat-NF-κB-GFP cells and proteins were prepared as described above. The CHO-K1 cells are adherent and they were harvested by trypsin-EDTA (1.5 ml for a T25 flask) and washed with excess media by centrifuging at 491 x g for 5 mins. Cells were then re-suspended in growth medium at the required density to have a 1:1 ratio with the Jurkat-NF-κB-GFP cells. Jurkat-NF-κB-GFP cells, CHO-K1 cells and proteins were distributed onto a 96-well plate (flat bottom) and incubated for 6 hrs at 37 °C. Then Jurkat-NF-κB-GFP cells were transferred into a U-bottom 96-well plate, leaving most of the adherent CHO-K1 cells in the flat bottom plate, and centrifuged to discard the supernatant. The cells were washed with 200 µl/well PBS again by centrifuging and finally re-suspended in 80 µl PBS to be analysed by flow cytometry by using the expression of GFP as the outcome of activation.

2.14 Titration of scmCD70-m1 binding to WT or DM CD27

To generate a titration curve of scmCD70-m1 binding to CD27 transfected Jurkat-NF-κB-GFP cells, cells were harvested, centrifuged and supernatant discarded. Cells were then re-suspended in 0.1% BSA/PBS solution and 50 µl/well distributed to have 2 x 10^5 cells per well. The ligand and isotype control were also prepared separately in a 96-well plate (U-bottom) and ½ dilutions were performed starting from a final 10 µg/ml concentration as the highest concentration. The cells were then added to the 96-well plate already prepared with ligand and isotype concentrations. The final volume per well was 100 µl with 2 x 10^5 cells and 10 µg/ml as the highest concentration and 0.0097 µg/ml as the lowest concentration. The cells were incubated with the proteins for 1 hr at 4 °C, washed 3 times with 200 µl/well

0.1% BSA/PBS and then re-suspended in 100 µl 0.1% BSA/PBS solution containing 1/200 dilution of the anti-mouse secondary antibody (Jackson Immunoresearch, 115-136-071). Cells were incubated for 30 mins at 4 °C, washed 3 times with 200 µl/well PBS and finally re-suspended in 80 µl PBS prior to analysis on a flow cytometer.

2.15 T-cell activation assay - ^{3}H-thymidine incorporation

To assess the capacity of scmCD70-m1 to influence T-cell activation in vitro, spleens were harvested from wild type (WT) C57BL/6 mice. Single cell suspensions prepared by passing through a nylon mesh cell strainer (100 µm, Corning) and cells washed twice with 20 ml PBS by centrifuging at 368 x g for 5 mins and discarding supernatant. Cells were then re-suspended in 5 ml red cell lysis buffer (8.4g NH_4Cl, 1g $KHCO_3$/L) and incubated for 5 mins at RT before the addition of 10 ml PBS and centrifugation. After discarding the supernatant, cells were washed twice with RPMI 1640 medium and re-suspended in 5 ml complete medium (RPMI 1640 supplemented with 10% FCS, 2 mM glutamine, 1 mM pyruvate, 100 µg/ml streptomycin, 100 units/ml penicillin and 50 µM 2-mercaptoethanol (Sigma)). After counting using a coulter counter or haemocytometer, 2 x 10^5 cells per well in 100 µl were plated in U shaped 96 well plates. Agonist anti-CD3 mAb (145-2C11, in house) was added in 50 µl at the concentrations indicated in figures. Finally additional agonistic mAb or scmCD70 fractions were added in 50 µl at the concentrations indicated in figure legends. Cells were incubated at 37 °C and 5% CO_2 in a humidified incubator for 48 hrs and then pulsed with 1 microcurie/well of ^{3}H-thymidine before incubation at 37 °C overnight (~17 hrs). The following day, cells were lysed using a harvesting system and lysates transferred to filter plates (Opti-plate-96, Perkin Elmer, Massachusetts, USA). Scintillant fluid (40 µl/well) (Perkin Elmer) was added and incorporation of ^{3}H-thymidine into proliferating cells was measured in a β-emission counter.

2.16 Mice

OT-1 transgenic mice in which T cells are specific for the OVA-derived peptide have been described previously (220). OT-1, WT, FcγRIIB KO, FcγR1,2,3,4 KO C57BL/6 and WT BALB/c mice were maintained in the Biomedical Research Facility unit of University of Southampton. For experiments, mice were age and sex matched. For OT-1 expansion and BCL1 studies, 8-10 weeks old mice were used as recipients. All in vivo experiments were performed under project licence PA4C79999 and under personal licence IE7C34E6C. All experimental work was approved by local ethics committee and was conducted in accordance with UK Home Office Guidelines.

2.17 In vivo experiments

2.17.1 OT-1 T-cell expansion

To determine the effect of CD27 agonists on T-cell activation in vivo, OT-1 TCR transgenic mice were used. In these experiments, T cells from OT-1 transgenic mice in PBS were adoptively transferred into WT, FcγRIIB KO and FcγR1,2,3,4 KO C57BL/6 recipients by intravenous (i.v.) injection on day -1. T cells were obtained from the spleens of sex-matched OT-1 mice and were passed through a nylon mesh cell strainer (100 µm) before use. To calculate the numbers of OT-1 cells present in the total splenocytes and confirm that they are naïve T cells, an aliquot of spleen cells was stained with anti-mouse CD8a antibody (eBioscience, Thermo Fisher, clone 53-6.7), $OVA_{257-264}$ tetramer-PE (in-house), anti-mouse CD62L antibody (eBioscience, clone MEL-14) and anti-mouse CD44 antibody (eBioscience, clone IM7). Approximately 0.5 x 10^6 cells were blocked with 10 µg/ml 2.4G2 (in-house, blocks non-specific binding to Fc receptors) in 100 µl 0.1% BSA/PBS for 15 mins at 4 °C. Then cells were stained with additional 100 µl 0.1% BSA/PBS with 1 µg/ml anti-mouse CD8a-APC, 1 µg/ml anti-mouse CD62L-eFluor450, 2.5 µg/ml anti-mouse CD44-FITC and 0.5 µl $OVA_{257-264}$ tetramer-PE for 30 mins at 4 °C in dark. Cells were then red cell lysed by incubating with 2 ml of red cell lysis buffer for 5 mins at 4 °C and washed twice with 4 ml of PBS. Samples were then analysed using BD FACS Canto II where a $CD44^{low}$ $CD62L^{high}$ profile indicated that the cells were naïve T cells.

In some experiments, $CD8^+$ T cells from OT-1 transgenic mice were first purified before adoptive transfer. For $CD8^+$ T cell purification, a MACS Miltenyi Biotec CD8a (Ly-2)

MicroBeads kit was used according to manufacturers' instructions. The purity of the cells was confirmed by comparison with unpurified population of splenocytes by staining with anti-CD8a and $OVA_{257-264}$tetramer-PE and analysing by flow cytometry. For this, an OT-1 spleen was harvested and processed to obtain a homogeneous single cell population. Approximately 0.5 x 10^6 cells were stained as described above and analysed using BD FACS Canto II. After confirming the abundance of $CD8^+Tet^+$ cells, $CD8^+$ T cells were purified as a single cell population. At this stage, again approximately 0.5 x 10^6 cells were stained in the same order as above (before purification) and analysed using BD FACS Canto II. Purity was always > 95%.

After adoptive transfer of either total OT-1 splenocytes or purified $CD8^+$ T cells from OT-1 transgenic mice, recipient mice were challenged with 30 nmol $OVA_{257-264}$ peptide (SIINFEKL) (Peptide Protein Research Ltd, Fareham, UK) in combination with 200 µg or 250 µg (indicated in figure legends) control, scmCD70-m1, scmCD70-mm1 or anti-CD27 mAb (AT124-1). All injections were performed intravenously. Expansion of the adoptively transferred $CD8^+$ T cells was detected by collection of peripheral blood at appropriate time points and performing flow cytometry staining. To examine the expansion of adoptively transferred OT-1 T cells, peripheral blood samples (20 µl) collected from mice were made up to 100 µl in 0.1% BSA/PBS and blocked with 10 µg/ml 2.4G2 for 15 mins at 4 °C. Then cells were stained with additional 100 µl 0.1% BSA/PBS with 1 µg/ml anti-mouse CD8a and $OVA_{257-264}$tetramer-PE or anti-mouse CD45.1 (eBioscience – clone A20) for 30 mins at 4 °C in dark. Cells were then red cell lysed by incubating with 2 ml of red cell lysis buffer for 5 mins at 4 °C and washed twice with 4 ml of PBS. Samples were then analysed using BD FACS Canto II.

In order to assess the magnitude of the memory T-cell pool, the primary response was allowed to contract to approximately 1% of OT-1 T cells forming the $CD8^+$ population. Then mice received intravenous injection of 30 nmol $OVA_{257-264}$ peptide in combination with 50 µg anti-CD40 (3/23, rIgG2a) as an adjuvant. The expansion of the OT-1 T cells was monitored by obtaining peripheral blood samples at appropriate time points and performing flow cytometry staining as detailed above.

2.17.2 BCL1 tumour model

To investigate the ability of CD27 agonists to stimulate tumour rejection, mice were challenged with a large dose of the BCL1 tumour and treated with the proteins indicated in the figures. BCL1 tumour was maintained by serial passage through mice and localises to the spleen resulting in splenomegaly in terminal mice. On the day of tumour challenge, a terminal spleen was therefore harvested from a previously BCL1-challenged WT BALB/c female mouse. The spleen was passed through a nylon mesh cell strainer (100 µm) in 20 ml PBS. Then 20 ml cell suspension was split into two with each 10 ml being added to 10 ml lymphoprep (Alere technologies, Oslo, Norway) solution by gentle pipetting, making sure that the solutions stay separated. The solutions were centrifuged at 872 xg for 20 min with gentle acceleration and deceleration of the centrifuge. Then each buffy coat containing the BCL1 cells was transferred into a tube with 25 ml PBS and washed by centrifuging at 491 xg for 5 min with normal acceleration and deceleration. The supernatant was discarded and tumour cells washed again with 20 ml PBS. Cells were re-suspended in 8 ml PBS and counted using a coulter counter, using zapoglobin (Beckman Coulter) to lyse the red blood cells. Cells were then diluted accordingly in PBS to inject 5 x 10^6 BCL1 cells per mouse in 200 µl by i.v. injection. Mice additionally received injections of endotoxin low control or CD27 agonist proteins as outlined in the relevant figure legends.

2.18 Endotoxin testing

All reagents throughout were prepared in endotoxin low buffers However, to be certain, proteins were additionally directly tested for contamination with endotoxin. For this, Endosafe-PTS portable test system cartridges (Charles River, Massachusetts, USA) using limulus amoebocyte lysate reagents were used. In brief, a 1 in 10 dilution of the test sample was prepared in sterile water and tested in the cartridges according to manufacturers' instructions. A value was obtained per mg of protein and 5 endotoxin units (EU) per mg of protein was used as the cut-off to consider the samples as endo low. All CD27 agonists described in this thesis which were used in in vivo experiments were endotoxin low.

2.19 Statistical analysis

Statistical analyses were performed using GraphPad Prism software (7.03). Unpaired Student's t test (two-tailed), one-way ANOVA, two-way ANOVA or Log-rank test for survival analysis were used to calculate statistical differences. P values are indicated in the figure legends; ns: not significant, *= $p<0.05$, **= $p<0.01$, ***= $p<0.001$, ****= $p<0.0001$.

Chapter 3 Generation of scmCD70-m1

3.1 Introduction

Previously in the laboratory, a version of recombinant soluble CD70 was developed. This comprised the Fc domain of human IgG1 (hinge, CH2 and CH3 domains) fused to the extracellular domain of mouse CD70. The structure can be seen in Figure 3.1 where CD70 domains form non-covalent trimers and by the interaction of Fc domains, a hexameric ligand domain is formed. The recombinant protein enhanced the proliferation of T cells in combination with peptide stimulation (signal 1) and improved effector cytokine production in vitro. Additionally, in combination with $OVA_{257-264}$ peptide immunisation it enhanced the expansion of adoptively transferred OT-1 T cells in vivo, improved their cytotoxic capacity and contributed to a greater secondary response (200).

However this first generation soluble CD70 protein formed higher-order structures and was rapidly cleared from the circulation. Potentially the higher-order structures were the result of the formation of multiple disulphide bonds between the Fc domains. The protein was also rapidly cleared potentially due to steric hindrance and the Fc domain not properly interacting with FcRn. Therefore the aim of this chapter was to synthesise a new generation scmCD70-m1 protein with a more homogeneous structure and improved half-life. A schematic diagram showing what I aim to manufacture is shown in Figure 3.1. The recombinant protein will be tested for its ability to interact with recombinant mouse CD27, induce in vitro T-cell activation/proliferation and if active, will be tested in vivo to stimulate the expansion of adoptively transferred T cells.

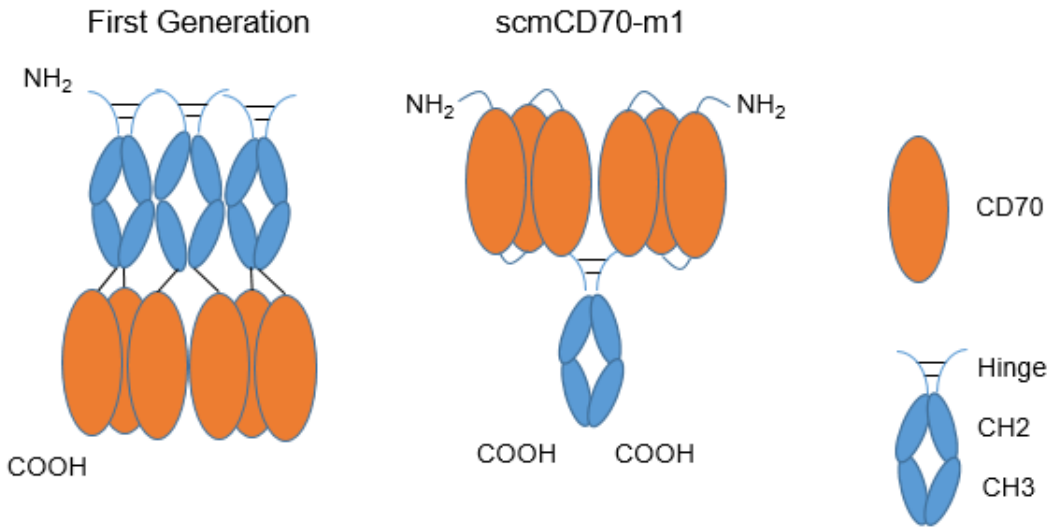

Figure 3.1. First generation soluble CD70 and new generation scmCD70-m1 structures. A hexameric ligand structure with three Fc domains for first generation sCD70 and a hexameric ligand structure with one Fc domain for scmCD70-m1 are illustrated. The orientation of hinge and CH2, CH3 domains in Fc are different for each protein. N-termini and C-termini are indicated on the figure. The disulphide bonds in the hinge region are also indicated. First generation CD70 protein was made up of fusing human IgG1 Fc domain directly with the CD70. The Fc domain had the WT hinge at the N-terminus and a modified hinge (lacking disulphide bonds) was conjugated to CD70 domain. For scmCD70-m1, The Fc domain of mouse IgG1 was conjugated to single chain CD70 trimer (each domain separated by 3xGGGS linkers) with a linker consisting of an XbaI restriction site and GGGS linker. The scmCD70-m1 domains are detailed in Figure 3.2. For sequence of scmCD70-m1, see Appendix Fig. 1.

3.2 Results

3.2.1 Cloning of scmCD70-m1

To generate a construct incorporating three copies of CD70 fused to a single Fc domain, Pubmed – Nucleotide tool (https://www.ncbi.nlm.nih.gov/nuccore) was used to identify sequence encoding murine CD70 (sequence NM_011617.2) and the murine IgG1 hinge, CH2 and CH3 domains (sequence LT160964). The construct was produced to reduce the number of Fc domains from 3 to 1 in a hexameric ligand protein (Fig. 3.1). A composite DNA sequence was generated in Seqbuilder (DNASTAR, Wisconsin, USA) to incorporate a sequence encoding three copies of the extracellular domain of murine CD70, each separated by a sequence encoding a short linker (3xGGGS; chosen based on flexibility and predicted lack of a strong secondary structure (221, 222)) upstream of a sequence encoding 2xGGGS, an XbaI site, an additional GGGS linker and sequence encoding the murine IgG1 Fc hinge region, CH2 and CH3 domains (Fig. 3.2.A).The sequence was designed to incorporate a leader peptide (taken from the heavy chain of mouse anti-tumour associated glycoprotein 72 mAb) upstream to enable secretion from the cells and was flanked by unique restriction sites HindIII and EcoRI. This entire sequence (see Appendix Fig. 1) was ordered commercially and was provided in pcDNA3.1 (+) plasmid DNA (Fig. 3.2.B).

In order to produce stable clones for large scale production of scmCD70-m1, the insert was cloned into the pEE14 expression vector using the unique restriction sites of HindIII and EcoRI (see Appendix Fig. 4). The vector pEE14 contains a glutamine synthetase (GS) minigene (Fig. 3.2.B) such that transfected cells which cannot normally grow in glutamine deficient medium are rescued by the expression of glutamine synthetase (223). The scmCD70-m1-pcDNA3.1 (+) was therefore double digested with HindIII and EcoRI for 2 hrs and products run on a 1% agarose gel (Fig. 3.3.A). The pEE14 vector was sequentially digested; first with EcoRI for 2.5 hrs (Fig. 3.3.B) and then with HindIII for 2 hrs (Fig. 3.3.C) and the products were run on 0.7% agarose gel. The gels were prepared with addition of EtBr and DNA bands were visualised using a UV light source. The insert from the pcDNA3.1 (+) vector ran at the expected size (2.3 kbp) and was isolated and cleaned from the gel. The digested pEE14 plasmid (9.4 kbp) was cleaned in solution in parallel and the DNA from both preparations was quantified by spectrometry. The products were then ligated together at a 3:1 insert to vector molar ratio at RT for 3 hrs and transformed into OneShot TOP10 cells. Individual colonies were grown on LB plates supplemented with amp to select only those clones successfully transformed with the pEE14 vector. Six colonies were then further grown in LB-amp in 5 ml cultures for 17 hrs and DNA isolated using commercial kits. DNA

was isolated in a volume of 50 µl and quantitated on a spectrophotometer. A small amount (400 ng) of the DNA product from 6 individual colonies was then double digested with HindIII and EcoRI for 1.5 hrs and visualised on a 1% agarose gel (Fig. 3.4). As all colonies showed a product consistent with incorporation of the pEE14-scmCD70-m1 plasmid (i.e. a band at 2.3 kbp), only one colony was grown further to increase the amount of DNA for subsequent stable transfection of CHO-K1S cells required for producing protein.

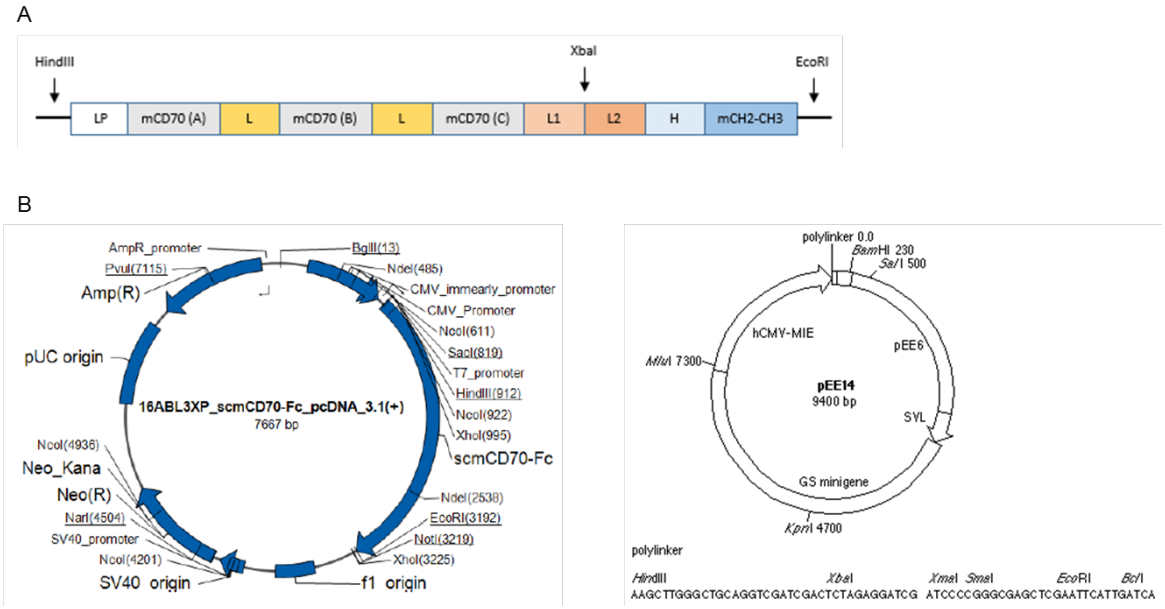

Figure 3.2. Schematic representation of scmCD70-m1 and plasmid maps. (A) The sequence of scmCD70-m1 insert. LP; leader peptide, mCD70; mouse CD70 extracellular domain, L; 3xGGGS linker, L1; 2xGGGS linker, L2; XbaI linker (XbaI restriction site and GGGS linker), H; mouse IgG1 Fc hinge region, mCH2-CH3; mouse IgG1 Fc domain. HindIII, XbaI and EcoRI are the restriction enzyme sites used with indicated digestion points. (B) Maps of the two expression vectors used for production of scmCD70-m1. The scmCD70-m1 insert was ordered in (left) pcDNA3.1 (+) and cloned into (right) pEE14 using HindIII and EcoRI restriction sites.

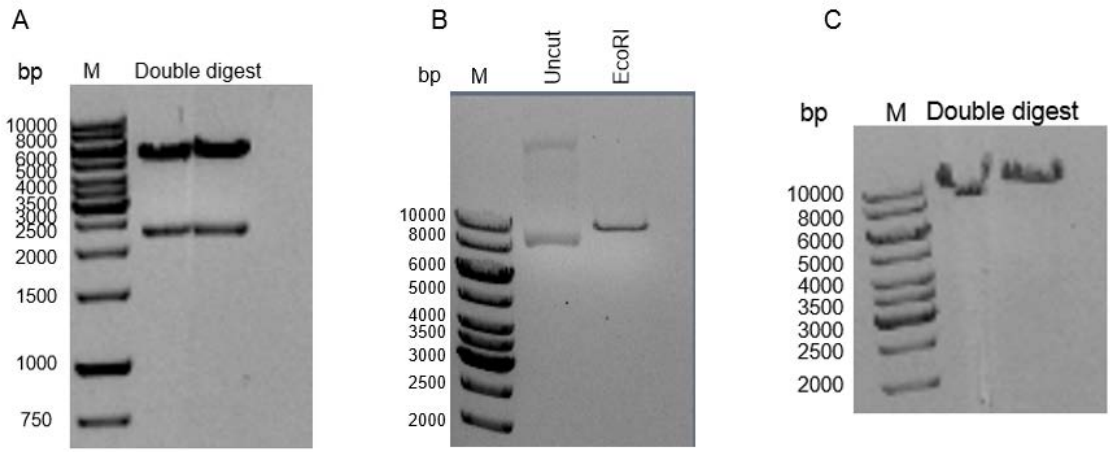

Figure 3.3. HindIII and EcoRI digestion of scmCD70-m1 pcDNA3.1 (+) and pEE14 expression vectors. (A) Double digested pcDNA3.1 (+) with the scmCD70-m1 insert. 6 µg plasmid was digested for 2 hrs at 37 °C using HindIII and EcoRI restriction enzymes; 200 ng DNA was run in each indicated lane and the rest in a major lane (not shown) from where insert was extracted without exposure to UV light. (B) Single EcoRI digest of pEE14; 4.2 µg of plasmid DNA was cut and a representative sample (200 ng) loaded onto the gel alongside uncut plasmid to confirm the reaction. The digestion was carried out for 2.5 hrs at 37 °C. (C) Double digested pEE14. Single EcoRI cut pEE14 plasmid DNA was recovered in solution using commercial kits (Qiaquick gel extraction, Qiagen). Then all of the recovered plasmid DNA was subjected to digestion with HindIII restriction enzyme for 2 hrs at 37 °C; 200 ng cut plasmid was then run in each lane and the rest was run in a major lane (not shown) to be extracted from the gel without exposure to UV light. pEE14 size; ~9.4 kbp, insert size; ~2.3 kbp M; marker lane, bp; basepair.

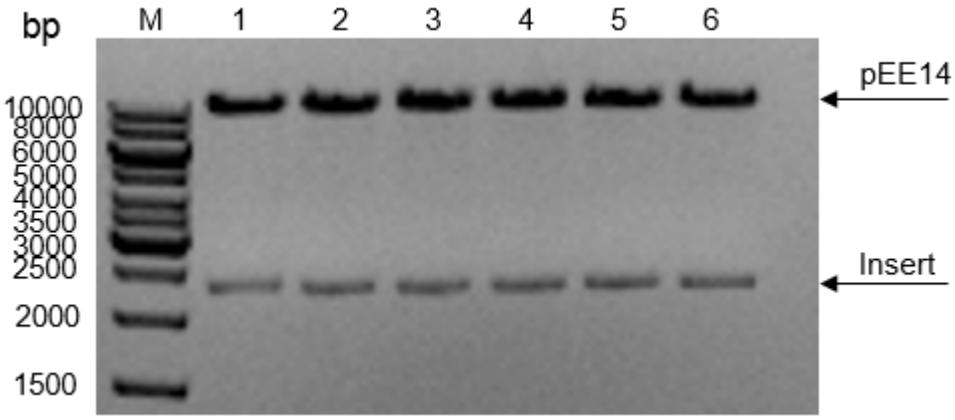

Figure 3.4. Restriction digest analysis of mini-prep plasmid DNA from six colonies of pEE14 containing the scmCD70-m1 insert. Six colonies of transformed OneShot Top10 cells were expanded in LB-amp for 17 hrs at 37 °C. Plasmid DNA was then isolated from the cultures using mini-prep kits (Qiagen) according to manufacturers' instructions. Plasmid DNA was eluted in 200 µl of elution buffer provided within the kit and quantified by spectrophotometer; 400 ng product was then digested using 2 units each of HindIII and EcoRI, for 1.5 hrs at 37 °C; 200 ng of each digest was visualised on a 1% agarose gel. pEE14 size; ~9.4 kbp, insert size; ~2.3 kbp. M; marker lane, bp; basepair.

3.2.2 Stable Clone Generation, Expression and Purification of scmCD70-m1

Colony #2 from the clones represented in Figure 3.4 was further grown in LB-amp for 17 hrs to a volume of 250 ml. DNA was then extracted using a maxi-prep kit (Qiagen). DNA was eluted in 1 ml TE buffer and quantitated. This yielded 289 µg of pEE14-scmCD70-m1 with a 260/280 ratio of 1.93, indicating low contamination with proteins. In order to generate cells capable of synthesising the protein product, CHO-K1S cells were then stably transfected with this DNA by lipid transfection in 6-well plates. Transfected cells were then plated at limiting dilutions in 96-well plates 72 hrs after transfection. Individual wells were regularly visualised for the presence of single colonies and growing cells. After 14-21 days, supernatants from wells with single colonies were screened by ELISA with the aim of identifying individual colonies secreting high concentrations of the scmCD70-m1 protein. An ELISA was therefore performed in which goat anti-mouse IgG was used to coat plates and goat anti-mouse Fc-HRP was used to detect the bound protein. Initial assays demonstrated that the primary and secondary antibodies do not prevent the other antibody from binding (data not shown).

Initially the six clones exhibiting the highest concentration of scmCD70-m1 were transferred from 96 well plates into 24 well plates and then into bigger flasks. Following this, supernatants from every clone were directly tested for the presence of secreted scmCD70-m1. At the time of supernatant collection, clones A, B and C were at 80-90% confluency whereas clones D, E and F were at 50-60% confluency. This screen was firstly to determine the levels of scmCD70-m1 secretion by each clone and, secondly to ensure that scmCD70-m1 could interact with recombinant mouse CD27. Results of the ELISA are shown in Figure 3.5. A standard curve (Fig. 3.5.A) was produced by using known concentrations of recombinant mouse-TIGIT-Fc protein (R&D systems) to measure the concentration of scmCD70-m1 secreted by each clone. Supernatant from clone A showed the highest concentration of protein at 25 µg/ml whereas supernatant from clone C showed the lowest concentration at 4 µg/ml. Other clones showed concentrations ranging from 10 µg/ml to 14 µg/ml (Fig. 3.5.B).

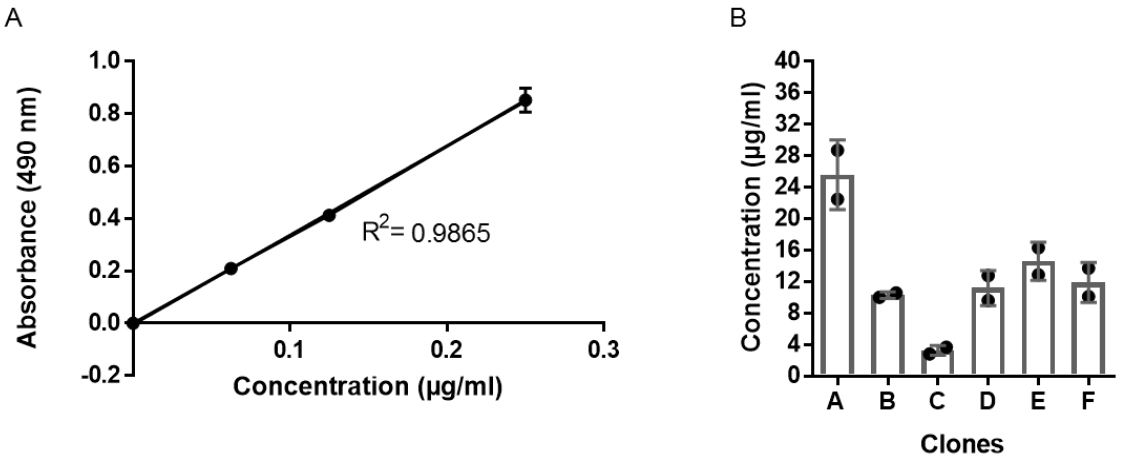

Figure 3.5. scmCD70-m1 expression by stable CHO-K1S clones. The concentration of scmCD70-m1 in supernatants of expanded transfected CHO-K1S clones was determined by ELISA. In brief, plates were coated with goat anti-mouse IgG, prior to incubation with supernatant. The presence of scmCD70-m1 in supernatants was then detected by goat anti-mouse-Fc HRP antibody. Blank wells containing neat cell culture medium were used as negative controls. (A) A standard curve from known concentrations of recombinant murine TIGIT-Fc protein was generated and was used to calculate the concentrations in supernatants. (B) The concentrations of scmCD70-m1 secreted by each CHO-K1S clone are shown. Mean +/- SD are representative of duplicates.

Additionally, surface plasmon resonance was used to confirm that the secreted products could bind recombinant mouse CD27. An anti-human Fc chip (anti-human IgG previously immobilised via amine coupling) was used to capture rmCD27-hFc protein. Supernatant from each clone was first injected through the chip to observe background binding. This was followed by injection and capture of rmCD27-hFc. Finally supernatants were injected again to confirm binding to recombinant CD27 captured on the chip. All the supernatants showed similar background binding with RU (indicating the level of bound protein on the chip surface) of 40 or lower which was considered negligible (Fig. 3.6). The amount of rmCD27-hFc captured on the chip for each clone was similar at approximately 750 RU. Supernatants from all of the clones could interact with rmCD27-hFc with RU in the order of A to E; 190 RU, 150 RU, 60 RU, 220 RU, 230 RU and 150 RU (measured by the change in the response level after rmCD27-hFc binding). Within the clones, clone C showed the least interaction with 60 RU and clones D and E showed highest interaction with 220 RU and 230 RU respectively (Fig. 3.6). By considering the level of confluency, amount of protein secretion (Fig. 3.5.B) and interaction with recombinant mouse CD27 (Fig. 3.6), clones D and E were selected for further processing. Both clones were therefore grown in bulk cultures in a shaking incubator. The scmCD70-m1 product secreted by clone E was purified whereas supernatant from clone D was stored at -20 °C.

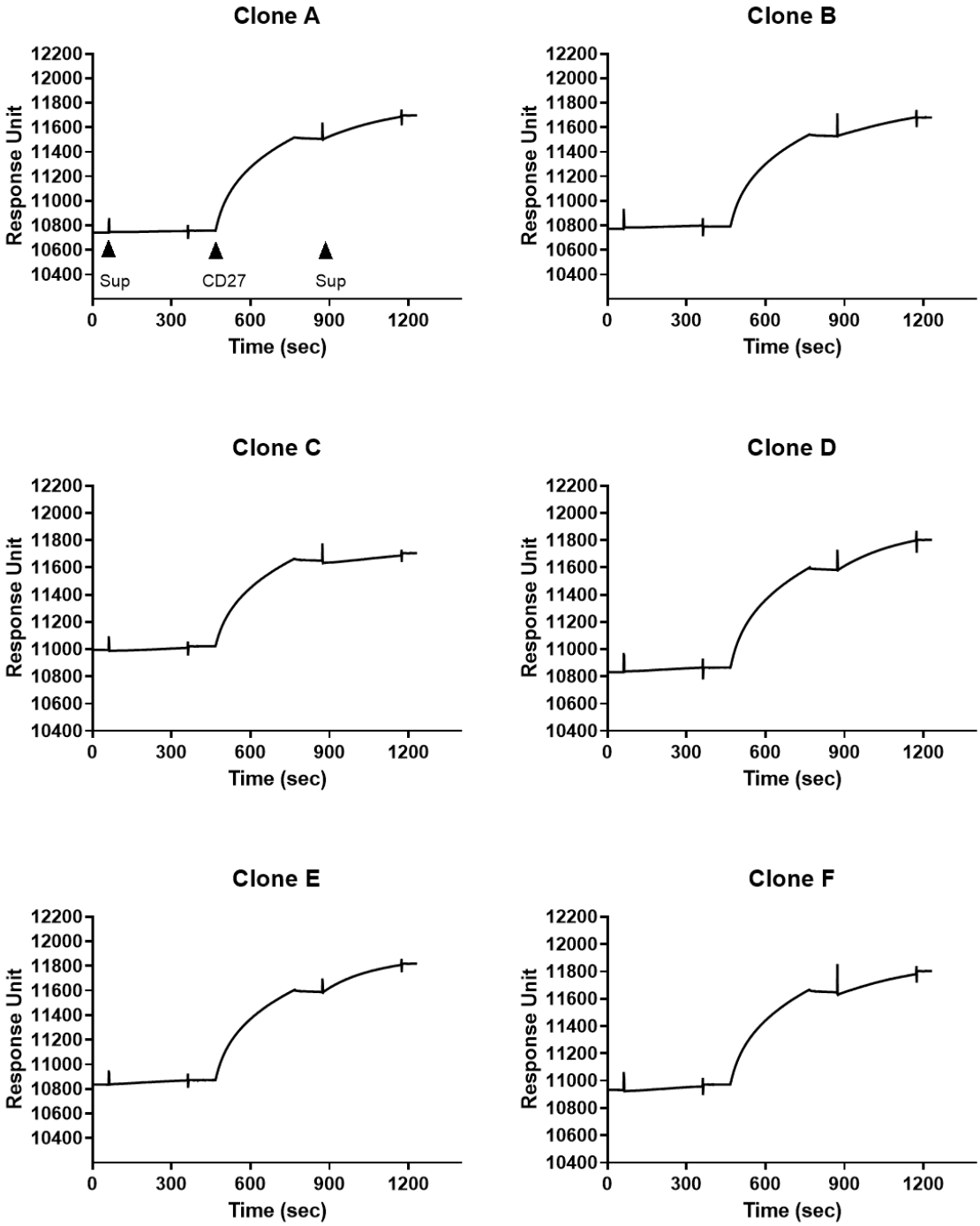

Figure 3.6. Interaction of supernatants from scmCD70-m1 secreting CHO-K1S clones with recombinant mouse CD27. Supernatants from stably transfected CHO-K1S clones were tested via SPR for binding to rmCD27-hFc which was captured by an anti-human Fc chip. Arrows on the graph representing the analysis of supernatant from clone A indicate the timings of solution injection. Supernatants were injected undiluted and rmCD27-hFc was injected at 5 µg/ml concentration in SPR running buffer (HBS-EP+). Flow rate; 10 µl/min for 5 mins for each injection. Sup; supernatant, CD27; rmCD27-hFc.

Purification of scmCD70-m1 from clone E was performed using a protein A column (in-house) in which the Fc region of the fusion protein is bound to the column and then eluted. The supernatant from the CHO-K1S cells, clone E, was concentrated down to 150 ml from approximately 2L. The concentrated solution was passed through the column and 136 mg of protein at 1.25 mg/ml concentration was subsequently eluted off the column. The purity and homogeneity of the eluted protein was then investigated via SDS-PAGE and SEC. The predicted molecular weight of the monomer polypeptide is 79.3 kDa (using Expasy compute pI/MW tool). There are 10 N-glycosylation sites in the monomer polypeptide and each N-glycosylation is 2.5 kDa (224). Accordingly, the predicted molecular weight of a monomer (single polypeptide) is 104.3 kDa and the dimer (dimer-of-trimer) is predicted to be 208.6 kDa. On SDS-PAGE, a reduced and non-reduced sample of purified scmCD70-m1 was visualised. For the non-reduced form, although a band was observed at approximately 210 kDa, the majority of the protein consisted of higher molecular weight products (Fig. 3.7.A). Under reduced conditions, the majority of proteins appeared at approximately 105 kDa which suggested that the formation of dimer and oligomeric structures was mainly due to disulphide bond formation.

Analysis by SEC (Fig. 3.7.B) showed a similar profile as SDS-PAGE. A peak slightly bigger than 158 kDa was observed, likely indicating a dimer-of-trimer form, but the majority of the proteins appeared to be at higher molecular weights, coming off the column earlier. The final peak at 19 ml corresponds to the salt peak coming off the column towards the end of the run (Fig. 3.7.B).

Finally the purified protein was tested via SPR to confirm interaction with recombinant mouse CD27, in the same way as supernatants. As for the supernatants, purified scmCD70-m1 showed negligible background binding to the anti-human Fc chip (Fig. 3.7.C). The amount of rmCD27-hFc captured on the chip was 1650 RU and binding of scmCD70-m1 to the captured rmCD27-hFc showed an additional 670 RU increase (Fig. 3.7.C). In this instance, the amount of rmCD27-hFc captured on the chip was higher than the amount captured during testing of the supernatants. This was likely due to using a freshly prepared chip in this assay. Also, the amount of scmCD70-m1 binding to captured rmCD27-hFc was higher compared to supernatants, which might be due to having more rmCD27-hFc captured on the chip. These data confirm that stably transfected CHO-K1S cells (clone E) secrete high levels of scmCD70-m1, which exists as a dimer-of-trimer, or a higher order oligomer, and is capable of binding to CD27 in vitro.

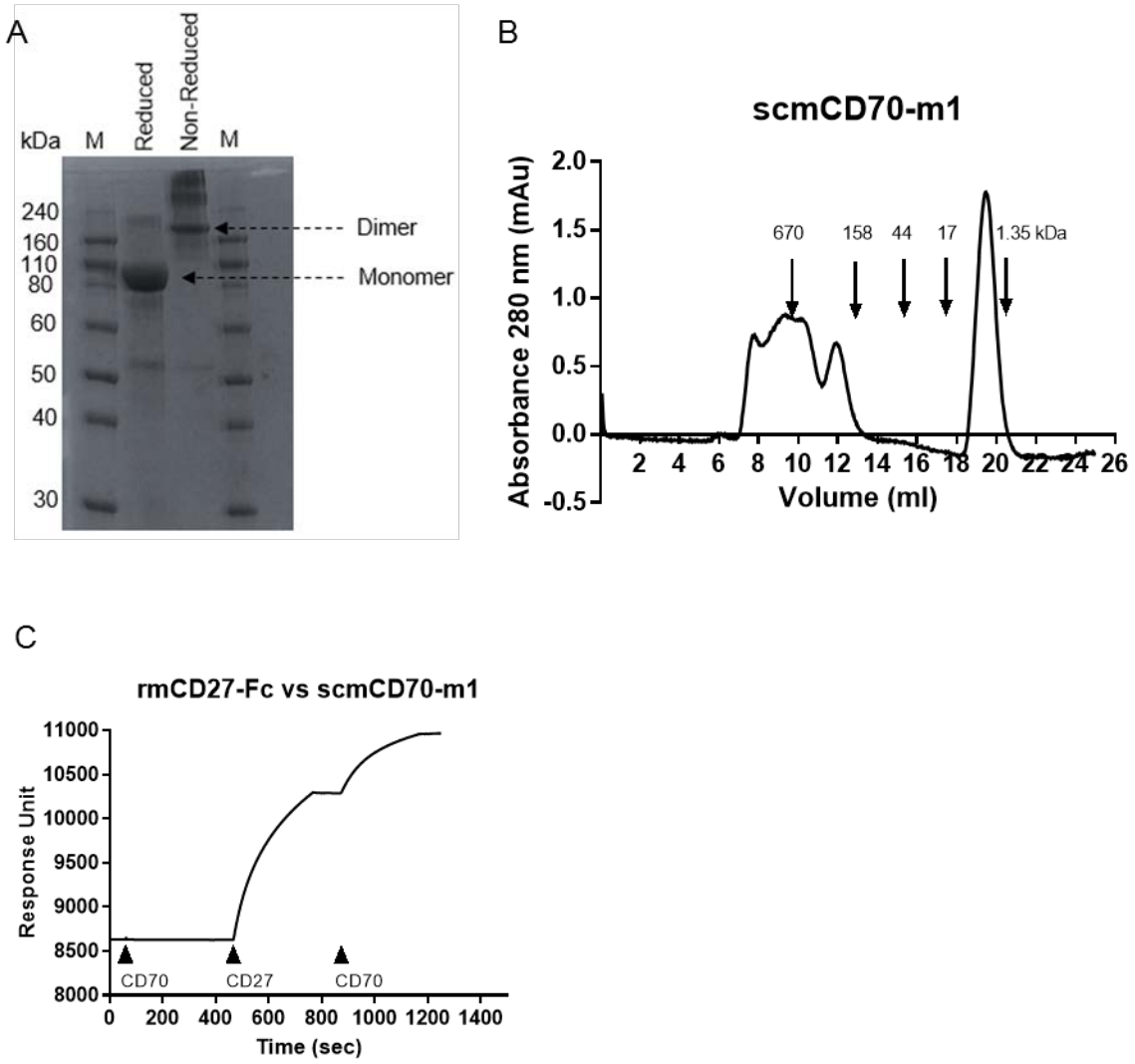

Figure 3.7. Size and purity confirmation of purified scmCD70-m1. (A) SDS-PAGE analysis of scmCD70-m1. Samples were analysed under reduced or non-reduced conditions; the reduced sample was prepared with a final concentration of 62.5 mM DTT as reducing agent. All samples were boiled at 95 °C for 5 mins prior to loading. 10 µg of protein was loaded per lane into a 10% Bis-Tris gel which was run at 150 V for 1.5 hrs. M; marker lane. (B) For SEC analysis of scmCD70-m1, 31.25 µg of protein was run on a Superdex 200 10/300 GL column. Molecular weight markers are indicated on the graph. (C) SPR analysis of the interaction between purified scmCD70-m1 and rmCD27-hFc. For this, an anti-human IgG chip was used to capture rmCD27-hFc and then scmCD70-m1 was injected. rmCD27-hFc was injected at 5 µg/ml and scmCD70-m1 was injected at 10 µg/ml in HBS-EP+. CD70; scmCD70-m1, CD27; rmCD27-hFc. Flow rate was 10 µl/min for 5 mins for each injection.

3.2.3 Fractionation and functional analysis of scmCD70-m1

To determine whether the eluted scmCD70-m1 exhibited functional activity, we next assessed its ability to stimulate T cells. It has been shown previously that stimulation of T cells with agonist anti-CD3 and via a co-stimulatory molecule such as CD28 is sufficient to drive in vitro activation and proliferation (225). In addition, previous work in our laboratory indicated that soluble CD70 could drive T-cell activation in the presence of anti-CD3 stimulation (200). Therefore a similar assay was used to test the functional activity of purified scmCD70-m1. Splenocytes were stimulated with varied doses of anti-CD3 in combination with scmCD70-m1 or a control mIgG1 antibody and uptake of ^{3}H-thymidine added at 48 hrs was assessed after ~17 hrs of incubation. As expected, cells showed a dose-dependent increase in ^{3}H-thymidine uptake with increasing anti-CD3 dose (Fig. 3.8). Across nearly all anti-CD3 concentrations, stimulation of cells with anti-CD3 mAb and scmCD70-m1 generated an approximately 2-fold higher response compared to stimulation with anti-CD3 and control mIgG1 (Fig. 3.8). Importantly, scmCD70-m1 did not induce T-cell activation in the absence of agonist anti-CD3 confirming that scmCD70-m1 acts as a co-stimulatory molecule and is dependent on additional TCR activation.

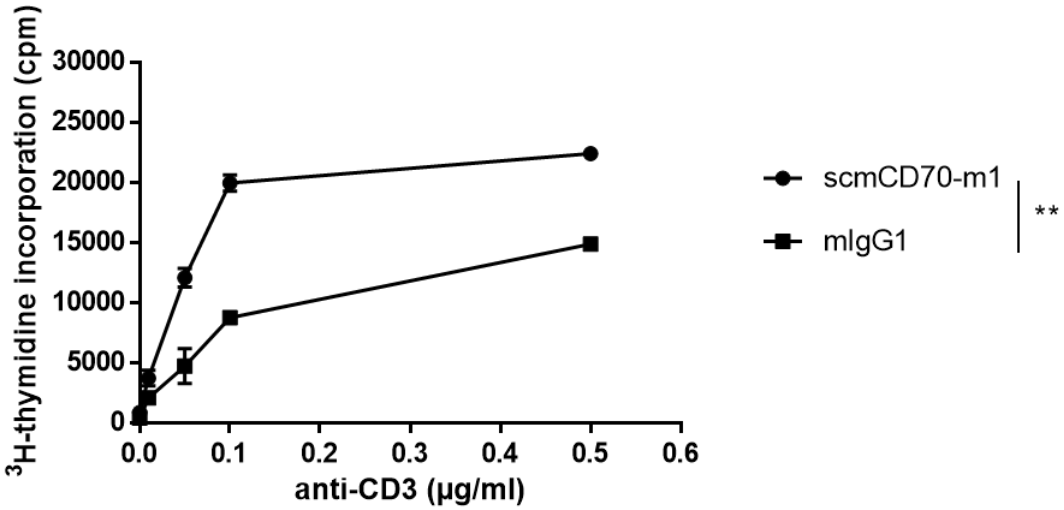

Figure 3.8. scmCD70-m1 induces T cell activation in vitro. 2 x 10^{5} splenocytes from a WT C57BL/6 mouse were stimulated with the doses of soluble anti-CD3 mAb (clone 145-2C11) indicated, in combination with either mIgG1 control (anti-human CD16 - clone 3G8) or scmCD70-m1 at 10 µg/ml. Cells were plated in triplicate for each condition. Activation of cells was determined by ^{3}H-thymidine incorporation which was added at 48 hrs post-stimulation and harvested after 17 hrs incubation. Two-way ANOVA with Tukey's multiple comparisons test was performed for statistical analyses and statistics at the highest anti-CD3 concentration is indicated. **= $p<0.01$. Plot represents mean +/- SEM of triplicates.

While these data confirm that the purified scmCD70-m1 has functional activity, in order to determine which multimer was active, the proteins were fractionated, via SEC, with the lowest number fraction being the highest oligomeric structure and the highest number fraction being the dimer-of-trimer form (Fig. 3.9 & 3.10).

The purity of the fractionated samples was confirmed by SDS-PAGE in reduced and non-reduced conditions (Fig. 3.11). Under reduced conditions, all fractions showed a similar profile with the majority of proteins in the monomeric form (104.3 kDa) and minimal presence of oligomers (250 kDa) and possible degradation products (53 kDa) (Fig. 3.11). Under non-reduced conditions, predicted dimer-of-trimer fractions (38-39 and 40-50) appeared to be in dimer-of-trimer form (208.6 kDa) with high purity and only a very low level of the oligomeric form. Unfractionated and other fractionated samples (12-14, 17-19, 21-25) appeared mainly in oligomeric form with low levels of the dimer-of-trimer form (Fig. 3.11).

In addition to investigate purity, the ability of each fraction to interact with recombinant CD27 was examined via SPR as previously described. All fractions showed negligible background binding to the chip with RU values of 15 or lower (Fig. 3.12). The amount of rmCD27-hFc captured on the chip was approximately 1500 RU. All of the fractions could interact with recombinant CD27 and showed a considerable amount of binding with RU values indicated on the graphs shown in Figure 3.12. Within the fractionated samples, the dimer-of-trimer forms 38-39 and 40-50 showed the highest level of interaction with recombinant CD27 with 690 RU and 810 RU respectively (Fig. 3.12). The RU values from SPR can be used to find the stoichiometry between the interacting molecules. To do this, the RU value achieved by each molecule is divided by its molecular weight to identify a value which can be used to derive a binding ratio between the two molecules. The predicted molecular weight of scmCD70-m1 (dimer-of-trimer, fraction 40-50) is 208.6 kDa and the RU value was 810. The molecular weight of rmCD27-hFc (dimer) is 90 kDa and the RU value achieved by rmCD27-hFc was 1500. With these values the stoichiometry between scmCD70-m1 and CD27 can be calculated as 3.88:16.67 and this is equal to approximately 1:4. This suggests that one scmCD70-m1 dimer-of-trimer interacts with four recombinant CD27 dimers. The dimer-of-trimer form of scmCD70-m1 has six CD70 domains, so a 1:3 ratio was expected but 1:4 is also acceptable due to a mixture of possible binding patterns. Working out the stoichiometry for the oligomers is difficult as there is a mixture of proteins of different molecular weights.

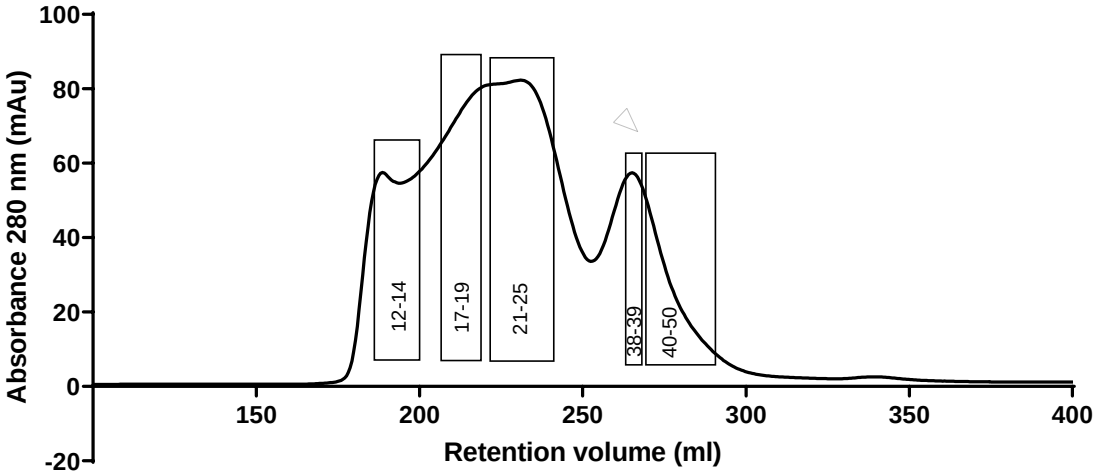

Figure 3.9. Fractionation of scmCD70-m1. Proteins produced by stable transfection of CHO-K1S cells were fractionated into five different fractions (indicated by rectangles) with lower fraction numbers consisting of the oligomer structures and fractions 38-39 and 40-50 consisting of the dimer-of-trimer structure. The peak corresponding to dimer-of-trimer products is indicated with an arrow. Samples were fractionated using the S200 26/950 column (in-house) with 3 ml/min flow rate.

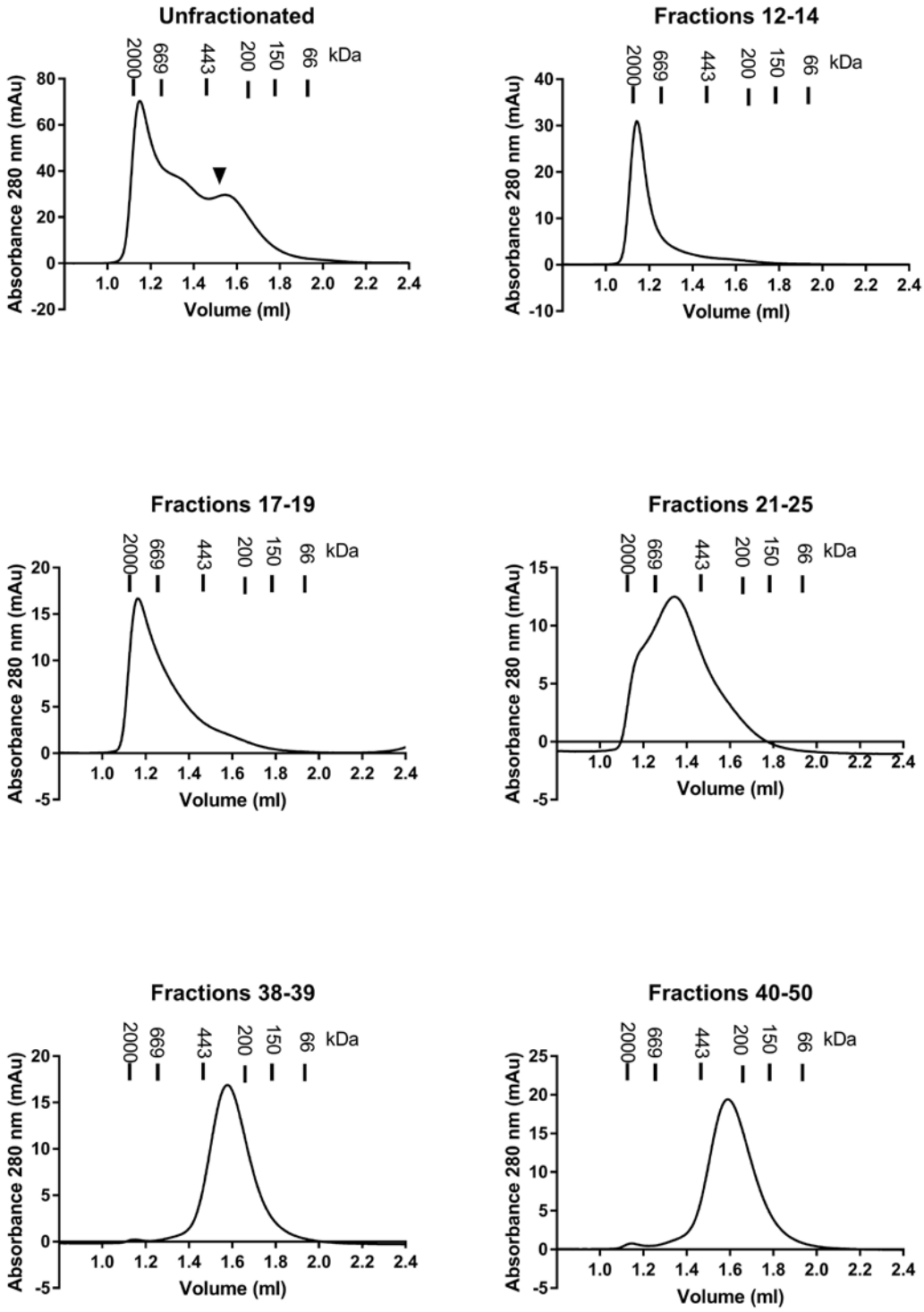

Figure 3.10. Analytical SEC on scmCD70-m1 fractions. Proteins produced by stable transfection of CHO-K1S cells were fractionated into five different fractions with lower fraction numbers consisting of the oligomer structures and fractions 38-39 and 40-50 consisting of the dimer-of-trimer structure. The peak corresponding to the dimer-of-trimer structure is indicated with an arrow on the unfractionated graph. 10 µg of each sample was run on Superdex 200, 5/150 GL (GE Healthcare) column with 0.3 ml/min flow rate.

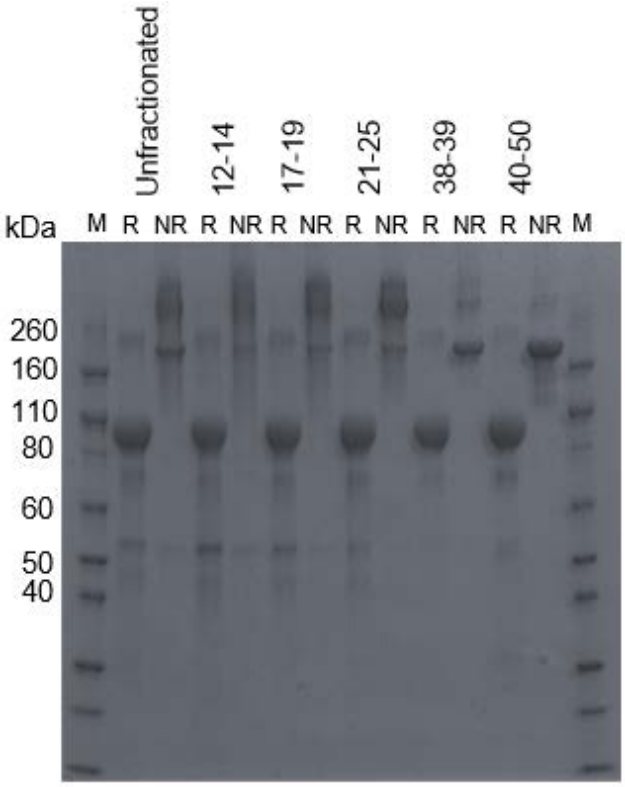

Figure 3.11. Purity of different scmCD70-m1 fractions. After being fractionated via SEC, the purity of different fractions of scmCD70-m1 was confirmed under reduced and non-reduced conditions via SDS-PAGE analysis. As before, final reducing agent (DTT) concentration was 62.5 mM. Samples were boiled at 95 °C for 5 mins before loading 10 µg of protein per lane into the 4-12% Bis-Tris gradient gel. The gel was run for 1.5 hrs at 150 V and stained with Coomassie brilliant blue. M; marker lane, R; reduced, NR; non-reduced. Values above indicate the fractions as indicated in Figure 3.9.

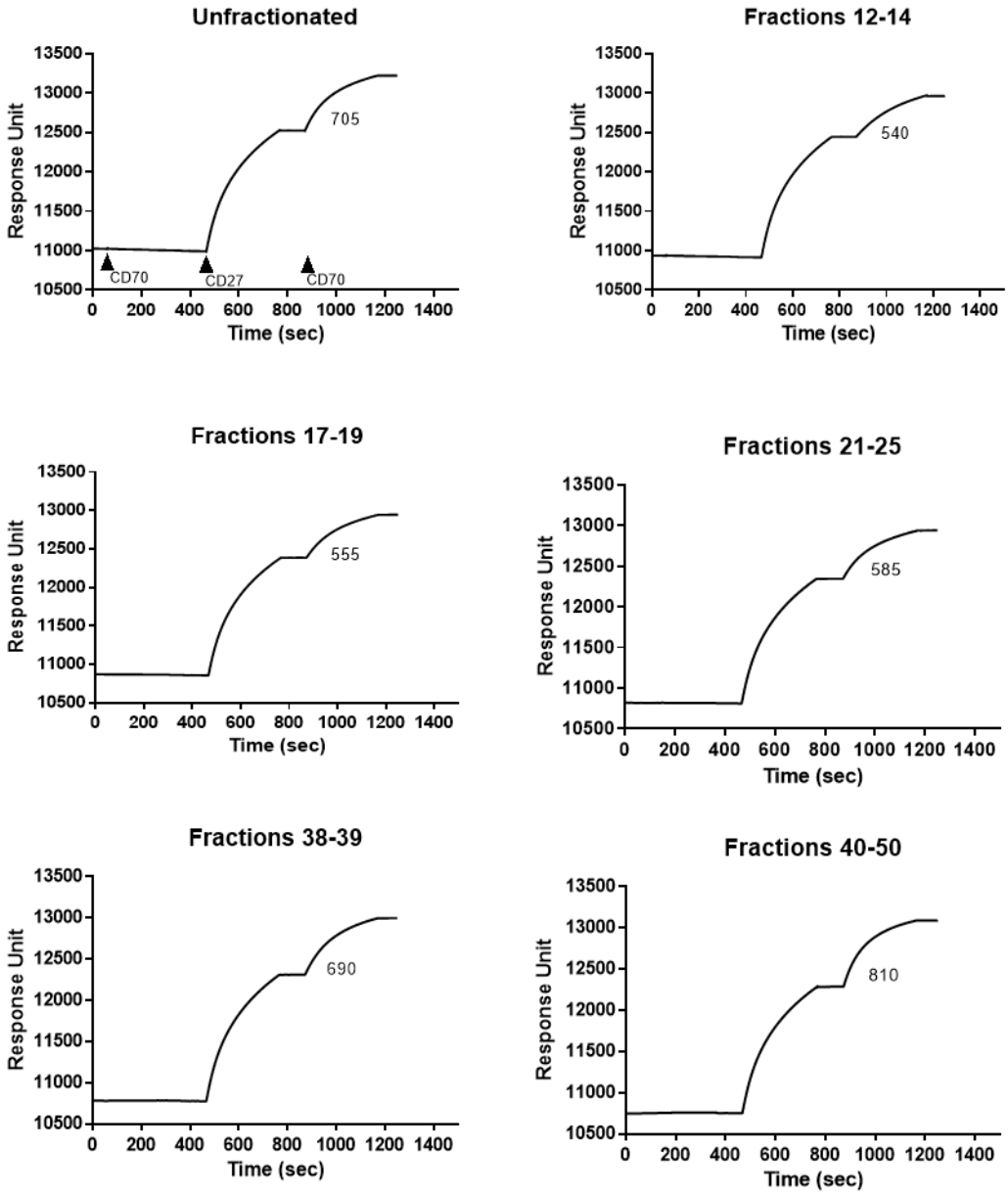

Figure 3.12. Interaction of different scmCD70-m1 fractions with rmCD27-hFc. Fractions of scmCD70-m1 were tested by SPR for their ability to interact with recombinant mouse CD27. A chip as described in Figure 3.7.C was used to detect binding. Fractions were first injected to detect background binding, then rmCD27-hFc was captured on the chip and scmCD70-m1 fractions were injected to confirm binding to rmCD27-hFc. A flow rate of 10 µl/min for 5 mins was used for each injection; rmCD27-hFc was used at 5 µg/ml and fractions were used at 10 µg/ml in HBS-EP+. Labels on the unfractionated graph indicate the timings of injections and apply to all graphs. Numbers on graphs indicate the RU achieved due to interaction between scmCD70-m1 and rmCD27-hFc. CD70; injected scmCD70-m1 fraction, CD27; rmCD27-hFc.

After confirming the purity of scmCD70-m1 fractions and their ability to interact with recombinant mouse CD27, the individual fractions were tested in an in vitro T-cell proliferation assay. Compared to the previous assay (Fig. 3.8) the background proliferation of cells treated with anti-CD3 and mIgG1 control stimulation appeared to be higher (Fig. 3.13) which may reflect the increased activation of T cells in this particular experiment. However, a dose-dependent response to anti-CD3 and mIgG1 was still apparent and similar to the previous assay. The unfractionated scmCD70-m1 sample contributed to a 3-fold higher level of proliferation of activated T cells compared with cells stimulated with anti-CD3 alone, which is similar to the results observed previously (Fig. 3.13, compare with Fig. 3.8).

Comparing the agonistic activity of individual fractions of scmCD70-m1 revealed that fractions 12-14 and 21-25 with only higher oligomeric structures contributed to a similar or higher response than the unfractionated scmCD70-m1 whereas fractions 17-19 were less active than unfractionated (Fig. 3.13). Fractions 38-39 and 40-50 were fractionated separately to ensure high purity of the 40-50 fraction. Both samples appeared very similar on analytical SEC and SDS-PAGE analysis (Figs. 3.10 and 3.11). Thus, with higher purity, only fraction 40-50 was tested in the T-cell activation assay. Dimer-of-trimer (fraction 40-50) induced a 2-fold higher response compared to control but was less active compared to unfractionated and higher oligomeric fractions. (Fig. 3.13).

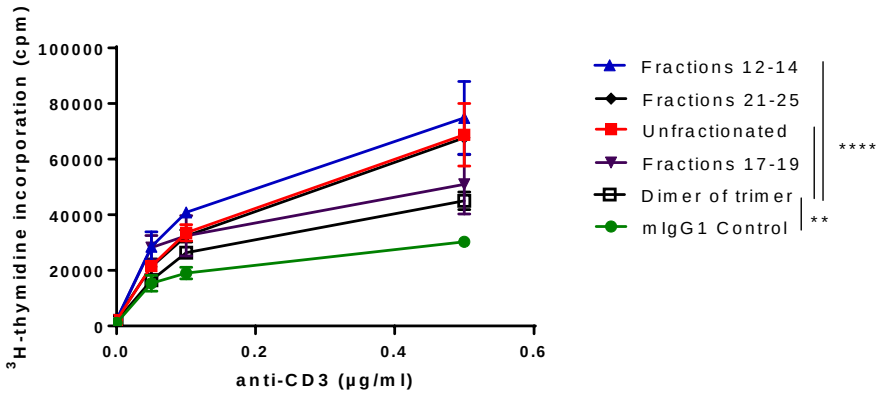

Figure 3.13. Proliferation of T cells induced by scmCD70-m1 fractions. Splenocytes from a WT C57BL/6 mouse were stimulated with anti-CD3 mAb (clone 145-2C11) in combination with either mIgG1 control (anti-human CD16-clone 3G8) or scmCD70-m1 fractions. 2 x 10^5 cells were stimulated with indicated concentrations of anti-CD3 and 10 µg/ml of scmCD70-m1 proteins. Triplicates were used for each anti-CD3 concentration. Lower fraction size indicates higher oligomeric structure. Activation of cells was confirmed by ^{3}H-thymidine incorporation which was added at 48 hrs post-stimulation and harvested after 17 hrs of incubation. Two-way ANOVA with post Tukey's multiple comparisons test was performed for statistical analyses and statistics at the highest concentration of anti-CD3 are indicated. **= p<0.01, ****=p<0.0001. Plots represent mean +/- SEM from one experiment.

According to the SPR (Fig. 3.12) and T-cell activation assay results (Fig. 3.13), the dimer-of-trimer (40-50) form of scmCD70-m1 could interact with recombinant mouse CD27 but was less able to induce activation compared with the oligomeric proteins (fraction 12-14, 17-19 and 21-25, Fig. 3.13) or the unfractionated form (Fig. 3.13). These data suggest that while all fractions can interact with CD27, the dimer-of-trimer may not be able to recruit enough receptors on the cell surface to form the multi-molecular signalling complex required for receptor activation. We therefore hypothesised that dimer-of-trimer proteins might not be able to effectively interact with Fc receptors to receive additional cross-linking which would contribute to an additive effect and a higher level of activation of T cells. Thus the Fc receptor interaction of the dimer-of-trimer fraction (40-50) was investigated. The unfractionated and fraction 40-50 versions of scmCD70-m1 were compared with Lob 12.0, an anti-mouse 4-1BB mouse IgG1 mAb, for their ability to bind to recombinant mouse FcγRIIB by SPR. Two different concentrations of FcγRIIB were tested and at both concentrations, the unfractionated sample showed only low binding whereas the dimer-of-trimer form showed slightly higher binding with Lob12.0 showing the highest binding to FcγRIIB (Fig. 3.14). In a separate experiment, the affinities of these three protein forms for FcγRIIB were determined using a range of concentrations. The dimer-of-trimer form of scmCD70-m1 showed a weak interaction with FcγRIIB with KD: 3.56×10^{-7} M (Fig 3.15). For comparison, the unfractionated form had an apparent KD of 4.16×10^{-7} M and Lob12.0, 3.1×10^{-7} M. Overall, these results indicate that the dimer-of-trimer can induce signalling through CD27 and can interact with FcγRIIB, indicating that it has the potential of being cross-linked, but the higher order structures are still more active.

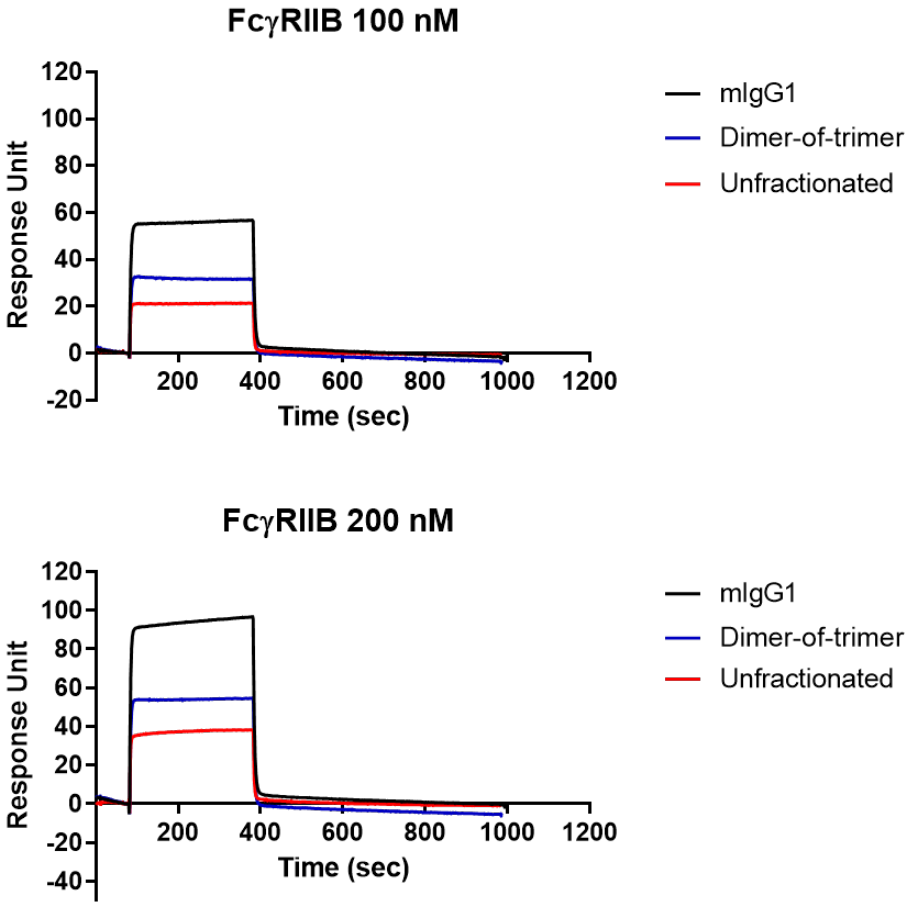

Figure 3.14. Interaction of scmCD70-m1 fractions with FcγRIIB. To investigate the ability of different forms of scmCD70-m1 to interact with FcγRIIB, mIgG1 control (Lob 12.0), fraction 40-50 and unfractionated samples were immobilized on flow cells in a CM5 sensor chip via amine coupling; approximately 3000 RU was reached for each protein sample. FcγRIIB was then injected over the flow cells at the indicated concentrations with 5 mins association (30 µl/min) and 10 mins dissociation time.

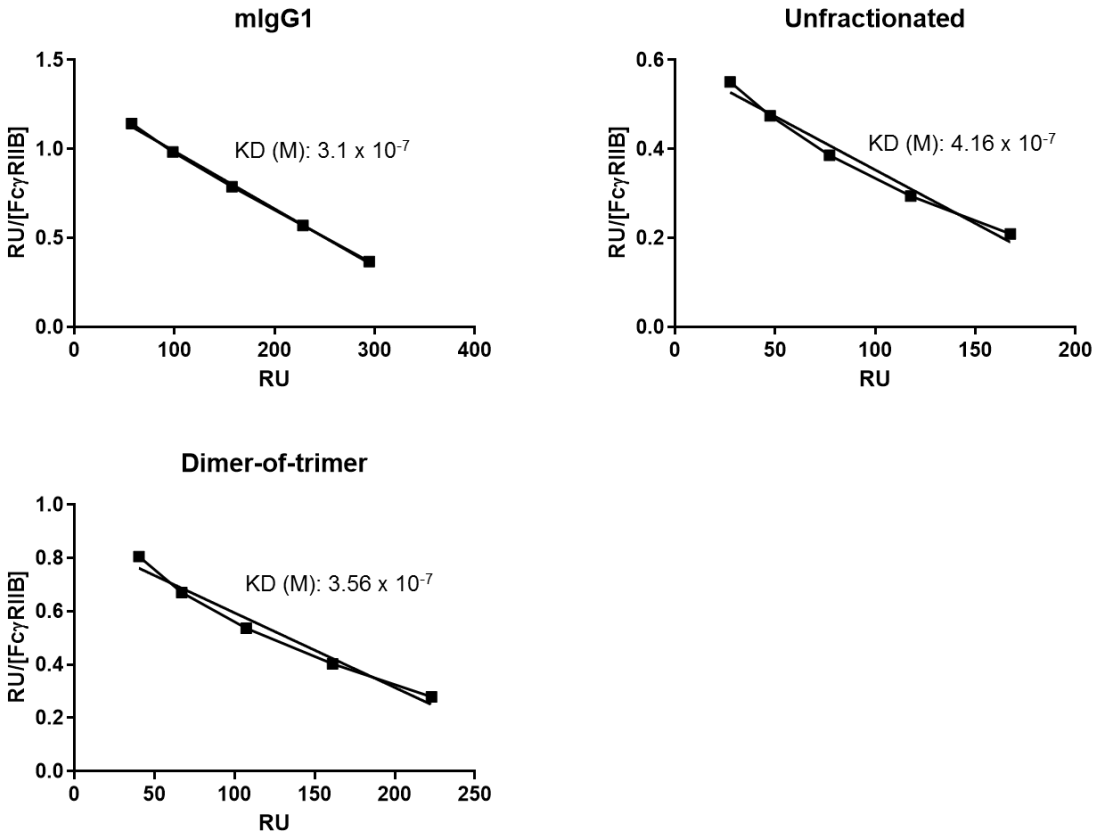

Figure 3.15. Affinity of scmCD70-m1 forms for FcγRIIB detected by SPR. FcγRIIB was run on flow cells with indicated proteins immobilized in the flow cell of CM5 sensor chip via amine coupling. Approximately 3000 RU was achieved for each protein sample during immobilization. Samples were run with 5 mins (30 µl/min) association and 10 mins dissociation time. Various FcγRIIB concentrations; 50, 100, 200, 400 and 800 nM, were used to generate a graph which was then transformed to calculate the KD. RU values for each FcγRIIB concentration were divided by the concentration and plotted against RU. The KD was calculated from the gradient using the equation m (gradient) = -1/KD. The plot with individual points and the line of best fit are illustrated on the graph.

Although unfractionated and oligomeric fractions induced a strong proliferation of T cells, it is unlikely that these will be suitable as therapeutics. Thus, further experiments focussed on characterising and enhancing the activity of the dimer-of-trimer form of scmCD70-m1.

In order to generate more protein, fractionation of scmCD70-m1 was repeated and only the dimer-of-trimer protein was isolated (Fig. 3.16.A). The purity of this product was confirmed by SDS-PAGE (Fig. 3.16.B) and analytical SEC (Fig. 3.16.C) as described previously. The dimer-of-trimer protein was then compared to anti-CD27 mAb (AT124-1) in a T-cell activation assay where splenocytes were stimulated with agonistic anti-CD3 mAb in combination with control, dimer-of-trimer scmCD70-m1 or anti-CD27 mAb (Fig. 3.17). AT124-1 is an anti-mouse CD27 rat IgG2a mAb that is known to have high agonistic activity (189) and which was therefore used as a positive control in these assays. Isotype controls for both scmCD70-m1 and AT124-1 were included in the assay. Activated cells form clumps and as expected, stimulation with anti-CD27 improved the clumping and activation of T cells (Fig. 3.17.A). Additionally, the dimer-of-trimer scmCD70-m1 induced enhanced clustering and activation of T cells compared to control (Fig. 3.17.A). Activation of cells was also assessed by ^{3}H-thymidine incorporation. As previously, a dose-dependent response to anti-CD3 mAb was observed in the control groups (Fig. 3.17.B). Similar to improved clustering of T cells, stimulation with scmCD70-m1 and anti-CD27 showed increased ^{3}H-thymidine uptake compared to control groups (Fig. 3.17.B) with scmCD70-m1 showing a similar level of activity compared with anti-CD27 mAb.

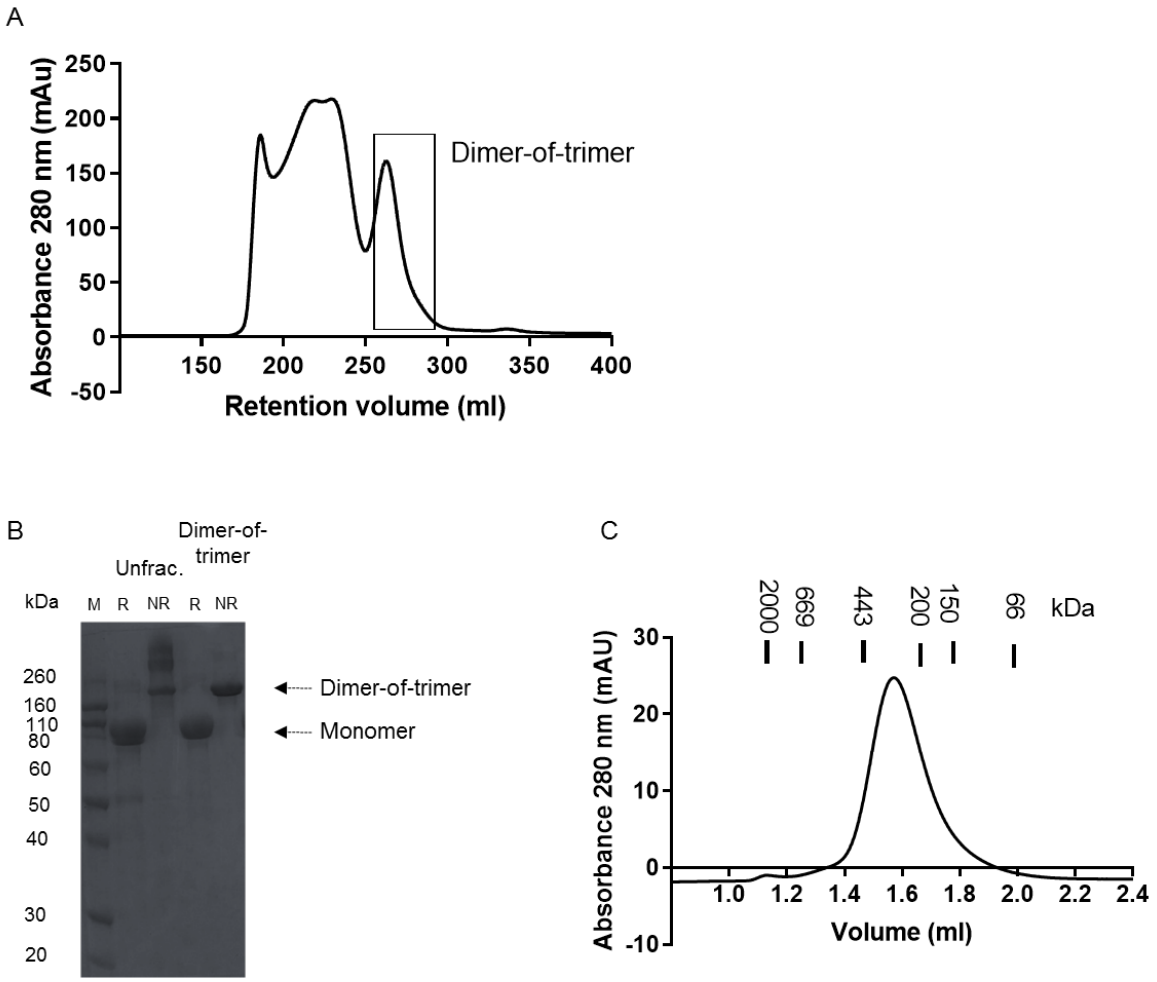

Figure 3.16. Fractionation and purity of dimer-of-trimer scmCD70-m1. Stable CHO-K1S produced scmCD70-m1 protein was purified by protein A affinity chromatography and further fractionated via SEC. (A) Dimer-of-trimer scmCD70-m1 was fractionated using the S200 26/950 column (in-house) with 3 ml/min flow rate. The fraction isolated is indicated on the graph. (B) SDS-PAGE analysis confirming the purity of dimer-of-trimer after fractionation. Unfractionated and dimer-of-trimer samples were run under reduced (R) and non-reduced (NR) conditions. Final reducing agent (DTT) concentration was 62.5 mM. Samples were boiled at 95 °C for 5 mins before loading into the 10% Bis-Tris gel. 10 µg of protein per lane was loaded and the gel was run for 1.5 hrs at 150 V before being stained with Coomassie brilliant blue. M; marker lane. (C) Analytical SEC of the isolated dimer-of-trimer. The sample (10 µg) was run on Superdex 200, 5/150 GL (GE Healthcare) with 0.3 ml/min flow rate.

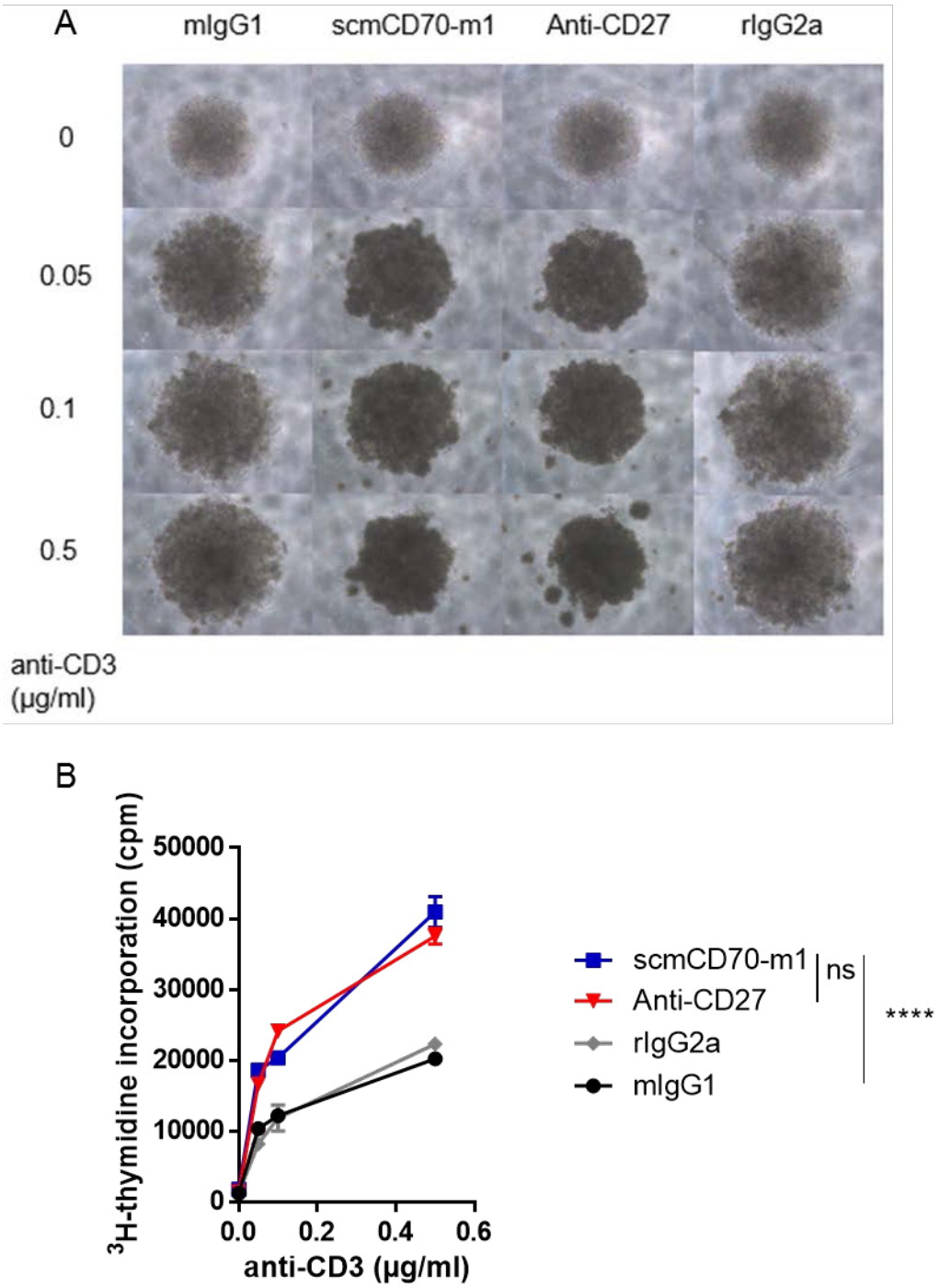

Figure 3.17. Comparison of T-cell activation by scmCD70-m1 dimer-of-trimer and anti-CD27 mAb. Splenocytes (2 x 10^5) from a WT C57BL/6 mouse were stimulated with agonistic anti-CD3 mAb (clone 145-2C11) at the concentrations indicated in combination with the indicated proteins at 10 µg/ml. Isotype mIgGI clone 3G8, isotype rIgG2a clone Mc106A5 and anti-CD27 clone AT124-1 rIgG2a were the mAbs used. (A) Phase contrast images of individual wells at 48 hrs time point. (B) Proliferation of T cells assessed by ^{3}H-thymidine incorporation which was added at 48 hrs time point and harvested after 17 hrs incubation in triplicate. Statistical analyses were performed by using two-way ANOVA with Tukey's multiple comparisons test and indicate statistics at the highest anti-CD3 concentration. Ns; not significant, ****= p<0.0001. Means of triplicate wells +/- SEM are indicated from one experiment.

3.2.4 scmCD70-m1 Fc Engineering

The aim of designing the single chain trimer of CD70 was to produce a homogeneous product as a dimer-of-trimer with minimal higher order structure formation. However, the majority of the scmCD70-m1 protein expressed by CHO-K1S cells was oligomeric with the dimer-of-trimer form being a relatively minor fraction. Although, the dimer-of-trimer form could be fractionated from the oligomers, a better expression system to produce more homogeneous product was required. Results from SDS-PAGE analysis (Fig. 3.11) suggested that production of oligomers could be due to disulphide bond formation. Therefore, we generated a new protein product (scmCD70-m1 Version II) in which the three Cys residues in the hinge region of the Fc domain of scmCD70-m1, at positions 535, 538 and 540 (see Appendix Fig. 1), were mutated to Ala residues to prevent disulphide formation (Fig. 3.18). The aim of mutating the Cys residues in the hinge region was to avoid the formation of disulphide bonds in the hinge region which may contribute to oligomer formation.

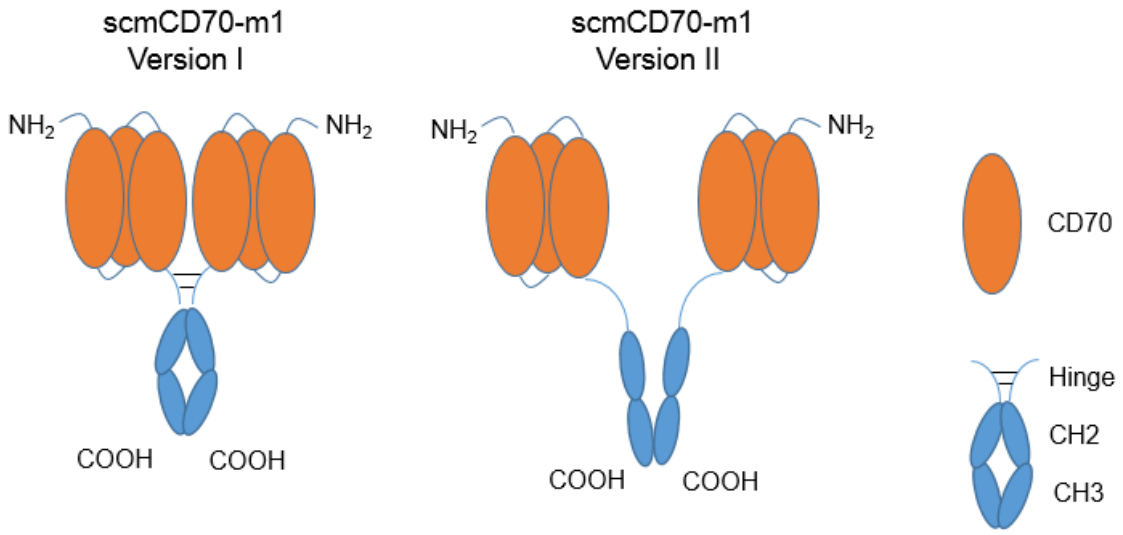

Figure 3.18. Structures of scmCD70-m1 Version I and Version II. Hexameric ligand structures with one Fc domain are illustrated. Version II has a mutant hinge region predicted to have no disulphide bonding.

Previously scmCD70-m1 was stably expressed by CHO-K1S cells. In order to obtain results in a shorter time period, Version (Ver) II was produced by transient transfection of 293F cells and for transient transfection, pcDNA3.1 (+) plasmid was used as the expression vector. The DNA sequence of the Ver II Fc domain with the mutations was ordered in a commercial plasmid (PMA-T) and the insert therefore needed to be moved into pcDNA3.1

(+). The DNA sequence of the original scmCD70-m1 construct was designed to have an XbaI restriction site to enable changing of the Fc domain only. Thus, Ver II Fc was first cloned into the pEE14-scmCD70-m1 vector to replace the original Fc domain using XbaI and EcoRI digestion. The entire insert was then cloned into pcDNA3.1 (+) vector with HindIII and EcoRI digestion (see Appendix Fig. 5). Therefore, pEE14-scmCD70-m1 plasmid was double digested with XbaI and EcoRI and the vector without the Fc domain was extracted from the gel (Fig. 3.19.A). Simultaneously, the PMA-T-Ver II Fc insert was digested with XbaI and EcoRI and the insert extracted from the gel (Fig. 3.19.B). Products were quantified and purity confirmed by ensuring the 260/280 ratio of the resultant DNA was between 1.8 and 2.0. Then the products were ligated at a 3:1 insert to vector Molar ratio using 3.9 ng of insert and 20 ng of vector in a 20 µl reaction. The reaction was carried out for 3 hrs at RT and 2 µl of ligation reaction was transformed into OneShot TOP10 cells. Mini-cultures from six individual colonies grown on amp supplemented plates were grown and DNA isolated using commercial kits. 400 ng of plasmid from each colony was digested with XbaI and EcoRI for 2 hrs at 37 °C and ligation confirmed by visualisation on a 1% agarose gel (Fig. 3.19.C). All six clones showed successful ligation and transformation of the pEE14-scmCD70-m1 Ver II construct.

After confirming the ligation of the Ver II insert into the pEE14 vector, pcDNA3.1 (+) containing scmCD70-m1 Ver I and pEE14 containing the Ver II insert were digested. pcDNA3.1 (+) vector was first digested with EcoRI only and a small amount of plasmid visualised on a 1% agarose gel to confirm EcoRI activity (Fig. 3.20.A). The remaining cut pcDNA3.1 (+) was cleaned in solution and the recovered DNA (3.2 µg) was then subjected to HindIII digestion (15 units) for 2 hrs at 37 °C prior to running on a 1% agarose gel to confirm double digestion. The cut vector was then extracted from the gel (Fig.3.20.B). Simultaneously, 3 µg of pEE14 – Ver II plasmid DNA was digested with 15 units of both HindIII and EcoRI at 37 °C for 2 hrs and the insert extracted from the gel after running the products on a 1% agarose gel (Fig. 3.20.C). The Ver II insert was ligated into the cut pcDNA3.1 (+) vector at a 3:1 insert to vector Molar ratio using 25.56 ng of insert and 20 ng of vector in a 20 µl reaction. The reaction was carried out for 3 hrs at RT and 2 µl of ligation reaction was transformed into OneShot TOP10 cells. Ligation was confirmed by growing mini-cultures from 4 colonies and digesting a small amount of isolated DNA. Specifically, 400 ng plasmid DNA from each colony was digested with HindIII and EcoRI and products visualised on 1% agarose gel to confirm ligation of the insert (Fig. 3.20.D).

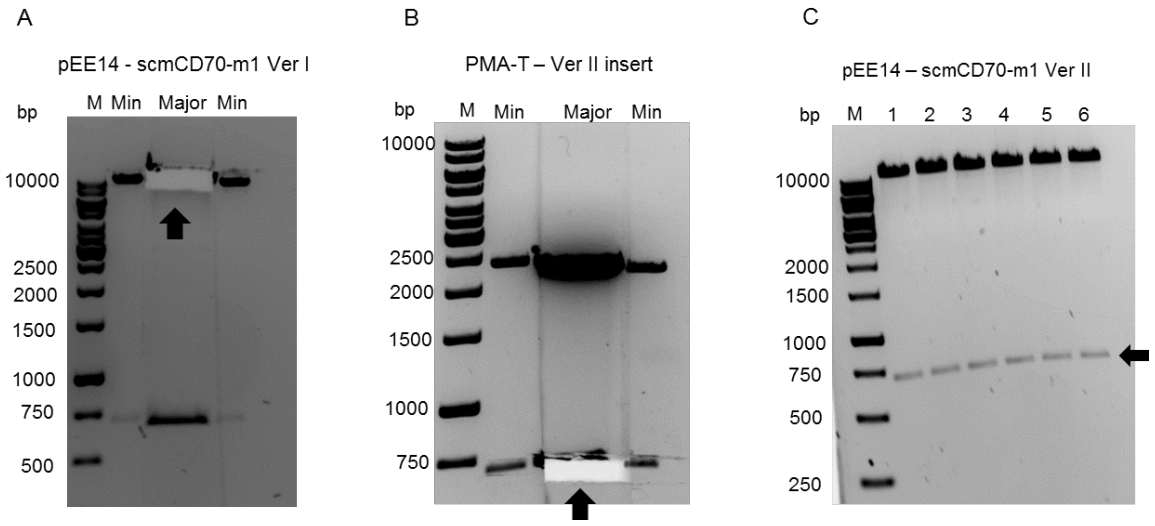

Figure 3.19. Cloning of scmCD70-m1 Ver II insert into pEE14 expression vector. (A) Digestion of pEE14 – scmCD70-m1 Ver I plasmid DNA. 3 µg of plasmid was digested with 15 units of both XbaI and EcoRI restriction enzymes at 37 °C for 2 hrs. 200 ng of digested sample was run in each minor (Min) lane and the rest was run in the major lane. The digested vector was extracted from the gel without exposure to UV light. (B) Digestion of PMA-T-Ver II plasmid DNA. 3 µg of plasmid was digested with 15 units of XbaI and 15 units of EcoRI for 2 hrs at 37 °C. 200 ng of digested sample was run in each minor (Min) lane and the rest was run in the major lane. The digested insert was extracted from the gel without exposure to UV light. (C) Six colonies of pEE14 – scmCD70-m1 Ver II transformed OneShot TOP10 cells were grown in LB-amp cultures for 17 hrs at 37 °C and plasmid DNA was isolated by using mini-prep kits (Qiagen). 400 ng of plasmid DNA from each colony was then digested with 2 units of XbaI and 2 units of EcoRI for 2 hrs at 37 °C and 200 ng of each digest was visualised on an agarose gel. All samples in (A), (B) and (C) were run on 1% agarose gel. Extracted gel samples and Ver II insert are indicated by arrows.

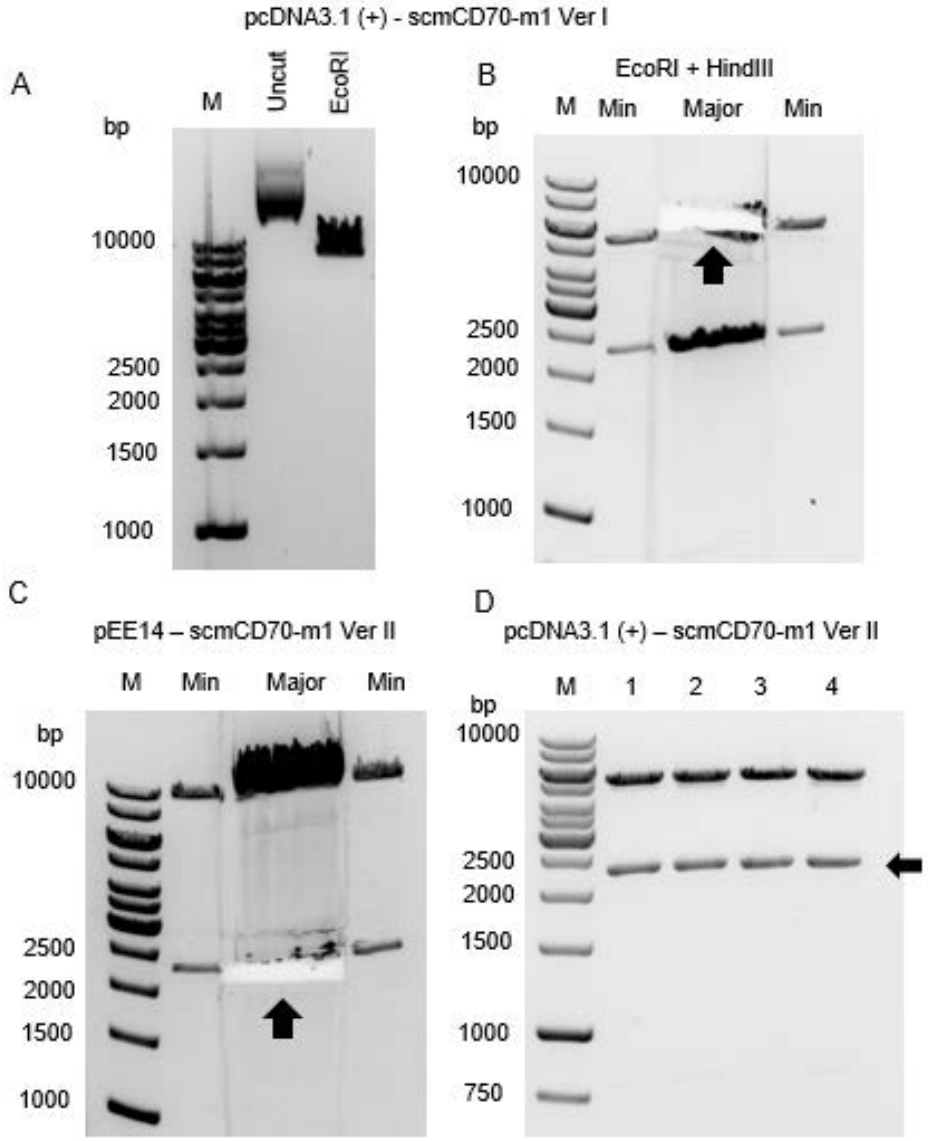

Figure 3.20. Cloning scmCD70-m1 Ver II into pcDNA3.1 (+) vector. (A) pcDNA3.1 (+) – scmCD70-m1 Ver I plasmid DNA was digested with EcoRI restriction enzyme; 4 µg of plasmid DNA was digested with 15 units of enzyme at 37 °C for 2 hrs. A small amount (200 ng) was run on an agarose gel alongside an uncut sample to confirm digestion. (B) EcoRI digested pcDNA3.1 (+) – scmCD70-m1 Ver I plasmid DNA was further digested with HindIII restriction enzyme; 3.2 µg of plasmid DNA was digested with 15 units of enzyme for 2 hrs at 37 °C. 200 ng of digested sample was run in each minor (Min) lane and the rest was run in the major lane. The digested insert was extracted from the gel without exposure to UV light. (C) pEE14 – scmCD70-m1 Ver II DNA was digested with HindIII and EcoRI restriction enzymes; 3 µg of plasmid DNA was digested with 15 units of each enzyme for 2 hrs at 37 °C. 200 ng of digested sample was run in each minor (Min) lane and the rest was run in the major lane. The digested insert was extracted from the gel without exposure to UV light. (D) Four colonies of pcDNA3.1 (+) – scmCD70-m1 Ver II transformed OneShot TOP10 cells were grown in LB-amp cultures for 17 hrs at 37 °C and plasmid DNA was isolated by using mini-prep kits (Qiagen). 400 ng of plasmid DNA from each colony was then digested with 2 units of XbaI and 2 units of EcoRI for 2 hrs at 37 °C and 200 ng of each digest was visualised on an agarose gel. All samples on (A), (B), (C) and (D) were run on 1% agarose gels. Extracted gel samples and Ver II insert are indicated by arrows.

A larger culture was then grown from colony #1 to obtain a greater stock of pcDNA3.1 (+) - scmCD70-m1 Ver II. DNA was then extracted using commercial kits yielding 1 mg DNA with an absorbance ratio at 260/280 nm of 1.97 which was then used to transfect 293F cells. To enable comparison with Ver I, a stock of Ver I protein was also produced in 293F cells. Supernatants were purified on protein A columns as before. The profile of purified Ver I protein from 293F transfection was different from that obtained from CHO-K1S purification (compare Fig. 3.9 with Fig. 3.21.A) such that Version I from 293F was predominantly in a dimer-of-trimer form whereas that from CHO-K1S was in oligomer form. Both Ver I and Ver II proteins from 293F cells showed a purification profile in which the majority of the protein was in the dimer-of-trimer form (major peak) with a low level of oligomer content as the smaller peaks (Fig. 3.21.A). To further purify the dimer-of-trimers, both versions were fractionated by SEC. Fractionation of Version I protein yielded a pure dimer-of-trimer product whereas Ver II contained a low level of additional oligomers (Fig. 3.21.B).

The purities of fractionated and unfractionated protein samples were also confirmed by SDS-PAGE. All of the samples showed a similar appearance under reduced conditions with the proteins being in the monomeric form at approximately 105 kDa (Fig. 3.22). Oligomers were observed under non-reduced conditions for both Ver I and Ver II proteins and these were not present in the fractionated samples. Although Ver I samples showed a faint band at approximately 105 kDa under non-reduced conditions, this was more apparent in Ver II samples indicating the prevention of disulphide bond formation in the latter. However, the dimer-of-trimer form was still present in Ver II samples under non-reduced conditions (Fig. 3.22). This suggested that there might be another interaction that keeps the two polypeptide chains together.

Overall, Ver I and Ver II proteins produced in 293F showed a similar profile and having a mutated hinge (Ver II) did not contribute to less oligomer formation compared to having a non-mutated hinge (Ver I). Further experiments were focussed on improving scmCD70-m1 Ver I production rather than characterising Ver II.

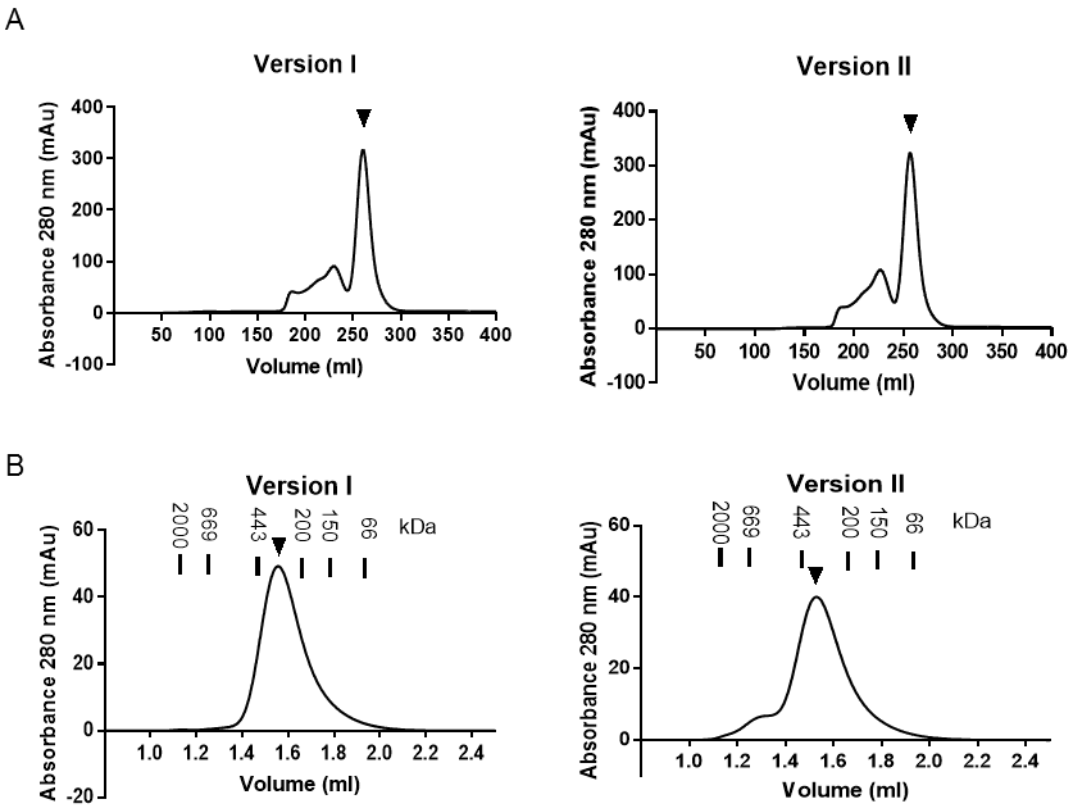

Figure 3.21. Purification of scmCD70-m1 Version I and Version II from transiently transfected 293F cells. 293F cells were transfected with scmCD70-m1 Ver I or Ver II and expanded for 7 days. Protein was isolated from supernatant by protein A purification and both versions were further fractionated by SEC. (A) Profiles of Ver I and Ver II before fractionation. Samples were run on Superdex 200 26/950 (in-house). (B) Profiles of proteins after fractionation and isolation of dimer-of-trimer. 10 µg of samples were run on the analytical Superdex 200 5/150 GL (GE Healthcare) column with 0.3 ml/min flow rate. The major peak corresponding to the dimer-of-trimer is indicated with an arrow. The minor peaks correspond to higher oligomers.

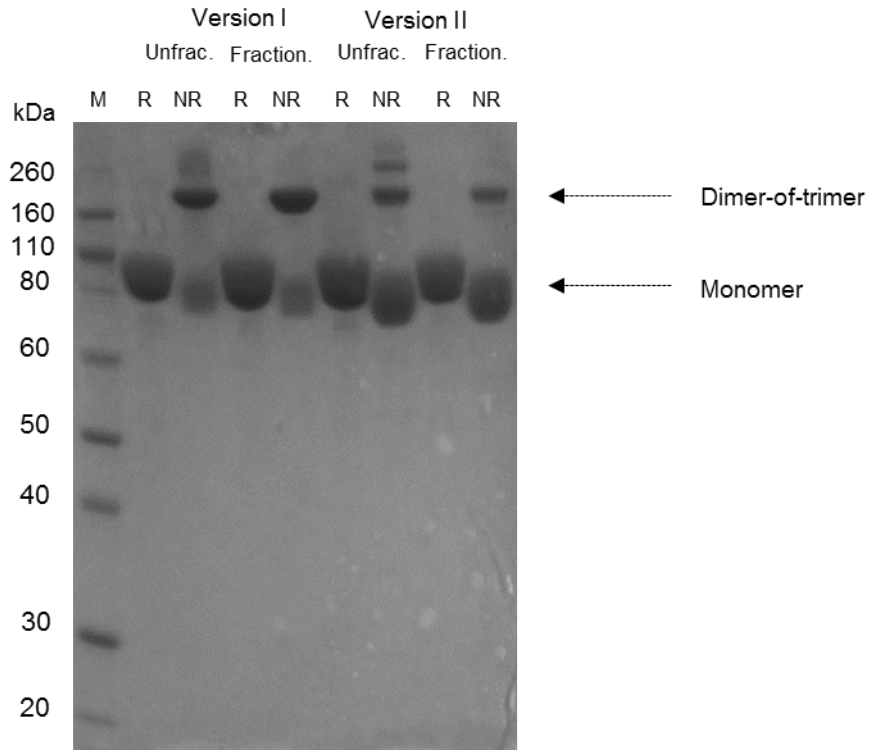

Figure 3.22. The purity of scmCD70-m1 Ver I and Ver II before and after fractionation. Proteins were purified by using a protein A column and further fractionated via SEC. Unfractionated and fractionated (dimer-of-trimer) samples were analysed under reduced and non-reduced conditions. Final reducing agent (DTT) concentration was 62.5 mM. Samples were boiled at 95 °C for 5 mins before loading 10 µg protein/lane into 10% Bis-Tris gel. Gel was Coomassie brilliant blue stained. Monomer and dimer-of-trimer bands are indicated with arrows. M; marker lane, R; reduced, NR; non-reduced, Unfrac; unfractionated, Fraction; fractionated.

For the generation of protein in 293F cells, cells were transiently transfected and cultured for 1 week before harvesting the supernatant and purifying proteins. In contrast, CHO-K1S cells were cultured for approximately 4 weeks before harvesting the supernatant. As both Ver I and Ver II produced a similar level of oligomers when produced in 293F cells and this was less than seen in Ver I protein produced in CHO-K1S cells, we hypothesised that the time in culture could be an important factor contributing to the level of oligomer formation. Thus, scmCD70-m1 Ver I transfected CHO-K1S cells were cultured and supernatants were harvested at 1 week, 2 weeks and 3 weeks intervals to compare the profile of scmCD70-m1 protein. Proteins were purified by protein A chromatography and their profiles analysed by SEC. As hypothesised, the profile of scmCD70-m1 proteins were different at each time point (Fig. 3.23). The highest purity of dimer-of-trimer proteins was observed with a 1 week culture whereas highest oligomer formation was observed with 3 weeks of culture. The profiles suggested that the longer the time in culture, the higher the level of oligomer formation. At the 1 week and 2 week time points, 1L of supernatant was harvested whereas

2L was harvested at 3 weeks. The amount of protein purified from each time point was approximately 13 mgs at 1 week, 55 mgs at 2 weeks and 150 mgs at 3 weeks. This suggested that although the highest purity of the dimer-of-trimer scmCD70-m1 was observed after 1 week of culture, the yield of protein was relatively low. As a good yield could be harvested after 2 weeks of culture and the profile favoured the production of a dimer-of-trimer compared with 3 weeks of culture, subsequent scmCD70-m1 batches were produced by culturing the CHO-K1S cells for 2 weeks and harvesting 5L supernatant to maximise the yield.

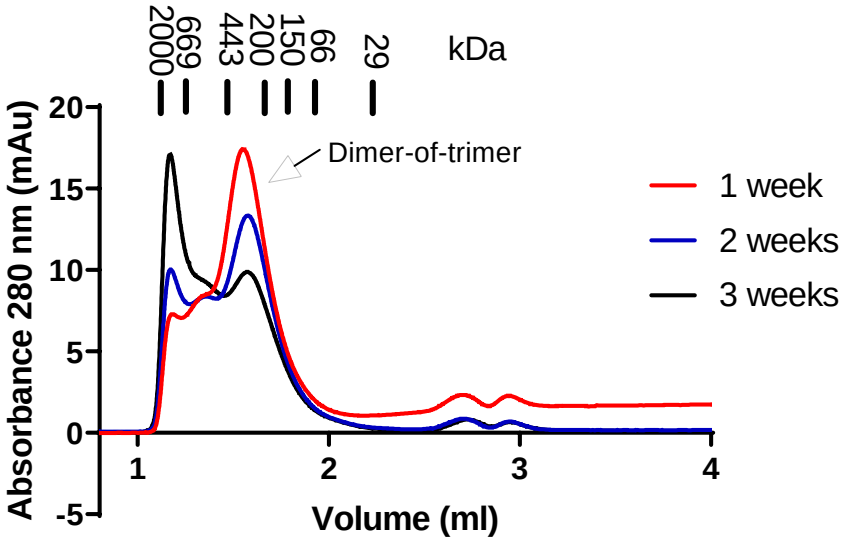

Figure 3.23. Comparison of scmCD70-m1 production in CHO-K1S cells harvested at different time points. CHO-K1S cells stably transfected with scmCD70-m1 were cultured and supernatant harvested at indicated time points. scmCD70-m1 protein was purified by protein A chromatography. Then 10 µg of the purified protein was run on analytical SEC column at 0.3 ml/min flow rate. Samples were run on Superdex 200, 5/150 GL (GE Healthcare).

3.2.5 Production of trimeric CD70 and comparison to dimer-of-trimer scmCD70-m1

Natural ligands of TNF superfamily receptors are expressed as homotrimers. The dimer-of-trimer scmCD70-m1 protein is a hexameric protein capable of inducing activation and proliferation of T cells. To establish the importance of dimer-of-trimeric activity and compare the activity to trimeric ligand, a non-dimerised trimeric version, i.e. a non-covalently linked CD70 trimer, was produced by fusing domains 3 and 4 of mouse CD4 to the extracellular domain of murine CD70 (mCD4-CD70) (Fig. 3.24.A). The CD4 domain was previously used as a tag for purification and is known to be monomeric in solution after being expressed (213). Thus the trimer is predicted to be formed by the non-covalent interactions between CD70 molecules. The DNA sequence of mCD4-CD70 was generated in Seqbuilder (see Appendix Fig. 2) and commercially ordered to be supplied in pcDNA3.1 (+) expression vector (Fig. 3.24.B). The plasmid DNA was amplified by growing transformed bacteria in LB/amp and 1 mg of DNA was isolated using commercial kits. Then 293F cells were transiently transfected and cells were grown for 1 week before harvesting the supernatant. The protein was purified by applying the supernatant on to a column with anti-mCD4 antibody (YTA3.1.2) and 2 mgs of protein was purified. Subsequent analytical SEC (Fig. 3.25.A) and SDS-PAGE (Fig. 3.25.B) analysis confirmed that a homogeneous product was obtained without oligomers. The theoretical MW of the trimer is approximately 39 kDa (using Expasy compute pI/MW tool) and the protein has 5 potential N-linked glycosylation sites which means that a monomeric protein of 51.5 kDa was predicted with the glycosylations. The trimeric protein (approximately 155 kDa) appeared bigger than 200 kDa by SEC and monomeric protein appeared at approximately 50 kDa in SDS-PAGE analysis. The protein is in the native form during SEC analysis and the conformation can influence the elution from the column, indicating a slightly bigger than predicted size. However, the non-covalent interactions are lost during SDS-PAGE analysis and the monomeric protein appears at the predicted size. The purified protein also bound to CD27 by using SPR analysis (Fig. 3.25.C).

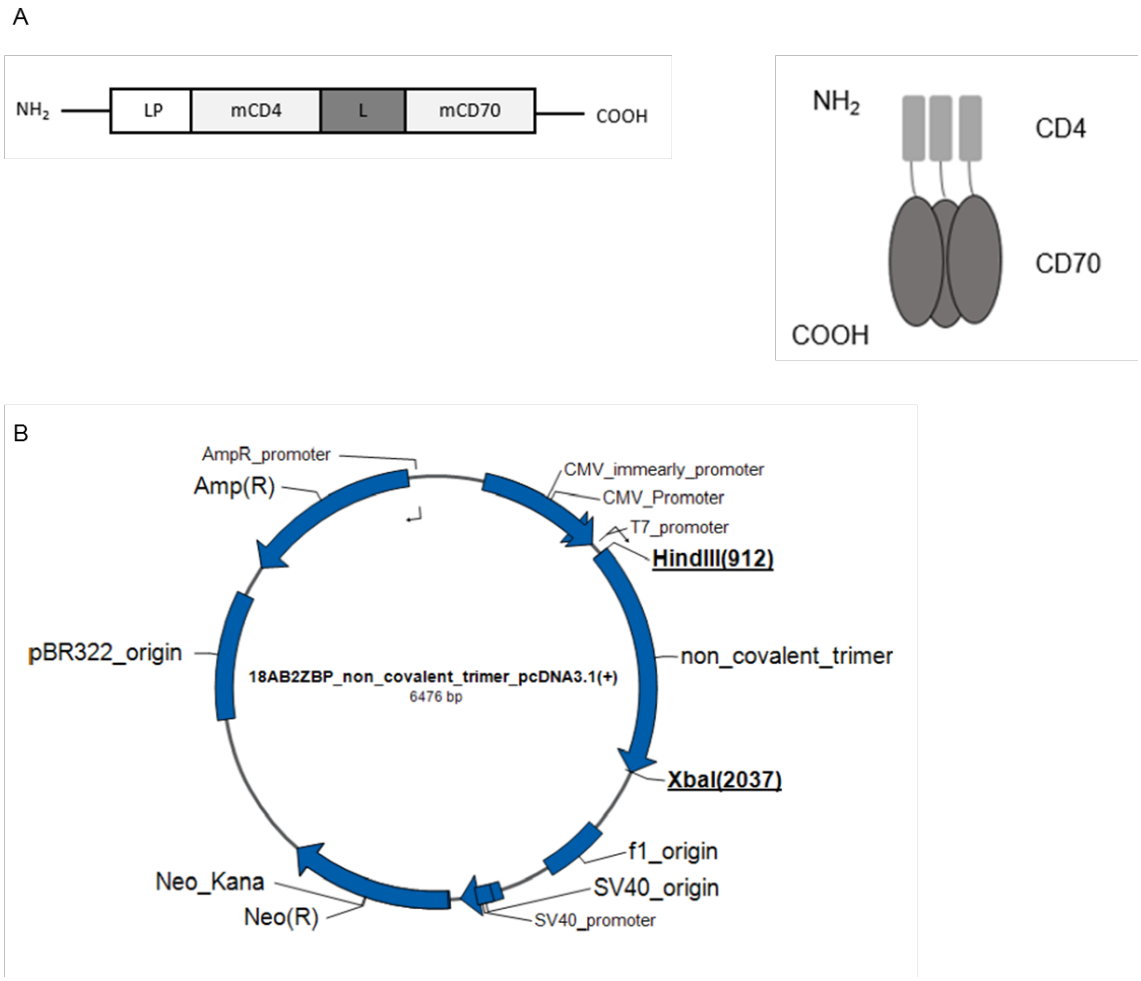

Figure 3.24. Schematic representation and predicted structure of trimeric CD70. (A) The sequence alignment of mCD4-CD70 insert and predicted structure of the mCD4-CD70 protein. The mCD4 domain was conjugated to the CD70 domain with a GGGS linker. The N and C-termini are indicated on the figure. LP; leader peptide, mCD4; mouse CD4 domains 3 and 4, L; GGGS linker, mCD70; mouse CD70. (B) Plasmid map of the mCD4-CD70 insert in pcDNA3.1 (+) expression vector. The insert was flanked with HindIII and XbaI restriction enzyme sites to enable further cloning into another expression vector.

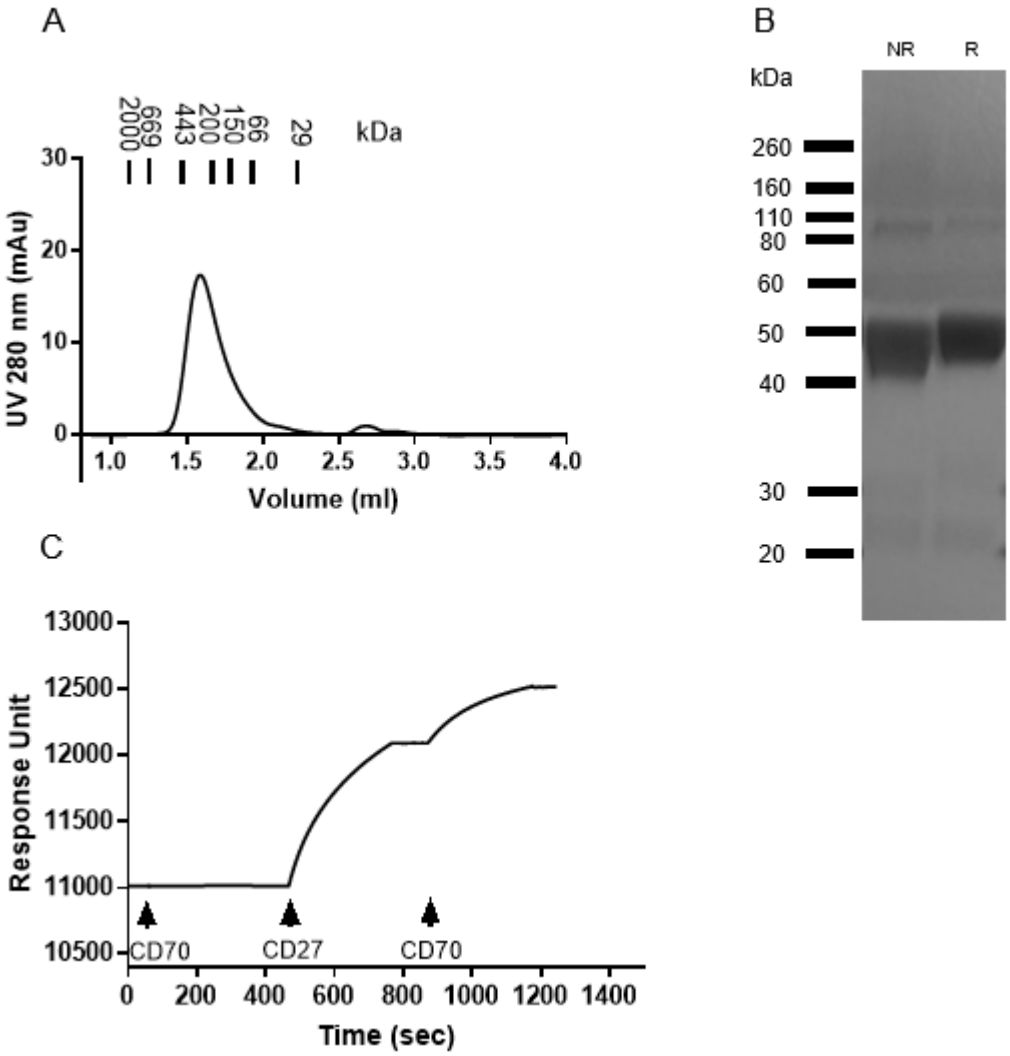

Figure 3.25. Confirmation of the purity and CD27-binding capacity of the mCD4-CD70 trimer. 293F cells were transiently transfected with mCD4-CD70 plasmid and supernatant harvested after 7 days. Protein was purified using immunoaffinity chromatography with a column prepared by conjugating CnBr activated Sepharose beads to anti-mouse CD4 antibody (YTA3.1.2). (A) Purified protein was run on an analytical SEC column. 10 µg of protein was run on Superdex 200 5/150 GL (GE Healthcare) with 0.3 ml/min flow rate. (B) Purity was also checked via SDS-PAGE under reduced (final reducing agent (DTT) concentration was 62.5 mM) or non-reduced conditions. In both cases, samples were boiled at 95 °C for 5 mins before loading 10 µg protein/lane into a 10% Bis-Tris gel. The gel was Coomassie brilliant blue stained. M; marker lane, NR; non-reduced, R; reduced. (C) Binding of mCD4-CD70 to rmCD27-hFc by SPR analysis. An anti-human IgG CM5 sensor chip was used to assess binding. The trimer was first injected to confirm no background binding to the chip. Then rmCD27-hFc was injected at 5 µg/ml and captured on the chip. Finally, mCD4-CD70 was injected at 10 µg/ml and binding to rmCD27-hFc was detected. Samples were prepared in HBS-EP+ running buffer and injected with the flow rate 10 µl/min for 5 mins. Arrows indicate the solution injected at that time point. CD70; mCD4-CD70, CD27; rmCD27-hFc.

After confirming the purity and CD27 interaction of mCD4-CD70, a T-cell proliferation assay was set up to compare the activity of the trimeric mCD4-CD70 with the dimer-of-trimer scmCD70-m1. An isotype control mAb was used as a negative control for scmCD70-m1; no negative control was used for the mCD4-CD70 protein. A positive control (anti-CD27 mAb, AT124-1 mIgG1) was also used in the assay. Previously, the parental AT124-1 mAb was used as a rIgG2a isotype (Fig. 3.17) but in this experiment the mIgG1 isotype was used as it possesses the same Fc domain with scmCD70-m1. Mouse splenocytes were stimulated with agonistic anti-CD3 mAb in combination with control, mCD4-CD70 trimer, scmCD70-m1 dimer-of-trimer or agonistic anti-CD27 mAb. As previously observed, increasing anti-CD3 concentration increased the level of proliferation in cells stimulated with mIgG1 control (Fig. 3.26). Interestingly, trimeric mCD4-CD70 did not induce any further proliferation whereas the dimer-of-trimer scmCD70-m1 induced a strong stimulation of T cells. The dimer-of-trimer scmCD70-m1 protein induced a similar level of stimulation compared to that induced by the agonistic anti-CD27 mAb at low anti-CD3 concentrations, but the activity was higher at the highest anti-CD3 concentration (Fig. 3.26).

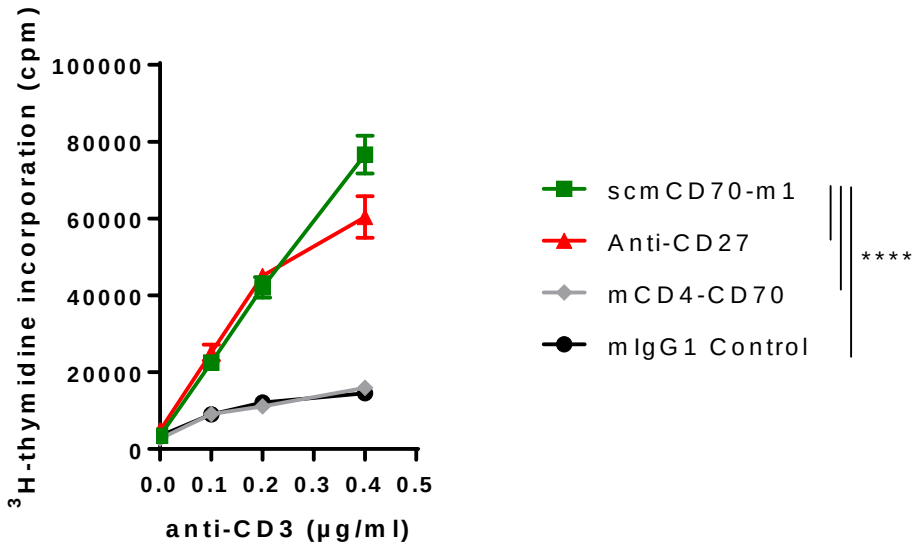

Figure 3.26. Proliferation of T cells stimulated with trimeric mCD4-CD70 or dimer-of-trimer scmCD70-m1. Splenocytes (2 x 10^5) from a WT C57BL/6 mouse were stimulated with agonistic anti-CD3 mAb (clone 145-2C11) at the indicated concentrations in combination with the indicated proteins at 10 µg/ml. ^{3}H-thymidine was added at 48 hrs post-stimulation and was harvested after 17 hrs of incubation. Cells were plated in triplicate and data show the mean +/- SEM of triplicates. Statistical analyses were performed using two-way ANOVA with Tukey's multiple comparisons test and statistics at the highest anti-CD3 concentration are indicated. ****= $p<0.0001$. Data representative of two independent experiments.

3.3 Discussion

Data presented in this chapter illustrate that an active soluble recombinant form of CD70, scmCD70-m1, can be produced and the recombinant protein can induce in vitro T-cell proliferation. Although, higher order structures induced a higher level of T-cell proliferation, the dimer-of-trimer scmCD70-m1 protein could also induce robust proliferation of T cells whereas trimeric CD70 ligand could not induce CD27 mediated activation. Additionally, the culture conditions during recombinant scmCD70-m1 production are important in order to obtain an optimal yield with high purity of the dimer-of-trimer product.

The recombinant protein scmCD70-m1, was designed to yield a homogeneous product, improved structure and improved in vivo half-life compared to first generation soluble CD70 (Fig. 3.1). Also, it was designed to act as a co-stimulatory agent to induce CD27 signalling without requiring FcγRs. Initially, the protein was synthesised in CHO-K1S cells, however, the majority of the proteins purified from CHO-K1S cells were in the oligomeric state which was similar to the profile observed when first generation soluble CD70 was produced in CHO-K1 cells (data not shown). Nonetheless, the purified sample could interact with recombinant mouse CD27 by SPR and importantly, significantly enhanced T-cell activation in vitro. Proteins were then fractionated in order to isolate higher order structures and dimer-of-trimer proteins separately to examine their ability to stimulate T-cell activation/proliferation. After fractionation, the dimer-of-trimer fractions (38-39 and 40-50) had minimal oligomer content and consisted of approximately >95% dimer-of-trimer structures.

Despite the ability of the dimer-of-trimer to interact with recombinant CD27, confirmed by SPR, this fraction (40-50) was slightly less active than oligomeric proteins in in vitro T-cell proliferation assay (Fig. 3.13) yet comparable to an agonist anti-CD27 antibody (Fig.3.17 & 3.26) and still able to induce substantial proliferation. It was previously shown that stimulating CD27 with soluble trimeric ligand was not sufficient to induce CD27 mediated activation, and higher order clustering was required to activate the receptor (215). This was also confirmed by results presented here, as the soluble recombinant trimeric ligand (mCD4-CD70) was not able to induce T-cell activation (Fig. 3.26) through CD27 whereas the dimer-of-trimer scmCD70-m1 was able to activate CD27 and T-cell proliferation. The higher order fractions of scmCD70-m1 possibly induce higher clustering of CD27 compared

to the dimer-of-trimer form, leading to stronger activation of T cells. Although the oligomeric fractions were more active in vitro, only the dimer-of-trimer protein was further characterised as a homogeneous product considering the ultimate aim of using it in in vivo studies. The main problem with higher order structures is not being able to obtain a homogeneous product. The product could be different after each production and this can influence the complete characterisation.

Initial purification and analysis of scmCD70-m1 under reduced and non-reduced condition with SDS-PAGE (Fig. 3.11), suggested that oligomerisation of the scmCD70-m1 could be disulphide-bonding related. For this reason, scmCD70-m1 Ver II was designed and produced in order to remove disulphide bonds in the hinge region of the Fc domain, to improve the homogeneity and reduce oligomer formation. When Ver II proteins were analysed under non-reducing conditions by SDS-PAGE, they still formed dimers and higher order structures (Fig. 3.22). Non-covalent interactions are broken under non-reducing conditions and results suggested that the higher order structures observed with Ver II protein were covalently linked, possibly indicating that there could be other Cys residues contributing to disulphide formation. There are 5 Cys residues in each CD70 domain and 4 Cys residues in each Fc domain in scmCD70-m1 and these might be involved in disulphide formation.

In order to obtain proteins in a shorter period, scmCD70-m1 Ver II was produced by transient transfection of 293F cells from which the supernatant was harvested after 1 week culture. To enable comparison of the two proteins, scmCD70-m1 Ver I was also produced in 293F cells and this revealed that both proteins were purified with similar profiles and generated a very similar low level of higher order structures. This suggested that the relatively high level of oligomerisation observed in the CHO-K1S-produced scmCD70-m1 Ver I compared with the 293F produced protein could be due to: 1) CHO-K1S cells producing the protein in a higher oligomeric state compared to 293F cells. 2) The time of culture, as the supernatant from 293F cells was harvested after 1 week whereas supernatant from CHO-K1S cells was harvested after a 4 week culture.

In order to address the role that time of culture may play in influencing the protein product, scmCD70-m1 Ver I was produced in CHO-K1S cells and supernatant was harvested after 1 week, 2 weeks and 3 weeks of culture. These results revealed that increasing the time of

culture increases the level of oligomer formation (Fig. 3.23) and suggested that scmCD70-m1 Ver I could be produced in CHO-K1S cells with a lower level of oligomers simply by culturing for a shorter period of time. Although, CHO-K1S cells could produce the dimer-of-trimer protein after 1 week of culture with a high level of purity, the amount of protein was much lower compared to that produced by 293F cells in the same time frame. However, protein could not easily be produced in 293F cells as this would require repeated transfections. Thus, we moved towards producing scmCD70-m1 in CHO-K1S cells after 2 weeks culture to obtain moderate levels of oligomers with a high level of overall protein. Although the time of culture might increase the level of oligomerisation of scmCD70-m1, it is important to note that the amount of protein produced also increases in longer cultures and this might be a reflection of higher protein concentration leading to higher oligomerisation. Additionally, the number of dead cells increase by increasing the time of culture and this might also play a role in inducing oligomerisation of scmCD70-m1 protein.

The initial hypothesis for the generation of scmCD70-m1 was to produce a protein capable of inducing T-cell responses in vivo independent of FcγRs. Results testing this aspect of the work are presented in chapter 4.

Chapter 4 Characterising and optimising the in vivo activity of scmCD70-m1

4.1 Introduction

It has been shown that targeting CD27 can promote a strong primary response of antigen specific T-cell expansion and also a strong secondary (memory) response. The in vitro characterisation of the dimer-of-trimer form of scmCD70-m1 showed that this protein can actively induce the proliferation of T cells as a co-stimulatory agent and the activity was similar to a strong agonistic anti-CD27 mAb. These data indicated that scmCD70-m1 might be used as an agent to induce in vivo expansion of antigen specific T cells. The Fc domain was included in the design of the scmCD70-m1 to provide dimerisation of the two polypeptide chains as well as to provide stability in circulation by interacting with FcRn.

In this chapter, the aim was to characterise the in vivo activity of scmCD70-m1. Initially, the ability of scmCD70-m1 to stimulate expansion of adoptively transferred antigen specific T cells and the in vivo stability of the protein were examined. These results led to studies aimed at improving in vivo stability and thus activity. The Fc domain was included in the design of the scmCD70-m1. While the Fc domain enables binding to FcγRIIB (as shown in chapter 3), the hexameric nature of the dimer-of-trimer form of scmCD70-m1 might enable Fc independent T-cell activation in vivo. Ultimately, FcγR independent activity and anti-tumour efficacy of scmCD70-m1 were also addressed using adoptive T-cell transfer models and a murine model of BCL1, respectively.

4.2 Results

Although the dimer-of-trimer scmCD70-m1 binds to FcγRIIB (Fig. 3.14), it was designed to act independent of FcγRIIB cross-linking. In order to investigate its efficacy in in vivo expansion of antigen specific T cells and to determine its dependence on FcγRIIB cross-linking, $CD8^+$ OT-1 T cells were adoptively transferred into WT or FcγRIIB KO recipients. For this, $CD8^+$ T cells were purified using commercial kits to eliminate the transfer of FcγRIIB expressing cells (B cells and myeloid cells) into FcγRIIB KO recipients. Figure 4.1 shows the percentage of $CD8^+$ OT-1 T cells before and after purification. $CD8^+$ T cells comprised 31% of singlets before purification and this was increased to 98.2% after purification. Out of the purified $CD8^+$ T cells, 95.1% were $tetramer^+$ indicating the percentage considered as $CD8^+$ OT-1 T cells. After confirming purity, 1×10^6 $CD8^+$ OT-1 T cells were transferred into recipient mice. Mice were then immunised with $OVA_{257-264}$ peptide in combination with control, scmCD70-m1 or anti-CD27 mAb (AT124-1 mIgG1). Agonistic anti-CD27 mAb stimulated strong expansion of OT-1 T cells in WT recipients (above 60% of lymphocytes on day 4; Fig. 4.2.A) but the activity was completely lost in FcγRIIB KO animals (2% of lymphocytes on day 4; Fig. 4.2.A & B), confirming the requirement for FcγRIIB engagement for the activity of the antibody. In contrast, scmCD70-m1 induced similar accumulation of OT-1 T cells in both WT and FcγRIIB KO recipients (approximately 22% of lymphocytes on day 4; Fig. 4.2.A) indicating that the activity is independent of FcγRIIB engagement (Fig. 4.2.B). Additionally, in the absence of FcγRIIB, the agonistic anti-CD27 mAb led to a strong depletion of $CD8^+$ T cells whereas no depletion was observed with scmCD70-m1 (Fig. 4.2.C).

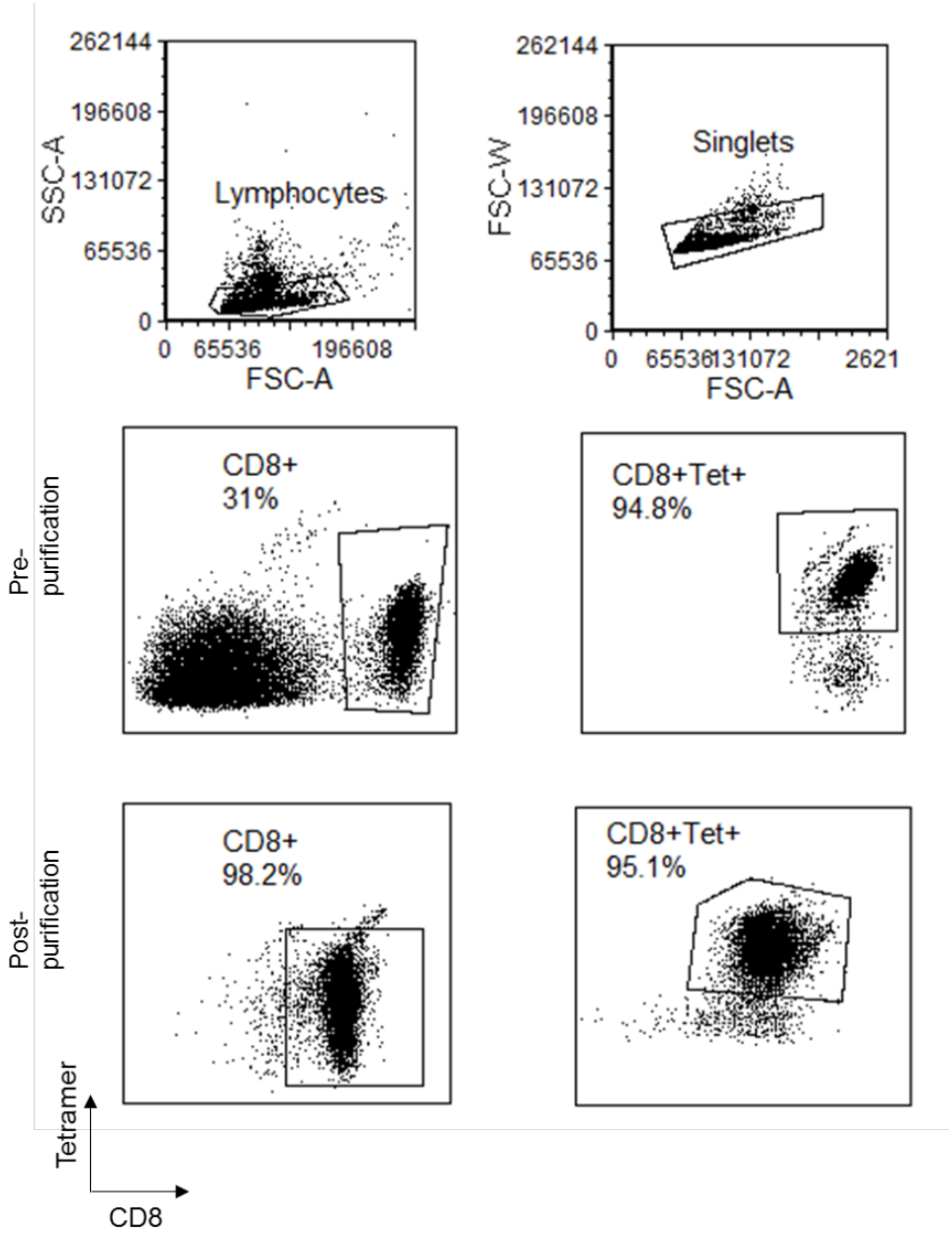

Figure 4.1. Purification of CD8⁺ OT-1 T cells for in vivo adoptive transfer. A spleen from an OT-1 TCR transgenic animal was harvested and processed to obtain a homogeneous population of splenocytes. The pre-purification profile of splenocytes was first analysed to confirm the presence of $CD8^+$ OT-1 T cells. For this, approximately 0.5 x 10^6 cells were stained with anti-mouse CD8a antibody and tetramer ($OVA_{257-264}$tetramer-PE) for 30 mins at 4 °C. Then the cells were analysed using a flow cytometer. The cells were then purified by using a $CD8^+$ T cell isolation kit according to manufacturers' instructions. Approximately 0.5 x 10^6 cells from the purified sample was stained with anti-mouse CD8a antibody and tetramer for 30 mins at 4 °C. The purity was then determined by flow cytometry analysis.

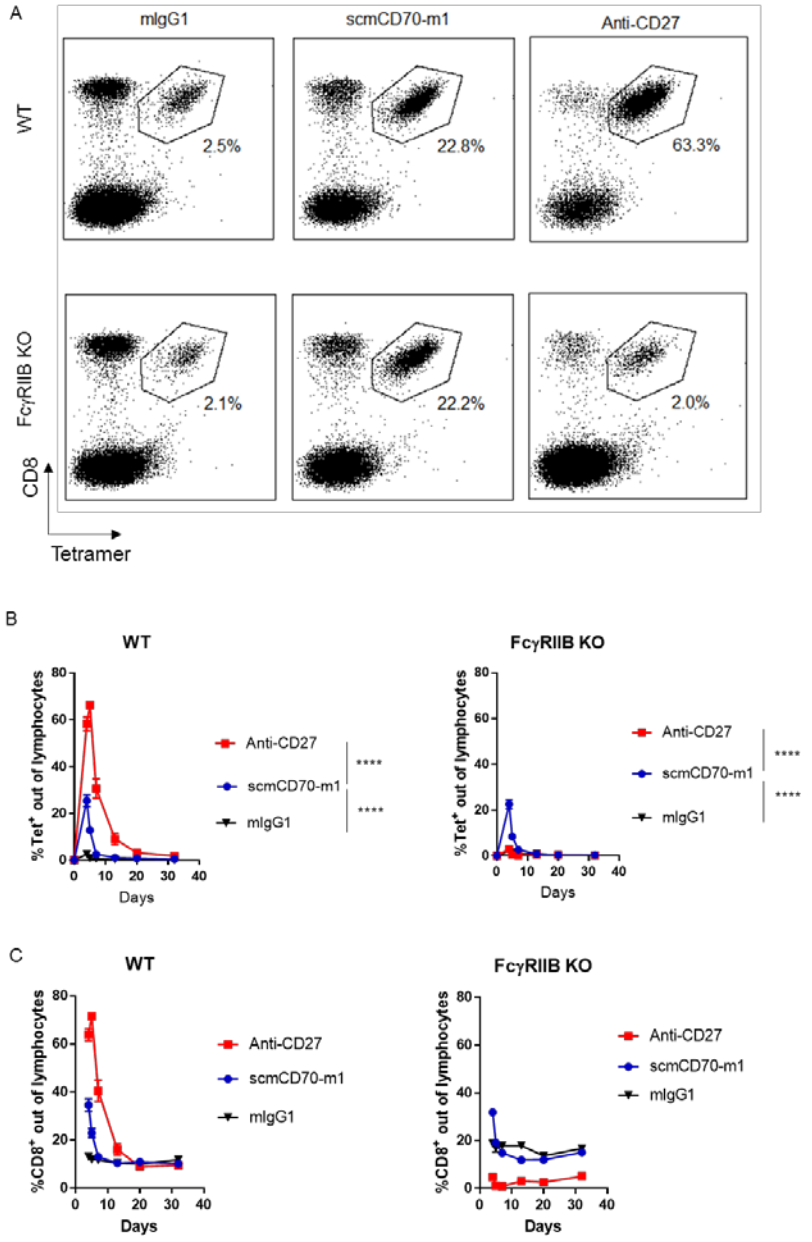

Figure 4.2. In vivo expansion of OT-1 T cells in WT and FcγRIIB KO mice induced by scmCD70-m1 or anti-CD27. 1 x 10^6 purified OT-1 Tg $CD8^+$ T cells were adoptively transferred into WT or FcγRIIB KO C57BL/6 recipients on day -1. Mice were immunised with 30 nmol $OVA_{257-264}$ in combination with 200 µg of indicated proteins at 0 hrs and another 200 µg of scmCD70-m1 or mIgG1 at 6 hrs on day 0. A third 200 µg injection of scmCD70-m1 and mIgG1 was performed on day 1. Agonistic anti-CD27 was only injected at 0 hrs on day 0. All injections were performed i.v. Peripheral blood samples were collected at days 4, 5, 7, 13, 20 and 32. Expansion of total and OT-1 specific $CD8^+$ T cells was monitored by staining with $OVA_{257-264}$ tetramer-PE and anti-CD8a antibody using flow cytometry. (A) Shows the frequency of tetramer+ cells out of lymphocytes on day 4. (B) Shows the frequency of tetramer+ cells out of lymphocytes during the expansion and contraction phases. (C) Shows the frequency of total $CD8^+$ T cells out of lymphocytes. In all cases 3 mice per group were used. Statistical analyses were performed by using two-way ANOVA with Tukey's multiple comparisons test and statistics at the peak of the response are indicated. ****= $p<0.0001$. Data points represent means +/- SEM from one experiment.

4.2.1 Characterisation and optimisation of in vivo stability

The in vitro activity of scmCD70-m1 was similar or stronger than anti-CD27 mAb (Fig. 3.17 and 3.26). However, its in vivo activity was significantly lower compared to mAb (Fig. 4.2.B) and we hypothesised that this could be a result of short in vivo stability of the scmCD70-m1 in circulation. In order to compare the half-lives of the dimer-of-trimer scmCD70-m1 protein and agonistic anti-CD27 mAb, mice were intravenously injected with a single dose (250 µg) of scmCD70-m1 or anti-CD27 mAb (AT124-1 mIgG1) and serum samples were collected at 1, 6, 25, 48, 72 and 168 hrs post-injection. The presence of scmCD70-m1 and anti-CD27 in serum samples was detected by ELISA. Known concentrations of both proteins were used to generate standard curves to determine the concentrations in the serum samples (Fig. 4.3.A). Anti-CD27 mAb had a long half-life (mean 115 µg/ml at 48 hrs) and was retained in the circulation, being detectable at high levels after 7 days post-injection (mean 42.4 µg/ml; Fig. 4.3.B). Interestingly, scmCD70-m1 was rapidly cleared from the circulation and could only be detected at low amounts at 1 hr post-injection (mean 14.2 µg/ml; Fig. 4.3.B). scmCD70-m1 was not detectable at later time points.

The Fc domain of scmCD70-m1 was included to facilitate in vivo stability by binding to FcRn. However, scmCD70-m1 showed a very short half-life and this might be due to the protein not being able to interact with FcRn. The trimeric CD70 domains which are linked to the Fc domain with flexible linkers might confer steric hindrance of the FcRn binding interface. Thus, the ability to bind to FcRn was investigated by SPR analysis. scmCD70-m1 and anti-CD27 mAb were directly immobilized onto flow cells in an SPR chip and different concentrations of recombinant FcRn were injected to flow through the flow cells. Interestingly, scmCD70-m1 showed a similar binding profile to the anti-CD27 mAb (Fig. 4.4) indicating that the short half-life was not due to scmCD70-m1 not being able to interact with FcRn.

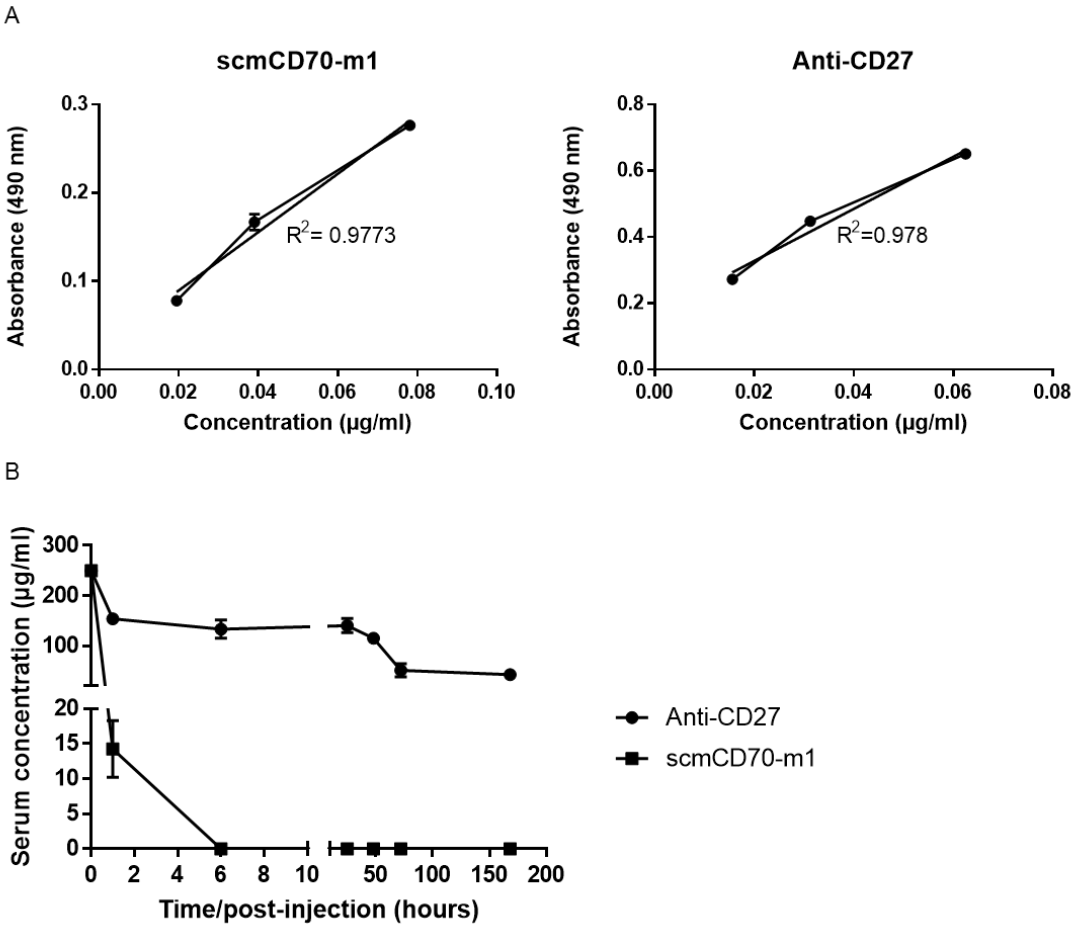

Figure 4.3. Serum half-lives of scmCD70-m1 and anti-CD27 mAb. A single dose of 250 µg of the indicated proteins was injected intravenously. Blood samples collected at 1, 6, 25, 48, 72 and 168 hrs and serum collected by centrifuging at 15700 xg at 4 °C for 30 mins. The concentrations of scmCD70-m1 and anti-CD27 mAb were detected by ELISA on serum samples. For scmCD70-m1; a plate was coated with anti-CD70 mAb and presence of scmCD70-m1 in serum samples was detected by rat anti-mouse-Fc HRP antibody. For anti-CD27; a plate was coated with rmCD27-hFc and presence of anti-CD27 in serum samples was detected by goat anti-mouse HRP. (A) Known concentrations of scmCD70-m1 and anti-CD27 were used to generate a standard curve to determine the concentrations in serum samples. Individual points and line of best fit are indicated on the graphs. (B) The serum concentrations of scmCD70-m1 and anti-CD27 mAb at indicated time points. Data points represent mean+/-SD of triplicates for scmCD70-m1 and duplicates for anti-CD27 from one experiment.

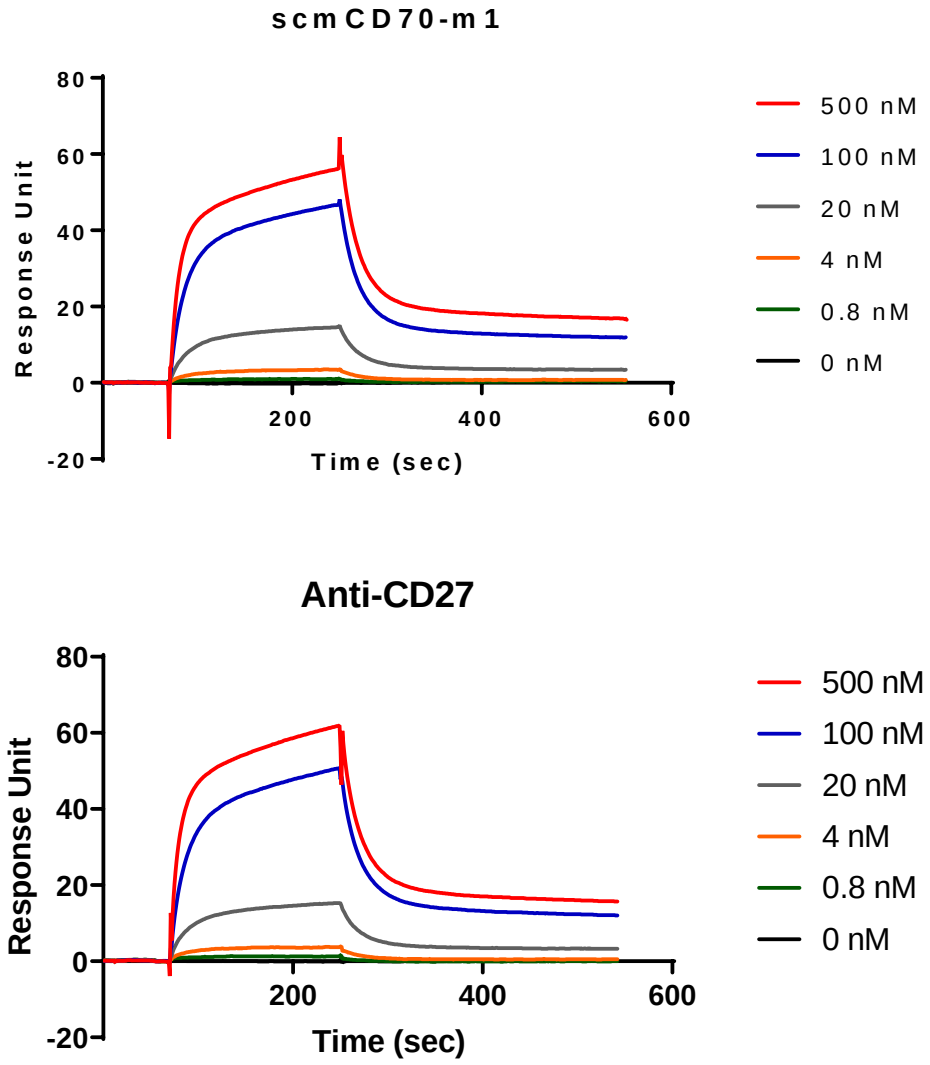

Figure 4.4. Binding of scmCD70-m1 and anti-CD27 mAb to FcRn. Proteins (scmCD70-m1 or anti-CD27) were immobilized onto a CM5 sensor chip by amine coupling and approximately 2000 RU was reached. Then FcRn was injected at the indicated concentrations in pH 6.0 HBS-EP+ buffer with 3 mins association and 5 mins dissociation. The flow rate was 30 µl/min and HBS-EP+ buffer at neutral pH was used for regeneration at the end of every injection.

The FcRn binding profile of scmCD70-m1 suggested that other factors were contributing to the short half-life of this protein in vivo. In order to support proper folding, recombinant proteins were produced in mammalian cells to enable appropriate glycosylation. scmCD70-m1 was produced in CHO-K1S cells and each CD70 domain and the Fc domain has 3 and 1 N-glycosylation site(s) respectively where the Asparagine (Asn (N)) residue in the N-X-S/T sequence, X being any amino acid apart from proline, is glycosylated (226, 227). So, a dimer-of-trimer protein has 20 potential N-glycosylation sites (Fig. 4.5.A) in total indicating that the protein is likely to be heavily glycosylated. It has been shown in many studies that

the type of glycosylation can impact on the in vivo stability of recombinant proteins (228). Thus, we hypothesised that the glycosylation on scmCD70-m1 could play a role in its short in vivo stability. Characterising the types of glycans on scmCD70-m1 (purified after 3 weeks of culture) and anti-CD27 mAb (which has 4 (2 in each heavy chain) potential N-glycosylation sites), both produced in CHO-K1S cells, revealed that scmCD70-m1 possessed a high level, 76.76% of glycans rich in mannose (oligomannose, Fig. 4.5.B) residues whereas anti-CD27 mAb had 10.37% of mannose rich glycans (Table 4.1) out of total glycans present on the proteins.

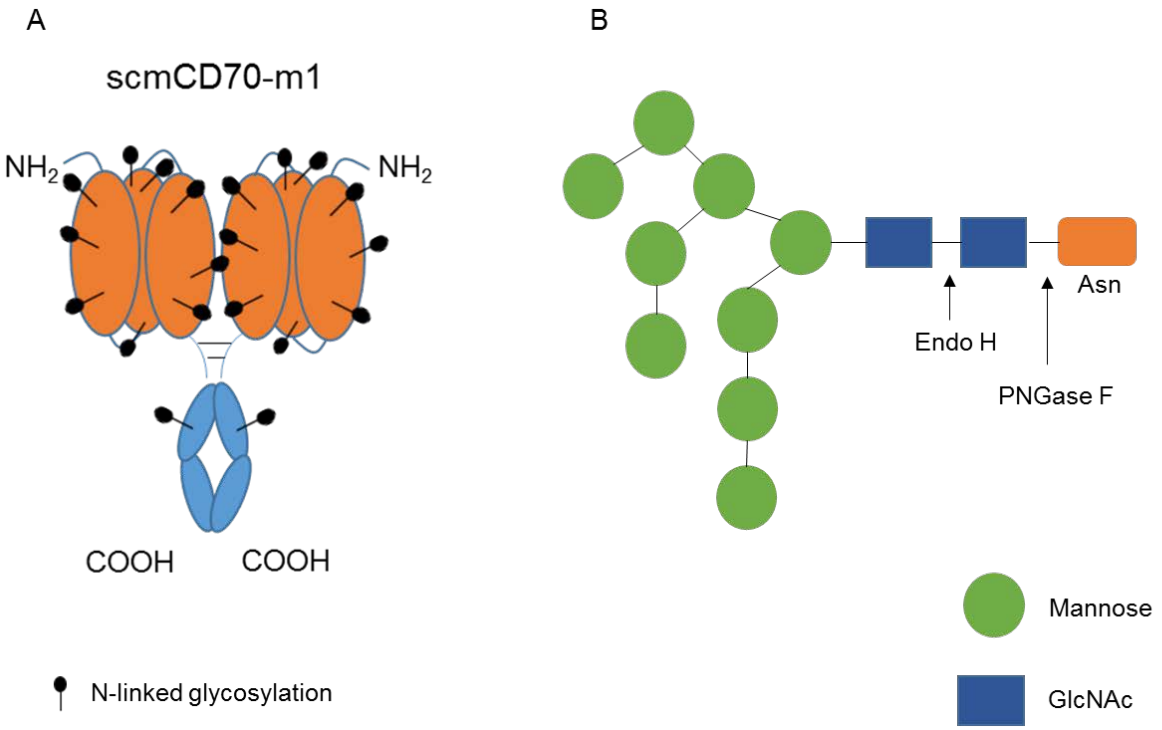

Figure 4.5. N-linked glycosylation sites on scmCD70-m1. (A) Possible N-linked glycosylation sites on scmCD70-m1 are indicated. There are 3 N-glycosylation sites in each CD70 domain and 1 N-glycosylation site in each Fc domain. (B) Structure of a high oligomannose glycan attached on to an Asn residue. The glycan consists of two N-acetyl glucosamine (GlcNAc) and nine mannose residues. The mannose residues can vary from five to nine residues but only the glycan structure with the highest mannose level is indicated on the figure. The cleavage sites of Endo H and PNGase F are also indicated.

Table 4.1. Level of oligomannose residues out of total glycans on scmCD70-m1 and anti-CD27 mAb.

	scmCD70-m1	Anti-CD27
Total Oligomannose	76.76%	10.37%
M9	3.33%	0.00%
M8	21.58%	0.00%
M7	11.19%	0.00%
M6	18.17%	0.00%
M5	22.48%	100%

Having oligomannose residues leads to rapid clearance from the circulation as the endocytic mannose receptors, mainly expressed on immune cells, bind to the terminal mannose residues on glycoproteins (229, 230). To investigate the effect of oligomannose glycans on scmCD70-m1 half-life, enzymatic activity was used to cleave the oligomannose residues followed by in vivo characterisation. Endo H is an enzyme that only cleaves glycans rich in mannose residues by cleaving between the two GlcNAc residues (231) in the glycan structure (Fig. 4.5.B). PNGase F is another enzyme that cleaves all types of N-linked sugar residues between the Asn and first GlcNAc residue (231) (Fig.4.5.B).

Initial analytical treatment of dimer-of-trimer scmCD70-m1 with Endo H or PNGase F revealed that Endo H exhibited activity under both denaturing and non-denaturing conditions (Fig. 4.6.A) whereas PNGase F was only active under denaturing conditions (Fig. 4.6.B). In order to maintain the structural and conformational stability of scmCD70-m1, further experiments focussed on using Endo H under non-denaturing conditions. To identify the optimal enzyme to protein ratio for large scale incubation, a titration of Endo H under non-denaturing conditions was carried out (Fig. 4.7). PNGase F treatment under denaturing conditions was also used as a positive control for complete de-glycosylation. Endo H treated samples migrated less than PNGase F treated samples indicating partial de-glycosylation by Endo H treatment. Titration of the Endo H enzyme amount per µg of scmCD70-m1 dimer-of-trimer protein indicated that 3.125 or higher units of Endo H per µg of protein led to similar levels of de-glycosylation and lower Endo H concentrations had slightly less activity (Fig. 4.7). Based on these results and considering the amount of enzyme required for large scale

Endo H treatment of scmCD70-m1, 5 units of Endo H per µg of protein was used for later large scale treatments.

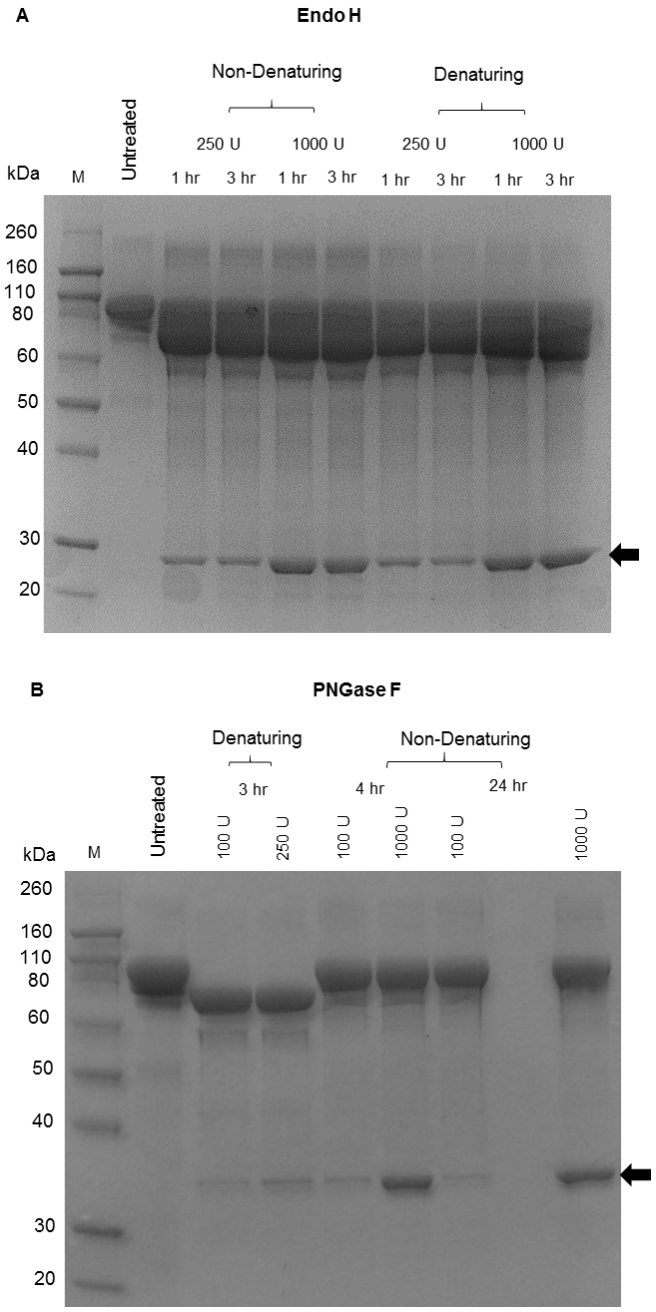

Figure 4.6. De-glycosylation of scmCD70-m1 by Endo H or PNGase F treatment. (A) Endo H treatment or (B) PNGase F treatment of scmCD70-m1 under denaturing and non-denaturing conditions with the indicated time and enzyme amounts. 10 µg of protein was treated for each indicated condition. For denaturation; proteins were incubated at 100 °C for 10 min with the appropriate buffers detailed in chapter 2. Then enzymes were added and reactions incubated for the indicated periods at 37 °C. For non-denaturing; enzymes were added to the reaction and incubated with the proteins for indicated time periods. After incubations, reducing agent (DTT) was added to all of the samples with final 62.5 mM DTT concentration. Samples were boiled at 95 °C for 5 mins and loaded 10 µg protein/lane into the 10% Bis-Tris gel. The gel was run at 100-120 V for 1.5 hrs and was Coomassie brilliant blue stained. Enzymes are indicated by arrows. U; units, M; molecular weight markers.

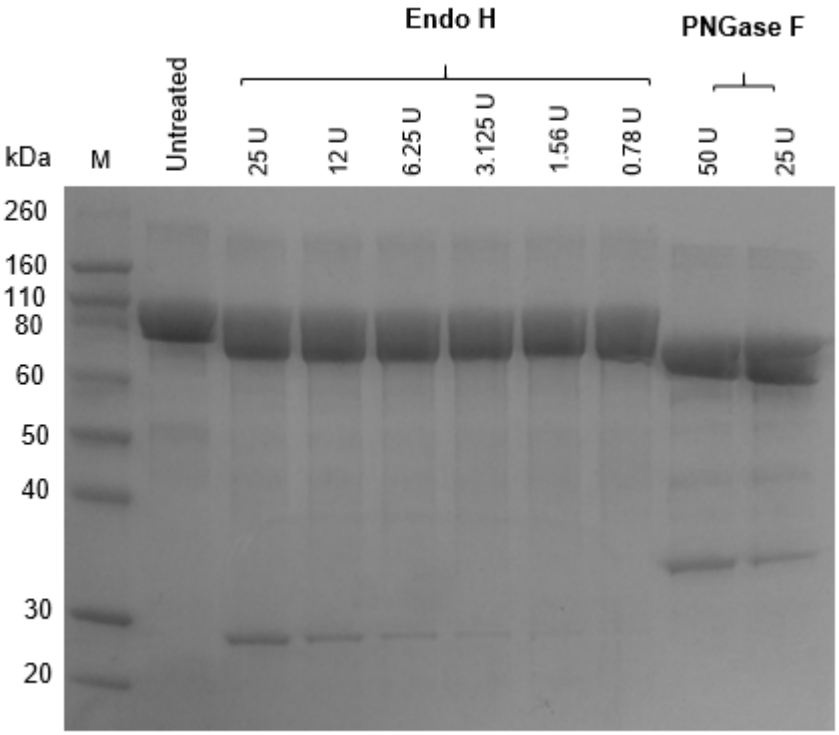

Figure 4.7. Titration of the amount of Endo H used for treatment of scmCD70-m1. A titration was carried out by using indicated amounts of Endo H per µg of protein under non-denaturing conditions. PNGase F treated proteins (indicated amounts per µg of protein) were loaded as a positive control to indicate the level of complete de-glycosylation under denaturing conditions. For Endo H treatment; indicated amounts of enzyme were incubated with scmCD70-m1 protein for 3 hrs at 37 °C. For denaturation; samples were first incubated at 100 °C for 10 mins and then PNGase F was added for further 3 hrs incubation at 37 °C. 10 µg of protein was loaded per lane under reducing conditions with 62.5 mM final reducing agent (DTT) concentration. Samples were boiled at 95 °C for 5 mins before loading into the 10% Bis-Tris gel. The gel was run at 100-120 V for 1.5 hrs and then Coomassie brilliant blue stained. U; units, M; molecular weight markers.

A new batch of scmCD70-m1 was produced in CHO-K1S cells after 2 weeks of culture and the dimer-of-trimer protein was fractionated. 20 mgs of this dimer-of-trimer scmCD70-m1 was treated with Endo H at a ratio of 5 units of enzyme per µg of protein for 3 hrs at 37 °C. The activity of Endo H and removal of glycan residues was confirmed via SDS-PAGE analysis by running a small amount of Endo H treated protein and comparing with untreated protein (Fig. 4.8.A). Then the whole sample was fractionated by SEC to remove the enzyme and isolate the Endo H treated protein (Fig. 4.8.B). The removal of Endo H was confirmed by comparing the samples before and after purification by SDS-PAGE (Fig. 4.8.C). Endo H treatment did not influence the ability of scmCD70-m1 to bind CD27 as determined by SPR analysis (Fig. 4.8.D). After purifying the Endo H treated protein, a small amount of untreated and Endo H treated scmCD70-m1, from the same batch, were analysed for the level of oligomannose residues. The untreated protein had 31.04% oligomannose residues out of total glycans whereas Endo H treatment reduced the level to 7.05% (Table 4.2). This level of oligomannose glycans in untreated scmCD70-m1 was lower than the previously analysed sample (76.76%) which was produced in a 3 week culture. Additionally, the majority of the oligomannose glycans were in the M5 form when the protein was produced in a 2 week culture and a low percentage of oligomannose residues with longer chains was observed compared to the protein produced in a 3 week culture (compare Tables 4.1 and 4.2).

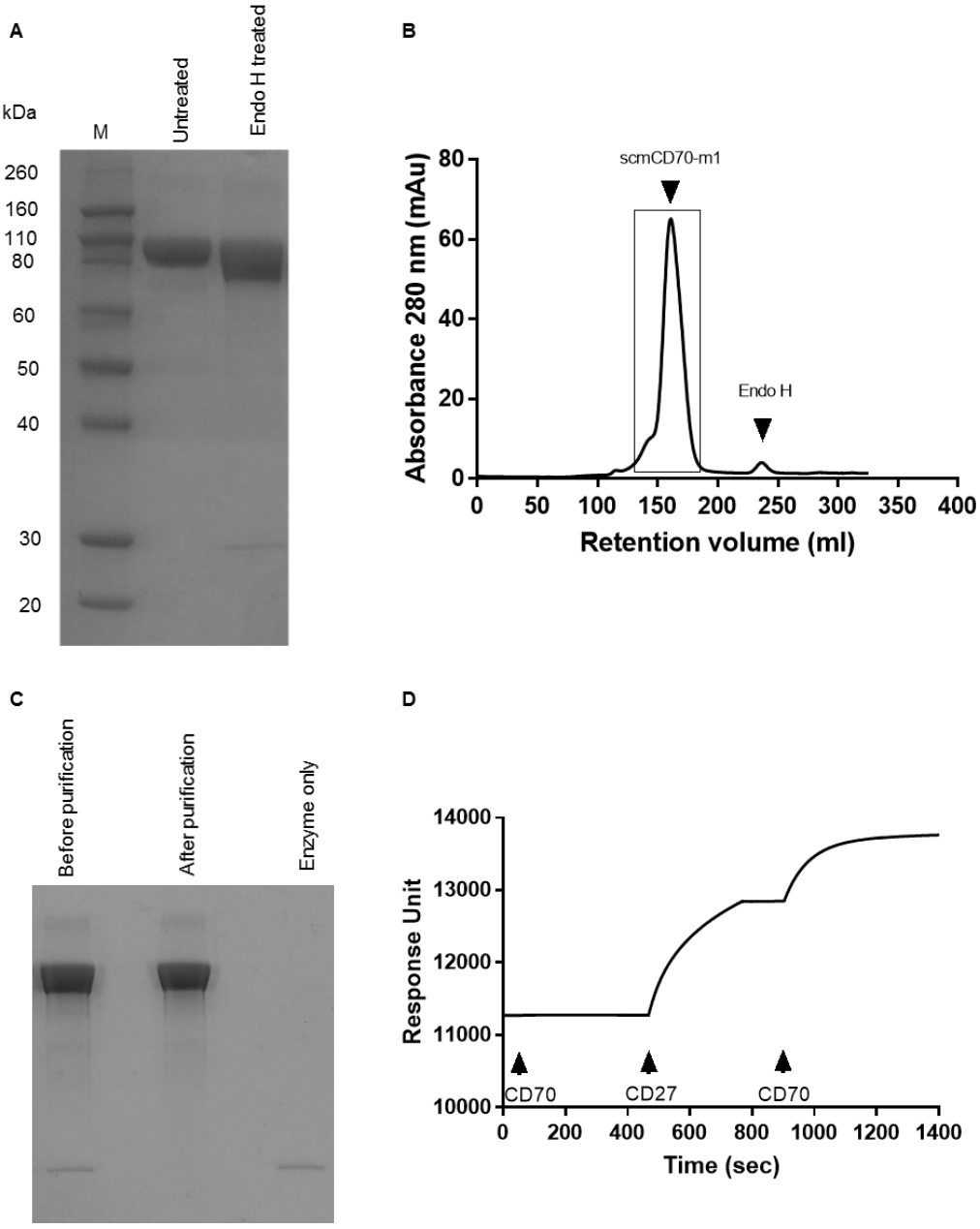

Figure 4.8. Large scale Endo H treatment of scmCD70-m1. A new batch of scmCD70-m1 was produced in CHO-K1S cells and dimer-of-trimer protein was isolated as described previously. 20 mgs of dimer-of-trimer scmCD70-m1 was then subjected to large scale Endo H treatment with a ratio of 5 units of enzyme per µg of protein. (A) SDS-PAGE analysis to confirm de-glycosylation of scmCD70-m1 after Endo H treatment. (B) SEC to isolate Endo H treated scmCD70-m1 from the enzyme. Indicated fraction was isolated to recover the Endo H treated scmCD70-m1 protein. The peaks for dimer-of -trimer scmCD70-m1 and Endo H enzyme are indicated. (C) SDS-PAGE to confirm removal of Endo H from scmCD70-m1. (D) SPR analysis to confirm CD27 binding of Endo H treated scmCD70-m1. An anti-human IgG chip was used to capture rmCD27-hFc which was injected at 5 µg/ml. Then Endo H treated scmCD70-m1 was injected at 10 µg/ml. All samples were prepared in HBS-EP+ buffer and injected with 10 µl/min flow rate for 5 mins. CD70; Endo H treated scmCD70-m1, CD27; rmCD27-hFc. For SDS-PAGE gels, 10 µg of protein was loaded per lane under reducing conditions with 62.5 mM final DTT concentration. Samples were boiled at 95 °C for 5 mins before loading into the 10% Bis-Tris gel. Gels were Coomassie brilliant blue stained. M; molecular weight markers.

Table 4.2. Level of oligomannose residues out of total glycans on untreated and Endo H treated scmCD70-m1.

	Untreated scmCD70-m1	Endo H treated scmCD70-m1
Total Oligomannose	31.04%	7.05%
M9	0.00%	0.00%
M8	2.09%	0.00%
M7	1.67%	0.64%
M6	7.33%	3.88%
M5	19.95%	2.53%

Although the ability of Endo H treated scmCD70-m1 protein to bind CD27 was confirmed via SPR analysis, to confirm that it still retained its activity, an in vitro T-cell proliferation assay was performed. T cells were stimulated with agonistic anti-CD3 mAb in combination with control or CD27-targeting proteins. Both untreated and Endo H treated scmCD70-m1 induced enhanced proliferation of T cells compared to control and the activity was similar to an agonistic anti-CD27 mAb (Fig. 4.9). The untreated sample showed a slightly higher activity compared to Endo H treated protein but this was not statistically significant. At the highest anti-CD3 concentration, the level of proliferation stimulated by untreated scmCD70-m1 was significantly higher than the agonistic anti-CD27 mAb (Fig. 4.9).

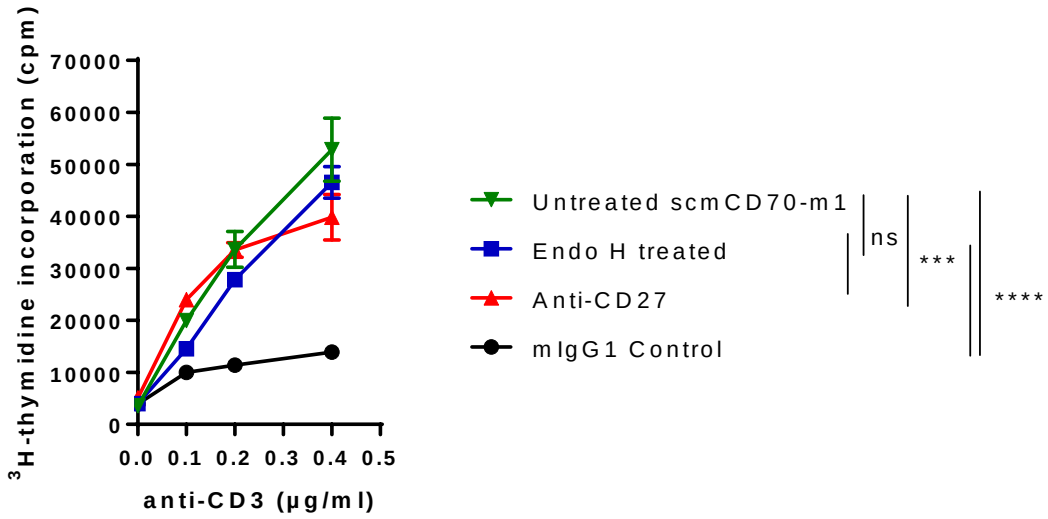

Figure 4.9. Comparison of proliferation of T cells stimulated with untreated and Endo H treated scmCD70-m1. Splenocytes (2 x 10^5) from a WT C57BL/6 mouse were stimulated with agonistic anti-CD3 mAb (clone 145-2C11) at the indicated concentrations in combination with indicated proteins at 10 µg/ml. ^{3}H-thymidine was added at 48 hrs and harvested after 17 hrs of further incubation. Each anti-CD3 concentration was plated in triplicate. Statistical analyses were performed by using two-way ANOVA with Tukey's multiple comparisons test and statistics at the highest anti-CD3 concentration are indicated. Ns; not significant, ***=p<0.001, ****=p<0.0001. Mean +/- SEM of triplicates are indicated. Data representative of two independent experiments.

4.2.2 Investigating the in vivo activity of Endo H treated scmCD70-m1

After confirming the similar in vitro activity of untreated and Endo H treated scmCD70-m1 proteins, the in vivo half-life of these proteins was investigated to test the hypothesis that removal of oligomannose type glycans will improve the in vivo stability of the protein. Mice received a single injection of untreated and Endo H treated proteins at time 0 and serum samples were obtained at 1, 6, 25 and 48 hrs post-injection. The concentration of the proteins in the serum was determined by ELISA as before. A standard curve was generated using known concentrations of scmCD70-m1 (Fig. 4.10.A) and was used to determine the concentrations in the serum samples. As predicted, the in vivo stability of the Endo H treated protein was significantly improved compared to the untreated protein. A higher concentration of Endo H treated scmCD70-m1 could be detected as early as 1 hr post injection and the Endo H treated protein could also be detected up to 48 hrs post injection whereas the untreated version could only be detected at the 1 hr time point (Fig. 4.10.B) consistent with previous results (Fig. 4.3.B). Although, the half-life of the Endo H treated protein was still shorter than the anti-CD27 mAb (compare to Fig. 4.3.B), these results

suggested that the in vivo activity of the Endo H treated scmCD70-m1 might be enhanced compared to the untreated version.

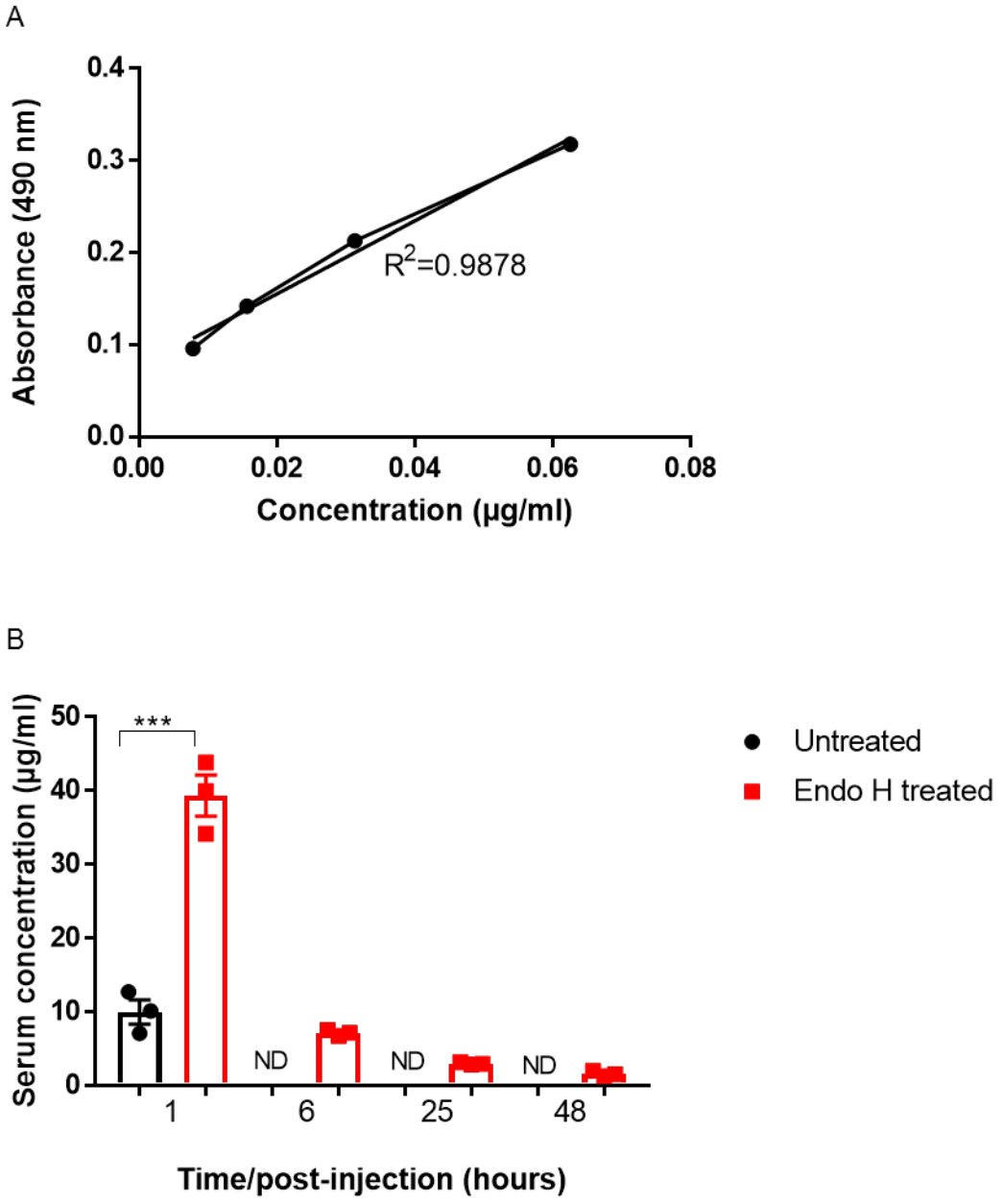

Figure 4.10. In vivo serum stability of untreated and Endo H treated scmCD70-m1. A single dose of 250 µg of the indicated proteins was injected i.v. into 3 mice for each group. Peripheral blood samples collected at 1, 6, 25 and 48 hrs and serum collected by centrifuging at 15700 xg at 4 °C for 30 mins. The concentrations of untreated and Endo H treated scmCD70-m1 were detected by ELISA on serum samples. A plate was coated with anti-CD70 mAb and presence of scmCD70-m1 in serum samples was detected by rat anti-mouse-Fc HRP antibody. (A) Known concentrations of scmCD70-m1 were used to generate a standard curve to determine the concentrations in serum samples. Individual points and line of best fit are shown on the graph. (B) The concentrations of untreated and Endo H treated scmCD70-m1 at indicated time points. Statistical analysis was performed by using Student's t test. ***=$p<0.001$. Data points represent mean +/- SEM from one experiment.

In order to test this hypothesis, 5 x 10^5 OT-1 T cells were adoptively transferred to WT recipient mice which were then immunised with the $OVA_{257-264}$ peptide in combination with control or CD27 agonist proteins. As observed previously (Fig. 4.2.B), untreated scmCD70-m1 and anti-CD27 mAb stimulated expansion of antigen specific T cells with anti-CD27 mAb generating a higher response (Fig. 4.11.A). However, Endo H treated scmCD70-m1 stimulated a response much higher than untreated scmCD70-m1 and the level was similar to anti-CD27 mAb with a slower contraction phase (Fig. 4.11.A).

Having confirmed the in vivo activity of Endo H treated scmCD70-m1 and observing a response similar to agonistic mAb, lower numbers of OT-1 T cells were transferred into WT recipients to better reflect physiological response levels. After transfer of 1 x 10^5 OT-1 T cells again the untreated scmCD70-m1 could stimulate the expansion of antigen specific T cells but only a low response was generated (Fig. 4.11.B). Endo H treated protein was significantly better than the untreated version but interestingly the response to the Endo H treated scmCD70-m1 was also higher than the anti-CD27 mAb at the peak of the response (Fig. 4.11.B). A similar activity was observed when 1 x 10^4 OT-1 T cells were transferred. Specifically, the activity of untreated scmCD70-m1 was negligible compared to control whereas anti-CD27 and Endo H treated scmCD70-m1 stimulated significantly higher expansion of antigen specific T cells with the Endo H treated protein generating the highest response (Fig. 4.11.C). Overall, these results, using different numbers of OT-1 T cells for transfer, suggested that the Endo H treatment of scmCD70-m1 contributed to enhanced in vivo half-life which resulted in a higher activity in stimulating the expansion of antigen specific T cells in vivo. Interestingly, despite the much shorter half-life, Endo H treated scmCD70-m1 generated a higher response than the anti-CD27 mAb when low numbers of OT-1 T cells were transferred.

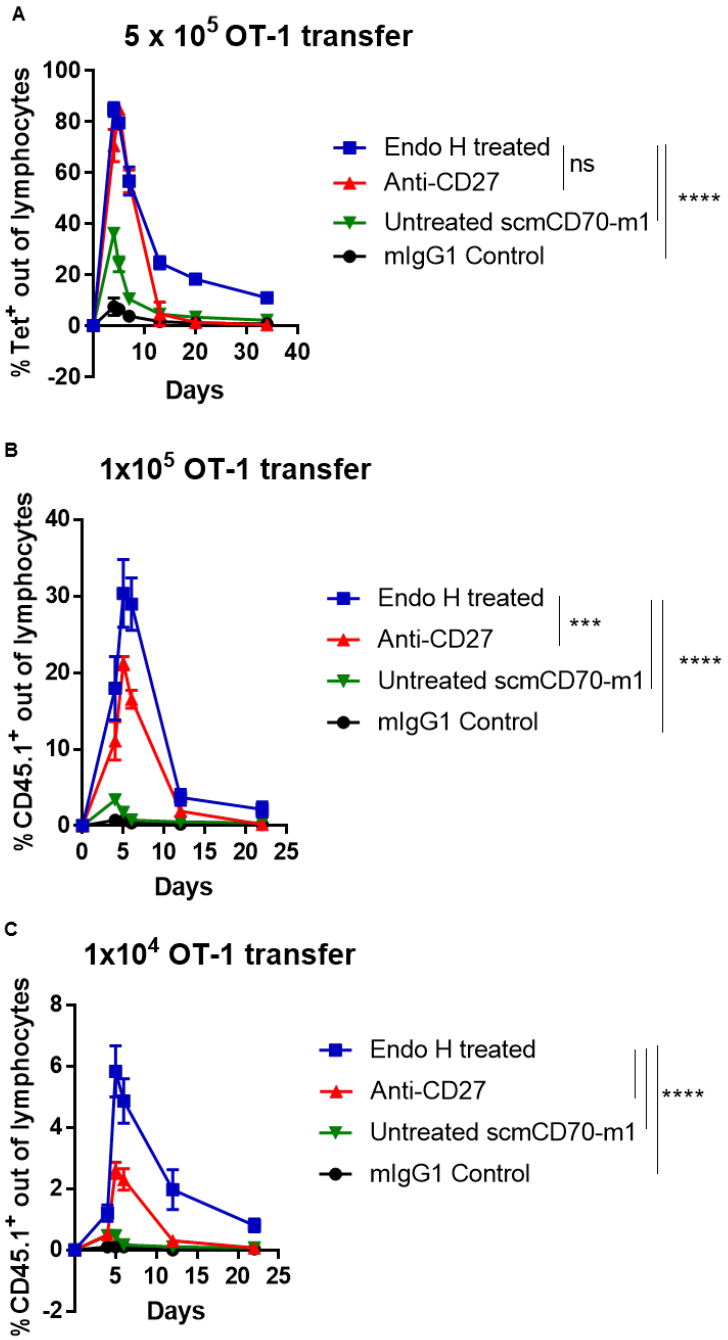

Figure 4.11. In vivo expansion of OT-1 T cells stimulated with CD27 agonists. Naïve 5 x 10^5 (A), 1 x 10^5 (B) and 1 x 10^4 (C) OT-1 T cells were adoptively transferred into WT recipients on day -1. Mice were immunised with 30 nmol $OVA_{257-264}$ in combination with 250 µg of indicated proteins on day 0 and another 250 µg dose of proteins on day 1. Peripheral blood was collected on indicated time points and expansion of OT-1 specific $CD8^+$ T cells was monitored by staining with anti-mouse CD8a and $OVA_{257-264}$ tetramer or anti-mouse CD45.1 antibody. Anti-mouse CD45.1 antibody was used where OT-1 T cells transferred were CD45.1 congenic (B and C). All samples were injected intravenously. Data were collected by flow cytometry and 3 mice per group were used. Statistical analyses were performed by using two-way ANOVA with Tukey's multiple comparisons test and statistics at the peak of the response are indicated. Ns; not significant, ***=p<0.001, ****= p<0.0001. Data indicate mean +/- SEM from one experiment for each transfer model.

After confirming the potency of Endo H treated scmCD70-m1 to stimulate antigen specific T-cell expansion in vivo, both with high and low dose adoptive transfer models, the anti-tumour efficacy of untreated and Endo H treated scmCD70-m1 and anti-CD27 was compared in a BCL1 model. For this, 5 x 10^6 BCL1 cells were intravenously injected into WT mice on day 0 and animals received the indicated proteins on days 5, 6, 7 and 8. The untreated scmCD70-m1 did not provide a survival benefit and activity was similar to the control group (Fig. 4.12). However, the Endo H treated scmCD70-m1 significantly improved the survival of mice, delaying tumour growth by an average of 32 days compared to control and untreated scmCD70-m1 groups. The activity observed with agonistic anti-CD27 mAb was similar to the activity of Endo H treated scmCD70-m1 (Fig. 4.12).

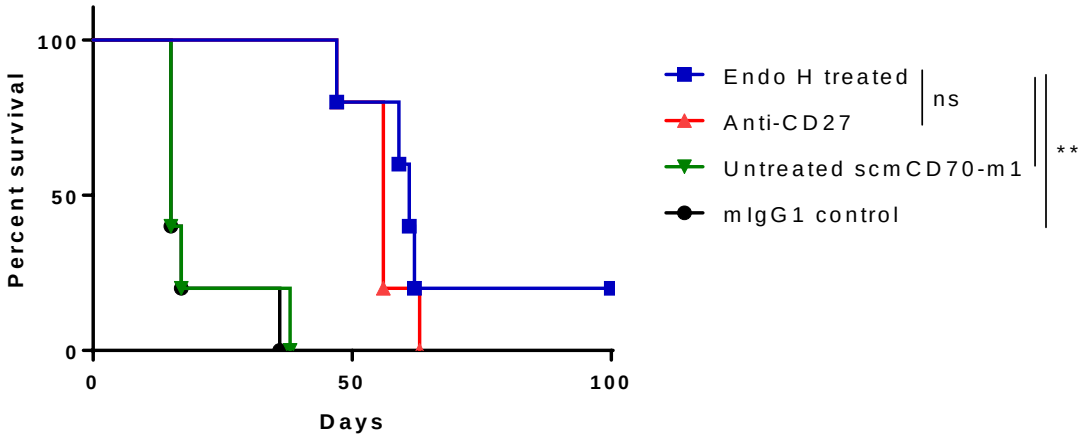

Figure 4.12. Anti-tumour efficacy of untreated and Endo H treated scmCD70-m1 in BCL1 model. 5 x 10^6 BCL1 cells were injected into WT BALB/c mice on day 0. Animals then received the indicated proteins on days 5, 6, 7 and 8. 200 µg of proteins injected at each time point. Five mice per group were used. Mice were culled when a humane end-point was reached. Statistical analyses were performed by using Log-rank test. Ns; not significant, **=p<0.01. Data for untreated scmCD70-m1, anti-CD27 and control are representative from two independent experiments. Data for Endo H treated scmCD70-m1 is from one experiment.

scmCD70-m1 was designed to act independently of FcγR cross-linking to induce co-stimulation of T cells. Previously, scmCD70-m1 was found to interact with FcγRIIB (Fig 3.14) and glycosylation of the Fc domain is critical for the interaction with FcγRs (232). As Endo H treated protein was partially de-glycosylated to remove oligomannose residues, this might have contributed to eliminating the interaction of Endo H treated protein with FcγRs. Thus, FcγR binding of untreated scmCD70-m1, Endo H treated scmCD70-m1 and anti-CD27 mAb (mIgG1) was investigated by SPR analysis. To test this, the CD27 agonist proteins were directly immobilized into the flow cells of an SPR chip and FcγR solutions were passed over the chip at different concentrations. Anti-CD27 mIgG1 mAb bound to FcγRIIB and FcγRIII but did not bind to FcγRI and FcγRIV (Fig. 4.13) as expected (167). The scmCD70-m1 protein contains the Fc domain of the mIgG1 isotype and both untreated and Endo H treated proteins showed the same binding profile as the mAb with binding only apparent to FcγRIIB and FcγRIII (Fig. 4.13). For FcγRI and FcγRIV binding, the highest concentration was injected first and as there was no binding, the rest of the concentrations were not injected.

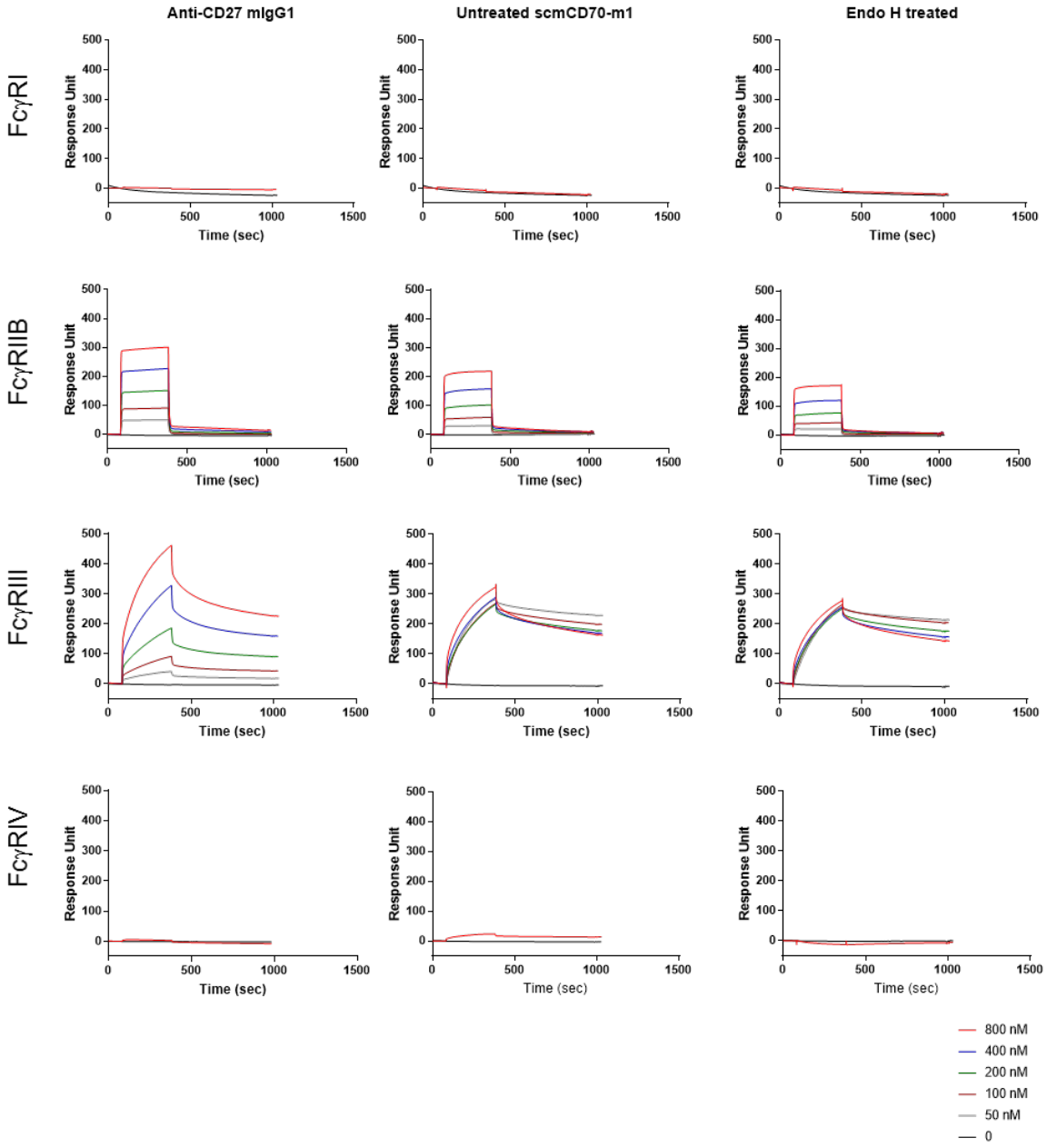

Figure 4.13. FcγR binding of anti-CD27 mAb, untreated scmCD70-m1 or Endo H treated scmCD70-m1. FcγR binding of indicated proteins investigated by SPR analysis. Proteins were directly immobilized into the flow cells of a CM5 sensor chip by amine coupling to achieve 2000-3000 RU and FcγR solutions were injected at indicated concentrations in HBS-EP+ running buffer (0, 50, 100, 200, 400 and 800 nM) with 5 mins association and 10 mins dissociation time with the flow rate; 30 µl/min.

The in vivo activity of untreated scmCD70-m1 is independent of FcγRIIB availability (Fig. 4.2.B) yet both untreated and Endo H treated proteins bind to both FcγRIIB and FcγRIII (Fig. 4.13) via SPR analysis. In order to investigate the role of all FcγRs on the activity of Endo H treated scmCD70-m1, OT-1 T cells were adoptively transferred into WT or FcγR1,2,3,4 KO recipients; the latter lack all FcγRs. Thus, 1 x 10^4 purified OT-1 T cells were transferred into mice prior to immunisation with $OVA_{257-264}$ peptide in combination with control or CD27 targeting proteins. The untreated scmCD70-m1 was only injected into WT recipients, and as previously observed in this low number transfer model (Fig 4.11), there was negligible (<0.5% of $CD8^+$ at the peak of the response) antigen specific T-cell expansion (Fig.4.14). Agonistic anti-CD27 mAb stimulated the expansion of antigen specific T cells in the WT recipients (7% of $CD8^+$ at the peak of the response) but as observed in the FcγRIIB KO animals previously (Fig. 4.2.B), activity was lost in the FcγR1,2,3,4 KO animals (Fig. 4.14). Endo H treated protein stimulated the highest level of antigen specific T-cell expansion in the WT recipients (15.4% of $CD8^+$ at the peak of the response) and was also active in the FcγR1,2,3,4 KO recipients (7% of $CD8^+$ at the peak of the response) (Fig. 4.14). Interestingly, the level of antigen specific T-cell expansion in FcγR1,2,3,4 KO animals was lower than in WT animals with the Endo H treated protein. As the Endo H treated protein can bind to FcγRIIB and FcγRIII (Fig. 4.13), the results suggested that while Endo H treated scmCD70-m1 still shows activity in the absence of FcγRs, its efficacy might be increased by being cross-linked by FcγR interaction.

Additionally, to investigate the ability of scmCD70-m1 to generate a memory T-cell population, WT mice were left until the primary response contracted to levels in which <1% of $CD8^+$ T cells were OT-1 cells, and were then immunised with $OVA_{257-264}$ peptide in combination with anti-CD40 mAb as an adjuvant. As observed with the primary response, the highest secondary response was generated in the group that was primarily immunised with Endo H treated scmCD70-m1 (Fig. 4.15). Interestingly, although the primary response was negligible with the untreated scmCD70-m1, a secondary response similar to that of the anti-CD27 group was generated (Fig. 4.15). This suggested that, the magnitude of the initial priming with untreated scmCD70-m1 was strong enough to generate a memory population to respond in the case of secondary encounter with the antigen. Only 2 out of 3 mice responded from each group. Thus, there was no statistical difference between the groups.

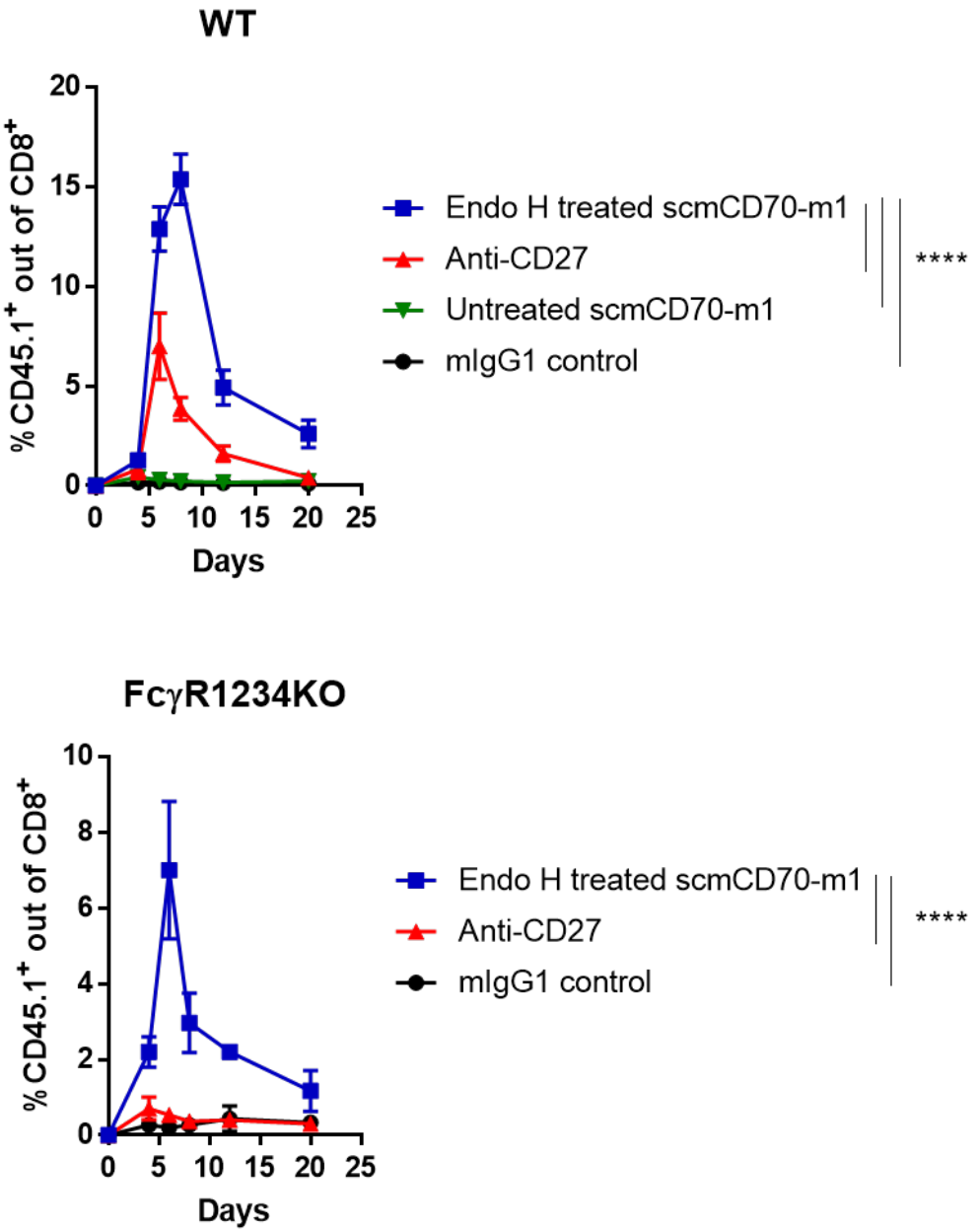

Figure 4.14. In vivo expansion of OT-1 T cells stimulated with Endo H treated scmCD70-m1 in the absence of FcγR. Naïve 1 x 10^4 purified CD45.1 congenic OT-1 T cells were adoptively transferred into WT or FcγR1,2,3,4 KO recipients on day -1. Mice were immunised with 30 nmol $OVA_{257-264}$ in combination with 250 µg of indicated proteins on day 0 and another 250 µg dose of proteins on day 1. Peripheral blood was collected on indicated time points and expansion of OT-1 specific $CD8^+$ T cells was monitored by staining with anti-mouse CD8a and anti-mouse CD45.1 antibody. All samples were injected intravenously. Data were collected by flow cytometry and 3 mice per group were used. Statistical analyses were performed by using two-way ANOVA with Tukey's multiple comparisons test and statistics at the peak of the response are indicated. Ns; not significant, ***=p<0.001, ****= p<0.0001. Mean +/- SEM are indicated. Data representative of two independent experiments.

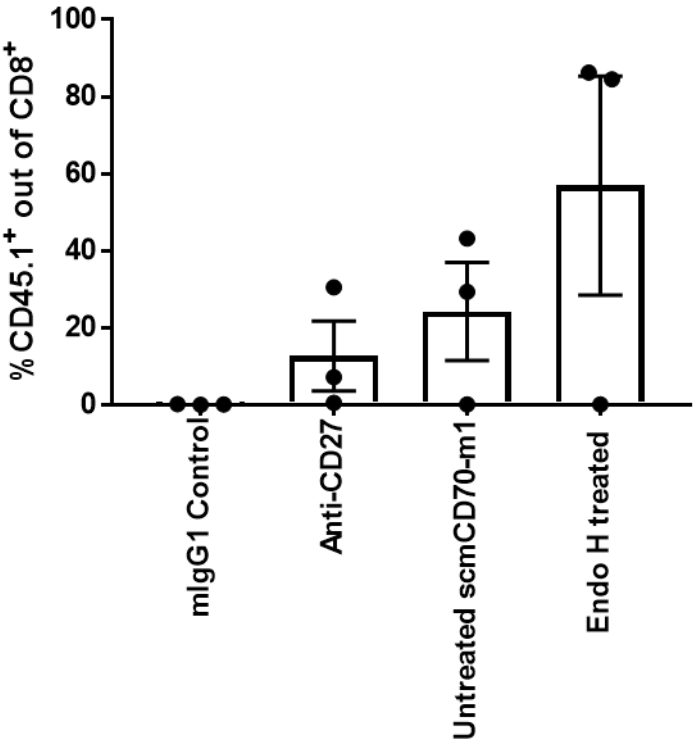

Figure 4.15. Secondary response after initial priming with anti-CD27, untreated scmCD70-m1 or Endo H treated scmCD70-m1. Mice were initially immunised as described in Figure 4.14. For the secondary response, mice received i.v. injection of 30 nmol $OVA_{257-264}$ in combination with 50 µg anti-CD40 (clone 3/23, rIgG2a). Peripheral blood was collected on day 6 after secondary immunisation and expansion of OT-1 specific $CD8^+$ T cells was monitored by staining with anti-mouse CD8a and anti-mouse CD45.1 antibody. Mean +/- SEM of 3 mice per group are indicated from one experiment.

4.2.3 Generation and characterisation of scmCD70 with "silent" Fc

In order to further investigate if FcγR cross-linking contributes to the enhanced activity of Endo H treated scmCD70-m1 in WT mice, a new construct with a D265A mutation in the Fc region, to generate a protein lacking FcγR interaction ("silent" Fc) (233) was generated as single chain mouse CD70 - mouse mutant 1 (scmCD70-mm1). The D at position 573 in scmCD70-m1 sequence was mutated to A (see Appendix Fig. 1). The DNA sequence for the mutated Fc domain was ordered commercially and supplied in PMA-T plasmid flanked with XbaI and EcoRI restriction sites. After transformation into bacteria and subsequent DNA extraction to amplify the amount of DNA, a preparative digest was performed by digesting 3 µg of plasmid DNA with 15 units of XbaI and EcoRI for 2 hrs at 37 °C. The digested DNA was run on a 1% agarose gel and the insert extracted (Fig. 4.16.A).

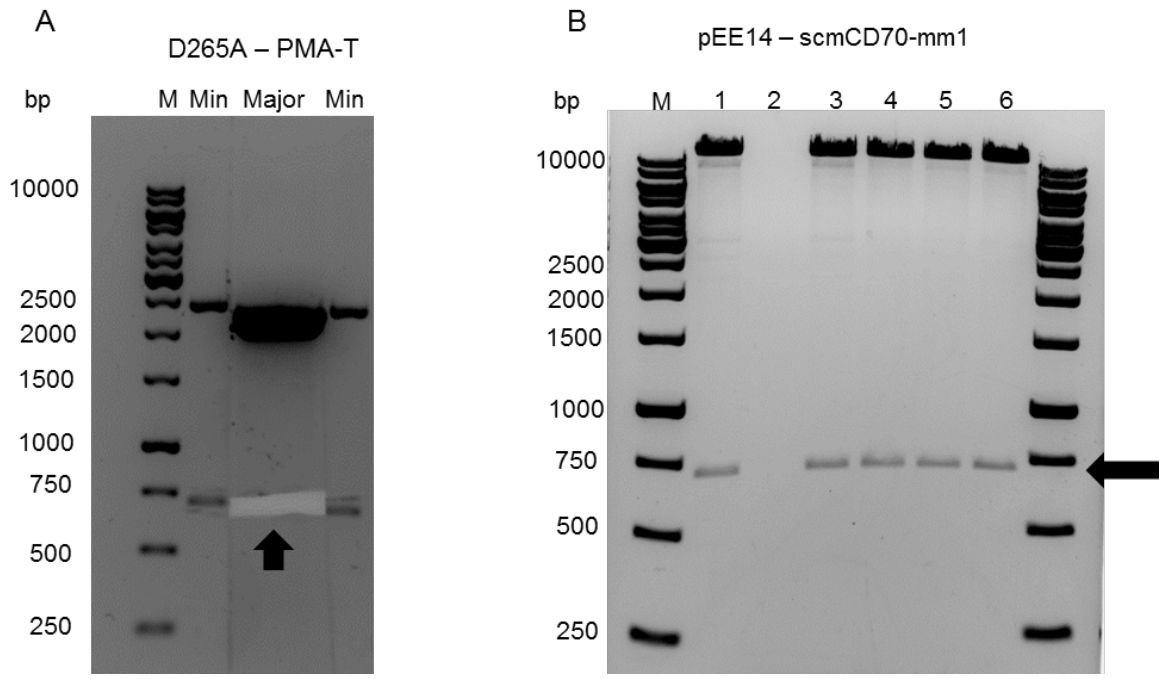

Figure 4.16. Cloning of scmCD70-mm1 into pEE14 expression vector. (A) The PMA-T plasmid DNA with the insert containing D265A mutation was digested with XbaI and EcoRI restriction enzymes. 3 µg of plasmid DNA was digested with 15 units of each enzyme at 37 °C for 2 hrs. 200 ng of digested sample was run in each minor (Min) lane and the rest was run in the major lane. The digested insert (indicated by the arrow) was extracted from the gel without exposure to UV light. (B) Six colonies of pEE14 – scmCD70-mm1 transformed OneShot TOP10 cells were grown in LB-amp cultures for 17 hrs at 37 °C and plasmid DNA was isolated by using mini-prep kits (Qiagen). 400 ng of isolated plasmid DNA from each colony was digested with 2 units of XbaI and 2 units of EcoRI for 2 hrs at 37 °C and 200 ng of each sample was visualised on an agarose gel. The digested insert is indicated by the arrow. All samples on (A) and (B) were run on 1% agarose gel. M; molecular weight markers.

In order to produce stable CHO-K1S clones, the insert was cloned into the pEE14 vector (see Appendix Fig. 6) which was previously digested with XbaI and EcoRI (Fig. 3.19.A) to enable the change of Fc domain. A 3:1 insert to vector Molar ratio was used for ligation and a small amount of the reaction was transformed into OneShot TOP10 cells. Mini-cultures were grown from individual colonies and plasmid DNA isolated from 6 colonies. A small amount of plasmid DNA from each colony was then digested with XbaI and EcoRI to confirm the ligation (Fig. 4.16. B). This digestion produced a DNA product of approximately 713 bp as expected and colony #6 was further grown to amplify the pEE14-scmCD70-mm1 vector. Then CHO-K1S cells were stably transfected and clones were generated as described previously (chapter 3). From the initial screening, two clones were found to secrete scmCD70-mm1 by ELISA (data not shown) and after further growth, the level of secretion was investigated. A standard curve was generated using scmCD70-m1 (Fig. 4.17.A) and was used to measure the concentration of scmCD70-mm1 secreted in CHO-K1S clone

supernatants (Fig. 4.17.B). The cells were at the same level of confluency and clone A produced 2.88 µg/ml whereas clone B produced 10 µg/ml of protein. The ability of scmCD70-mm1 to bind recombinant CD27 was also confirmed via SPR analysis and clone B showed a higher level of binding. Clone A generated 270 RU whereas clone B generated 544 RU (Fig.4.17.C).

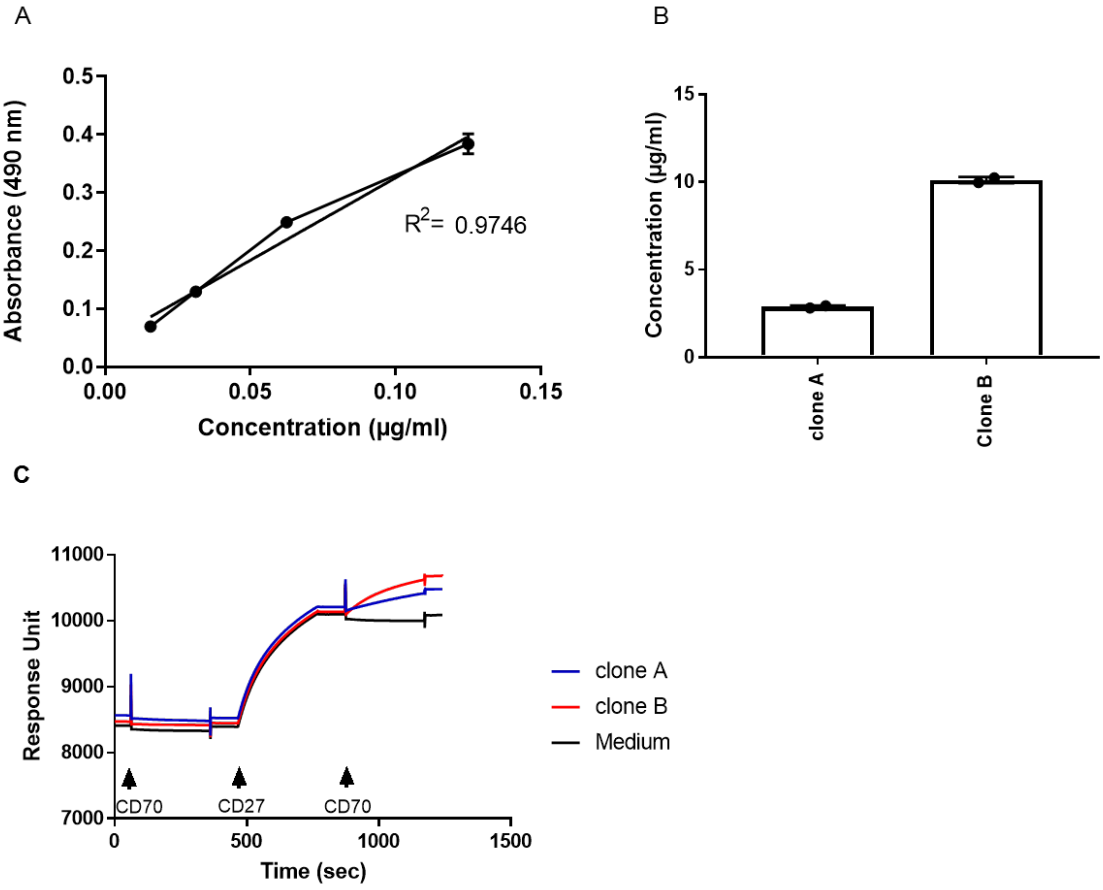

Figure 4.17. Expression of scmCD70-mm1 and binding to CD27. Concentration of scmCD70-mm1 in supernatants from CHO-K1S cells was determined by ELISA. The plate was coated with goat anti-mouse IgG and presence of scmCD70-m1 in supernatants was detected by goat anti-mouse-Fc HRP antibody. (A) A standard curve was generated using known concentrations of scmCD70-m1 and was used to determine the concentration of scmCD70-mm1 in supernatants. Individual points and line of best fit are shown on the graph. (B) Concentration of scmCD70-mm1 secreted by each clone. Blank wells containing neat cell culture medium were used as negative controls. Mean +/- SD are representative of duplicates. (C) CD27 binding of scmCD70-mm1 in supernatants was confirmed by SPR. An anti-human IgG chip was used to determine the binding of scmCD70-mm1 to CD27. First the supernatants were injected to confirm no background binding. Then rmCD27-hFc was captured on the chip and finally supernatant was injected again to determine binding to rmCD27-hFc. rmCD27-hFc was injected at 5 µg/ml in HBS-EP+ running buffer. Supernatants were injected as neat samples. Blank medium was used to confirm the background binding to the chip and rmCD27-hFc. Samples were injected with a flow rate of 10 µl/min for 5 mins. The labels in the graph indicate the solution injected at that time point. CD70; scmCD70-mm1 supernatant, CD27; rmCD27-hFc.

Considering the level of protein secretion and binding to CD27, clone B was used for further bulk culture and protein was produced by growing CHO-K1S cells for 2 weeks and harvesting the supernatant. The protein was purified in the same way as scmCD70-m1 (detailed in chapter 3) and the dimer-of-trimer protein was further purified by SEC (Fig. 4.18.A). The profile of the protein at this time was similar to that of the parental scmCD70-m1 protein with a mix of dimer-of-trimer and higher-order structures. The purity of the isolated dimer-of-trimer protein was confirmed by analytical SEC (Fig. 4.18.B). In order to compare this new protein with the Endo H treated scmCD70-m1, 20 mgs of protein was treated with Endo H with a ratio of 5 units of enzyme per µg of protein for 3 hrs at 37 °C. The protein was then fractionated again by SEC to remove the Endo H and purify the Endo H treated scmCD70-mm1 protein (Fig. 4.18.C). The purity and removal of enzyme was confirmed by analytical SEC (Fig. 4.18.D). Additionally, the purity of the untreated and Endo H treated proteins, and removal of the enzyme was also confirmed by SDS-PAGE (Fig. 4.19). The shift in the size of the Endo H treated protein was very low compared to the untreated protein. However, glycosylation analysis revealed that untreated scmCD70-mm1 had 21.12% of total oligomannose content, which was significantly lower than the amount present on scmCD70-m1, and this was reduced to 1.50% after Endo H treatment (Table 4.3).

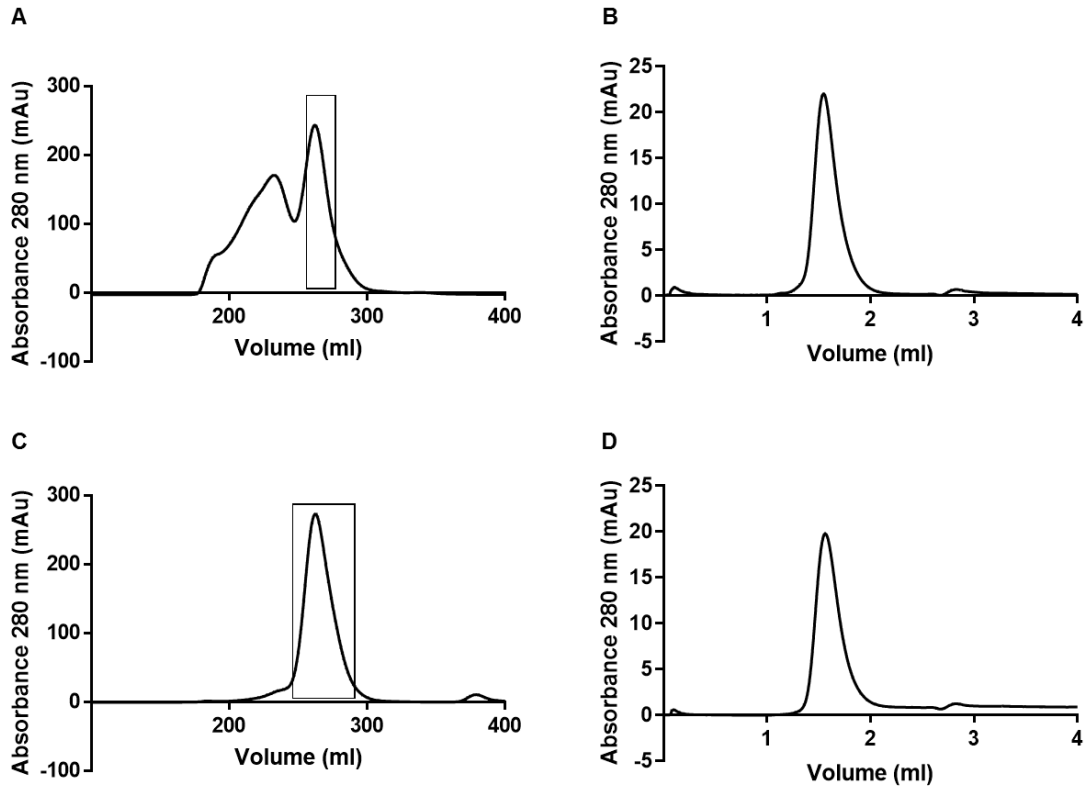

Figure 4.18. Purification and fractionation of scmCD70-mm1. CHO-K1S cells were grown for 2 weeks and supernatant was harvested. scmCD70-mm1 protein was first purified by protein A purification and then fractionated by SEC. (A) Purification of dimer-of-trimer fractions. The dimer-of-trimer fraction isolated (256 ml – 276 ml) is indicated on the graph. (B) Profile of isolated scmCD70-mm1 on analytical SEC column. (C) Fractionation of scmCD70-mm1 after Endo H treatment. 15 mgs of scmCD70-mm1 dimer-of-trimer protein was treated with Endo H with 5 units of enzyme to 1 µg of protein ratio (detailed in chapter 2). Then the enzyme treated protein was isolated by SEC. The isolated dimer-of-trimer fraction (246 ml – 290 ml) is indicated on the graph. (D) Profile of Endo H treated scmCD70-mm1 dimer-of-trimer protein after purification on analytical SEC column. For fractionation, samples were run on Superdex 200 26/950 (in-house). For analytical analysis, samples were run on Superdex 200 5/150 GL (GE Healthcare).

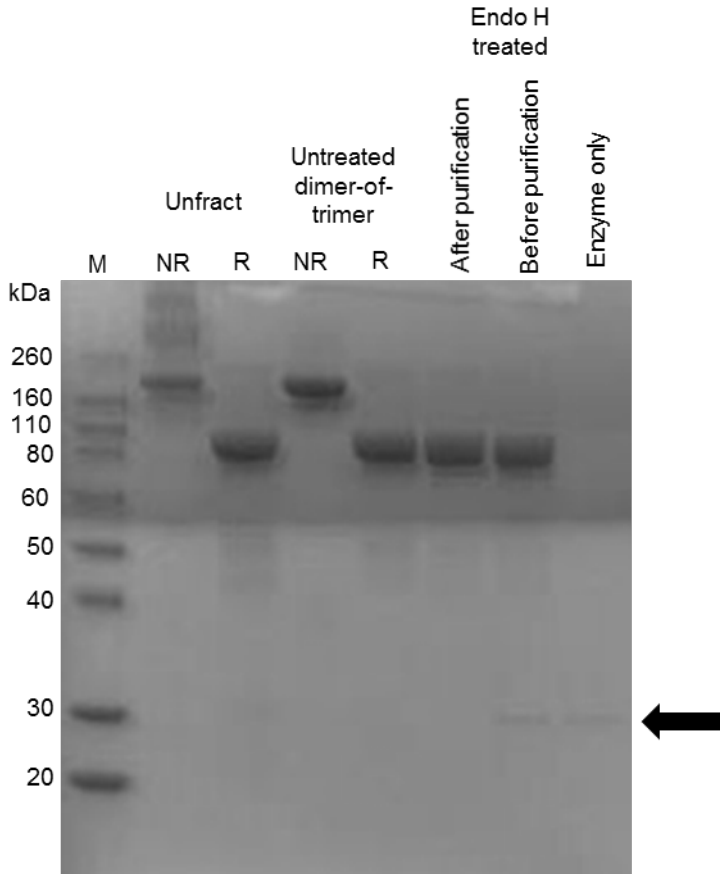

Figure 4.19. Purity and Endo H treatment of scmCD70-mm1. Samples from unfractionated (unfract) scmCD70-mm1, untreated scmCD70-mm1 and Endo H treated scmCD70-mm1 were analysed by SDS-PAGE. For unfractionated and untreated scmCD70-mm1, samples were prepared under reducing and non-reducing conditions. Endo H treated samples were prepared under reduced conditions. Reduced samples had a final concentration of 62.5 mM reducing agent (DTT). Samples were boiled at 95 °C for 5 mins and 10 µg of protein was loaded on 10% Bis-Tris gel. The gel was run at 100-120 V for 1.5 hrs and then Coomassie brilliant blue stained. The band corresponding to Endo H is indicated by the arrow. M; molecular weight markers, NR; non-reduced, R; reduced.

Table 4.3. Level of oligomannose residues out of total glycans on untreated and Endo H treated scmCD70-mm1.

	Untreated scmCD70-mm1	Endo H treated scmCD70-mm1
Total Oligomannose	21.12%	1.50%
M9	0.63%	0.00%
M8	1.18%	0.00%
M7	1.02%	0.00%
M6	3.17%	0.56%
M5	15.13%	0.94%

As scmCD70-mm1 was produced to eliminate binding to FcγR, the ability of scmCD70-mm1 to bind FcγR was investigated by SPR analysis and compared to scmCD70-m1. As previously observed, scmCD70-m1 showed binding to FcγRIIB and FcγRIII but not FcγRI and FcγRIV (Fig. 4.20). However, scmCD70-mm1 did not bind any of the FcγRs (Fig. 4.20) confirming that the mutation eliminated the interaction with FcγRs.

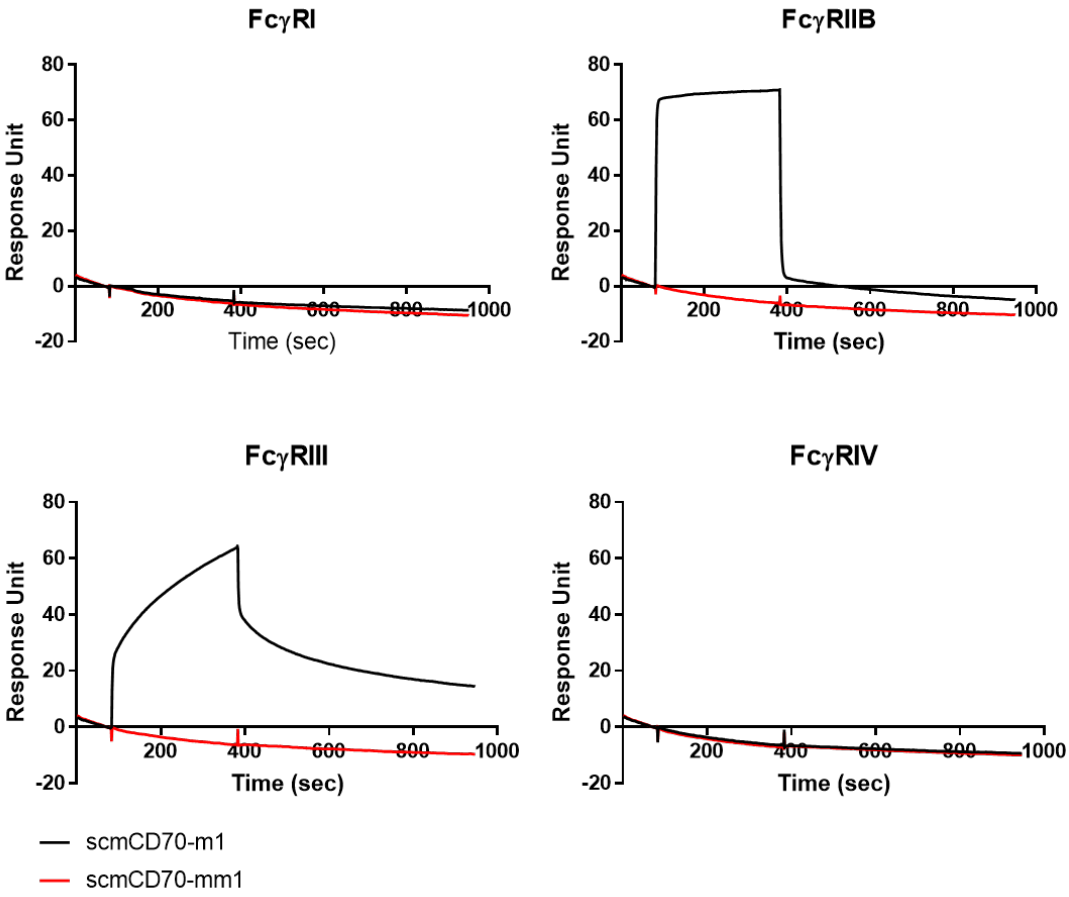

Figure 4.20. Comparison of FcγR binding of scmCD70-m1 and scmCD70-mm1. FcγR binding of scmCD70-mm1 was investigated by SPR analysis and compared to scmCD70-m1. Proteins (scmCD70-m1 and scmCD70-mm1) were directly immobilized via amine coupling into the flow cells of a CM5 sensor chip to achieve 2000 RU. Then the indicated FcγR solutions were injected at 200 nM in HBS-EP+ buffer with 5 mins association and 10 mins dissociation time with a flow rate of 30 µl/min.

Initially to confirm the lack of FcγR binding in a cell activation assay, Jurkat cells with NF-κB GFP reporter activity and stably transfected with WT mouse CD27 (detailed in chapter 5) were cultured with or without mouse FcγRIIB expressing CHO-K1 cells and stimulated with scmCD70-m1 or scmCD70-mm1. This assay enables GFP to be used as a read-out of NF-κB activity downstream of CD27. Both proteins similarly stimulated the activation of Jurkat cells (Fig. 4.21) in the absence of CHO-K1 mediated cross-linking. Co-culturing the Jurkat cells with FcγRIIB expressing CHO-K1 cells increased the percentage of GFP+ cells induced by scmCD70-m1 but not scmCD70-mm1 (Fig. 4.21). These results indicated that additional FcγR mediated cross-linking can improve the activity of scmCD70-m1 but not scmCD70-mm1.

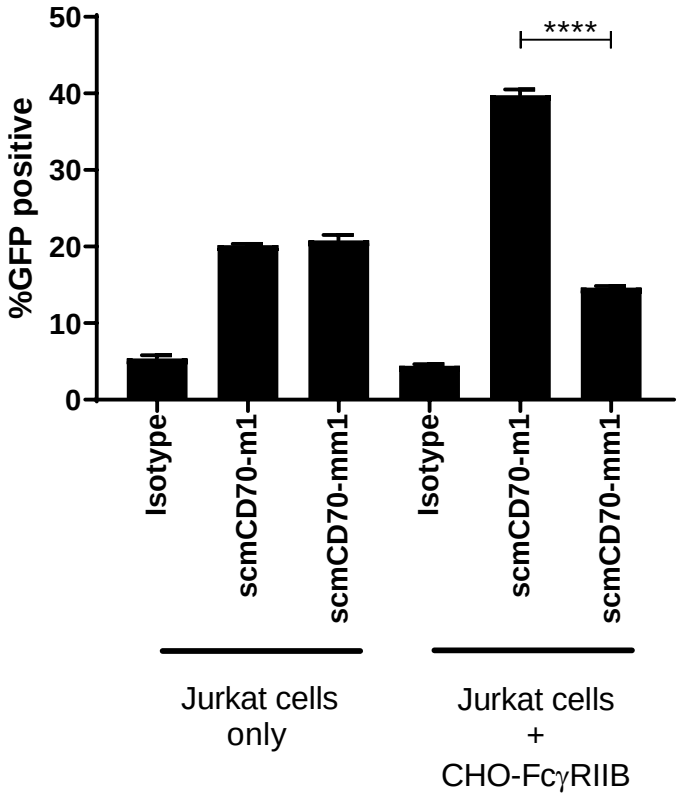

Figure 4.21. Activation of CD27 transfected Jurkat-NF-κB-GFP reporter cells upon stimulation with scmCD70-m1 and scmCD70-mm1. Jurkat-NF-κB-GFP reporter cells transfected with WT mouse CD27 were stimulated with indicated proteins with or without mouse FcγRIIB expressing CHO-K1 cells. The Jurkat and CHO-K1 cells were co-cultured at a 1:1 ratio and 1 x 10^5 of each cell type was used in the culture. Cells were incubated with the indicated proteins at 10 µg/ml for 6 hrs at 37 °C before measuring the level of GFP positive cells as the outcome of activation by flow cytometry. Statistical analysis was performed using one-way ANOVA with Tukey's multiple comparisons test. ****= $p<0.0001$. Mean +/- SD of duplicates are indicated from one experiment.

4.2.4 In vivo comparison of Endo H treated scmCD70-m1 and scmCD70-mm1

After confirming that scmCD70-mm1 is capable of initiating CD27 mediated signalling in vitro yet does not interact with FcγR, the in vivo activity of scmCD70-mm1 was investigated. In order to compare with scmCD70-mm1, a new batch of untreated and Endo H treated scmCD70-m1 was also generated (as described previously). Initially the in vivo half-lives of the new scmCD70-m1 and scmCD70-mm1 batches were examined. WT mice received a single injection of proteins and serum samples were obtained at 1, 6, 25 and 48 hrs post-injection and the concentration of proteins was determined by ELISA. Standard curves were generated for each protein by using known concentrations (Fig. 4.22.A) and used to determine the concentrations in serum samples. As observed previously, untreated scmCD70-m1 could only be detected at 1 hr post-injection whereas Endo H treated scmCD70-m1 could be detected up to 48 hrs post-injection (Fig. 4.22.B). Untreated scmCD70-mm1 showed much higher stability than untreated scmCD70-m1 but Endo H treated scmCD70-mm1 showed the highest stability which indicates that removing oligomannose residues also improved the in vivo stability of scmCD70-mm1 (Fig. 4.22.B).

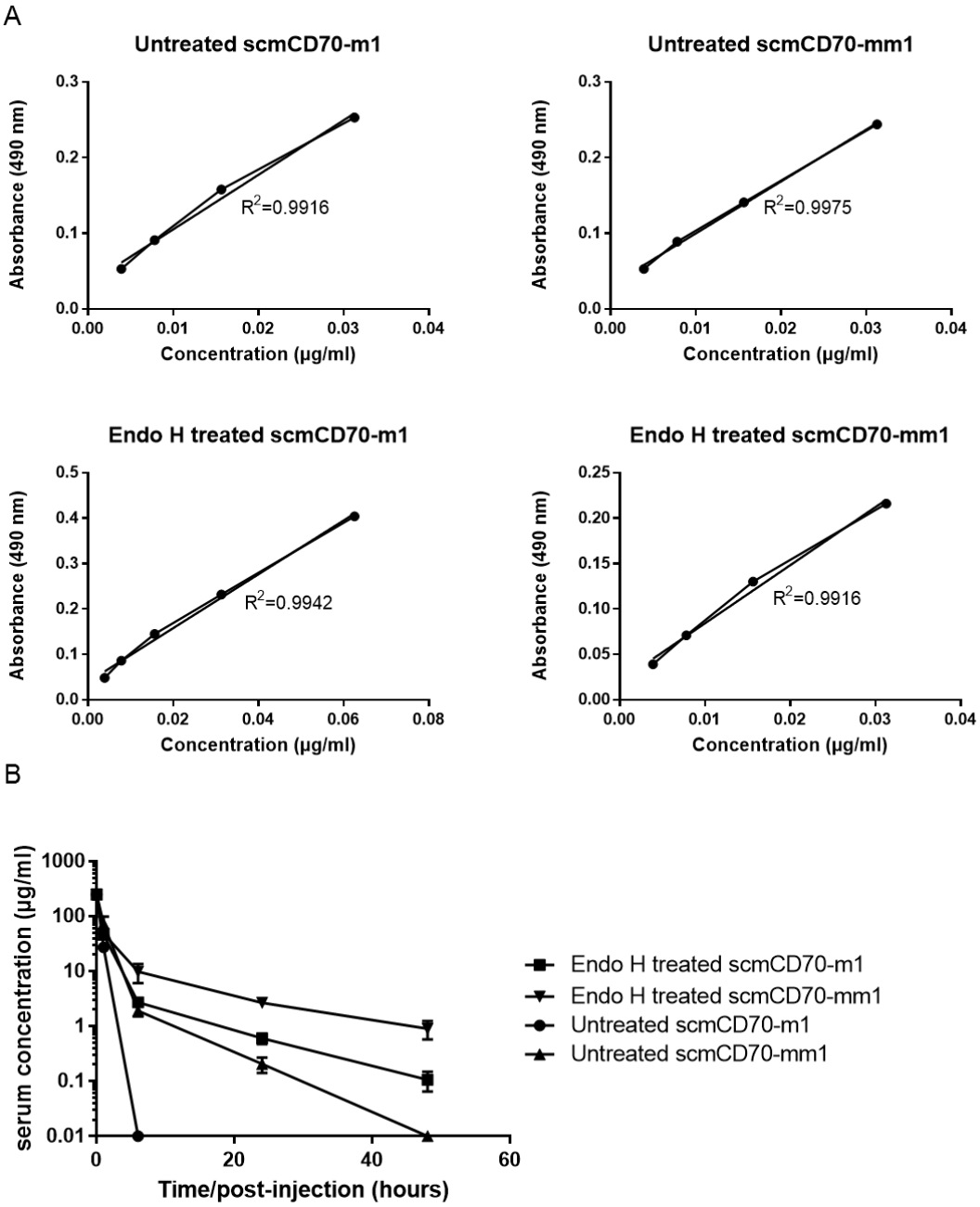

Figure 4.22. Serum half-lives of scmCD70-m1 and scmCD70-mm1 proteins. A single dose of 250 µg of indicated proteins was injected intravenously into 3 mice for each group. Peripheral blood samples collected at 1, 6, 25 and 48 hrs and serum collected by centrifuging at 15700 xg at 4 °C for 30 mins. Concentration of the proteins in serum samples was determined by ELISA. The plates were coated with anti-CD70 mAb (TAN 1-7) and the presence of proteins in serum samples was detected with rat anti-mouse-HRP. (A) Known concentrations of scmCD70-m1 were used to generate a standard curve to determine the concentrations in serum samples. Individual points and line of best fit are shown on each graph. (B) The concentrations of scmCD70-m1 and scmCD70-mm1 proteins at indicated time points. Mean +/- SEM are indicated from one experiment.

In order to investigate the in vivo activity of scmCD70-mm1 and compare to the activity of scmCD70-m1, 1 x 10^4 purified OT-1 T cells were adoptively transferred into WT and FcγR1,2,3,4 KO recipients. Then mice were immunised with $OVA_{257-264}$ peptide in combination with control, untreated scmCD70-mm1, Endo H treated scmCD70-mm1 or Endo H treated scmCD70-m1. Untreated scmCD70-m1 was not used in this experiment as the activity was thoroughly characterised in previous assays and the response was negligible with this very low cell number transfer (Fig. 4.11.C & 4.14). Untreated scmCD70-mm1 was included in this experiment as the in vivo stability was higher than untreated scmCD70-m1 which indicated that it might show better activity than scmCD70-m1 protein. However, in WT recipients, untreated scmCD70-mm1 did not induce expansion of antigen specific OT-1 cells (Fig. 4.23). Although in WT mice, Endo H treated scmCD70-mm1 stimulated the expansion of antigen specific T cells, the highest activity was achieved by Endo H treated scmCD70-m1. Interestingly, in FcγR1,2,3,4 KO mice, Endo H treated scmCD70-mm1 induced a response slightly higher than Endo H treated scmCD70-m1 (Fig. 4.23). This indicated that as hypothesised, in WT mice, Endo H treated scmCD70-m1 receives cross-linking via FcγRs and this enhances its activity. In FcγR1,2,3,4 KO mice, there are no FcγRs and both proteins act only via dimer-of-trimeric interactions indicating that, where there are no FcγRs available, Endo H treated scmCD70-mm1 shows better activity possibly as a result of having better in vivo stability (Fig. 4.23).

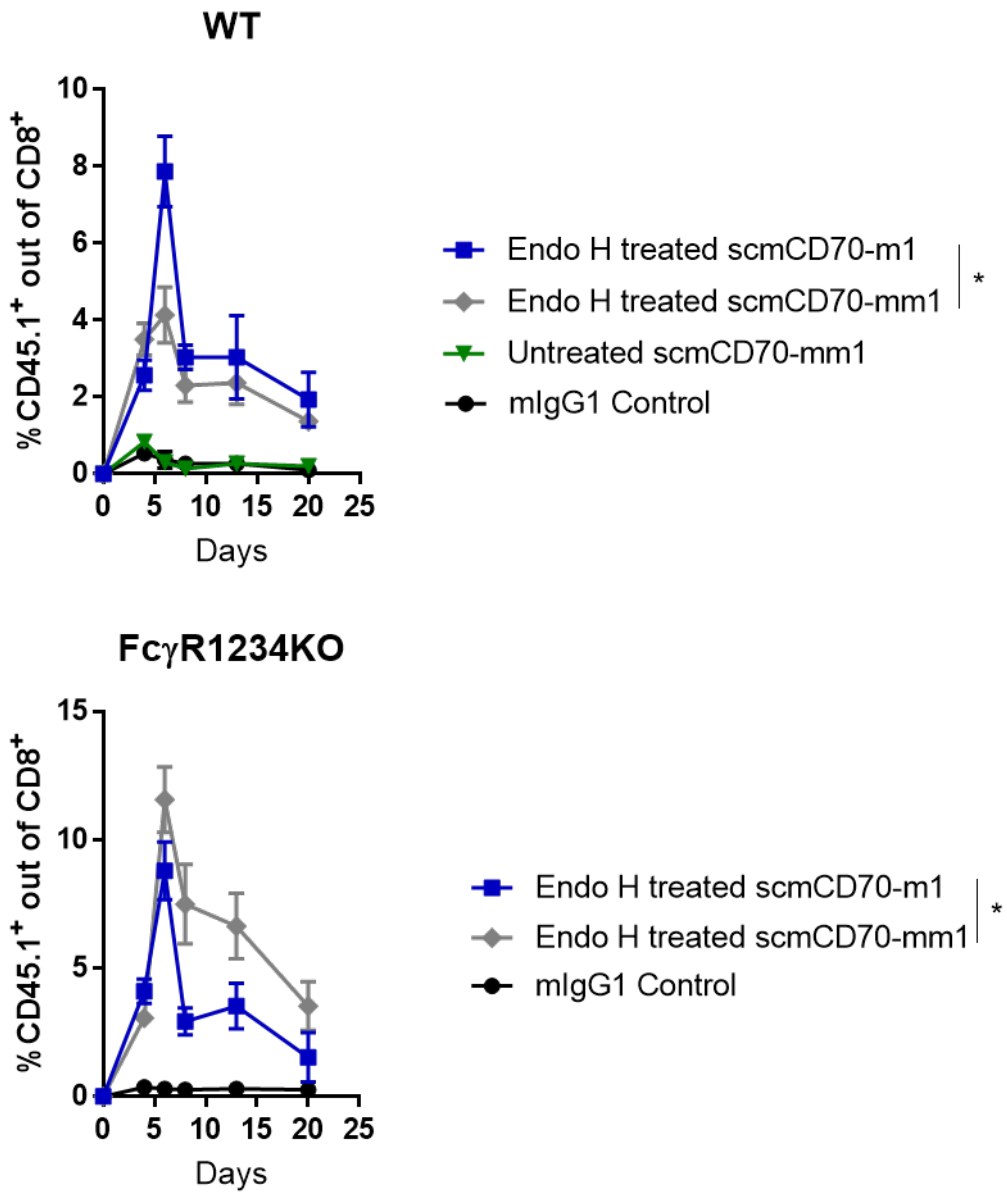

Figure 4.23. Comparison of in vivo expansion of OT-1 T cells stimulated with Endo H treated scmCD70-m1 or scmCD70-mm1. Naïve 1 x 10^4 CD45.1 congenic OT-1 T cells were adoptively transferred into WT or FcγR1,2,3,4 KO recipients on day -1. Mice were then immunised with 30 nmol $OVA_{257-264}$ in combination with 250 µg of indicated proteins on day 0 and another 250 µg dose of proteins on day 1. All samples were injected intravenously. Peripheral blood was collected on indicated time points and expansion of OT-1 specific $CD8^+$ T cells was monitored by staining with anti-mouse CD8a and anti-mouse CD45.1 antibody. Data were collected by flow cytometry and 3 mice per group were used. Statistical analyses were performed by using two-way ANOVA with Tukey's multiple comparisons test and statistics at the peak of the response are indicated. *=$p<0.05$. Mean +/- SEM are indicated. Data representative of two independent experiments.

As Endo H treated scmCD70-mm1 could induce in vivo expansion of antigen specific $CD8^+$ T cells, anti-tumour efficacy was investigated in a BCL1 model and compared to Endo H treated scmCD70-m1 and agonistic anti-CD27 mAb. As before, 5 x 10^6 BCL1 cells were injected into WT mice on day 0 prior to treatment with the indicated proteins on days 5, 6, 7 and 8 with 200 µg of proteins at every injection. The results indicated that Endo H treated scmCD70-mm1 could improve survival compared to the control group and activity was similar to Endo H treated scmCD70-m1 and agonistic anti-CD27 mAb (Fig. 4.24). Together the data presented here show that dimer-of-trimer activity is sufficient to induce activation and expansion of antigen specific T cells and can also induce an anti-tumour response.

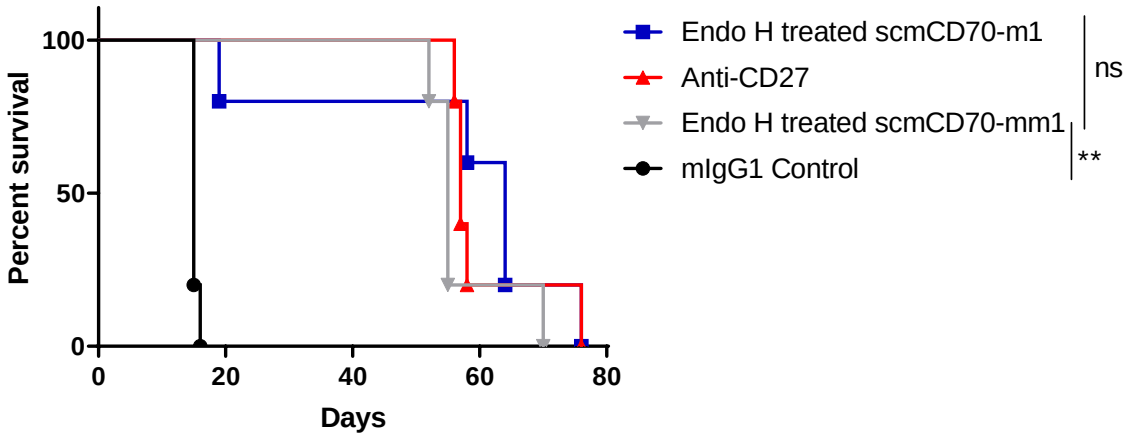

Figure 4.24. Anti-tumour efficacy of Endo H treated scmCD70-mm1 in BCL1 model. 5 x 10^6 BCL1 cells were injected into WT BALB/c mice on day 0. Animals then received the indicated proteins on days 5, 6, 7 and 8 with 200 µg of proteins being injected at each time point. All injections were performed intravenously. Mice were culled when a humane end-point was reached. Statistical analyses were performed by using Log-rank test. Ns; not significant, **=p<0.01. Data are from one experiment.

4.3 Discussion

Data presented in this chapter illustrate that scmCD70-m1 can induce in vivo expansion of antigen specific T cells and stimulate an anti-tumour response in a BCL1 model. The presence of oligomannose type glycans negatively influences the in vivo stability and activity of scmCD70-m1 but this can be rectified by enzymatic removal using Endo H. In keeping with the rationale of designing scmCD70-m1, the protein can induce in vivo expansion of T cells independent of FcγR availability whereas the activity of agonistic anti-CD27 mAb is completely dependent on FcγR cross-linking. Additionally, the dimer-of-trimer scmCD70-m1 can induce in vivo T-cell expansion with only dimer-of-trimeric interactions but having an intact Fc, enabling FcγR cross-linking, can further enhance the activity.

Although the potency of anti-mouse CD27 mAb (AT124-1, rIgG2a) was previously demonstrated (234), initial experiments shown here confirm the potency of the highly agonistic mIgG1 isotype of AT124-1 to stimulate in vivo expansion of antigen specific T cells (Fig. 4.2.B). In line with data from anti-human CD27 mAb (43), its efficacy was completely dependent on the availability of FcγRs, specifically FcγRIIB. In line with data on the mIgG1 isotype (167), further assays showed that anti-CD27 mIgG1 binds to FcγRIIB and FcγRIII by SPR analysis (Fig. 4.13). In FcγRIIB KO mice, the antibody depleted $CD8^+$ T cells to very low levels (Fig. 4.2.C) which was likely a reflection of mAb binding to FcγRIII as direct targeting mAbs bind to activatory FcγRs (FcγRI, FcγRIII and FcγRIV) and induce depletion of target cells (235). The data presented here indicate that in the absence of FcγRIIB, agonistic anti-CD27 mAb may bind to FcγRIII and induce an activity similar to a direct targeting mAb. This finding is important as it suggests that depending on the availability of FcγRs, the activity of the mAbs can change significantly and mAbs can produce different effects in different tissues or in the tumour microenvironment.

Encouragingly, scmCD70-m1 also promoted expansion of T cells in vivo. However, unlike anti-CD27, this protein was still active in mice lacking FcγRIIB and there was no depletion of $CD8^+$ T cells with scmCD70-m1 regardless of availability of FcγRs (Fig. 4.2). These data indicated that scmCD70-m1 can still work without the dependence on FcγR availability, creating an advantage compared to anti-CD27 mAb.

4.3.1 The activity of scmCD70-m1 can be enhanced by oligomannose removal

Although scmCD70-m1 could activate expansion of antigen specific T cells in WT mice, responses were lower than obtained after stimulation with anti-CD27 and $CD8^+$ T cell responses were more short-lived (Fig. 4.2). In light of this, we investigated the half-life of the protein in vivo and found it to be very short; it could not be detected after 1 hr post-injection in contrast to the mAb which could be detected at high concentrations up to 1 week post-injection (Fig. 4.3). Initial demonstration of FcRn binding of scmCD70-m1 and anti-CD27 (Fig. 4.4), indicated that other factors were contributing to short in vivo stability.

One of the factors influencing in vivo stability is glycosylation. scmCD70-m1 and anti-CD27 have potential 20 and 4 N-glycosylation sites respectively. Analysis of the glycosylation of scmCD70-m1 and anti-CD27 revealed that scmCD70-m1 protein had high levels of oligomannose residues which could range from 76.76% to 31% depending on the culture conditions during production and anti-CD27 had 10% oligomannose residues out of total glycans. Using Endo H activity to reduce the level of oligomannose residues, significantly improved the in vivo stability of scmCD70-m1 (Fig. 4.10). Although the frequency of oligomannose residues on Endo H treated protein was similar to anti-CD27, the half-life was still much shorter than anti-CD27, indicating that there are additional factors which contribute to rapid clearance from circulation (discussed in detail in Chapter 6).

Improving the in vivo stability of scmCD70-m1 by Endo H treatment, also significantly improved its ability to induce expansion of antigen specific T cells in vivo. While untreated scmCD70-m1 protein could stimulate the expansion of T cells when high numbers (1×10^6) of antigen specific T cells were transferred (Fig. 4.2), its activity was minimal at more modest (1×10^4) physiological levels (Fig. 4.11). The number of SIINFEKL-antigen specific T cells in an unimmunised mouse are less than 1000 (236, 237) and 1×10^4 adoptive transfer therefore reflects a more physiological frequency of T cells, considering that approximately 10% of the transferred cells survive. While Endo H treatment improved the half-life of the scmCD70-m1 protein compared to untreated scmCD70-m1 this was not to the same level as the anti-CD27 mAb. Interestingly, despite the shorter half-life compared to mAb, Endo H treated protein showed a higher activity in stimulating antigen specific T cells compared to agonistic mAb (Fig. 4.11). This is an important finding as it suggests that in a tumour setting, where there are low numbers of tumour specific T cells, Endo H treated scmCD70-m1 might generate a greater response than agonistic anti-CD27 mAb.

Initial activation and commitment of $CD8^+$ T cells to divide requires a short time of exposure to antigen and co-stimulatory signalling. In a study, where $CD8^+$ T cells were stimulated with antigen expressing APCs in combination with co-stimulatory signalling in vitro, as short as 2 hrs of stimulation was sufficient to drive further expansion of activated $CD8^+$ T cells (238). In another study in which the antigen expressing APCs could be selectively depleted in vivo, antigen exposure of less than 7 hrs was sufficient to allow $CD8^+$ T cells to become activated and committed for further expansion (239). The availability of the untreated scmCD70-m1 in circulation for only around 1 hr may have not been sufficient to prime a high T-cell response. In contrast, Endo H treated scmCD70-m1 could generate a strong response and was available in circulation for up to 48 hrs (Fig. 4.10). Although the levels of Endo H treated scmCD70-m1 were not as high as a mAb, the concentration of Endo H treated protein available in the initial 6 hrs is sufficient to drive activation of OT-1 $CD8^+$ T cells by providing a strong co-stimulatory interaction in the presence of antigen. The response generated by Endo H treated scmCD70-m1 was as good as anti-CD27 mAb when high OT-1 numbers were transferred yet stronger than anti-CD27 when low OT-1 numbers were transferred indicating that it can induce a better activity than anti-CD27.

4.3.2 The activity of scmCD70-m1 can be enhanced by FcγR cross-linking

Data presented in this thesis show that, while the anti-CD27 mAb and Endo H treated scmCD70-m1 both induced T-cell expansion in WT mice, only Endo H treated scmCD70-m1 induced expansion of T cells in FcγR1,2,3,4 KO mice when 1 x 10^4 cells were adoptively transferred. This is likely due to increased CD27 cross-linking afforded by Endo H treated scmCD70-m1 compared with anti-CD27. However, the activity of Endo H treated scmCD70-m1 in FcγR1,2,3,4 KO mice was lower than in WT mice (Fig. 4.14). Endo H treated scmCD70-m1 showed binding to FcγRIIB and FcγRIII in SPR analysis (Fig. 4.13) indicating that there could be additional cross-linking which further improves the activity of Endo H treated scmCD70-m1 in WT compared to FcγR1,2,3,4 KO mice.

To test the hypothesis that the activity of Endo H treated scmCD70-m1 is improved by cross-linking in WT mice, a version of scmCD70-m1, scmCD70-mm1, which lacks FcγR binding was designed and its lack of interaction with FcγRs was confirmed (Fig. 4.20). Then Endo H treated versions of scmCD70-m1 and scmCD70-mm1 were compared for their ability to stimulate OT-1 T-cell expansion in WT or FcγR1,2,3,4 KO mice. Results showed that in WT

mice, Endo H treated scmCD70-m1 showed a higher activity than Endo H treated scmCD70-mm1. However, in FcγR1,2,3,4 KO mice, Endo H treated scmCD70-mm1 induced a slightly higher response than Endo H treated scmCD70-m1 (Fig. 4.23). Notably the Endo H treated scmCD70-mm1 had a slightly higher in vivo stability than Endo H treated scmCD70-m1 (Fig. 4.22.B). These data suggest that, in FcγR1,2,3,4 KO mice, in which the activity is only based on dimer-of-trimeric interaction of proteins and both proteins are expected to stimulate the same magnitude of response, the Endo H treated scmCD70-mm1 showed slightly better activity as a consequence of having higher stability than Endo H treated scmCD70-m1. However, in WT mice, Endo H treated scmCD70-m1 stimulated a higher expansion of antigen specific T cells, indicating that Endo H treated scmCD70-m1 receives additional cross-linking by FcγRs and this compensates for the slightly lower stability and contributes to a better activity compared with Endo H treated scmCD70-mm1.

In contrast to the results with Endo H treated scmCD70-m1, untreated scmCD70-m1 showed a similar activity in WT and FcγRIIB KO mice (Fig. 4.2.B). Of note, untreated scmCD70-m1 could not be detected in circulation after 1 hr post-injection suggesting that the activity of untreated scmCD70-m1 in both WT and FcγRIIB KO mice is based on the dimer-of-trimeric interactions and the rapid clearance may not allow enough time for additional cross-linking to occur to further enhance activity in WT mice. Untreated scmCD70-m1 shows the same FcγR binding profile as Endo H treated scmCD70-m1 and the difference between the two proteins is the improved in vivo stability of Endo H treated protein. Also, both versions show similar in vitro activity in stimulating T-cell proliferation. These observations further support the idea that Endo H treated protein may be cross-linked by FcγR interaction in WT mice whereas untreated protein does not undergo that interaction in vivo.

4.3.3 scmCD70-m1 and its Fc “silent” variant can promote anti-tumour immunity

The anti-tumour efficacy of targeting CD27 by agonism in the BCL1 model has been previously established in several pre-clinical studies (95, 157) and the results with the agonistic anti-CD27 used in here are consistent with previous studies. In contrast, untreated scmCD70-m1 failed to induce an anti-tumour response in the BCL1 model. Considering the relatively weak activity of scmCD70-m1 compared with anti-CD27 for OT-1 T-cell stimulation, the anti-tumour activity was not expected to be as high as that induced by anti-

CD27. Endo H treatment of scmCD70-m1 improved its activity in stimulating antigen specific T-cell expansion and this also generated a significantly better anti-tumour activity compared to untreated scmCD70-m1 (Fig. 4.12). Indeed Endo H treated protein generated an anti-tumour response very similar to the agonistic anti-CD27 mAb. Interestingly, Endo H treated scmCD70-mm1 also generated a strong anti-tumour response in the BCL1 model which was similar to mAb and Endo H treated scmCD70-m1 responses (Fig. 4.24). These data indicate that dimer-of-trimeric interactions, without additional cross-linking, can be sufficient to generate a strong anti-tumour response.

In summary, data presented in this chapter show that scmCD70-m1 and the Fc "silent" variant, scmCD70-mm1, can act as in vivo co-stimulatory agents to induce expansion of antigen specific T cells independent of FcγR engagement. The in vivo stability of the ligand forms can be enhanced by removing oligomannose residues and this in turn leads to significantly better in vivo activity. The ligands with improved in vivo stability induce anti-tumour immunity and increase survival in murine BCL1 model.

Chapter 5 Influence of CD27 dimerisation on signal activation

5.1 Introduction

The majority of the co-stimulatory members of the TNFRSF are expressed as monomers on the cell surface and CD27 is expressed as a disulphide linked homodimer (86). As previously described (section 1.10), TNFRSF proteins require clustering to be activated and being a dimer and thus partially oligomerised, might therefore provide an advantage to CD27 in activation. However, the impact of the disulphide bonds on CD27 activity has not been studied but we hypothesised that eliminating disulphide linked dimerisation might influence the structural stability and conformation of CD27 on the cell surface, ultimately influencing downstream signalling.

The crystal structure of human CD27 revealed that there is a Cys residue residing at position 185 before the transmembrane domain which is not involved in the CRD domains or the ligand binding domain. It resides in a flexible region of the ECD and as human CD27 is expressed as a dimer on the cell surface, it has been predicted that the free Cys residue at position 185 contributes to disulphide linked dimerisation of hCD27 (240).

In this chapter, the aim was to characterise the importance of disulphide linked dimerisation of murine CD27 for cell surface expression and downstream signal activation. In order to investigate these, two mutant forms of CD27 with mutated Cys residues (residing before the transmembrane domain) to eliminate dimerisation were produced and compared with the WT CD27 protein.

5.2 Results

In order to test the hypothesis that disulphide bond linked dimerisation of murine CD27 is important for expression and signal activation, the murine CD27 protein sequence was aligned with other species to examine how conserved the Cys residues are and identify the Cys residues contributing to disulphide bond formation. The murine, rat, gorilla and human CD27 sequences were aligned by using the Uniprot protein sequence database website (Fig. 5.1) and Clustal Omega program. The overall % similarity between the four sequences was 60.92%.

The Cys at position 185 of human CD27 has been postulated to contribute to disulphide linked dimerisation of human CD27 (240). This residue (C185) corresponds to residue 176 on the murine sequence (Fig. 5.1) which is also a Cys suggesting that this might contribute to disulphide linked dimerisation of mouse CD27. In addition, the Cys residue at position 176 was conserved amongst all species.

Another Cys residue (position 180 in the mouse, Fig. 5.1) was also present in the mouse sequence which was conserved in the rat but not in the other sequences. It could be that Cys at position 176 (conserved in all species) is responsible for disulphide linked dimerisation of murine CD27. However, as Cys at position 180 is also located before the transmembrane domain, we hypothesised that it could also be forming disulphide bonds, contributing to CD27 dimerisation. Thus, we generated two mutant forms of CD27; one incorporating a single Cys mutation at position 176 and another mutant with mutation of both Cys residues at positions 176 and 180.

To examine the role of both Cys residues, a single mutant (SM) (C176A) and a double mutant (DM) (C176A and C180A) form of murine CD27 were produced by mutating Cys residues to Ala residues. DNA sequences for WT (from Unigene, (NM_001042564.1)), single mutant and double mutant CD27 were generated in Seqbuilder. The sequences were then ordered commercially to be provided in pcDNA3.1 (+) plasmid DNA (Fig. 5.2).

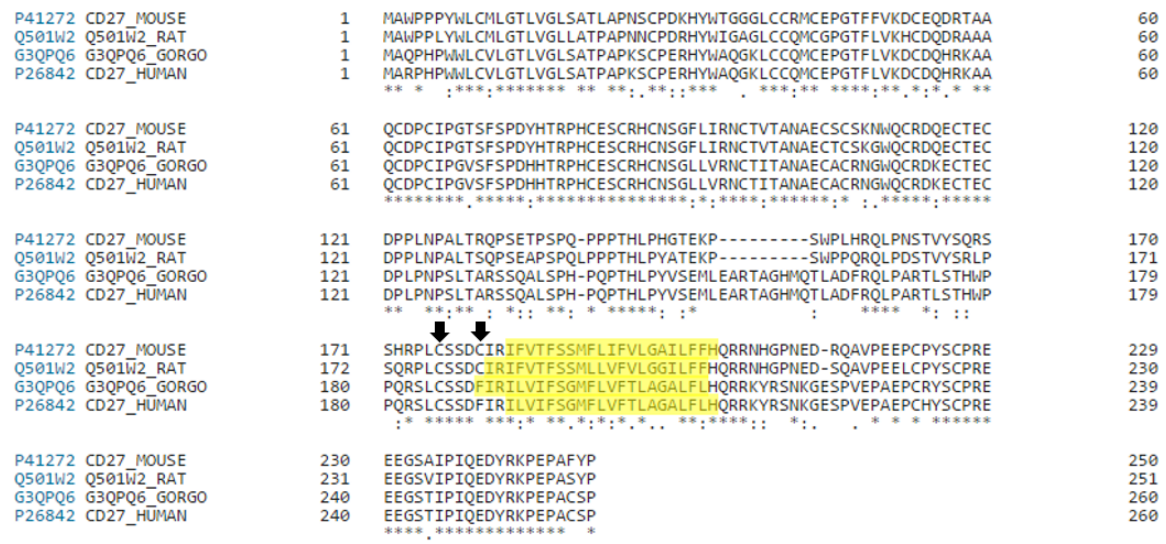

Figure 5.1. Amino acid sequence alignment of CD27 protein from mouse, rat, gorilla and human. The amino acid sequence of murine CD27 was aligned with the amino acid sequences of rat, gorilla and human CD27. Sequences were aligned using Uniprot protein database website and Clustal Omega program. The accession numbers of the protein sequences on Uniprot website were; P41272 for mouse, Q501W2 for rat, G3QPQ6 for gorilla and P26842 for human CD27. The highlighted regions indicate the transmembrane domains. '–' indicates missing sequence, '*' indicates amino acids conserved in all aligned sequences, ':' indicates conservation between groups of strongly similar properties and '.' indicates conservation between groups of weakly similar properties. The mutated Cys residues at positions 176 and 180 in murine CD27 are indicated with arrows.

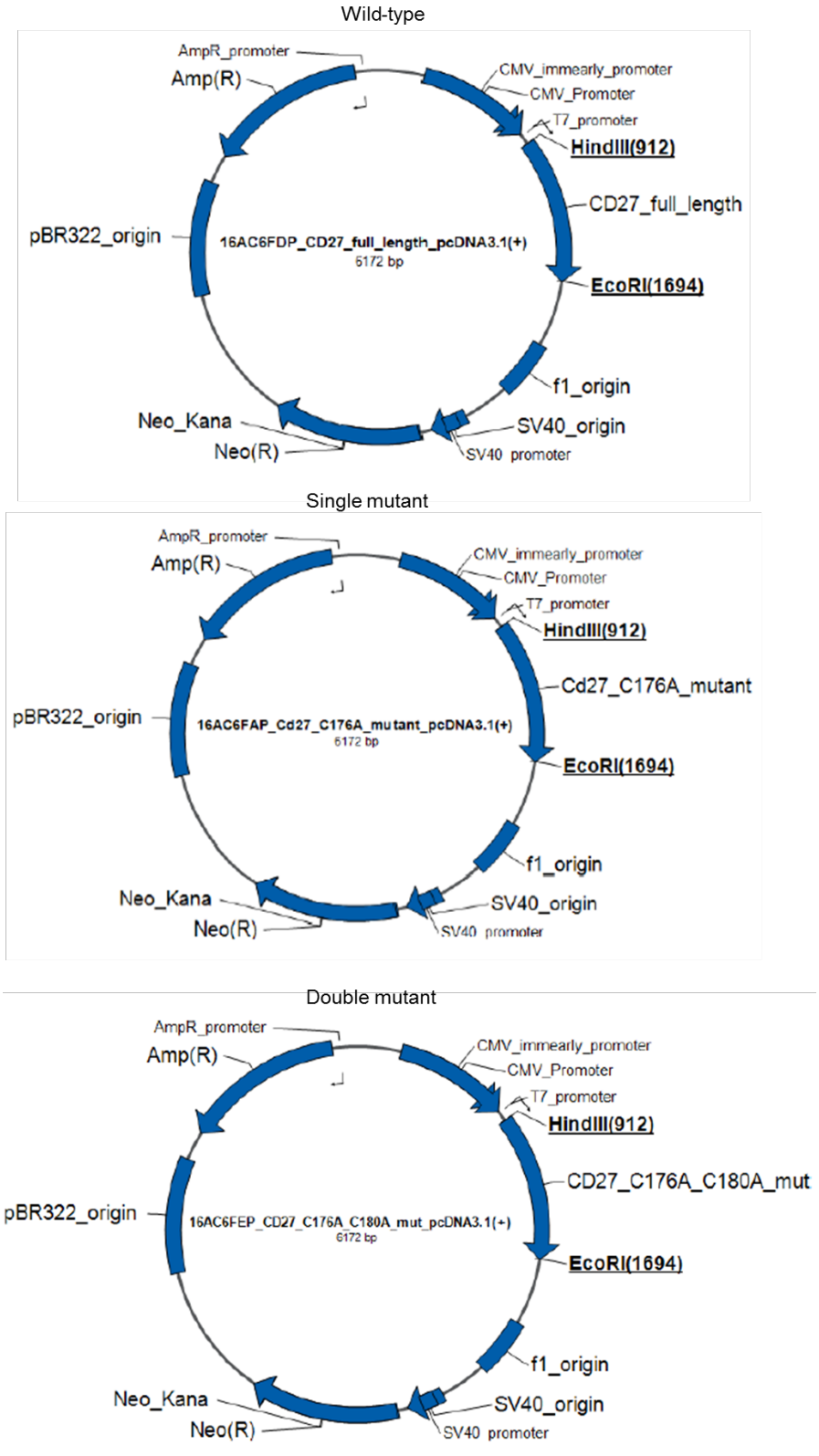

Figure 5.2. WT and mutant CD27 plasmid maps. The WT, SM and DM murine CD27 sequences were ordered commercially in pcDNA3.1 (+) expression vector. The SM contained a C176A mutation whereas the DM contained both C176A and C180A mutations. Inserts were flanked with HindIII and EcoRI restriction sites to enable further cloning if required.

5.2.1 Expression and dimerisation of WT and mutant CD27 forms

In order to investigate if the Cys residues are important for expression of the CD27 protein, 293T cells were transiently transfected with WT, SM or DM CD27 and expression of the protein was examined 72 hrs post-transfection via flow cytometry. Two different anti-CD27 mAbs were used to detect the protein to circumvent the potential loss of mAb epitope by the introduced mutations. Staining with in-house anti-CD27 mAb (AT124-1) revealed that both mutant forms of CD27 were expressed by 293T cells and this indicated that mutating the Cys residues to remove disulphide bonds did not influence the expression of protein (Fig. 5.3). Additional staining with a commercial anti-CD27 antibody (LG.3A10) similarly showed that both mutant forms were expressed (Fig. 5.4). These results show that eliminating dimerisation does not prevent surface expression of CD27 or significantly influence the availability of epitopes of these antibodies.

To confirm that loss of Cys 176 only or loss of both 176 and 180 inhibited CD27 dimerisation, cell lysates were obtained from transiently transfected 293T cells and the CD27 protein was detected by Western Blot using anti-CD27 mAb (AT124-1). The antibody did not recognise its epitope when the proteins were in the reduced form but did show binding to CD27 under non-reduced conditions (Fig. 5.5). The molecular weight of monomeric CD27 without glycosylation is approximately 29 kDa. However, CD27 has both N-linked (2 on each monomer) and O-linked glycosylation sites, meaning that the molecular weight of the monomer is predicted to be larger than 29 kDa and the dimer is predicted to be larger than 58 kDa. Although only the dimeric form of CD27 should have been observed after transfection with the WT protein, multiple bands were detected between 60 – 80 kDa (Fig. 5.5). These could be dimers with different levels of glycosylation. In addition, bands between 35 – 45 kDa were also observed. These could be degradation products or monomeric proteins with different levels of glycosylation that did not form dimers during rapid protein production in 293T cells. The higher molecular weight bands were also detected in cells transfected with the SM form of CD27 with an additional very faint band evident at a lower molecular weight (Fig. 5.5). This result indicated that the SM form could still form disulphide linked dimers of CD27 and mutating Cys at position 176 was not sufficient to eliminate dimerisation. In contrast, only low molecular weight products (35 – 45 kDa) were detected in cells transfected with the DM CD27 construct (Fig. 5.5) indicating that mutating both Cys residues eliminated the disulphide linked dimerisation of CD27 such that protein was expressed in the monomeric form.

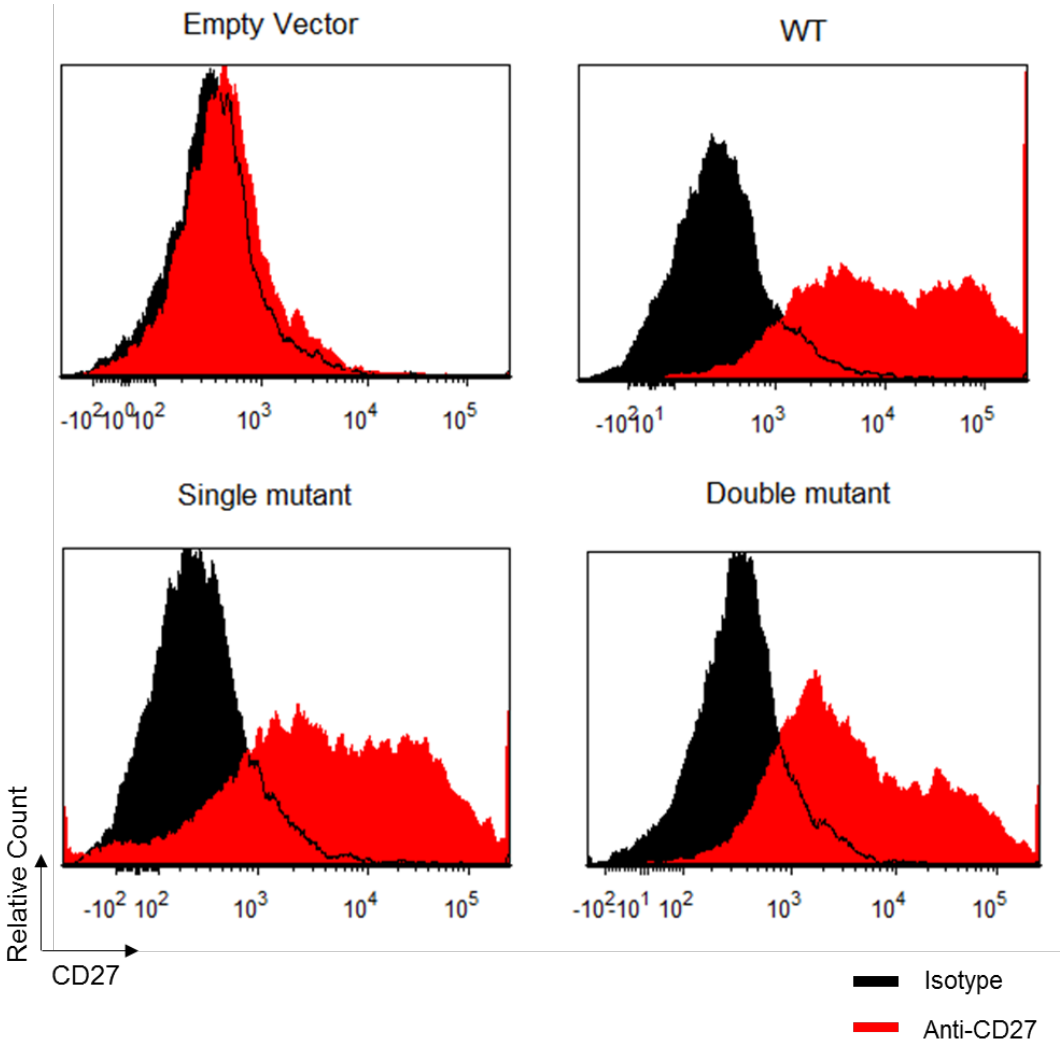

Figure 5.3. Cell surface expression of WT and mutant CD27 forms on 293T cells stained with in-house anti-CD27 mAb. 293T cells were transiently transfected with the expression vectors of indicated proteins. 1 x 10^5 293T cells per well were plated into a 6-well plate and allowed to grow for 72 hrs. The cells were then transfected with 5 µg plasmid DNA of the indicated constructs. The expression of CD27 was determined at 72 hrs post-transfection using flow cytometry. The cells were stained with the isotype (Mc106A5, rIgG2a) or anti-CD27 mAb (AT124-1 rIgG2a, in-house) as the primary antibody for 30 mins at 4 °C. Then the cells were stained with anti-rat secondary APC (Jackson Immunoresearch 712-136-153) for 30 mins at 4 °C for detection of CD27 expression.

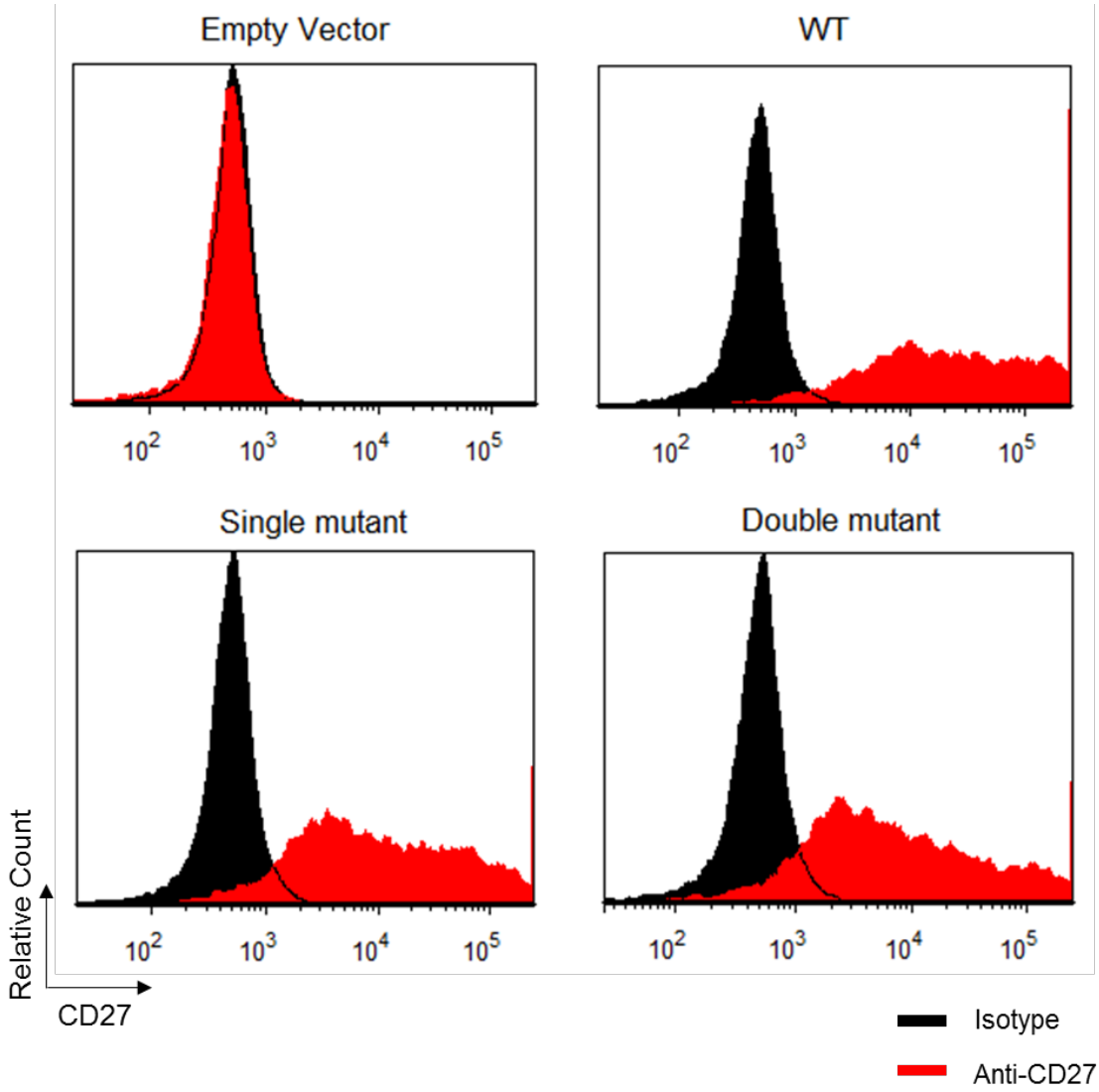

Figure 5.4. Cell surface expression of WT and mutant CD27 forms on 293T cells stained with commercial anti-CD27 mAb. 293T cells were transiently transfected with the expression vectors of indicated proteins. 1 x 10^5 293T cells per well were plated into a 6-well plate and allowed to grow for 72 hrs. The cells were then transfected with 5 µg plasmid DNA of the indicated constructs. The expression of CD27 was determined at 72 hrs post-transfection via flow cytometry. The cells were stained with the isotype (hamster IgG) or directly labelled commercial anti-CD27 mAb (LG.3A10-PE) for 30 mins at 4 °C before detecting CD27 expression.

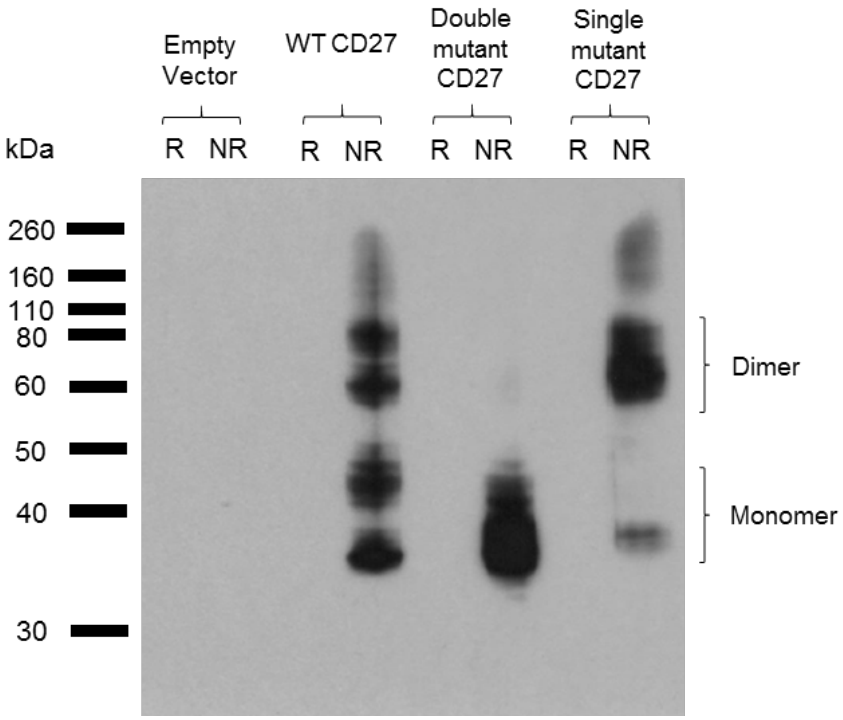

Figure 5.5. Western blot analysis of WT, SM and DM CD27. 293T cells were transiently transfected as above (Fig 5.3) and cell lysates were obtained at 72 hrs post-transfection. Lysate from 1 x 10^6 cells was run per lane under reduced and non-reduced conditions. Reduced samples had a final reducing agent (DTT) concentration of 62.5 mM. Samples were boiled for 5 mins at 95 °C and loaded onto a 10% Bis-Tris gel. Gel was run at 120 V for 1.5 hrs in MOPS running buffer. Then transferred onto Immobilon-P membrane by running at 100 V for 1 hr in Nu-PAGE transfer buffer. The membrane was blocked for 1 hr in 5% milk solution prepared in western blot wash buffer. Then the membrane was incubated with anti-CD27 mAb (AT124-1, rIgG2a) for ~17 hrs at 4 °C. Finally the membrane was incubated with anti-rat secondary HRP for 1 hr at RT before detecting the signal by using an ECL substrate. The bands corresponding to monomeric and dimeric CD27 are indicated on the figure.

5.2.2 Generation of stable clones to characterise signalling activity of WT and DM CD27

After confirming that both SM and DM forms of CD27 could be expressed at the cell surface and that the SM form, but not the DM form, still formed disulphide linked dimers, further experiments were carried out using the DM form only. In order to investigate the influence of dimerisation on signalling, WT and DM CD27 were stably transfected into Jurkat cell lines with NF-κB-GFP reporter activity to generate cell lines with similar levels of CD27 expression. These Jurkat cells produce GFP as a downstream effect of NF-κB activation and the level of GFP positive cells was used as a readout of CD27 signalling. Jurkat cells were transfected with the pcDNA3.1 (+) plasmids and plated into 96 well plates at 1 x 10^4 cells per well to grow individual clones. The single clones were selected with geneticin (neomycin) antibiotic resistance and were screened for cell surface CD27 expression by flow cytometry. From the initial screening, six WT and six DM clones with different levels of CD27 expression were chosen for further growth (Fig. 5.6). Although clones with different expression levels were grown and frozen, initial experiments were carried out using the clones with a high level of CD27 expression; WT clone A and DM clone D which showed similar levels of expression (Fig. 5.6). In order to have a negative cell line, Jurkat-NF-κB-GFP cells stably transfected with empty vector pcDNA3.1 (+) were also produced with geneticin resistance and lack of CD27 expression was confirmed (Fig. 5.7.A). As, WT clone A and DM clone D were going to be used for further assays, cells were grown to confirm that CD27 was retained on the cell surface and remained expressed at similar levels; the level of CD27 expression was found to be similar as confirmed by overlaying the WT and DM plots (Fig. 5.7.B).

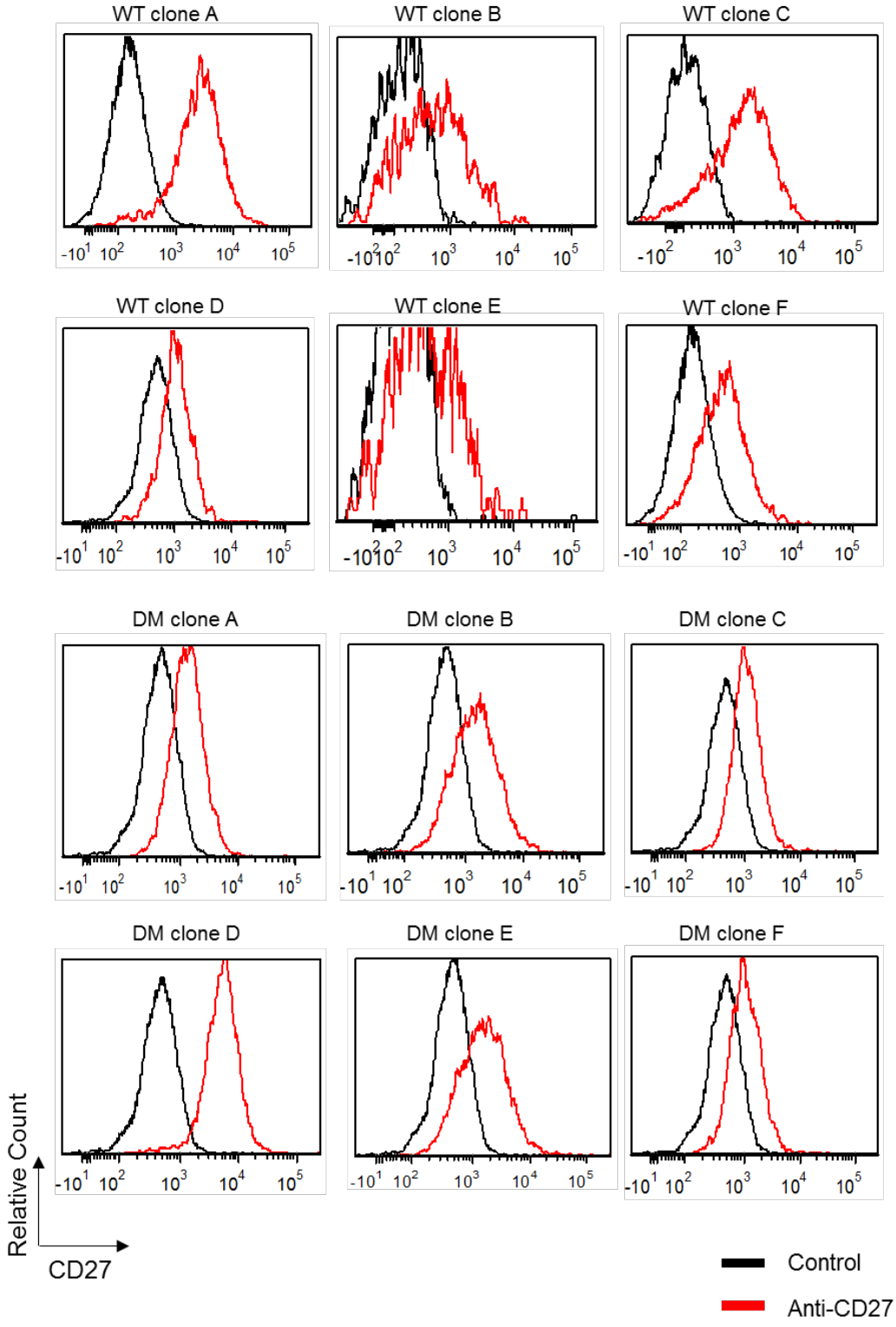

Figure 5.6. WT and DM CD27 expression on stable Jurkat-NF-κB-GFP clones. Jurkat-NF-κB-GFP cells were stably transfected with either WT or DM CD27 and cells were plated onto 96-well plates (flat bottom) as 1 x 10^4 cells per well. Cells were allowed to grow for 2-3 weeks and the single clone populations were detected under the microscope. A small number of cells was harvested from each clone and stained with anti-CD27 mAb (AT124-1 or LG.3A10-PE) for 30 mins at 4 °C before determining CD27 expression via flow cytometry. After AT124-1 incubation, cells were further incubated with anti-mouse secondary antibody for 30 mins at 4 °C before analysing on a flow cytometer.

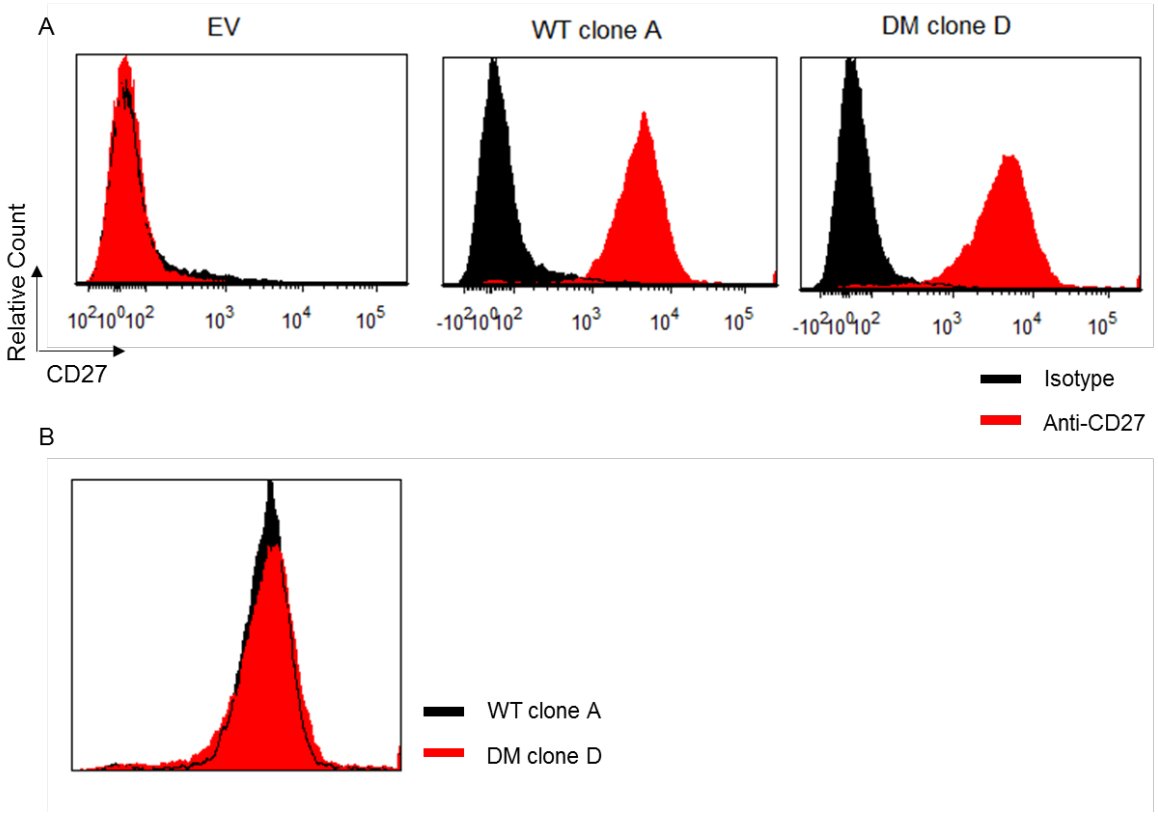

Figure 5.7. Level of CD27 expression on WT clone A or DM clone D Jurkat-NF-κB-GFP cells. EV, WT or DM cells (2 x 10^5) were stained with isotype (clone 3G8 mIgG1) or anti-CD27 (AT124-1 mIgG1) for 30 mins at 4 °C. The cells were then washed to remove excess primary mAb and further stained with anti-mouse secondary antibody for 30 mins at 4 °C. The level of CD27 expression was detected via flow cytometry.

For initial characterisation of NF-κB activation by CD27, Jurkat-NF-κB-GFP transfectants were stimulated with proteins with different valency to investigate the activity of bivalent, trimeric, hexameric and oligomeric clustering on CD27 activation. For this, bivalent anti-CD27 mAb, trimeric ligand, dimer-of-trimer (hexamer) scmCD70-m1 and unfractionated scmCD70-m1 (oligomers) were used to stimulate the CD27 transfected Jurkat-NF-κB-GFP cells (Fig. 5.8). Preliminary experiments in which only WT CD27 transfected Jurkat cells were used showed that 6 hrs of stimulation produced the optimal activation (data not shown) and this time point was used for subsequent experiments. Thus, EV, WT and DM transfected Jurkat-NF-κB-GFP cells were stimulated with 10 µg/ml of proteins for 6 hrs at 37 °C. Although the level of cell surface expression of CD27 was similar on both CD27 transfected populations, overall the DM CD27 transfected cells showed a higher level of activation compared to WT CD27 transfected cells (Fig. 5.8). The highest level of activation for both WT and DM CD27 transfected cells was observed with the unfractionated (oligomeric) scmCD70-m1 (Fig. 5.8). Although the dimer-of-trimer could also induce activation, the percentage of GFP+ cells was lower than after incubation with unfractionated

protein. The bivalent antibody and trimer did not activate either WT or DM transfected Jurkat-NF-κB-GFP cells, suggesting that the level of clustering achieved was not sufficient (Fig. 5.8). Also, the lower level of activation induced by the dimer-of-trimer compared to the unfractionated scmCD70-m1 protein suggested that hexameric engagement of the receptor is sufficient to induce signalling but a higher level of clustering is required for maximal downstream signal initiation.

DM CD27 transfected cells showed higher activation compared to WT CD27 transfected cells when stimulated with dimer-of-trimer and unfractionated scmCD70-m1. In order to confirm that binding of scmCD70-m1 was similar to both WT and DM CD27 and the difference in the level of activation was not due to improved scmCD70-m1 binding to DM CD27, binding curves for the dimer-of-trimer protein were generated. Starting with the highest 10 µg/ml dimer-of-trimer concentration and performing 1 in 2 dilutions revealed that the protein bound to WT and DM CD27 in a similar pattern (Fig. 5.9).

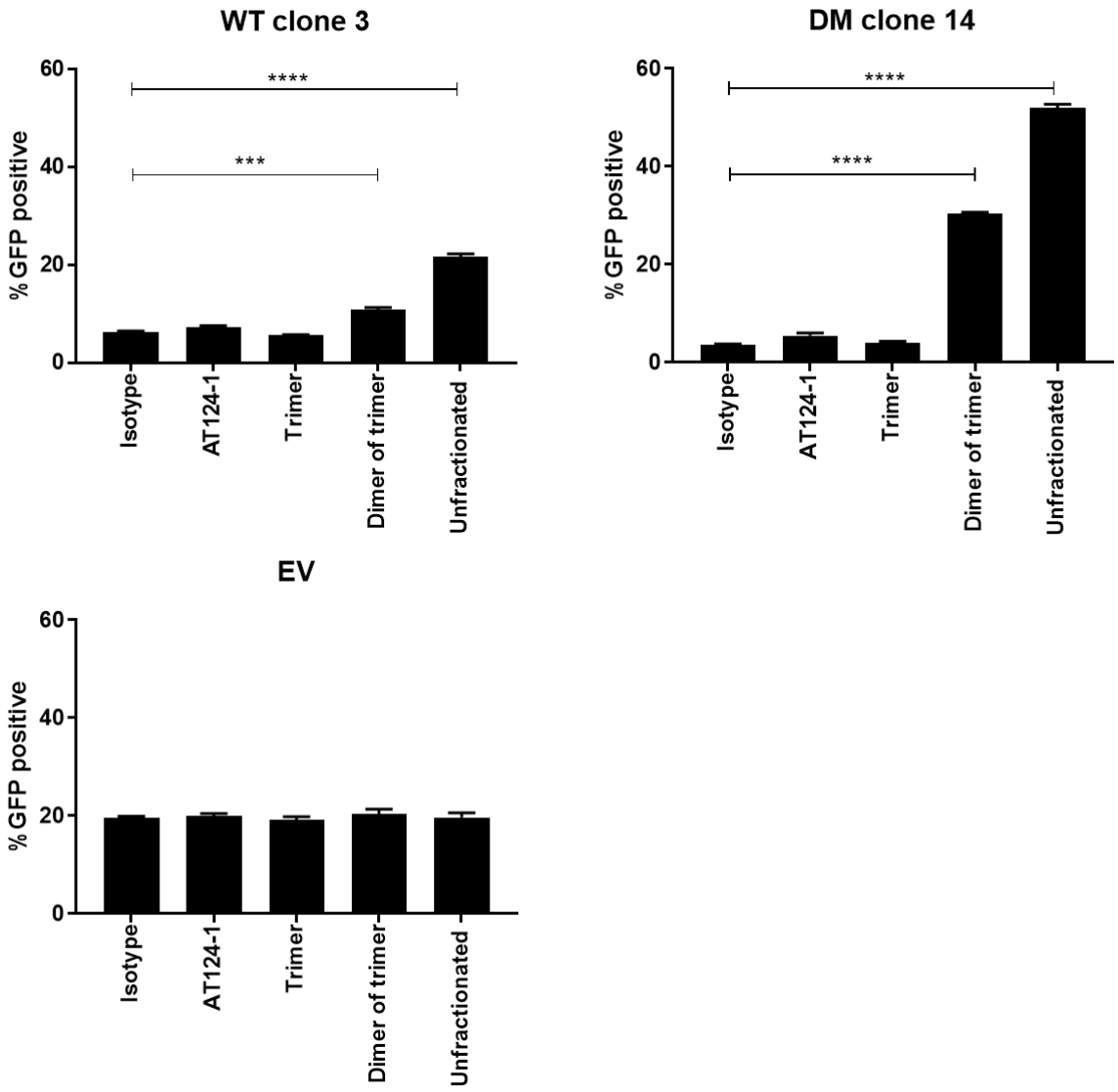

Figure 5.8. Stimulation of EV, WT CD27 or DM CD27 transfected Jurkat-NF-κB-GFP cells. Jurkat-NF-κB-GFP cells were plated into 96-well plates (U bottom) as 1 x 10^5 cells/well. The cells were stimulated with the indicated proteins at 10 μg/ml concentration for 6 hrs at 37 °C and GFP production was measured using flow cytometry as the readout of activation. Mean +/- SD of duplicates are indicated. Statistical analyses were performed by using one way ANOVA with Tukey's multiple comparisons test. ***=p<0.001, ****=p<0.0001. Data representative of two independent experiments.

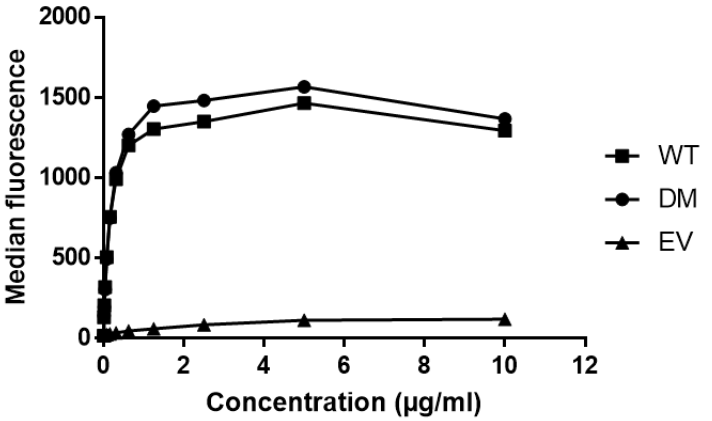

Figure 5.9. Dimer-of-trimer scmCD70-m1 binding to WT or DM CD27 expressed on Jurkat-NF-κB-GFP cells. Jurkat-NF-κB-GFP transfectants (2 x 10^5) were incubated with the indicated concentrations of dimer-of-trimer scmCD70-m1 for 1 hr at 4 °C. Then the cells were washed to remove excess ligand and incubated with APC-labelled anti-mouse secondary antibody for 30 mins at 4 °C. The level of bound dimer-of-trimer was detected using flow cytometry. Data indicate the median fluorescence of APC signal under the singlets gate (not shown).

The finding that DM CD27 elicited greater signalling than the WT CD27 was unexpected. The WT and DM CD27 transfected Jurkat-NF-κB-GFP cells are monoclonal populations and the differences observed in their levels of activation could be a consequence of selecting clones with different levels of NF-κB-GFP reporter activity i.e. the DM CD27 transfected clone might have more GFP reporter activity. In order to eliminate this possibility, polyclonal populations of WT and DM CD27 transfected cells were produced by sorting for positive cells using FACSAria. For this, cells were labelled with anti-mouse CD27 mAb and sorted based on a gate set against EV transfected cells. Both WT and DM populations showed high purity after sorting and they possessed similar levels of CD27 expression (Fig. 5.10). Each polyclonal population contained cells with a similar range of CD27 expression and contained a heterogeneous population with respect to reporter activity. To test again the activation of WT and DM CD27 transfected cells, polyclonal populations were stimulated with 10 µg/ml of unfractionated scmCD70-m1 for 6 hrs at 37 °C and the percentage of cells exhibiting NF-κB activation was evaluated as before by flow cytometry. After stimulation, an average of 32.6% of WT and 44% of DM cells were GFP positive (Fig. 5.11). Although both populations were activated, DM CD27 transfected cells showed a higher level of activation compared to WT CD27 transfected cells in line with the findings in Fig 5.8.

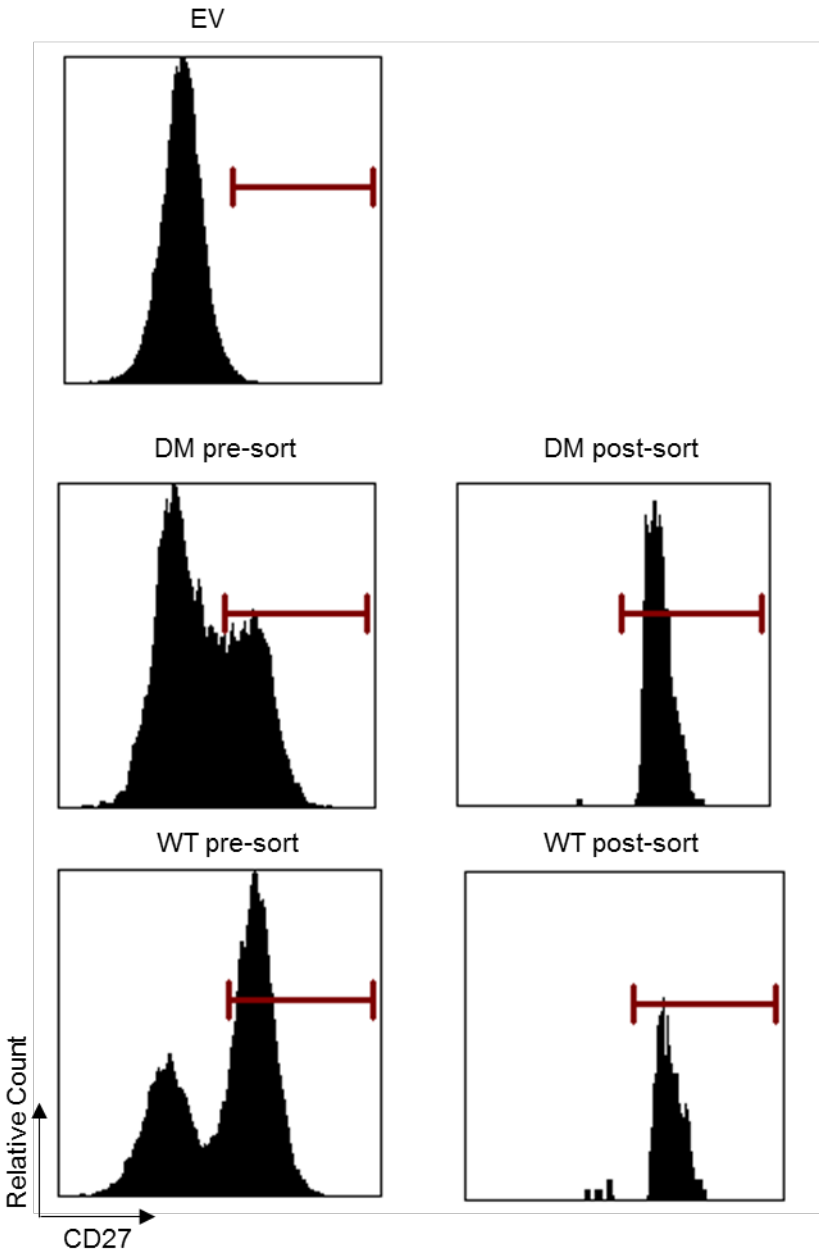

Figure 5.10. Sorting WT or DM CD27 transfected polyclonal Jurkat-NF-κB-GFP cells. Polyclonal Jurkat-NF-κB-GFP cells transfected with EV, WT CD27 or DM CD27 constructs were labelled with anti-CD27 mAb (LG.3A10) at a density of 1 x 10^6 cells being labelled with 1 µg of antibody. The cells were incubated with the antibody for 30 mins at 4 °C. Then the cells were sorted based on the gate created with EV transfected cells. Approximately 70000 cells were recovered from sorting for each population using FACSAria instrument.

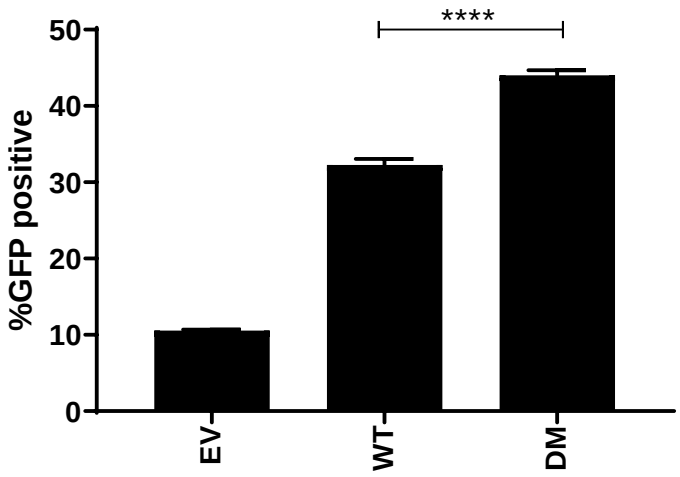

Figure 5.11. Activation of sorted polyclonal Jurkat-NF-κB-GFP populations stimulated with unfractionated scmCD70-m1. EV, WT CD27 or DM CD27 transfected polyclonal Jurkat-NF-κB-GFP reporter cells were plated at 1 x 10^5 cells/well in a 96-well plate (U-bottom) and stimulated with 10 µg/ml of unfractionated scmCD70-m1 for 6 hrs at 37 °C. The percentage of cells with GFP production was measured using flow cytometry as a readout of activation. Mean +/- SEM of triplicates are indicated from one experiment. Statistical analysis was performed by using one way ANOVA with Tukey's multiple comparisons test. ****=p<0.0001.

Both monoclonal and polyclonal DM CD27 transfected populations showed a higher level of NF-κB activation after CD27 stimulation compared to WT CD27 populations suggesting that disulphide bonds hinder signalling through CD27. However in order to formally demonstrate that the differences observed are not due to higher expression of the reporter construct in the DM cells; the EV, WT and DM transfectants were stimulated with TNFα for which all populations should show a similar response. TNFα is known to be an inducer of NF-κB activation (241) and was used in the assay to stimulate all (monoclonal and polyclonal) Jurkat NF-κB-GFP reporter populations. The cells were stimulated with different concentrations of TNFα and incubated at 37 °C for 6 hrs. Both monoclonal and polyclonal populations of WT and DM CD27 expressors, showed a similar level of activation compared to EV transfected cells with increasing activation in response to increasing TNFα concentration (Fig. 5.12). These results show that there was no inherent difference in the level of reporter activity between the populations and the difference in activation observed between WT and DM CD27 transfected populations is a reflection of CD27 activity. Thus, these data imply that the disulphide linkers between the CD27 monomers reduce the level of CD27 signal activation.

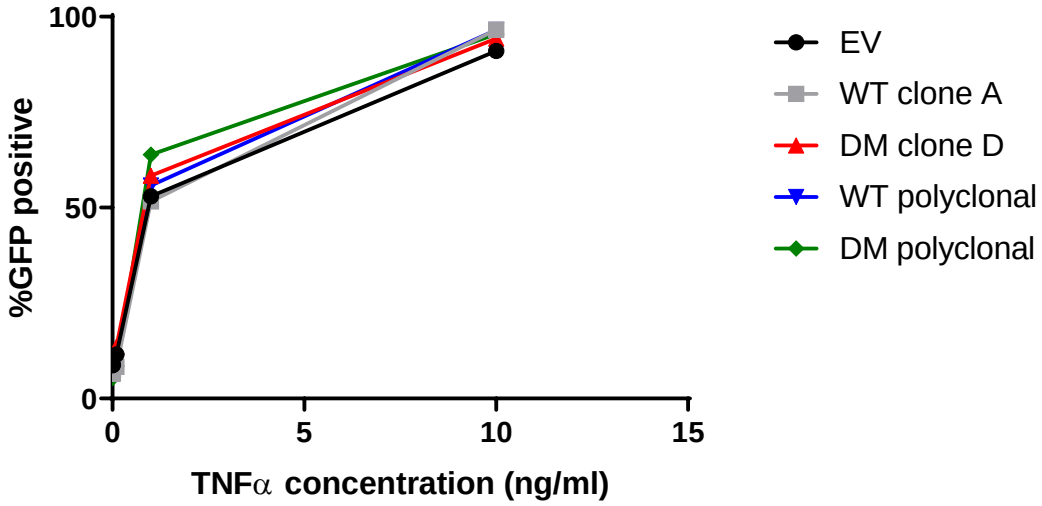

Figure 5.12. Activation of Jurkat-NF-κB-GFP populations upon TNFα stimulation. Indicated Jurkat-NF-κB-GFP reporter cell populations were plated into 96-well plates (U-bottom) as 1 x 10^5 cells/well and stimulated with indicated concentrations of TNFα (0.01, 0.1, 1 and 10 ng/ml) for 6 hrs at 37 °C. The percentage of GFP positive cells were then determined using flow cytometry as the outcome of activation. Mean +/- SD of duplicates are indicated. Data for 10 ng/ml TNFα concentration are representative of two independent experiments.

One of the initial experiments indicated that CD27 activation requires hexameric clustering and this can be enhanced with increasing level of clustering (Fig. 5.8). The bivalent anti-CD27 mAb failed to induce activation through WT or DM CD27 but we hypothesised that it might generate a strong stimulation in presence of cross-linking. Similarly, the activity of the dimer-of-trimer scmCD70-m1 might be enhanced with additional cross-linking; both the antibody and scmCD70-m1 proteins are known to interact with FcγRIIB (chapter 4). In order to investigate if cross-linking the anti-CD27 mAb and dimer-of-trimer scmCD70-m1 can increase activation of CD27 transfected Jurkat-NF-κB-GFP cells to a level comparable to the unfractionated scmCD70-m1, and to investigate if the activity of the unfractionated scmCD70-m1 can be enhanced by additional cross-linking, CD27 transfected cells were co-cultured with murine FcγRIIB-expressing CHO-K1 cells.

Thus monoclonal and polyclonal WT and DM Jurkat-NF-κB-GFP cells were co-cultured with murine FcγRIIB-expressing CHO-K1 cells and incubated with the indicated proteins at 10 µg/ml for 6 hrs at 37 °C. As previously observed (Fig. 5.8), the anti-CD27 antibody (AT124-1 mIgG1) did not induce activation without the co-culture; however when cross-linked by FcγRIIB the mAb induced much greater activation of both WT and DM populations (Fig.

5.13). The increase in the %GFP+ cells after incubation with FcγRIIB-expressing cells and mAb were similar in both monoclonal and polyclonal populations of WT and DM cells (Fig. 5.13).

In line with the data shown in Fig. 5.8, the dimer-of-trimer scmCD70-m1 induced activation of all populations (WT and DM monoclonal and polyclonal) without additional cross-linking. However, the %GFP+ cells induced by the dimer-of-trimer was enhanced by additional FcγRIIB cross-linking when evaluating WT transfectants (both monoclonal and polyclonal) and the DM polyclonal population (Fig. 5.13). The activation of the DM clone D cells induced by the dimer-of-trimer did not increase with additional cross-linking but this was likely due to the high level of activation induced by uncross-linked scmCD70-m1 meaning that it was not possible to further promote activation. The unfractionated scmCD70-m1 protein alone induced strong activation of all WT and DM populations and this was independent of FcγRIIB cross-linking (Fig. 5.13). These findings suggested that, once maximal clustering and activation is induced, providing extra clustering does not induce further activation. Of note, hexameric clustering of DM clone D cells (with dimer-of-trimer scmCD70-m1) was sufficient to provide maximal activity whereas WT clone A cells required additional clustering to reach maximal activation. It is important to note that both populations had similar levels of CD27 expression; this finding reinforces the results from earlier (Fig 5.8) showing that the presence of disulphide bonds hinders CD27 signalling.

The WT and DM polyclonal populations did not show higher activity when unfractionated scmCD70-m1 was further cross-linked with FcγRIIB but both populations showed higher activation when dimer-of-trimer scmCD70-m1 was cross-linked (Fig. 5.13). The data showing that unfractionated scmCD70-m1 could induce maximal clustering of DM polyclonal population but dimer-of-trimer scmCD70-m1 required cross-linking to achieve this, suggested that the dimer-of-trimer protein was sufficient to provide maximal clustering for monoclonal DM population but not for polyclonal DM population. This could be a reflection of the level of CD27 expressed on cell surface as polyclonal population had slightly lower level of CD27 expression compared to DM clone D cells.

Overall, the DM cells (clone D and polyclonal) were stimulated more effectively when compared to WT cells, consistent with findings presented in Figs 5.8 and 5.11.

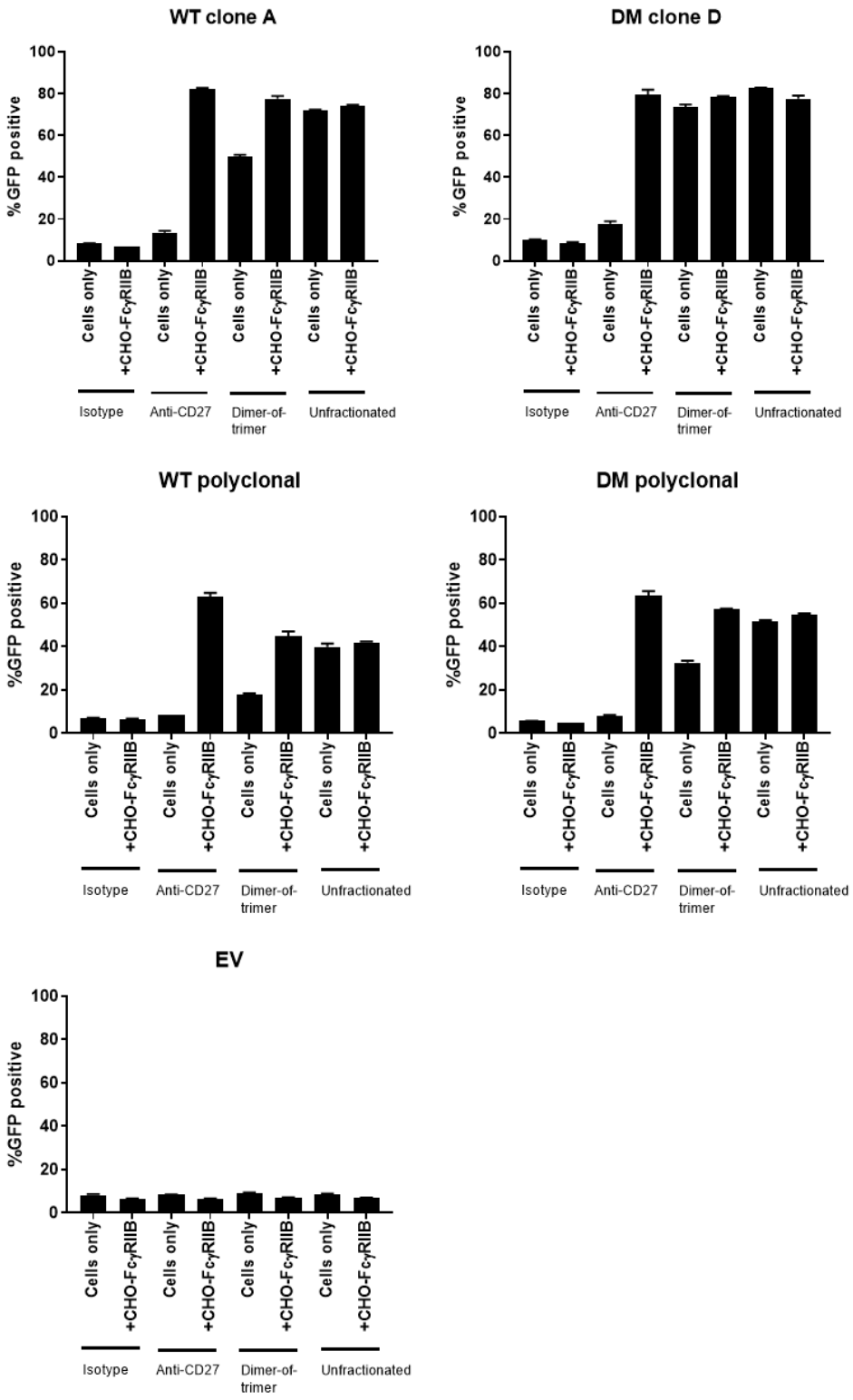

Figure 5.13. Stimulation of EV or CD27 transfected Jurkat-NF-κB-GFP cells with CD27 agonists in absence or presence of FcγRIIB cross-linking. Jurkat-NF-κB-GFP reporter cells stably expressing WT or DM CD27 or control transfectants were plated into 96-well plates with or without the presence of murine FcγRIIB-expressing CHO-K1 cells as 1 x 10^5 cells of each cell type per well. The cells were incubated with indicated proteins at 10 μg/ml for 6 hrs at 37 °C. The percentage of GFP positive cells was measured using flow cytometry as the outcome of activation. Mean +/- SD of duplicates are indicated from one experiment.

5.3 Discussion

Data in this chapter addressed the importance of disulphide linked dimerisation of murine CD27 on expression and activation of the receptor. Data presented in the chapter show that DM CD27 can be expressed as a monomer on the cell surface and can initiate downstream signal transduction. Bivalent and trimeric interactions are not sufficient to activate either WT or DM CD27 whereas hexameric or higher order clustering can activate both WT and DM CD27. Further increasing the level of receptor clustering increases the activation through both WT and DM CD27. Finally the mutant form lacking the disulphide bonds required for dimerisation shows higher activation compared to WT CD27.

Although a form of CD27 incorporating mutations at two disulphide bonding sites, DM CD27, could be expressed on the cell surface as detected by flow cytometry, the level of expression was slightly lower compared to WT CD27 following transient transfection of 293T cells (Fig. 5.3 & 5.4). Initial western blot analysis confirmed that DM CD27 did not form disulphide-linked dimers whereas for WT CD27, multiple bands approximately corresponding to dimeric CD27 and bands similar in size to the monomeric CD27 were observed (Fig. 5.5). During transient transfection, a very high level of protein is expressed and this could lead to proteins being presented with a range of different glycosylation states possibly forming dimers of different sizes. Similarly, the bands corresponding to monomeric protein might be monomers which did not get to the stage of dimerisation due to the nature of high level protein production. An alternative explanation is that these smaller bands could be degradation products of the dimeric CD27. For DM CD27, no dimers were observed and the broad band observed for the monomeric protein could be due to differential and incomplete glycosylation of the protein. The main observation of the form with single mutation, SM CD27, was that, it existed mainly as a dimer and no further characterization was carried out. Although it was not characterised for its signalling activity, we would expect that the SM protein would be comparable to WT CD27 in its ability to transduce downstream signalling.

In order to assess differences in the signalling activity of WT and DM CD27, stable clones of WT CD27 or DM CD27 transfected Jurkat cells with NF-kB reporter activity were produced with equivalent levels of WT and DM CD27 expression. It is important to note that, eliminating the dimerisation did not influence the binding of ligand (scmCD70-m1) to CD27

(Fig. 5.9) and this enabled comparison of signal transduction activity purely based on activation of the WT and DM form of CD27.

In line with data presented in chapter 3 (Fig. 3.26) and chapter 4 (Fig. 4.2) and previous studies (215), trimeric CD70 and bivalent mAb were not able to induce activation of CD27 indicating that the receptor requires higher order clustering to be activated (Fig. 5.14). Identification of the crystal structure of hCD27 and detailed characterisation of the epitopes of two mAbs binding to hCD27, suggested that one of those mAbs could be bringing two CD27 dimers together and this was also not enough to induce activation of CD27 (240, 242). Thus, tetramerization of CD27 is also insufficient to induce activation and at least hexamerisation is required. Although, hexameric ligand (dimer-of-trimer scmCD70-m1) could induce activation of CD27 (Fig. 5.8 & 5.13), maximal activation was observed with unfractionated scmCD70-m1 indicating that increasing the level of CD27 clustering increases the level of downstream signal initiation (Fig. 5.14).

Unexpectedly, DM CD27 was found to lead to higher activation of Jurkat-NF-kB-GFP cells compared to WT CD27. This was an interesting observation which suggested that the disulphide linked dimerisation of CD27 might act as a regulatory mechanism to ensure that the receptor becomes activated only when there is sufficient clustering. It has recently been shown that DR5, a member of TNFRSF, stays inactive on cell surface by the extracellular domain preventing the clustering of intracellular domains. Oligomerisation in the transmembrane region of DR5 is sufficient to drive initiation of downstream signalling, however in absence of ligand binding, the extracellular domain prevents oligomerisation of the transmembrane domain (243). Once the extracellular domain interacts with the ligand, this removes the inhibition and transmembrane domain can acquire a higher order structure leading to signal initiation (243). This phenomenon can support our hypothesis that the disulphide bonds in CD27 can keep the receptor in a conformation to increase the threshold for activation whereas without disulphides, the threshold can be reduced and the receptor can show higher activity.

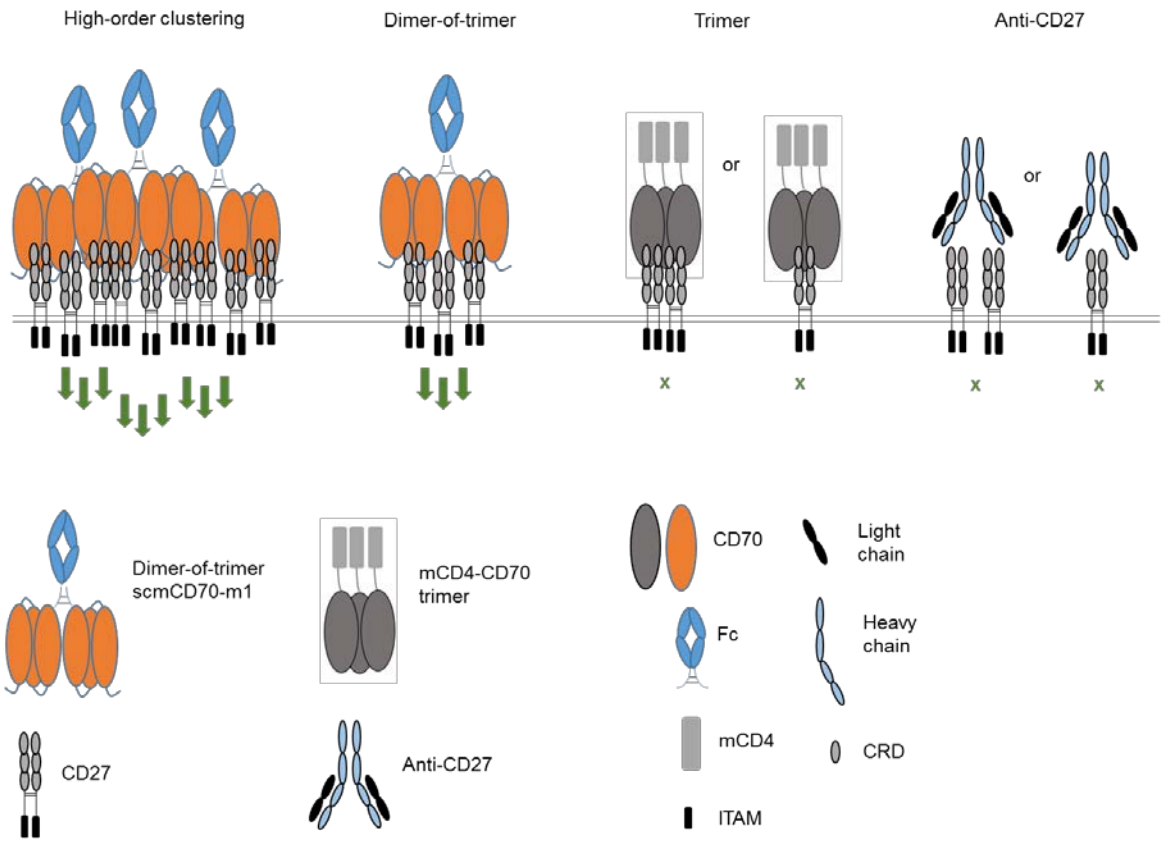

Figure 5.14. Schematic of CD27 clustering induced by bivalent, trimer, hexamer or higher-order interaction. Schematic of interaction between WT CD27 and bivalent mAb or different ligand forms are indicated. Anti-CD27 mAb and trimeric CD70 might be interacting with one or two CD27 dimers and in both cases, signal transduction is not initiated (indicated by a cross). Dimer-of-trimer is predicted to be interacting with three CD27 dimers with its hexameric ligand domain which is sufficient to induce signal transduction (indicated by arrows). Higher order clustering of CD27, either by cross-linking of dimer-of-trimer or unfractionated scmCD70-m1, can drive stronger signal transduction.

Overall, the data presented in this chapter confirm that signal transduction downstream of CD27 requires high order clustering. The cell surface expression of disulphide linked WT CD27 might act as a regulatory mechanism to control downstream signal initiation to ensure that CD27 is activated when a certain level of clustering is achieved. However, lacking the disulphide bonds (DM CD27) can contribute to higher level of activation and signal transduction.

Chapter 6 Overall Discussion

This thesis describes the expression and characterisation (in vitro and in vivo) of a recombinant single chain dimer-of-trimer ligand of CD27 which is capable of driving expansion of $CD8^+$ T cells through CD27 mediated co-stimulation independent of FcγR engagement. The data presented shows the first direct comparison of agonistic anti-CD27 mAb, dimer-of-trimer ligand with WT Fc (scmCD70-m1) and also dimer-of-trimer ligand with a "silent" Fc (scmCD70-mm1). Both of the ligand forms (scmCD70-m1 and scmCD70-mm1) could induce in vivo expansion of antigen specific T cells in OT-1 adoptive transfer model and anti-tumour response in murine BCL1 model. Additionally, the importance of CD27 being expressed as a dimer on cell surface was characterised providing evidence that the disulphide linked dimerisation may act as a mechanism of controlling signal transduction through CD27.

Soluble recombinant single chain trimeric TNFSF ligands have been previously produced for members of the family such as; TNFα, TRAIL and RANKL (244-247). A single chain trimer TNF was designed by covalently linking three monomers which were separated by flexible linkers. The single chain trimer TNF (scTNF) showed improved stability, both in vitro and in vivo, compared to wild type non-covalent TNF trimer and could lead to increased biological activity (244). The TRAIL ligand functions as a homotrimer but soluble recombinant trimer versions of the protein are prone to dissociation into monomers and thus loss of biological activity. In order to improve stability, a single chain trimer version (TR3) was generated which showed improved stability and biological activity through in vitro and in vivo characterisation (245). TRAIL has two receptors; DR4 and DR5. Although DR4 can become activated by interacting with soluble trimeric ligand, DR5 requires higher order clustering. In order to further improve the stability and activity of the soluble recombinant trimeric TRAIL, a version of TR3 by addition of a target specific scFv region (targeting red blood cells) was generated. This protein further improved the biological activity compared to the single chain trimer without the scFv fusion. In a separate study, another single chain trimer TRAIL was compared to a single chain trimer fused to a target specific scFv (targeting ERBB2). The fusion protein was used to provide cross-linking of trimeric ligands by targeting them to an antigen on target cell surface to enable sufficient cross-linking of the receptor. The fusion protein showed improved stability and biological activity indicating that modifications to improve the therapeutic effect are possible and tolerated with no loss of biological activity (246).

These covalently linked single chain trimers showed improved in vivo half-life compared to the trimers formed from monomers by non-covalent interactions. However, the time period for clearance of single chain trimers was still short. The scTNF serum availability was reduced to 10% 110 mins post-injection (244). The scFv-TRAIL (targeting ERBB2) had α half-life of 35 mins and β half-life of 160 mins (246). These single chain trimers did not have Fc fusions and short half-lives are expected. The new generation scmCD70-m1 described in this thesis was produced as an Fc fusion protein and was expected to have a long in vivo half-life. However, scmCD70-m1 was found to be cleared very quickly from circulation. There might be several explanations for the short half-life of scmCD70-m1. 1) The protein consists of two CD70 trimers and this gives it the ability to signal immediately after administration into the body. The protein might quickly interact with CD27 expressing cells in circulation and this might induce internalization of the protein, leading to rapid clearance. 2) The glycosylation status of the protein might affect stability (detailed below). 3) It has been shown for human IgG antibodies that oxidation of methionine (Met) residues in the CH2-CH3 region can have a significant impact on stability (248). This might be a factor for the mouse IgG CH2-CH3 domain used to generate scmCD70-m1, as there are four Met residues within this region. scmCD70-m1 possesses the same Fc isotype as AT124-1 mIgG1 and AT124-1 mIgG1 was produced in CHO-K1S cells. This suggests that the oxidation of Met residues on scmCD70-m1 produced in CHO-K1S cells is likely to be the same as the antibody. However, the rest of the protein is different and we cannot rule out the possibility of scmCD70-m1 having Met residues with different oxidation states. 4) FcRn interacts with the Fc region in the CH2-CH3 interface (249). The flexible linkers between the final CD70 domain and hinge region in scmCD70-m1 might allow the CD70 trimer domain to hinder the FcRn binding interface. While the ability of scmCD70-m1 to interact with FcRn was investigated via SPR and it showed the same binding pattern as anti-CD27 mAb, this does not completely rule out the possibility of the structure causing steric hindrance in vivo.

The glycosylation status of recombinant proteins can be an important factor in determining therapeutic efficacy and in vivo half-life (228). For instance, the presence of sialic acid on glycan structures can enhance the half-life of recombinant proteins (250). N-linked glycans can have an impact on the plasma stability of therapeutic proteins (229) and having high mannose residues can contribute to significantly reduced half-life (229). In a study in which pharmacokinetics of therapeutic IgGs in human subjects were studied, IgGs with high mannose glycans on their Fc regions were cleared more rapidly than IgGs with other glycan forms (251). It has been shown that high mannose content on recombinant proteins leads

to rapid clearance by cells with high mannose receptors in organs such as the liver (252). When the first batch of scmCD70-m1, produced in 3 weeks culture, was analysed, 76.76% of glycans on the protein were of oligomannose type. However, when a batch was produced after 2 weeks culture, only 31.04% of glycans were of oligomannose type. It was also shown that, proteins produced in 3 weeks of culture had higher oligomerisation compared to proteins produced after 2 weeks of culture. The increased oligomerisation and oligomannose over time could be due to an increase in the level of dead cells (data not shown). This can create a stress response in other cells leading to production of aggregated and also high oligomannosylated proteins. Despite the difference in the level of oligomannose residues between the proteins produced in 2 weeks and 3 weeks cultures, both proteins were not detectable in circulation after 1 hr post-injection (Fig. 4.3 & 4.10). This suggested that even 31% of oligomannose residues was sufficient to contribute to rapid removal from circulation.

Interestingly, when scmCD70-mm1 was produced in CHO-K1S cells in a 2 week culture, the level of oligomannose residues was lower than on scmCD70-m1. The only difference between the two proteins was the D265A mutation in the Fc domain of scmCD70-mm1. It has been previously shown that D265A mutation can influence the type of glycosylation on the Fc domain (253, 254). It could be that the Fc domain of scmCD70-m1 was oligomannosylated and the D265A mutation in scmCD70-mm1 changed the type of glycosylation, contributing to reduction in the level of oligomannose residues which leads to longer stability in in vivo circulation.

The dimer-of-trimer proteins have the CD70 domains attached to the Fc domain by flexible linkers. When the trimeric CD70 domains form, they are bulky and can be mobile due to flexibility enabled by the linkers between the CD70 and Fc domains. During the processing of N-linked glycans, the initial glycan structure is added as a pre-assembled complex consisting of two N-acetyl glucosamines, nine mannose residues and three glucose residues (255, 256). The glycan is then trimmed and processed in the ER and Golgi by several glycosidases and glycosyltransferases (255, 256). One possible reason for the dimer-of-trimer proteins having high oligomannose residues might be that the enzymes responsible of removing the mannose residues cannot access the glycan sites due to the bulky structure of the protein. It is not known if the natural CD70 protein has oligomannose residues. In order to study the effect of CD70 trimeric domains in more detail, soluble recombinant single chain CD70 trimer or non-covalent CD70 trimer could have been

produced in CHO-K1S cells in the same culture conditions as dimer-of-trimer and the level of oligomannose residues compared.

We have found that increasing the time of culture during scmCD70-m1 production by CHO-K1S cells, leads to increased oligomannose levels with longer mannose chains. It might be expected that the protein with shorter mannose chains would have a better in vivo stability than the protein with longer mannose chains. However, in a study in which a protein was produced with different mannose chain lengths (ranging from 2 to 9 mannose residues), it was shown that binding and uptake by the mannose receptors on macrophages did not change (257), indicating that chain length does not impact on uptake by the mannose receptors as long as the mannose residues are the terminal residues exposed on the sugar chain of the protein.

Glycosylation is important for the proper folding, stability and expression of proteins (256). As Endo H treatment improved the in vivo stability of scmCD70-m1, we attempted to mutate all of the Asn residues in the protein to Ala residues to completely eliminate N-glycosylation to study the effects on in vivo stability (data not shown). However, the protein could not be expressed by transfection of CHO-K1S cells. Single colonies transfected with the plasmid were generated but as the protein was not secreted, this suggested that the protein was being degraded during the production process. N-linked glycosylation is required for appropriate folding of proteins in the ER; chaperones such as calnexin and calreticulin require glycans to bind to the protein and facilitate proper folding and improve stability (256). The proteins which do not adapt their conformation after calnexin/calreticulin interaction, are directed from the ER back into the cytosol to be degraded by the ubiquitin-proteasome system (258). When all of the Asn residues were mutated, it is possible that the interaction of the protein (without N-glycosylation) with calnexin/calreticulin was diminished and this resulted in the protein being directed for degradation during the folding process.

As previously discussed in detail (chapter 1), targeting TNFRSF members with agonistic mAbs requires FcγR cross-linking for optimal activity and this can be a limiting factor. Thus, as shown here and by others, it is possible to generate alternative mechanisms to develop FcγR independent approaches to target TNFRSF members. A recombinant hexameric human CD70 protein to target CD27 has recently been reported which consists of three extracellular domains of hCD70 fused to a hIgG1 Fc domain (259). The product is made up

of a hexameric ligand domain and a full Fc domain with a mutation that eliminated FcγR interaction. The protein could induce activation and expansion of T cells in both in vitro and in vivo studies without requiring FcγR mediated cross-linking. Although, the hexameric ligand protein was compared to an anti-CD27 mAb in absence of FcγR, showing that mAb required FcγRs whereas the ligand was active without requiring cross-linking, there was no direct in vivo comparison with an agonistic mAb. Additionally the hexameric protein was only tested as an Fc silent variant and the activity observed with a WT Fc could have been different. Here, WT Fc clearly has an advantage of FcγR mediated cross-linking contributing to enhance in vivo activity in inducing the expansion of antigen specific T cells when only low number of antigen specific cells are available. Fc engineering approaches to facilitate on target multimerisation of IgGs have also been developed. Several mutations within the human Fc domain such as E345R and T437R/K248E double mutations have been identified to facilitate on target hexamerisation of mAbs. Incorporating these mutations into anti-OX40 mAbs, induced downstream activation of the receptor and thus FcγR independent agonism (180, 260) compared to the parental mAb. In a recent study, anti-TNFR mAbs against several members of the family were designed by addition of various proteins as conjugates to the heavy chain of the mAb which lacked FcγR interaction (261). By interacting with their specific targets, the conjugated domains anchor the anti-TNFR mAb on the cell surface which mimics FcγR mediated cross-linking. By that mechanism, specific antigens at specific tissue sites such as the tumour microenvironment can be targeted to allow site specific accumulation and effect of the anti-TNFR mAbs.

In this project, CHO-K1S cells were used for stable clone generation and 293F cells were used for transient transfections. Data showed that the time of culture or cell type might play an important role in the purity and yield of the end product. Transient transfection of mammalian cells gives a good protein yield in a short period of time whereas generation of stable clones requires a longer procedure with several independent screening and selection steps. When the products from 1 week 293F and CHO-K1S cultures were prepared, the products were similar in terms of purity. Although 293F cells could produce a good yield in a short time, some protein is always lost during the fractionation step after protein A purification. This means that, in order to obtain enough protein for in vivo experiments, repeated transfections would be required. The disadvantages of this approach would have been that the transfection efficiency and yield would not have been the same after every transfection and also a high amount of plasmid DNA would have been required for each transfection. Thus, although it was a longer procedure to obtain clones of CHO-K1S cells,

this approach is more advantageous for long-term large-scale protein production as a similar yield is obtained at every repeated procedure and despite losing protein during fractionation, a high yield can still be obtained.

The anti-CD27 mAb (without being cross-linked) and soluble recombinant trimeric CD70 were not able to induce activation of CD27 mediated signalling. CD27 is expressed as a dimer on the cell surface. It has not been established if the mAb binds in the inner region of the CD27 or if it can pull two dimers together. The trimer binds at the CRD2 domain (240, 242) and similarly it is not known if it only binds to a dimer or if it can bring two dimers together. In both cases, the clustering of CD27 is not enough to induce activation. The dimer-of-trimer can induce sufficient clustering of CD27 to induce signalling which supports previous studies showing that for TNFRSF, six or more receptors need to be clustered for signal activation (214, 262). However, the unfractionated scmCD70-m1, with oligomers, induced the highest level of CD27 mediated activation in in vitro assays. This indicated that the higher the level of clustering, the higher the level of activation. However, it is also not known if CD27 internalizes the soluble ligand when they interact. One of the reasons for not having activity with mAb and trimer could be that they interact with only one or two dimers of CD27 which is insufficient to drive signal transduction. Another reason of not having activation with mAb and trimer but having such a high level of activation with the unfractionated scmCD70-m1 might be that CD27 can internalize the mAb and trimeric CD70 and to some extent the dimer-of-trimer scmCD70-m1 but not the higher order protein. As the dimer-of-trimer can induce activation of CD27, even if it becomes internalized, clearly not all the protein is internalized or the receptor is activated prior to internalization. However, as unfractionated scmCD70-m1 consists mainly of high order structures, internalization might be more difficult or not possible, meaning that CD27 remains clustered at the cell surface and this contributes to enhanced activation. In order to investigate this, mAb, trimeric CD70, dimer-of-trimer scmCD70-m1 and unfractionated scmCD70-m1 would need to be labelled with a fluorescent tag (using commercial kits) and after incubating them with CD27 expressing cells, the level of internalization could be measured via a fluorescence microscope.

In the BCL1 model, Endo H treated scmCD70-m1, Endo H treated scmCD70-mm1 and agonistic anti-CD27 mAb generated similar responses, all improving the survival compared to control group. It is important to note that the effects of these agents might be different in solid tumour models. The BCL1 tumour mainly develops in the spleen which is a lymphoid

tissue and there is likely to be sufficient cross-linking of the mAb at this site due to FcγRs expressed by B cells and myeloid cells. However, this might be a limiting factor in a solid tumour model and in fact data generated in other studies suggest that the activity of agonistic anti-CD27 mAb is much less in a solid tumour model compared to BCL1 model. In solid tumour models, depleting mAbs have higher efficacy than agonistic mAb and the activity of agonistic anti-CD27 is minimal (157). The advantage of Endo H treated scmCD70-m1 is that it does not require FcγR cross-linking to generate an anti-tumour response. Although, FcγR cross-linking can improve the activity, there wasn't a significant difference between Endo H treated scmCD70-m1 and Endo H treated scmCD70-mm1 in BCL1 anti-tumour activity. The reason for that could possibly be related to the BCL1 tumour model used which uses a large inoculum of tumour cells to establish. 5×10^6 BCL1 tumour cells were transferred and allowed to establish for five days before initiation of the treatment. This might have generated a high number of antigen specific T cells already and it might have been difficult to see a difference between Endo H treated scmCD70-m1 and Endo H treated scmCD70-mm1. It is important to note that Endo H treated scmCD70-m1 induced a similar T-cell response as anti-CD27 when 5×10^5 OT-1 T cells were transferred but the activity of Endo H treated scmCD70-m1 was better than anti-CD27 when lower numbers were transferred (Fig. 4.11). Also, when low numbers of OT-1 cells were transferred into WT animals, Endo H treated scmCD70-m1 generated a higher response than Endo H treated scmCD70-mm1. These data indicate that, although the dimer-of-trimer was sufficient to stimulate antigen specific T cells and generate an anti-tumour response, having additional cross-linking can further enhance the activity of scmCD70-m1 which might be advantageous in a solid tumour model. In fact, the hexameric human CD70 protein induced anti-tumour efficacy in murine solid tumour models indicating that hexameric targeting of CD27 without additional cross-linking can be efficacious (259). However, as previously mentioned, there was no comparison with an anti-CD27 mAb in that study and it is hard to draw a conclusion on how the activity of the hexameric CD70 ligand would compare to agonistic anti-CD27.

Together the data presented in this thesis highlight scmCD70-m1 as a potential FcγR independent reagent to increase in vivo expansion of antigen specific T-cells and induce anti-tumour response. Overall the data indicates that a soluble recombinant TNFSF ligand can be generated to be as active as an agonistic mAb with the advantage of inducing FcγR independent activity. Additionally it has been demonstrated that, although in vivo FcγR independent activity could be achieved with the Fc "silent" version of the ligand, having WT

Fc with additional FcγR cross-linking proved to be advantageous to enhance the activity of the ligand. Also, despite the fact that a mIgG1 mAb is considered as agonistic, depending on availability of the FcγR in the surrounding microenvironment, the mAb could demonstrate a depleting activity leading to significantly decreased levels of $CD8^+$ T cells. However, this was not observed with the ligand, adding another important advantage for the use of the ligand over the mAb. Furthermore it has been shown that the disulphide linked dimerisation of CD27 under physiological conditions might act as a potential regulatory mechanism to only induce signal transduction when a certain level of receptor clustering is achieved.

List of References

1. Parkin J, Cohen B. An overview of the immune system. The Lancet. 2001;357(9270):1777-89.
2. Dempsey PW, Vaidya SA, Cheng G. The art of war: Innate and adaptive immune responses. Cellular and molecular life sciences : CMLS. 2003;60(12):2604-21.
3. Kumar H, Kawai T, Akira S. Pathogen Recognition by the Innate Immune System. International Reviews of Immunology. 2011;30(1):16-34.
4. Bonilla FA, Oettgen HC. Adaptive immunity. The Journal of allergy and clinical immunology. 2010;125(2 Suppl 2):S33-40.
5. Koch U, Radtke F. Mechanisms of T cell development and transformation. Annual review of cell and developmental biology. 2011;27:539-62.
6. Ma D, Wei Y, Liu F. Regulatory mechanisms of thymus and T cell development. Developmental and comparative immunology. 2013;39(1-2):91-102.
7. Carpenter AC, Bosselut R. Decision checkpoints in the thymus. Nat Immunol. 2010;11(8):666-73.
8. Klein L, Hinterberger M, Wirnsberger G, Kyewski B. Antigen presentation in the thymus for positive selection and central tolerance induction. Nat Rev Immunol. 2009;9(12):833-44.
9. Matloubian M, Lo CG, Cinamon G, Lesneski MJ, Xu Y, Brinkmann V, et al. Lymphocyte egress from thymus and peripheral lymphoid organs is dependent on S1P receptor 1. Nature. 2004;427(6972):355-60.
10. Jelley-Gibbs DM, Strutt TM, McKinstry KK, Swain SL. Influencing the fates of CD4 T cells on the path to memory: lessons from influenza. Immunol Cell Biol. 2008;86(4):343-52.
11. Luckheeram RV, Zhou R, Verma AD, Xia B. CD4(+)T cells: differentiation and functions. Clin Dev Immunol. 2012;2012:925135.
12. Smith CM, Wilson NS, Waithman J, Villadangos JA, Carbone FR, Heath WR, et al. Cognate CD4(+) T cell licensing of dendritic cells in CD8(+) T cell immunity. Nat Immunol. 2004;5(11):1143-8.
13. Behrens G, Li M, Smith CM, Belz GT, Mintern J, Carbone FR, et al. Helper T cells, dendritic cells and CTL Immunity. Immunol Cell Biol. 2004;82(1):84-90.
14. Wherry EJ, Kurachi M. Molecular and cellular insights into T cell exhaustion. Nature reviews Immunology. 2015;15(8):486-99.
15. Wherry EJ. T cell exhaustion. Nat Immunol. 2011;12(6):492-9.
16. Goral S. The three-signal hypothesis of lymphocyte activation/targets for immunosuppression. Dialysis & Transplantation. 2011;40(1):14-6.
17. Shahinian A, Pfeffer K, Lee KP, Kundig TM, Kishihara K, Wakeham A, et al. Differential T cell costimulatory requirements in CD28-deficient mice. Science (New York, NY). 1993;261(5121):609-12.
18. Curtsinger JM, Schmidt CS, Mondino A, Lins DC, Kedl RM, Jenkins MK, et al. Inflammatory cytokines provide a third signal for activation of naive CD4+ and CD8+ T cells. Journal of immunology (Baltimore, Md : 1950). 1999;162(6):3256-62.
19. Plumlee CR, Obar JJ, Colpitts SL, Jellison ER, Haining WN, Lefrancois L, et al. Early Effector CD8 T Cells Display Plasticity in Populating the Short-Lived Effector and Memory-Precursor Pools Following Bacterial or Viral Infection. Scientific Reports. 2015;5:12264.
20. Blum JS, Wearsch PA, Cresswell P. Pathways of Antigen Processing. Annual review of immunology. 2013;31:443-73.
21. Oancea G, O'Mara ML, Bennett WF, Tieleman DP, Abele R, Tampe R. Structural arrangement of the transmission interface in the antigen ABC transport complex TAP. Proceedings of the National Academy of Sciences of the United States of America. 2009;106(14):5551-6.

22. Koopmann JO, Post M, Neefjes JJ, Hammerling GJ, Momburg F. Translocation of long peptides by transporters associated with antigen processing (TAP). European journal of immunology. 1996;26(8):1720-8.
23. Saric T, Chang SC, Hattori A, York IA, Markant S, Rock KL, et al. An IFN-gamma-induced aminopeptidase in the ER, ERAP1, trims precursors to MHC class I-presented peptides. Nat Immunol. 2002;3(12):1169-76.
24. Rudensky AY, Preston-Hurlburt P, Hong S-C, Barlow A, Janeway CA. Sequence analysis of peptides bound to MHC class II molecules. Nature. 1991;353(6345):622-7.
25. Belz GT, Carbone FR, Heath WR. Cross-presentation of antigens by dendritic cells. Critical reviews in immunology. 2002;22(5-6):439-48.
26. Rock KL, Shen L. Cross-presentation: underlying mechanisms and role in immune surveillance. Immunol Rev. 2005;207:166-83.
27. Cantrell DA. T-cell antigen receptor signal transduction. Immunology. 2002;105(4):369-74.
28. Call ME, Wucherpfennig KW. Molecular mechanisms for the assembly of the T cell receptor–CD3 complex. Molecular immunology. 2004;40(18):1295-305.
29. Ferber M, Zoete V, Michielin O. T-Cell Receptors Binding Orientation over Peptide/MHC Class I Is Driven by Long-Range Interactions. PloS one. 2012;7(12):e51943.
30. Acuto O, Cantrell D. T cell activation and the cytoskeleton. Annual review of immunology. 2000;18:165-84.
31. van Leeuwen JE, Samelson LE. T cell antigen-receptor signal transduction. Curr Opin Immunol. 1999;11(3):242-8.
32. Artyomov MN, Lis M, Devadas S, Davis MM, Chakraborty AK. CD4 and CD8 binding to MHC molecules primarily acts to enhance Lck delivery. Proceedings of the National Academy of Sciences of the United States of America. 2010;107(39):16916-21.
33. Lin J, Weiss A. T cell receptor signalling. Journal of Cell Science. 2001;114(2):243-4.
34. Myung PS, Boerthe NJ, Koretzky GA. Adapter proteins in lymphocyte antigen-receptor signaling. Curr Opin Immunol. 2000;12(3):256-66.
35. Imboden JB, Stobo JD. Transmembrane signalling by the T cell antigen receptor. Perturbation of the T3-antigen receptor complex generates inositol phosphates and releases calcium ions from intracellular stores. J Exp Med. 1985;161(3):446-56.
36. Crabtree GR. Generic signals and specific outcomes: signaling through Ca2+, calcineurin, and NF-AT. Cell. 1999;96(5):611-4.
37. Ranger AM, Gerstenfeld LC, Wang J, Kon T, Bae H, Gravallese EM, et al. The Nuclear Factor of Activated T Cells (Nfat) Transcription Factor Nfatp (Nfatc2) Is a Repressor of Chondrogenesis. The Journal of Experimental Medicine. 2000;191(1):9-22.
38. Thaker YR, Schneider H, Rudd CE. TCR and CD28 activate the transcription factor NF-κB in T-cells via distinct adaptor signaling complexes. Immunology Letters. 2015;163(1):113-9.
39. Los M, Schenk H, Hexel K, Baeuerle PA, Dröge W, Schulze-Osthoff K. IL-2 gene expression and NF-kappa B activation through CD28 requires reactive oxygen production by 5-lipoxygenase. The EMBO Journal. 1995;14(15):3731-40.
40. Bai D, Ueno L, Vogt PK. Akt-mediated regulation of NFκB and the essentialness of NFκB for the oncogenicity of PI3K and Akt. International journal of cancer Journal international du cancer. 2009;125(12):2863-70.
41. June CH, Bluestone JA, Nadler LM, Thompson CB. The B7 and CD28 receptor families. Immunol Today. 1994;15(7):321-31.
42. Appleman LJ, Boussiotis VA. T cell anergy and costimulation. Immunol Rev. 2003;192:161-80.
43. He LZ, Prostak N, Thomas LJ, Vitale L, Weidlick J, Crocker A, et al. Agonist anti-human CD27 monoclonal antibody induces T cell activation and tumor immunity in human CD27-transgenic mice. Journal of immunology (Baltimore, Md : 1950). 2013;191(8):4174-83.
44. Vitale LA, He LZ, Thomas LJ, Widger J, Weidlick J, Crocker A, et al. Development of a human monoclonal antibody for potential therapy of CD27-expressing lymphoma and leukemia.

Clinical cancer research : an official journal of the American Association for Cancer Research. 2012;18(14):3812-21.
45. June CH, Ledbetter JA, Linsley PS, Thompson CB. Role of the CD28 receptor in T-cell activation. Immunol Today. 1990;11(6):211-6.
46. Beier KC, Kallinich T, Hamelmann E. Master switches of T-cell activation and differentiation. The European respiratory journal. 2007;29(4):804-12.
47. Beyersdorf N, Kerkau T, Hünig T. CD28 co-stimulation in T-cell homeostasis: a recent perspective. Immunotargets and Therapy. 2015;4:111-22.
48. Chen L, Flies DB. Molecular mechanisms of T cell co-stimulation and co-inhibition. Nature reviews Immunology. 2013;13(4):227-42.
49. Lumsden JM, Roberts JM, Harris NL, Peach RJ, Ronchese F. Differential requirement for CD80 and CD80/CD86-dependent costimulation in the lung immune response to an influenza virus infection. Journal of immunology (Baltimore, Md : 1950). 2000;164(1):79-85.
50. Bertram EM, Lau P, Watts TH. Temporal segregation of 4-1BB versus CD28-mediated costimulation: 4-1BB ligand influences T cell numbers late in the primary response and regulates the size of the T cell memory response following influenza infection. Journal of immunology (Baltimore, Md : 1950). 2002;168(8):3777-85.
51. Thompson CB, Lindsten T, Ledbetter JA, Kunkel SL, Young HA, Emerson SG, et al. CD28 activation pathway regulates the production of multiple T-cell-derived lymphokines/cytokines. Proceedings of the National Academy of Sciences of the United States of America. 1989;86(4):1333-7.
52. Curtsinger JM, Mescher MF. Inflammatory Cytokines as a Third Signal for T Cell Activation. Current opinion in immunology. 2010;22(3):333-40.
53. Nolz JC, Starbeck-Miller GR, Harty JT. Naive, effector and memory CD8 T-cell trafficking: parallels and distinctions. Immunotherapy. 2011;3(10):1223-33.
54. Voskoboinik I, Whisstock JC, Trapani JA. Perforin and granzymes: function, dysfunction and human pathology. Nature Reviews Immunology. 2015;15:388.
55. Trambas CM, Griffiths GM. Delivering the kiss of death. Nature Immunology. 2003;4(5):399-403.
56. Lieberman J. The ABCs of granule-mediated cytotoxicity: new weapons in the arsenal. Nature Reviews Immunology. 2003;3(5):361-70.
57. Farhood B, Najafi M, Mortezaee K. CD8(+) cytotoxic T lymphocytes in cancer immunotherapy: A review. Journal of cellular physiology. 2019;234(6):8509-21.
58. Tau GZ, Cowan SN, Weisburg J, Braunstein NS, Rothman PB. Regulation of IFN-gamma signaling is essential for the cytotoxic activity of CD8(+) T cells. Journal of immunology (Baltimore, Md : 1950). 2001;167(10):5574-82.
59. Obar JJ, Lefrançois L. Memory CD8(+) T cell differentiation. Annals of the New York Academy of Sciences. 2010;1183:251-66.
60. Kaech SM, Wherry EJ, Ahmed R. Effector and memory T-cell differentiation: implications for vaccine development. Nature Reviews Immunology. 2002;2(4):251-62.
61. Veiga-Fernandes H, Walter U, Bourgeois C, McLean A, Rocha B. Response of naive and memory CD8+ T cells to antigen stimulation in vivo. Nat Immunol. 2000;1(1):47-53.
62. Gray D. Thanks for the memory. Nature Immunology. 2000;1(1):11-2.
63. Veiga-Fernandes H, Rocha B. High expression of active CDK6 in the cytoplasm of CD8 memory cells favors rapid division. Nat Immunol. 2004;5(1):31-7.
64. Sallusto F, Lenig D, Forster R, Lipp M, Lanzavecchia A. Two subsets of memory T lymphocytes with distinct homing potentials and effector functions. Nature. 1999;401(6754):708-12.
65. Martin MD, Badovinac VP. Defining Memory CD8 T Cell. Front Immunol. 2018;9:2692.
66. Gerlach C, Moseman EA, Loughhead SM, Alvarez D, Zwijnenburg AJ, Waanders L, et al. The Chemokine Receptor CX3CR1 Defines Three Antigen-Experienced CD8 T Cell Subsets with Distinct Roles in Immune Surveillance and Homeostasis. Immunity. 2016;45(6):1270-84.

67. Shin H, Iwasaki A. Tissue-resident memory T cells. Immunological reviews. 2013;255(1):165-81.
68. Mueller SN, Mackay LK. Tissue-resident memory T cells: local specialists in immune defence. Nature Reviews Immunology. 2015;16:79.
69. Bremer E. Targeting of the Tumor Necrosis Factor Receptor Superfamily for Cancer Immunotherapy. ISRN Oncology. 2013;2013:25.
70. Croft M. The role of TNF superfamily members in T-cell function and diseases. Nat Rev Immunol. 2009;9(4):271-85.
71. Sonar S, Lal G. Role of Tumor Necrosis Factor Superfamily in Neuroinflammation and Autoimmunity. Front Immunol. 2015;6:364.
72. Dempsey PW, Doyle SE, He JQ, Cheng G. The signaling adaptors and pathways activated by TNF superfamily. Cytokine & growth factor reviews. 2003;14(3-4):193-209.
73. Dawicki W, Watts TH. Expression and function of 4-1BB during CD4 versus CD8 T cell responses in vivo. European journal of immunology. 2004;34(3):743-51.
74. Schaer DA, Hirschhorn-Cymerman D, Wolchok JD. Targeting tumor-necrosis factor receptor pathways for tumor immunotherapy. J Immunother Cancer. 2014;2.
75. Wajant H. Principles of antibody-mediated TNF receptor activation. Cell Death and Differentiation. 2015;22(11):1727-41.
76. MacEwan DJ. TNF ligands and receptors – a matter of life and death. British Journal of Pharmacology. 2002;135(4):855-75.
77. Hehlgans T, Pfeffer K. The intriguing biology of the tumour necrosis factor/tumour necrosis factor receptor superfamily: players, rules and the games. Immunology. 2005;115(1):1-20.
78. Aggarwal BB. Signalling pathways of the TNF superfamily: a double-edged sword. Nat Rev Immunol. 2003;3(9):745-56.
79. van de Ven K, Borst J. Targeting the T-cell co-stimulatory CD27/CD70 pathway in cancer immunotherapy: rationale and potential. Immunotherapy. 2015;7(6):655-67.
80. Vonderheide RH, Glennie MJ. Agonistic CD40 antibodies and cancer therapy. Clinical cancer research : an official journal of the American Association for Cancer Research. 2013;19(5):1035-43.
81. Linch SN, McNamara MJ, Redmond WL. OX40 Agonists and Combination Immunotherapy: Putting the Pedal to the Metal. Frontiers in oncology. 2015;5:34.
82. Bartkowiak T, Curran MA. 4-1BB Agonists: Multi-Potent Potentiators of Tumor Immunity. Frontiers in oncology. 2015;5:117.
83. Hendriks J, Xiao Y, Rossen JW, van der Sluijs KF, Sugamura K, Ishii N, et al. During viral infection of the respiratory tract, CD27, 4-1BB, and OX40 collectively determine formation of CD8+ memory T cells and their capacity for secondary expansion. Journal of immunology (Baltimore, Md : 1950). 2005;175(3):1665-76.
84. Buchan SL, Fallatah M, Thirdborough SM, Taraban VY, Rogel A, Thomas LJ, et al. PD-1 Blockade and CD27 Stimulation Activate Distinct Transcriptional Programs That Synergize for CD8(+) T-Cell-Driven Antitumor Immunity. Clinical cancer research : an official journal of the American Association for Cancer Research. 2018;24(10):2383-94.
85. Prasad KV, Ao Z, Yoon Y, Wu MX, Rizk M, Jacquot S, et al. CD27, a member of the tumor necrosis factor receptor family, induces apoptosis and binds to Siva, a proapoptotic protein. Proceedings of the National Academy of Sciences of the United States of America. 1997;94(12):6346-51.
86. Camerini D, Walz G, Loenen WA, Borst J, Seed B. The T cell activation antigen CD27 is a member of the nerve growth factor/tumor necrosis factor receptor gene family. Journal of immunology (Baltimore, Md : 1950). 1991;147(9):3165-9.
87. Taraban VY, Rowley TF, Kerr JP, Willoughby JE, Johnson PM, Al-Shamkhani A, et al. CD27 costimulation contributes substantially to the expansion of functional memory CD8(+) T cells after peptide immunization. European journal of immunology. 2013;43(12):3314-23.

88. Borst J, Hendriks J, Xiao Y. CD27 and CD70 in T cell and B cell activation. Curr Opin Immunol. 2005;17(3):275-81.
89. Peperzak V, Veraar EA, Keller AM, Xiao Y, Borst J. The Pim kinase pathway contributes to survival signaling in primed CD8+ T cells upon CD27 costimulation. Journal of immunology (Baltimore, Md : 1950). 2010;185(11):6670-8.
90. Dolfi DV, Boesteanu AC, Petrovas C, Xia D, Butz EA, Katsikis PD. Late signals from CD27 prevent Fas-dependent apoptosis of primary CD8+ T cells. Journal of immunology (Baltimore, Md : 1950). 2008;180(5):2912-21.
91. Grant EJ, Nussing S, Sant S, Clemens EB, Kedzierska K. The role of CD27 in anti-viral T-cell immunity. Current opinion in virology. 2017;22:77-88.
92. Amaravadi R, Thompson CB. The survival kinases Akt and Pim as potential pharmacological targets. Journal of Clinical Investigation. 2005;115(10):2618-24.
93. Peperzak V, Veraar EA, Xiao Y, Babala N, Thiadens K, Brugmans M, et al. CD8+ T cells produce the chemokine CXCL10 in response to CD27/CD70 costimulation to promote generation of the CD8+ effector T cell pool. Journal of immunology (Baltimore, Md : 1950). 2013;191(6):3025-36.
94. Taraban VY, Rowley TF, Al-Shamkhani A. Cutting edge: a critical role for CD70 in CD8 T cell priming by CD40-licensed APCs. Journal of immunology (Baltimore, Md : 1950). 2004;173(11):6542-6.
95. French RR, Taraban VY, Crowther GR, Rowley TF, Gray JC, Johnson PW, et al. Eradication of lymphoma by CD8 T cells following anti-CD40 monoclonal antibody therapy is critically dependent on CD27 costimulation. Blood. 2007;109(11):4810-5.
96. Feau S, Garcia Z, Arens R, Yagita H, Borst J, Schoenberger SP. The CD4(+) T-cell help signal is transmitted from APC to CD8(+) T-cells via CD27-CD70 interactions. Nature communications. 2012;3:948.
97. Dong H, Franklin NA, Ritchea SB, Yagita H, Glennie MJ, Bullock TN. CD70 and IFN-1 selectively induce eomesodermin or T-bet and synergize to promote CD8+ T-cell responses. European journal of immunology. 2015;45(12):3289-301.
98. Peperzak V, Xiao Y, Veraar EAM, Borst J. CD27 sustains survival of CTLs in virus-infected nonlymphoid tissue in mice by inducing autocrine IL-2 production. The Journal of clinical investigation. 2010;120(1):168-78.
99. Bullock TN. Stimulating CD27 to quantitatively and qualitatively shape adaptive immunity to cancer. Curr Opin Immunol. 2017;45:82-8.
100. van Gisbergen KP, Klarenbeek PL, Kragten NA, Unger PP, Nieuwenhuis MB, Wensveen FM, et al. The costimulatory molecule CD27 maintains clonally diverse CD8(+) T cell responses of low antigen affinity to protect against viral variants. Immunity. 2011;35(1):97-108.
101. Wherry EJ, Teichgraber V, Becker TC, Masopust D, Kaech SM, Antia R, et al. Lineage relationship and protective immunity of memory CD8 T cell subsets. Nat Immunol. 2003;4(3):225-34.
102. Yamaura K, Boenisch O, Watanabe T, Ueno T, Vanguri V, Yang J, et al. Differential requirement of CD27 costimulatory signaling for naive versus alloantigen-primed effector/memory CD8+ T cells. American journal of transplantation : official journal of the American Society of Transplantation and the American Society of Transplant Surgeons. 2010;10(5):1210-20.
103. Dong H, Franklin NA, Roberts DJ, Yagita H, Glennie MJ, Bullock TNJ. CD27 stimulation promotes the frequency of IL-7 receptor-expressing memory precursors and prevents IL-12-mediated loss of CD8(+) T cell memory in the absence of CD4(+) T cell help. Journal of immunology (Baltimore, Md : 1950). 2012;188(8):3829-38.
104. Dong H, Buckner A, Prince J, Bullock T. Frontline Science: Late CD27 stimulation promotes IL-7Ralpha transcriptional re-expression and memory T cell qualities in effector CD8(+) T cells. J Leukoc Biol. 2019.

105. van Montfrans JM, Hoepelman AIM, Otto S, van Gijn M, van de Corput L, de Weger RA, et al. CD27 deficiency is associated with combined immunodeficiency and persistent symptomatic EBV viremia. The Journal of allergy and clinical immunology. 2012;129(3):787-93.e6.
106. Makedonas G, Hutnick N, Haney D, Amick AC, Gardner J, Cosma G, et al. Perforin and IL-2 upregulation define qualitative differences among highly functional virus-specific human CD8 T cells. PLoS pathogens. 2010;6(3):e1000798.
107. Savoldo B, Huls MH, Liu Z, Okamura T, Volk HD, Reinke P, et al. Autologous Epstein-Barr virus (EBV)-specific cytotoxic T cells for the treatment of persistent active EBV infection. Blood. 2002;100(12):4059-66.
108. Salzer E, Daschkey S, Choo S, Gombert M, Santos-Valente E, Ginzel S, et al. Combined immunodeficiency with life-threatening EBV-associated lymphoproliferative disorder in patients lacking functional CD27. Haematologica. 2013;98(3):473-8.
109. Alkhairy OK, Perez-Becker R, Driessen GJ, Abolhassani H, van Montfrans J, Borte S, et al. Novel mutations in TNFRSF7/CD27: Clinical, immunologic, and genetic characterization of human CD27 deficiency. The Journal of allergy and clinical immunology. 2015;136(3):703-12.e10.
110. Izawa K, Martin E, Soudais C, Bruneau J, Boutboul D, Rodriguez R, et al. Inherited CD70 deficiency in humans reveals a critical role for the CD70-CD27 pathway in immunity to Epstein-Barr virus infection. J Exp Med. 2017;214(1):73-89.
111. Abolhassani H, Edwards ES, Ikinciogullari A, Jing H, Borte S, Buggert M, et al. Combined immunodeficiency and Epstein-Barr virus-induced B cell malignancy in humans with inherited CD70 deficiency. J Exp Med. 2017;214(1):91-106.
112. Caorsi R, Rusmini M, Volpi S, Chiesa S, Pastorino C, Sementa AR, et al. CD70 Deficiency due to a Novel Mutation in a Patient with Severe Chronic EBV Infection Presenting As a Periodic Fever. Frontiers in immunology. 2018;8:2015-.
113. Sudhakar A. History of Cancer, Ancient and Modern Treatment Methods. Journal of cancer science & therapy. 2009;1(2):1-4.
114. Hanahan D, Weinberg Robert A. Hallmarks of Cancer: The Next Generation. Cell. 2011;144(5):646-74.
115. Hanahan D, Weinberg RA. The Hallmarks of Cancer. Cell. 2000;100(1):57-70.
116. Dunn GP, Old LJ, Schreiber RD. The immunobiology of cancer immunosurveillance and immunoediting. Immunity. 2004;21(2):137-48.
117. Swann JB, Smyth MJ. Immune surveillance of tumors. Journal of Clinical Investigation. 2007;117(5):1137-46.
118. Shankaran V, Ikeda H, Bruce AT, White JM, Swanson PE, Old LJ, et al. IFNgamma and lymphocytes prevent primary tumour development and shape tumour immunogenicity. Nature. 2001;410(6832):1107-11.
119. Smyth MJ, Thia KY, Street SE, MacGregor D, Godfrey DI, Trapani JA. Perforin-mediated cytotoxicity is critical for surveillance of spontaneous lymphoma. J Exp Med. 2000;192(5):755-60.
120. Corthay A. Does the Immune System Naturally Protect Against Cancer? Frontiers in Immunology. 2014;5(197).
121. Mueller BU, Pizzo PA. Cancer in children with primary or secondary immunodeficiencies. The Journal of pediatrics. 1995;126(1):1-10.
122. Farkona S, Diamandis EP, Blasutig IM. Cancer immunotherapy: the beginning of the end of cancer? BMC Medicine. 2016;14(1):73.
123. Menez-Jamet J, Gallou C, Rougeot A, Kosmatopoulos K. Optimized tumor cryptic peptides: the basis for universal neo-antigen-like tumor vaccines. Annals of Translational Medicine. 2016;4(14):266.
124. Hamai A, Benlalam H, Meslin F, Hasmim M, Carre T, Akalay I, et al. Immune surveillance of human cancer: if the cytotoxic T-lymphocytes play the music, does the tumoral system call the tune? Tissue antigens. 2010;75(1):1-8.

125. Zhang L, Conejo-Garcia JR, Katsaros D, Gimotty PA, Massobrio M, Regnani G, et al. Intratumoral T Cells, Recurrence, and Survival in Epithelial Ovarian Cancer. New England Journal of Medicine. 2003;348(3):203-13.
126. Kim R, Emi M, Tanabe K. Cancer immunoediting from immune surveillance to immune escape. Immunology. 2007;121(1):1-14.
127. Badalamenti G, Fanale D, Incorvaia L, Barraco N, Listi A, Maragliano R, et al. Role of tumor-infiltrating lymphocytes in patients with solid tumors: Can a drop dig a stone? Cell Immunol. 2019;343:103753.
128. Fridman WH, Pages F, Sautes-Fridman C, Galon J. The immune contexture in human tumours: impact on clinical outcome. Nature reviews Cancer. 2012;12(4):298-306.
129. Sharma P, Allison JP. The future of immune checkpoint therapy. Science (New York, NY). 2015;348(6230):56-61.
130. Tormoen GW, Crittenden MR, Gough MJ. Role of the immunosuppressive microenvironment in immunotherapy. Advances in radiation oncology. 2018;3(4):520-6.
131. Kantoff PW, Higano CS, Shore ND, Berger ER, Small EJ, Penson DF. Sipuleucel-T immunotherapy for castration-resistant prostate cancer. The New England journal of medicine. 2010;363.
132. Rosenberg SA, Yang JC, Sherry RM, Kammula US, Hughes MS, Phan GQ. Durable complete responses in heavily pretreated patients with metastatic melanoma using T-cell transfer immunotherapy. Clinical cancer research : an official journal of the American Association for Cancer Research. 2011;17.
133. June CH, O'Connor RS, Kawalekar OU, Ghassemi S, Milone MC. CAR T cell immunotherapy for human cancer. Science (New York, NY). 2018;359(6382):1361-5.
134. Miliotou AN, Papadopoulou LC. CAR T-cell Therapy: A New Era in Cancer Immunotherapy. Current pharmaceutical biotechnology. 2018;19(1):5-18.
135. Brentjens RJ, Davila ML, Riviere I, Park J, Wang X, Cowell LG, et al. CD19-targeted T cells rapidly induce molecular remissions in adults with chemotherapy-refractory acute lymphoblastic leukemia. Sci Transl Med. 2013;5(177):177ra38.
136. Grupp SA, Kalos M, Barrett D, Aplenc R, Porter DL, Rheingold SR, et al. Chimeric Antigen Receptor–Modified T Cells for Acute Lymphoid Leukemia. New England Journal of Medicine. 2013;368(16):1509-18.
137. Porter DL, Levine BL, Kalos M, Bagg A, June CH. Chimeric antigen receptor-modified T cells in chronic lymphoid leukemia. The New England journal of medicine. 2011;365(8):725-33.
138. Rosenberg SA, Restifo NP, Yang JC, Morgan RA, Dudley ME. Adoptive cell transfer: a clinical path to effective cancer immunotherapy. Nature reviews Cancer. 2008;8.
139. Berger M, Kreutz FT, Horst JL, Baldi AC, Koff WJ. Phase I study with an autologous tumor cell vaccine for locally advanced or metastatic prostate cancer. Journal of pharmacy & pharmaceutical sciences : a publication of the Canadian Society for Pharmaceutical Sciences, Societe canadienne des sciences pharmaceutiques. 2007;10(2):144-52.
140. Guo C, Manjili MH, Subjeck JR, Sarkar D, Fisher PB, Wang X-Y. Therapeutic Cancer Vaccines: Past, Present and Future. Advances in cancer research. 2013;119:421-75.
141. Morton DL, Foshag LJ, Hoon DS, Nizze JA, Famatiga E, Wanek LA, et al. Prolongation of survival in metastatic melanoma after active specific immunotherapy with a new polyvalent melanoma vaccine. Annals of surgery. 1992;216(4):463-82.
142. Morton DL, Hsueh EC, Essner R, Foshag LJ, O'Day SJ, Bilchik A, et al. Prolonged survival of patients receiving active immunotherapy with Canvaxin therapeutic polyvalent vaccine after complete resection of melanoma metastatic to regional lymph nodes. Annals of surgery. 2002;236(4):438-48; discussion 48-9.
143. Weiner GJ. Rituximab: mechanism of action. Seminars in hematology. 2010;47(2):115-23.
144. Weiner Louis M, Murray Joseph C, Shuptrine Casey W. Antibody-Based Immunotherapy of Cancer. Cell.148(6):1081-4.

145. Salles G, Barrett M, Foa R, Maurer J, O'Brien S, Valente N, et al. Rituximab in B-Cell Hematologic Malignancies: A Review of 20 Years of Clinical Experience. Advances in therapy. 2017;34(10):2232-73.
146. Buchbinder EI, Desai A. CTLA-4 and PD-1 Pathways: Similarities, Differences, and Implications of Their Inhibition. American Journal of Clinical Oncology. 2016;39(1):98-106.
147. Hodi FS, O'Day SJ, McDermott DF, Weber RW, Sosman JA, Haanen JB. Improved survival with ipilimumab in patients with metastatic melanoma. The New England journal of medicine. 2010;363.
148. Ansell SM, Lesokhin AM, Borrello I, Halwani A, Scott EC, Gutierrez M, et al. PD-1 Blockade with Nivolumab in Relapsed or Refractory Hodgkin's Lymphoma. New England Journal of Medicine. 2015;372(4):311-9.
149. Rizvi NA, Mazieres J, Planchard D, Stinchcombe TE, Dy GK, Antonia SJ, et al. Activity and safety of nivolumab, an anti-PD-1 immune checkpoint inhibitor, for patients with advanced, refractory squamous non-small-cell lung cancer (CheckMate 063): a phase 2, single-arm trial. Lancet Oncol. 2015;16(3):257-65.
150. Brahmer JR, Drake CG, Wollner I, Powderly JD, Picus J, Sharfman WH, et al. Phase I study of single-agent anti-programmed death-1 (MDX-1106) in refractory solid tumors: safety, clinical activity, pharmacodynamics, and immunologic correlates. Journal of clinical oncology : official journal of the American Society of Clinical Oncology. 2010;28(19):3167-75.
151. Guo L, Zhang H, Chen B. Nivolumab as Programmed Death-1 (PD-1) Inhibitor for Targeted Immunotherapy in Tumor. Journal of Cancer. 2017;8(3):410-6.
152. Dang TO, Ogunniyi A, Barbee MS, Drilon A. Pembrolizumab for the treatment of PD-L1 positive advanced or metastatic non-small cell lung cancer. Expert review of anticancer therapy. 2016;16(1):13-20.
153. Hui R, Garon EB, Goldman JW, Leighl NB, Hellmann MD, Patnaik A, et al. Pembrolizumab as first-line therapy for patients with PD-L1-positive advanced non-small cell lung cancer: a phase 1 trial. Annals of oncology : official journal of the European Society for Medical Oncology / ESMO. 2017;28(4):874-81.
154. Wolchok JD, Kluger H, Callahan MK, Postow MA, Rizvi NA, Lesokhin AM, et al. Nivolumab plus ipilimumab in advanced melanoma. The New England journal of medicine. 2013;369(2):122-33.
155. Postow MA, Chesney J, Pavlick AC, Robert C, Grossmann K, McDermott D, et al. Nivolumab and ipilimumab versus ipilimumab in untreated melanoma. The New England journal of medicine. 2015;372(21):2006-17.
156. Hodi FS, Chiarion-Sileni V, Gonzalez R, Grob J-J, Rutkowski P, Cowey CL, et al. Nivolumab plus ipilimumab or nivolumab alone versus ipilimumab alone in advanced melanoma (CheckMate 067): 4-year outcomes of a multicentre, randomised, phase 3 trial. The Lancet Oncology. 2018;19(11):1480-92.
157. Wasiuk A, Testa J, Weidlick J, Sisson C, Vitale L, Widger J, et al. CD27-Mediated Regulatory T Cell Depletion and Effector T Cell Costimulation Both Contribute to Antitumor Efficacy. Journal of immunology (Baltimore, Md : 1950). 2017;199(12):4110-23.
158. Bournazos S, Wang TT, Ravetch JV. The Role and Function of Fcγ Receptors on Myeloid Cells. Microbiol Spectr. 2016;4(6):10.1128/microbiolspec.MCHD-0045-2016.
159. Bruhns P. Properties of mouse and human IgG receptors and their contribution to disease models. Blood. 2012;119(24):5640-9.
160. Bournazos S, Ravetch JV. Fcγ Receptor Function and the Design of Vaccination Strategies. Immunity. 2017;47(2):224-33.
161. Stewart R, Hammond SA, Oberst M, Wilkinson RW. The role of Fc gamma receptors in the activity of immunomodulatory antibodies for cancer. Journal for ImmunoTherapy of Cancer. 2014;2(1):29.
162. Bournazos S, Ravetch JV. Fcgamma receptor pathways during active and passive immunization. Immunol Rev. 2015;268(1):88-103.

163. Bournazos S, Wang TT, Dahan R, Maamary J, Ravetch JV. Signaling by Antibodies: Recent Progress. Annual review of immunology. 2017;35:285-311.
164. Bruhns P, Iannascoli B, England P, Mancardi DA, Fernandez N, Jorieux S, et al. Specificity and affinity of human Fcgamma receptors and their polymorphic variants for human IgG subclasses. Blood. 2009;113(16):3716-25.
165. Beatty GL, Torigian DA, Chiorean EG, Saboury B, Brothers A, Alavi A, et al. A phase I study of an agonist CD40 monoclonal antibody (CP-870,893) in combination with gemcitabine in patients with advanced pancreatic ductal adenocarcinoma. Clinical cancer research : an official journal of the American Association for Cancer Research. 2013;19(22):6286-95.
166. Beatty GL, Li Y, Long KB. Cancer immunotherapy: activating innate and adaptive immunity through CD40 agonists. Expert review of anticancer therapy. 2017;17(2):175-86.
167. White AL, Chan HT, Roghanian A, French RR, Mockridge CI, Tutt AL, et al. Interaction with FcgammaRIIB is critical for the agonistic activity of anti-CD40 monoclonal antibody. Journal of immunology (Baltimore, Md : 1950). 2011;187(4):1754-63.
168. White AL, Dou L, Chan HT, Field VL, Mockridge CI, Moss K, et al. Fcgamma receptor dependency of agonistic CD40 antibody in lymphoma therapy can be overcome through antibody multimerization. Journal of immunology (Baltimore, Md : 1950). 2014;193(4):1828-35.
169. White AL, Chan HT, French RR, Willoughby J, Mockridge CI, Roghanian A, et al. Conformation of the human immunoglobulin G2 hinge imparts superagonistic properties to immunostimulatory anticancer antibodies. Cancer cell. 2015;27(1):138-48.
170. Dahan R, Barnhart BC, Li F, Yamniuk AP, Korman AJ, Ravetch JV. Therapeutic Activity of Agonistic, Human Anti-CD40 Monoclonal Antibodies Requires Selective FcgammaR Engagement. Cancer cell. 2016;29(6):820-31.
171. Houot R, Goldstein MJ, Kohrt HE, Myklebust JH, Alizadeh AA, Lin JT, et al. Therapeutic effect of CD137 immunomodulation in lymphoma and its enhancement by Treg depletion. Blood. 2009;114(16):3431-8.
172. Adappa ND, Sung CK, Choi B, Huang TG, Genden EM, Shin EJ. The administration of IL-12/GM-CSF and Ig-4-1BB ligand markedly decreases murine floor of mouth squamous cell cancer. Otolaryngology--head and neck surgery : official journal of American Academy of Otolaryngology-Head and Neck Surgery. 2008;139(3):442-8.
173. Gauttier V, Judor JP, Le Guen V, Cany J, Ferry N, Conchon S. Agonistic anti-CD137 antibody treatment leads to antitumor response in mice with liver cancer. International journal of cancer Journal international du cancer. 2014;135(12):2857-67.
174. Buchan SL, Dou L, Remer M, Booth SG, Dunn SN, Lai C, et al. Antibodies to Costimulatory Receptor 4-1BB Enhance Anti-tumor Immunity via T Regulatory Cell Depletion and Promotion of CD8 T Cell Effector Function. Immunity. 2018;49(5):958-70.e7.
175. Molckovsky A, Siu LL. First-in-class, first-in-human phase I results of targeted agents: Highlights of the 2008 American Society of Clinical Oncology meeting. Journal of Hematology & Oncology. 2008;1(1):20.
176. Segal NH, He AR, Doi T, Levy R, Bhatia S, Pishvaian MJ, et al. Phase I Study of Single-Agent Utomilumab (PF-05082566), a 4-1BB/CD137 Agonist, in Patients with Advanced Cancer. Clinical cancer research : an official journal of the American Association for Cancer Research. 2018;24(8):1816-23.
177. Jensen SM, Maston LD, Gough MJ, Ruby CE, Redmond WL, Crittenden M, et al. Signaling through OX40 enhances antitumor immunity. Semin Oncol. 2010;37(5):524-32.
178. Morris A, Vetto JT, Ramstad T, Funatake CJ, Choolun E, Entwisle C, et al. Induction of anti-mammary cancer immunity by engaging the OX-40 receptor in vivo. Breast cancer research and treatment. 2001;67(1):71-80.
179. Willoughby J, Griffiths J, Tews I, Cragg MS. OX40: Structure and function - What questions remain? Molecular immunology. 2017;83:13-22.

180. Zhang D, Goldberg MV, Chiu ML. Fc Engineering Approaches to Enhance the Agonism and Effector Functions of an Anti-OX40 Antibody. The Journal of biological chemistry. 2016;291(53):27134-46.
181. Curti BD, Kovacsovics-Bankowski M, Morris N, Walker E, Chisholm L, Floyd K, et al. OX40 is a potent immune-stimulating target in late-stage cancer patients. Cancer research. 2013;73(24):7189-98.
182. Aspeslagh S, Postel-Vinay S, Rusakiewicz S, Soria J-C, Zitvogel L, Marabelle A. Rationale for anti-OX40 cancer immunotherapy. European Journal of Cancer. 2016;52:50-66.
183. Knee DA, Hewes B, Brogdon JL. Rationale for anti-GITR cancer immunotherapy. European journal of cancer (Oxford, England : 1990). 2016;67:1-10.
184. Bulliard Y, Jolicoeur R, Windman M, Rue SM, Ettenberg S, Knee DA, et al. Activating Fc gamma receptors contribute to the antitumor activities of immunoregulatory receptor-targeting antibodies. J Exp Med. 2013;210(9):1685-93.
185. Mayes PA, Hance KW, Hoos A. The promise and challenges of immune agonist antibody development in cancer. Nature Reviews Drug Discovery. 2018;17:509.
186. Roberts DJ, Franklin NA, Kingeter LM, Yagita H, Tutt AL, Glennie MJ, et al. Control of established melanoma by CD27 stimulation is associated with enhanced effector function and persistence, and reduced PD-1 expression of tumor infiltrating CD8(+) T cells. Journal of immunotherapy (Hagerstown, Md : 1997). 2010;33(8):769-79.
187. Arens R, Schepers K, Nolte MA, van Oosterwijk MF, van Lier RAW, Schumacher TNM, et al. Tumor Rejection Induced by CD70-mediated Quantitative and Qualitative Effects on Effector CD8⁺ T Cell Formation. The Journal of Experimental Medicine. 2004;199(11):1595-605.
188. Keller AM, Schildknecht A, Xiao Y, van den Broek M, Borst J. Expression of costimulatory ligand CD70 on steady-state dendritic cells breaks CD8+ T cell tolerance and permits effective immunity. Immunity. 2008;29(6):934-46.
189. Buchan S, Manzo T, Flutter B, Rogel A, Edwards N, Zhang L, et al. OX40- and CD27-mediated co-stimulation synergize with anti-PD-L1 blockade by forcing exhausted CD8(+) T cells to exit quiescence. Journal of immunology (Baltimore, Md : 1950). 2015;194(1):125-33.
190. Ahrends T, Babala N, Xiao Y, Yagita H, van Eenennaam H, Borst J. CD27 Agonism Plus PD-1 Blockade Recapitulates CD4+ T-cell Help in Therapeutic Anticancer Vaccination. Cancer research. 2016;76(10):2921-31.
191. Turaj AH, Hussain K, Cox KL, Rose-Zerilli MJJ, Testa J, Dahal LN, et al. Antibody Tumor Targeting Is Enhanced by CD27 Agonists through Myeloid Recruitment. Cancer cell. 2017;32(6):777-91.e6.
192. Ansell S, Northfelt D, Flinn I, Burris H, Dinner S, Villalobos V, et al. A phase I study of an agonist anti-CD27 human antibody (CDX-1127) in patients with advanced hematologic malignancies or solid tumors. Journal for ImmunoTherapy of Cancer. 2013;1(1):P259.
193. Burris HA, Infante JR, Ansell SM, Nemunaitis JJ, Weiss GR, Villalobos VM, et al. Safety and Activity of Varlilumab, a Novel and First-in-Class Agonist Anti-CD27 Antibody, in Patients With Advanced Solid Tumors. Journal of Clinical Oncology. 2017;35(18):2028-36.
194. Sanborn RE, Pishvaian MJ, Kluger HM, Callahan MK, Weise AM, Lutzky J, et al. Clinical results with combination of anti-CD27 agonist antibody, varlilumab, with anti-PD1 antibody nivolumab in advanced cancer patients. Journal of Clinical Oncology. 2017;35(15_suppl):3007-.
195. Villasboas JC, Reeder CB, Tun HW, Bartlett NL, Sharon E, LaPlant B, et al. The DIAL Study (Dual Immunomodulation in Aggressive Lymphoma): A randomized phase 2 study of CDX-1127 (varlilumab) in combination with nivolumab in patients with relapsed or refractory aggressive B-cell lymphomas (NCI 10089/NCT03038672). Journal of Clinical Oncology. 2019;37(15_suppl):TPS7570-TPS.
196. Lim SH, Linton KM, Collins GP, Dhondt J, Caddy J, Rossiter L, et al. RIVA - a phase IIa study of rituximab and varlilumab in relapsed or refractory B-cell malignancies: study protocol for a randomized controlled trial. Trials. 2018;19(1):619.

197. Melero I, Shuford WW, Newby SA, Aruffo A, Ledbetter JA, Hellstrom KE, et al. Monoclonal antibodies against the 4-1BB T-cell activation molecule eradicate established tumors. Nat Med. 1997;3(6):682-5.
198. French RR, Chan HT, Tutt AL, Glennie MJ. CD40 antibody evokes a cytotoxic T-cell response that eradicates lymphoma and bypasses T-cell help. Nat Med. 1999;5(5):548-53.
199. Weinberg AD, Rivera MM, Prell R, Morris A, Ramstad T, Vetto JT, et al. Engagement of the OX-40 receptor in vivo enhances antitumor immunity. Journal of immunology (Baltimore, Md : 1950). 2000;164(4):2160-9.
200. Rowley TF, Al-Shamkhani A. Stimulation by soluble CD70 promotes strong primary and secondary CD8+ cytotoxic T cell responses in vivo. Journal of immunology (Baltimore, Md : 1950). 2004;172(10):6039-46.
201. McNamara JO, Kolonias D, Pastor F, Mittler RS, Chen L, Giangrande PH, et al. Multivalent 4-1BB binding aptamers costimulate CD8+ T cells and inhibit tumor growth in mice. The Journal of clinical investigation. 2008;118(1):376-86.
202. Wiethe C, Dittmar K, Doan T, Lindenmaier W, Tindle R. Provision of 4-1BB ligand enhances effector and memory CTL responses generated by immunization with dendritic cells expressing a human tumor-associated antigen. Journal of immunology (Baltimore, Md : 1950). 2003;170(6):2912-22.
203. Melero I, Bach N, Hellstrom KE, Aruffo A, Mittler RS, Chen L. Amplification of tumor immunity by gene transfer of the co-stimulatory 4-1BB ligand: synergy with the CD28 co-stimulatory pathway. European journal of immunology. 1998;28(3):1116-21.
204. Moraes TJ, Lin GH, Wen T, Watts TH. Incorporation of 4-1BB ligand into an adenovirus vaccine vector increases the number of functional antigen-specific CD8 T cells and enhances the duration of protection against influenza-induced respiratory disease. Vaccine. 2011;29(37):6301-12.
205. Li F, Ravetch JV. Inhibitory Fcgamma receptor engagement drives adjuvant and anti-tumor activities of agonistic CD40 antibodies. Science (New York, NY). 2011;333(6045):1030-4.
206. Smith KG, Clatworthy MR. FcgammaRIIB in autoimmunity and infection: evolutionary and therapeutic implications. Nat Rev Immunol. 2010;10(5):328-43.
207. Grugan KD, McCabe FL, Kinder M, Greenplate AR, Harman BC, Ekert JE, et al. Tumor-associated macrophages promote invasion while retaining Fc-dependent anti-tumor function. Journal of immunology (Baltimore, Md : 1950). 2012;189(11):5457-66.
208. Pritchard NR, Cutler AJ, Uribe S, Chadban SJ, Morley BJ, Smith KG. Autoimmune-prone mice share a promoter haplotype associated with reduced expression and function of the Fc receptor FcgammaRII. Curr Biol. 2000;10(4):227-30.
209. Su K, Yang H, Li X, Li X, Gibson AW, Cafardi JM, et al. Expression profile of FcgammaRIIb on leukocytes and its dysregulation in systemic lupus erythematosus. Journal of immunology (Baltimore, Md : 1950). 2007;178(5):3272-80.
210. Li F, Ravetch JV. Antitumor activities of agonistic anti-TNFR antibodies require differential FcgammaRIIB coengagement in vivo. Proceedings of the National Academy of Sciences of the United States of America. 2013;110(48):19501-6.
211. Henkler F, Behrle E, Dennehy KM, Wicovsky A, Peters N, Warnke C, et al. The extracellular domains of FasL and Fas are sufficient for the formation of supramolecular FasL-Fas clusters of high stability. The Journal of cell biology. 2005;168(7):1087-98.
212. Siegel RM, Muppidi JR, Sarker M, Lobito A, Jen M, Martin D, et al. SPOTS: signaling protein oligomeric transduction structures are early mediators of death receptor-induced apoptosis at the plasma membrane. The Journal of cell biology. 2004;167(4):735-44.
213. Hargreaves PG, Al-Shamkhani A. Soluble CD30 binds to CD153 with high affinity and blocks transmembrane signaling by CD30. European journal of immunology. 2002;32(1):163-73.
214. Haswell LE, Glennie MJ, Al-Shamkhani A. Analysis of the oligomeric requirement for signaling by CD40 using soluble multimeric forms of its ligand, CD154. European journal of immunology. 2001;31(10):3094-100.

215. Wyzgol A, Muller N, Fick A, Munkel S, Grigoleit GU, Pfizenmaier K, et al. Trimer stabilization, oligomerization, and antibody-mediated cell surface immobilization improve the activity of soluble trimers of CD27L, CD40L, 41BBL, and glucocorticoid-induced TNF receptor ligand. Journal of immunology (Baltimore, Md : 1950). 2009;183(3):1851-61.
216. Diebold SS, Montoya M, Unger H, Alexopoulou L, Roy P, Haswell LE, et al. Viral infection switches non-plasmacytoid dendritic cells into high interferon producers. Nature. 2003;424(6946):324-8.
217. Rowley TF. Functional analysis of the costimulatory molecules CD27 and CD137 during T-cell mediated immune responses. : University of Southampton 2004.
218. Pyzik M, Rath T, Lencer WI, Baker K, Blumberg RS. FcRn: The Architect Behind the Immune and Nonimmune Functions of IgG and Albumin. Journal of immunology (Baltimore, Md : 1950). 2015;194(10):4595-603.
219. Jensen PF, Schoch A, Larraillet V, Hilger M, Schlothauer T, Emrich T, et al. A Two-pronged Binding Mechanism of IgG to the Neonatal Fc Receptor Controls Complex Stability and IgG Serum Half-life. Mol Cell Proteomics. 2017;16(3):451-6.
220. Clarke SR, Barnden M, Kurts C, Carbone FR, Miller JF, Heath WR. Characterization of the ovalbumin-specific TCR transgenic line OT-I: MHC elements for positive and negative selection. Immunol Cell Biol. 2000;78(2):110-7.
221. Klein JS, Jiang S, Galimidi RP, Keeffe JR, Bjorkman PJ. Design and characterization of structured protein linkers with differing flexibilities. Protein engineering, design & selection : PEDS. 2014;27(10):325-30.
222. Chen X, Zaro JL, Shen W-C. Fusion protein linkers: property, design and functionality. Adv Drug Deliv Rev. 2013;65(10):1357-69.
223. Brown ME, Renner G, Field RP, Hassell T. Process development for the production of recombinant antibodies using the glutamine synthetase (GS) system. Cytotechnology. 1992;9(1-3):231-6.
224. Ansari IH, Kwon B, Osorio FA, Pattnaik AK. Influence of N-linked glycosylation of porcine reproductive and respiratory syndrome virus GP5 on virus infectivity, antigenicity, and ability to induce neutralizing antibodies. Journal of virology. 2006;80(8):3994-4004.
225. Trickett A, Kwan YL. T cell stimulation and expansion using anti-CD3/CD28 beads. Journal of Immunological Methods. 2003;275(1):251-5.
226. Gavel Y, von Heijne G. Sequence differences between glycosylated and non-glycosylated Asn-X-Thr/Ser acceptor sites: implications for protein engineering. Protein engineering. 1990;3(5):433-42.
227. Breitling J, Aebi M. N-linked protein glycosylation in the endoplasmic reticulum. Cold Spring Harbor perspectives in biology. 2013;5(8):a013359-a.
228. Hossler P, Khattak SF, Li ZJ. Optimal and consistent protein glycosylation in mammalian cell culture. Glycobiology. 2009;19(9):936-49.
229. Higel F, Seidl A, Sörgel F, Friess W. N-glycosylation heterogeneity and the influence on structure, function and pharmacokinetics of monoclonal antibodies and Fc fusion proteins. European Journal of Pharmaceutics and Biopharmaceutics. 2016;100:94-100.
230. Lee SJ, Evers S, Roeder D, Parlow AF, Risteli J, Risteli L, et al. Mannose receptor-mediated regulation of serum glycoprotein homeostasis. Science (New York, NY). 2002;295(5561):1898-901.
231. Freeze HH, Kranz C. Endoglycosidase and glycoamidase release of N-linked glycans. Curr Protoc Mol Biol. 2010;Chapter 17:10.1002/0471142727.mb1713as89-17.13A.
232. Abès R, Teillaud J-L. Impact of Glycosylation on Effector Functions of Therapeutic IgG. Pharmaceuticals (Basel). 2010;3(1):146-57.
233. Clynes RA, Towers TL, Presta LG, Ravetch JV. Inhibitory Fc receptors modulate in vivo cytoxicity against tumor targets. Nature Medicine. 2000;6(4):443-6.
234. Willoughby JE, Kerr JP, Rogel A, Taraban VY, Buchan SL, Johnson PW, et al. Differential impact of CD27 and 4-1BB costimulation on effector and memory CD8 T cell generation following peptide immunization. Journal of immunology (Baltimore, Md : 1950). 2014;193(1):244-51.

235. Nimmerjahn F, Ravetch JV. Fcgamma receptors: old friends and new family members. Immunity. 2006;24(1):19-28.
236. Jenkins MK, Moon JJ. The role of naive T cell precursor frequency and recruitment in dictating immune response magnitude. Journal of immunology (Baltimore, Md : 1950). 2012;188(9):4135-40.
237. Haluszczak C, Akue AD, Hamilton SE, Johnson LDS, Pujanauski L, Teodorovic L, et al. The antigen-specific CD8+ T cell repertoire in unimmunized mice includes memory phenotype cells bearing markers of homeostatic expansion. The Journal of experimental medicine. 2009;206(2):435-48.
238. van Stipdonk MJ, Lemmens EE, Schoenberger SP. Naive CTLs require a single brief period of antigenic stimulation for clonal expansion and differentiation. Nat Immunol. 2001;2(5):423-9.
239. Prlic M, Hernandez-Hoyos G, Bevan MJ. Duration of the initial TCR stimulus controls the magnitude but not functionality of the CD8+ T cell response. The Journal of experimental medicine. 2006;203(9):2135-43.
240. Teplyakov A, Obmolova G, Malia TJ, Gilliland GL. Crystal structure of CD27 in complex with a neutralizing noncompeting antibody. Acta Crystallogr F Struct Biol Commun. 2017;73(Pt 5):294-9.
241. Egan LJ, Toruner M. NF-kappaB signaling: pros and cons of altering NF-kappaB as a therapeutic approach. Ann N Y Acad Sci. 2006;1072:114-22.
242. Obmolova G, Teplyakov A, Malia TJ, Wunderler N, Kwok D, Barone L, et al. Epitope-dependent mechanisms of CD27 neutralization revealed by X-ray crystallography. Molecular immunology. 2017;83:92-9.
243. Pan L, Fu TM, Zhao W, Zhao L, Chen W, Qiu C, et al. Higher-Order Clustering of the Transmembrane Anchor of DR5 Drives Signaling. Cell. 2019;176(6):1477-89.e14.
244. Krippner-Heidenreich A, Grunwald I, Zimmermann G, Kühnle M, Gerspach J, Sterns T, et al. Single-Chain TNF, a TNF Derivative with Enhanced Stability and Antitumoral Activity. The Journal of Immunology. 2008;180(12):8176-83.
245. Spitzer D, McDunn JE, Plambeck-Suess S, Goedegebuure PS, Hotchkiss RS, Hawkins WG. A genetically encoded multifunctional TRAIL trimer facilitates cell-specific targeting and tumor cell killing. Molecular cancer therapeutics. 2010;9(7):2142-51.
246. Schneider B, Munkel S, Krippner-Heidenreich A, Grunwald I, Wels WS, Wajant H, et al. Potent antitumoral activity of TRAIL through generation of tumor-targeted single-chain fusion proteins. Cell death & disease. 2010;1:e68.
247. Warren JT, Nelson CA, Decker CE, Zou W, Fremont DH, Teitelbaum SL. Manipulation of receptor oligomerization as a strategy to inhibit signaling by TNF superfamily members. Science signaling. 2014;7(339):ra80.
248. Wang W, Vlasak J, Li Y, Pristatsky P, Fang Y, Pittman T, et al. Impact of methionine oxidation in human IgG1 Fc on serum half-life of monoclonal antibodies. Molecular immunology. 2011;48(6-7):860-6.
249. Wines BD, Powell MS, Parren PW, Barnes N, Hogarth PM. The IgG Fc contains distinct Fc receptor (FcR) binding sites: the leukocyte receptors Fc gamma RI and Fc gamma RIIa bind to a region in the Fc distinct from that recognized by neonatal FcR and protein A. Journal of immunology (Baltimore, Md : 1950). 2000;164(10):5313-8.
250. Varki A. Sialic acids in human health and disease. Trends in molecular medicine. 2008;14(8):351-60.
251. Goetze AM, Liu YD, Zhang Z, Shah B, Lee E, Bondarenko PV, et al. High-mannose glycans on the Fc region of therapeutic IgG antibodies increase serum clearance in humans. Glycobiology. 2011;21(7):949-59.
252. Mi Y, Coonce M, Fiete D, Steirer L, Dveksler G, Townsend RR, et al. Functional Consequences of Mannose and Asialoglycoprotein Receptor Ablation. The Journal of biological chemistry. 2016;291(36):18700-17.

253. Lund J, Takahashi N, Pound JD, Goodall M, Jefferis R. Multiple interactions of IgG with its core oligosaccharide can modulate recognition by complement and human Fc gamma receptor I and influence the synthesis of its oligosaccharide chains. Journal of immunology (Baltimore, Md : 1950). 1996;157(11):4963-9.
254. Lux A, Yu X, Scanlan CN, Nimmerjahn F. Impact of immune complex size and glycosylation on IgG binding to human FcgammaRs. Journal of immunology (Baltimore, Md : 1950). 2013;190(8):4315-23.
255. Matsuo I, Kashiwagi T, Totani K, Ito Y. First chemical synthesis of triglucosylated tetradecasaccharide (Glc3Man9GlcNAc2), a common precursor of asparagine-linked oligosaccharides. Tetrahedron Letters. 2005;46(24):4197-200.
256. Braakman I, Hebert DN. Protein folding in the endoplasmic reticulum. Cold Spring Harbor perspectives in biology. 2013;5(5):a013201-a.
257. Van Patten SM, Hughes H, Huff MR, Piepenhagen PA, Waire J, Qiu H, et al. Effect of mannose chain length on targeting of glucocerebrosidase for enzyme replacement therapy of Gaucher disease. Glycobiology. 2007;17(5):467-78.
258. Ferris SP, Kodali VK, Kaufman RJ. Glycoprotein folding and quality-control mechanisms in protein-folding diseases. Dis Model Mech. 2014;7(3):331-41.
259. Thiemann M, Richards DM, Heinonen K, Kluge M, Marschall V, Merz C, et al. A Single-Chain-Based Hexavalent CD27 Agonist Enhances T Cell Activation and Induces Anti-Tumor Immunity. Frontiers in oncology. 2018;8:387.
260. Zhang D, Armstrong AA, Tam SH, McCarthy SG, Luo J, Gilliland GL, et al. Functional optimization of agonistic antibodies to OX40 receptor with novel Fc mutations to promote antibody multimerization. MAbs. 2017;9(7):1129-42.
261. Medler J, Nelke J, Weisenberger D, Steinfatt T, Rothaug M, Berr S, et al. TNFRSF receptor-specific antibody fusion proteins with targeting controlled FcγR-independent agonistic activity. Cell death & disease. 2019;10(3):224.
262. Holler N, Tardivel A, Kovacsovics-Bankowski M, Hertig S, Gaide O, Martinon F, et al. Two adjacent trimeric Fas ligands are required for Fas signaling and formation of a death-inducing signaling complex. Mol Cell Biol. 2003;23(4):1428-40.

Appendix

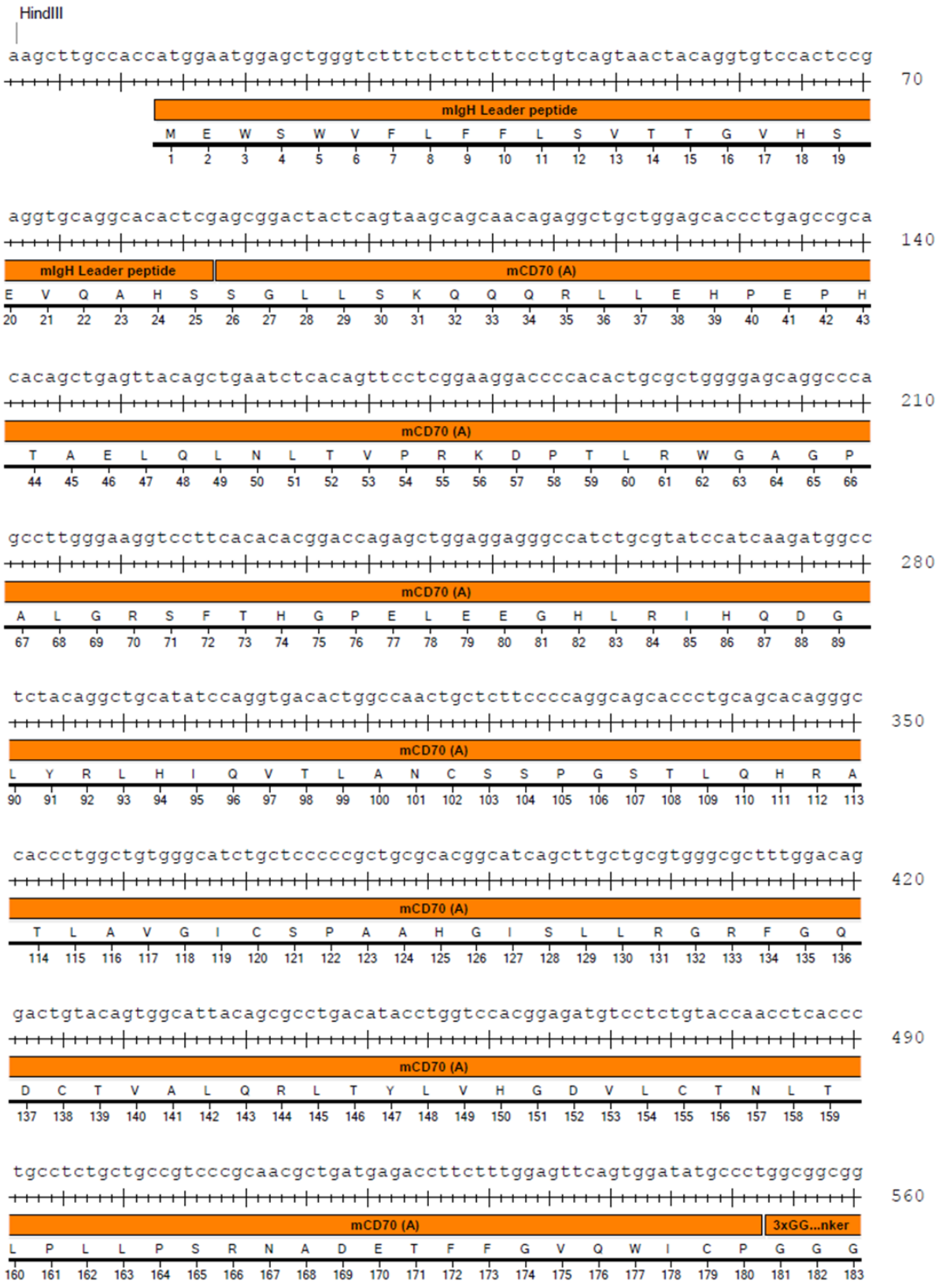
HindIII
aagcttgccaccatggaatggagctgggtctttctcttcttcctgtcagtaactacaggtgtccactccg
70
mIgH Leader peptide
M E W S W V F L F F L S V T T G V H S
1 2 3 4 5 6 7 8 9 10 11 12 13 14 15 16 17 18 19
aggtgcaggcacactcgagcggactactcagtaagcagcaacagaggctgctggagcaccctgagccgca
140
mIgH Leader peptide
mCD70 (A)
E V Q A H S S G L L S K Q Q Q R L L E H P E P H
20 21 22 23 24 25 26 27 28 29 30 31 32 33 34 35 36 37 38 39 40 41 42 43
cacagctgagttacagctgaatctcacagttcctcggaaggaccccacactgcgctggggagcaggccca
210
mCD70 (A)
T A E L Q L N L T V P R K D P T L R W G A G P
44 45 46 47 48 49 50 51 52 53 54 55 56 57 58 59 60 61 62 63 64 65 66
gccttgggaaggtccttcacacacggaccagagctggaggagggccatctgcgtatccatcaagatggcc
280
mCD70 (A)
A L G R S F T H G P E L E E G H L R I H Q D G
67 68 69 70 71 72 73 74 75 76 77 78 79 80 81 82 83 84 85 86 87 88 89
tctacaggctgcatatccaggtgacactggccaactgctcttccccaggcagcaccctgcagcacagggc
350
mCD70 (A)
L Y R L H I Q V T L A N C S S P G S T L Q H R A
90 91 92 93 94 95 96 97 98 99 100 101 102 103 104 105 106 107 108 109 110 111 112 113
caccctggctgtgggcatctgctcccccgctgcgcacggcatcagcttgctgcgtgggcgctttggacag
420
mCD70 (A)
T L A V G I C S P A A H G I S L L R G R F G Q
114 115 116 117 118 119 120 121 122 123 124 125 126 127 128 129 130 131 132 133 134 135 136
gactgtacagtggcattacagcgcctgacatacctggtccacggagatgtcctctgtaccaacctcaccc
490
mCD70 (A)
D C T V A L Q R L T Y L V H G D V L C T N L T
137 138 139 140 141 142 143 144 145 146 147 148 149 150 151 152 153 154 155 156 157 158 159
tgcctctgctgccgtcccgcaacgctgatgagaccttctttggagttcagtggatatgccctggcggcgg
560
mCD70 (A)
3xGG...nker
L P L L P S R N A D E T F F G V Q W I C P G G G
160 161 162 163 164 165 166 167 168 169 170 171 172 173 174 175 176 177 178 179 180 181 182 183

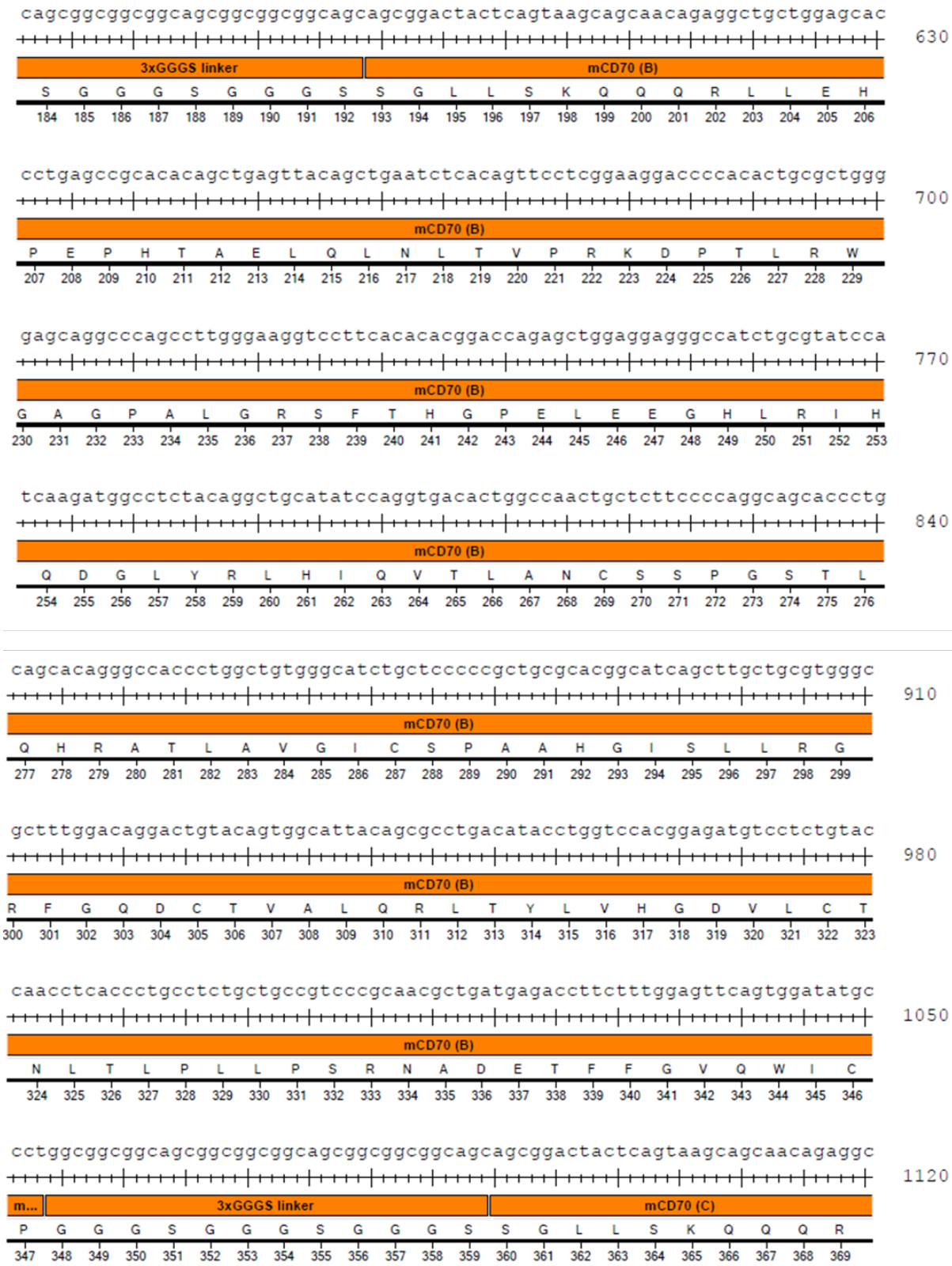
cagcggcggcggcagcggcggcggcagcagcggactactcagtaagcagcaacagaggctgctggagcac
630
3xGGGS linker
mCD70 (B)
S G G G S G G G S S G L L S K Q Q Q R L L E H
184 185 186 187 188 189 190 191 192 193 194 195 196 197 198 199 200 201 202 203 204 205 206
cctgagccgcacacagctgagttacagctgaatctcacagttcctcggaaggaccccacactgcgctggg
700
mCD70 (B)
P E P H T A E L Q L N L T V P R K D P T L R W
207 208 209 210 211 212 213 214 215 216 217 218 219 220 221 222 223 224 225 226 227 228 229
gagcaggcccagccttgggaaggtccttcacacacggaccagagctggaggagggccatctgcgtatcca
770
mCD70 (B)
G A G P A L G R S F T H G P E L E E G H L R I H
230 231 232 233 234 235 236 237 238 239 240 241 242 243 244 245 246 247 248 249 250 251 252 253
tcaagatggcctctacaggctgcatatccaggtgacactggccaactgctcttccccaggcagcaccctg
840
mCD70 (B)
Q D G L Y R L H I Q V T L A N C S S P G S T L
254 255 256 257 258 259 260 261 262 263 264 265 266 267 268 269 270 271 272 273 274 275 276
cagcacagggccaccctggctgtgggcatctgctccccgctgcgcacggcatcagcttgctgcgtgggc
910
mCD70 (B)
Q H R A T L A V G I C S P A A H G I S L L R G
277 278 279 280 281 282 283 284 285 286 287 288 289 290 291 292 293 294 295 296 297 298 299
gctttggacaggactgtacagtggcattacagcgcctgacatacctggtccacggagatgtcctctgtac
980
mCD70 (B)
R F G Q D C T V A L Q R L T Y L V H G D V L C T
300 301 302 303 304 305 306 307 308 309 310 311 312 313 314 315 316 317 318 319 320 321 322 323
caacctcaccctgcctctgctgccgtcccgcaacgctgatgagaccttctttggagttcagtggatatgc
1050
mCD70 (B)
N L T L P L L P S R N A D E T F F G V Q W I C
324 325 326 327 328 329 330 331 332 333 334 335 336 337 338 339 340 341 342 343 344 345 346
cctggcggcggcagcggcggcggcagcggcggcggcagcagcggactactcagtaagcagcaacagaggc
1120
m...
3xGGGS linker
mCD70 (C)
P G G G S G G G S G G G S S G L L S K Q Q Q R
347 348 349 350 351 352 353 354 355 356 357 358 359 360 361 362 363 364 365 366 367 368 369


tgctggagcaccctgagccgcacacagctgagttacagctgaatctcacagttcctcggaaggaccccac
1190
mCD70 (C)
L L E H P E P H T A E L Q L N L T V P R K D P T
370 371 372 373 374 375 376 377 378 379 380 381 382 383 384 385 386 387 388 389 390 391 392 393
actgcgctggggagcaggcccagccttgggaaggtccttcacacacggaccagagctggaggagggccat
1260
mCD70 (C)
L R W G A G P A L G R S F T H G P E L E E G H
394 395 396 397 398 399 400 401 402 403 404 405 406 407 408 409 410 411 412 413 414 415 416
ctgcgtatccatcaagatggcctctacaggctgcatatccaggtgacactggccaactgctcttccccag
1330
mCD70 (C)
L R I H Q D G L Y R L H I Q V T L A N C S S P
417 418 419 420 421 422 423 424 425 426 427 428 429 430 431 432 433 434 435 436 437 438 439
gcagcaccctgcagcacagggccaccctggctgtgggcatctgctccccgctgcgcacggcatcagctt
1400
mCD70 (C)
G S T L Q H R A T L A V G I C S P A A H G I S L
440 441 442 443 444 445 446 447 448 449 450 451 452 453 454 455 456 457 458 459 460 461 462 463
gctgcgtgggcgctttggacaggactgtacagtggcattacagcgcctgacatacctggtccacggagat
1470
mCD70 (C)
L R G R F G Q D C T V A L Q R L T Y L V H G D
464 465 466 467 468 469 470 471 472 473 474 475 476 477 478 479 480 481 482 483 484 485 486
gtcctctgtaccaacctcaccctgcctctgctgccgtcccgcaacgctgatgagaccttctttggagttc
1540
mCD70 (C)
V L C T N L T L P L L P S R N A D E T F F G V
487 488 489 490 491 492 493 494 495 496 497 498 499 500 501 502 503 504 505 506 507 508 509
XbaI
agtggatatgccctggcggcggcagcggcggcggcagctctagaggcggcggcagcGTGCCCAGGGATTC
1610
mCD70 (C)
2xGGGS linker
Hinge
Xba I linker
Q W I C P G G G S G G G S S R G G G S V P R D S
510 511 512 513 514 515 516 517 518 519 520 521 522 523 524 525 526 527 528 529 530 531 532 533

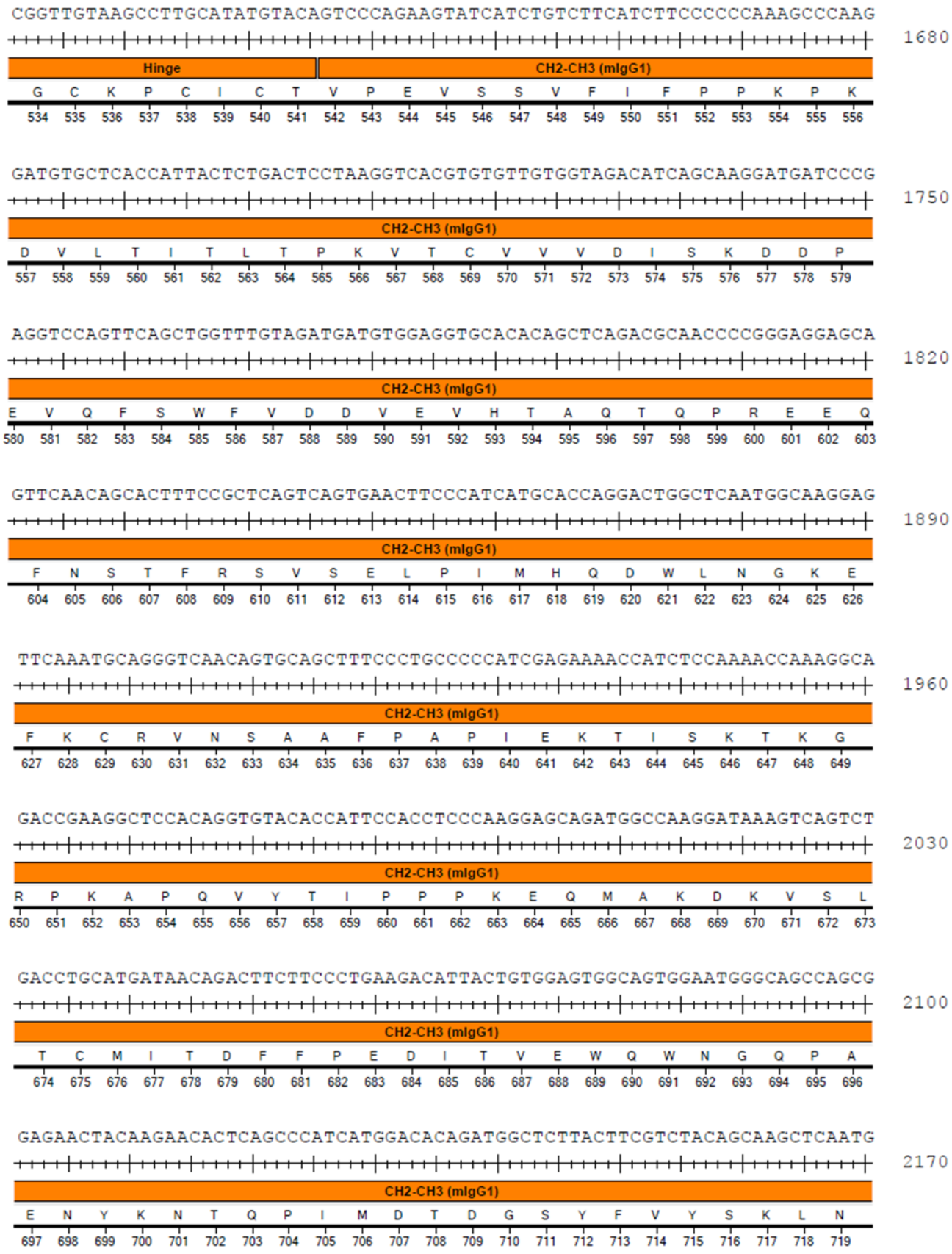
CGGTTGTAAGCCTTGCATATGTACAGTCCCAGAAGTATCATCTGTCTTCATCTTCCCCCCAAAGCCCAAG
1680
Hinge
CH2-CH3 (mIgG1)
G C K P C I C T V P E V S S V F I F P P K P K
534 535 536 537 538 539 540 541 542 543 544 545 546 547 548 549 550 551 552 553 554 555 556
GATGTGCTCACCATTACTCTGACTCCTAAGGTCACGTGTGTTGTGGTAGACATCAGCAAGGATGATCCCG
1750
CH2-CH3 (mIgG1)
D V L T I T L T P K V T C V V V D I S K D D P
557 558 559 560 561 562 563 564 565 566 567 568 569 570 571 572 573 574 575 576 577 578 579
AGGTCCAGTTCAGCTGGTTTGTAGATGATGTGGAGGTGCACACAGCTCAGACGCAACCCCGGGAGGAGCA
1820
CH2-CH3 (mIgG1)
E V Q F S W F V D D V E V H T A Q T Q P R E E Q
580 581 582 583 584 585 586 587 588 589 590 591 592 593 594 595 596 597 598 599 600 601 602 603
GTTCAACAGCACTTTCCGCTCAGTCAGTGAACTTCCCATCATGCACCAGGACTGGCTCAATGGCAAGGAG
1890
CH2-CH3 (mIgG1)
F N S T F R S V S E L P I M H Q D W L N G K E
604 605 606 607 608 609 610 611 612 613 614 615 616 617 618 619 620 621 622 623 624 625 626
TTCAAATGCAGGGTCAACAGTGCAGCTTTCCCTGCCCCCATCGAGAAAACCATCTCCAAAACCAAAGGCA
1960
CH2-CH3 (mIgG1)
F K C R V N S A A F P A P I E K T I S K T K G
627 628 629 630 631 632 633 634 635 636 637 638 639 640 641 642 643 644 645 646 647 648 649
GACCGAAGGCTCCACAGGTGTACACCATTCCACCTCCCAAGGAGCAGATGGCCAAGGATAAAGTCAGTCT
2030
CH2-CH3 (mIgG1)
R P K A P Q V Y T I P P P K E Q M A K D K V S L
650 651 652 653 654 655 656 657 658 659 660 661 662 663 664 665 666 667 668 669 670 671 672 673
GACCTGCATGATAACAGACTTCTTCCCTGAAGACATTACTGTGGAGTGGCAGTGGAATGGGCAGCCAGCG
2100
CH2-CH3 (mIgG1)
T C M I T D F F P E D I T V E W Q W N G Q P A
674 675 676 677 678 679 680 681 682 683 684 685 686 687 688 689 690 691 692 693 694 695 696
GAGAACTACAAGAACACTCAGCCCATCATGGACACAGATGGCTCTTACTTCGTCTACAGCAAGCTCAATG
2170
CH2-CH3 (mIgG1)
E N Y K N T Q P I M D T D G S Y F V Y S K L N
697 698 699 700 701 702 703 704 705 706 707 708 709 710 711 712 713 714 715 716 717 718 719

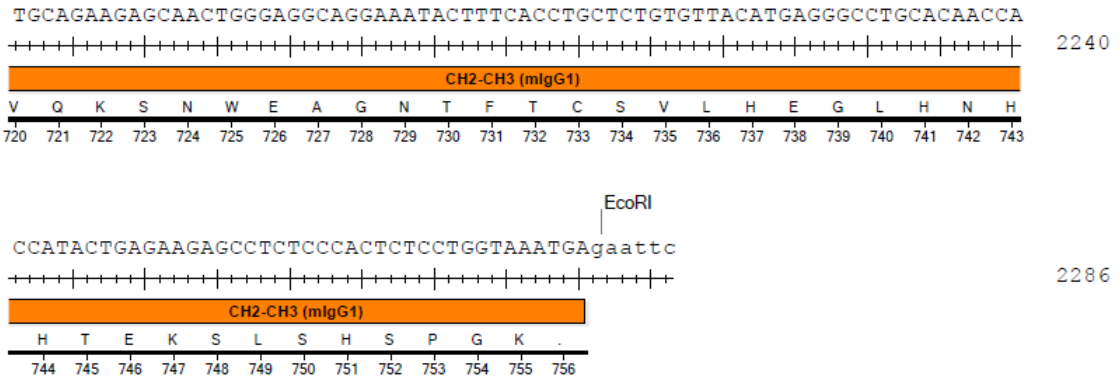

Figure 1. Translated DNA sequence of scmCD70-m1. The translated DNA sequence with single letter amino acid code is illustrated. CD70, hinge and CH2-CH3 domains of mIgG1 Fc are labelled. HindIII, XbaI and EcoRI restriction sites are indicated. The sequence was designed as detailed in section 3.2.

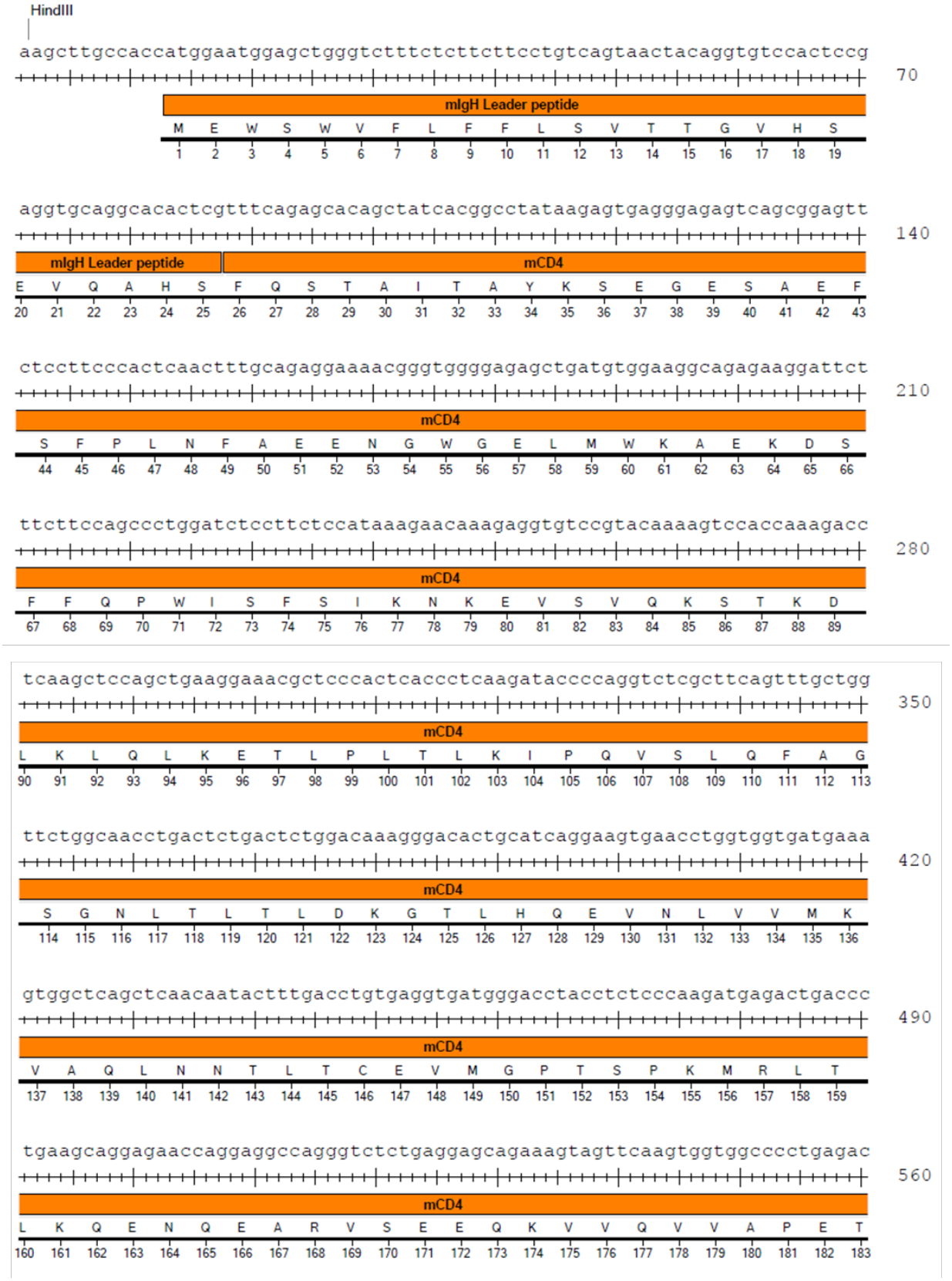
HindIII
aagcttgccaccatggaatggagctgggtctttctcttcttcctgtcagtaactacaggtgtccactccg
70
mIgH Leader peptide
M E W S W V F L F F L S V T T G V H S
1 2 3 4 5 6 7 8 9 10 11 12 13 14 15 16 17 18 19
aggtgcaggcacactcgtttcagagcacagctatcacggcctataagagtgagggagagtcagcggagtt
140
mIgH Leader peptide
mCD4
E V Q A H S F Q S T A I T A Y K S E G E S A E F
20 21 22 23 24 25 26 27 28 29 30 31 32 33 34 35 36 37 38 39 40 41 42 43
ctccttcccactcaactttgcagaggaaaacgggtggggagagctgatgtggaaggcagagaaggattct
210
mCD4
S F P L N F A E E N G W G E L M W K A E K D S
44 45 46 47 48 49 50 51 52 53 54 55 56 57 58 59 60 61 62 63 64 65 66
ttcttccagccctggatctccttctccataaagaacaaagaggtgtccgtacaaaagtccaccaaagacc
280
mCD4
F F Q P W I S F S I K N K E V S V Q K S T K D
67 68 69 70 71 72 73 74 75 76 77 78 79 80 81 82 83 84 85 86 87 88 89
tcaagctccagctgaaggaaacgctcccactcaccctcaagataccccaggtctcgcttcagtttgctgg
350
mCD4
L K L Q L K E T L P L T L K I P Q V S L Q F A G
90 91 92 93 94 95 96 97 98 99 100 101 102 103 104 105 106 107 108 109 110 111 112 113
ttctggcaacctgactctgactctggacaaagggacactgcatcaggaagtgaacctggtggtgatgaaa
420
mCD4
S G N L T L T L D K G T L H Q E V N L V V M K
114 115 116 117 118 119 120 121 122 123 124 125 126 127 128 129 130 131 132 133 134 135 136
gtggctcagctcaacaatactttgacctgtgaggtgatgggacctacctctcccaagatgagactgaccc
490
mCD4
V A Q L N N T L T C E V M G P T S P K M R L T
137 138 139 140 141 142 143 144 145 146 147 148 149 150 151 152 153 154 155 156 157 158 159
tgaagcaggagaaccaggaggccagggtctctgaggagcagaaagtagttcaagtggtggcccctgagac
560
mCD4
L K Q E N Q E A R V S E E Q K V V Q V V A P E T
160 161 162 163 164 165 166 167 168 169 170 171 172 173 174 175 176 177 178 179 180 181 182 183

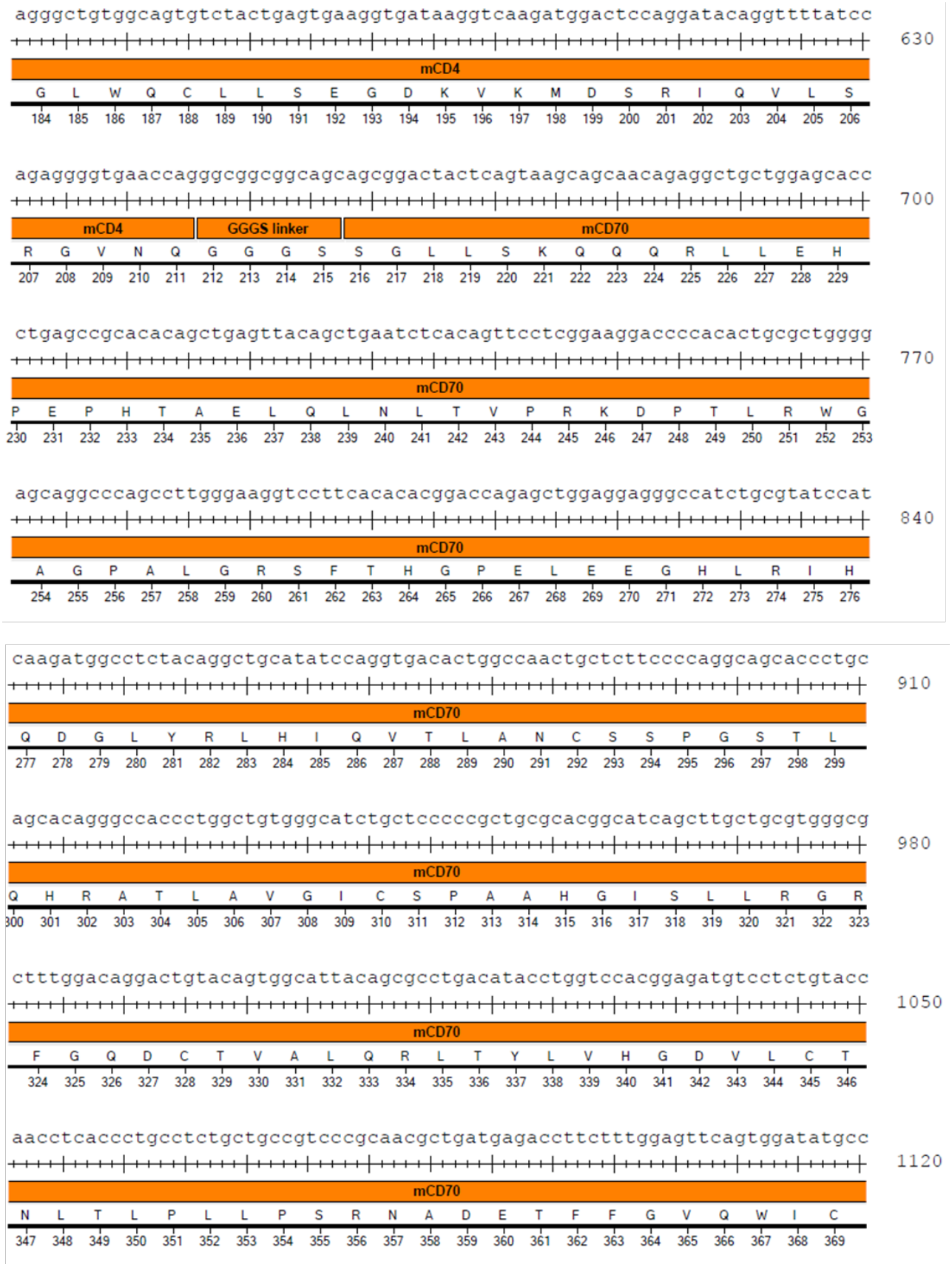
agggctgtggcagtgtctactgagtgaaggtgataaggtcaagatggactccaggatacaggttttatcc
630
mCD4
G L W Q C L L S E G D K V K M D S R I Q V L S
184 185 186 187 188 189 190 191 192 193 194 195 196 197 198 199 200 201 202 203 204 205 206
agaggggtgaaccagggcggcggcagcagcggactactcagtaagcagcaacagaggctgctggagcacc
700
mCD4
GGGS linker
mCD70
R G V N Q G G G S S G L L S K Q Q Q R L L E H
207 208 209 210 211 212 213 214 215 216 217 218 219 220 221 222 223 224 225 226 227 228 229
ctgagccgcacacagctgagttacagctgaatctcacagttcctcggaaggaccccacactgcgctgggg
770
mCD70
P E P H T A E L Q L N L T V P R K D P T L R W G
230 231 232 233 234 235 236 237 238 239 240 241 242 243 244 245 246 247 248 249 250 251 252 253
agcaggcccagccttgggaaggtccttcacacacggaccagagctggaggagggccatctgcgtatccat
840
mCD70
A G P A L G R S F T H G P E L E E G H L R I H
254 255 256 257 258 259 260 261 262 263 264 265 266 267 268 269 270 271 272 273 274 275 276
caagatggcctctacaggctgcatatccaggtgacactggccaactgctcttccccaggcagcaccctgc
910
mCD70
Q D G L Y R L H I Q V T L A N C S S P G S T L
277 278 279 280 281 282 283 284 285 286 287 288 289 290 291 292 293 294 295 296 297 298 299
agcacagggccaccctggctgtgggcatctgctcccccgctgcgcacggcatcagcttgctgcgtgggcg
980
mCD70
Q H R A T L A V G I C S P A A H G I S L L R G R
300 301 302 303 304 305 306 307 308 309 310 311 312 313 314 315 316 317 318 319 320 321 322 323
ctttggacaggactgtacagtggcattacagcgcctgacatacctggtccacggagatgtcctctgtacc
1050
mCD70
F G Q D C T V A L Q R L T Y L V H G D V L C T
324 325 326 327 328 329 330 331 332 333 334 335 336 337 338 339 340 341 342 343 344 345 346
aacctcaccctgcctctgctgccgtcccgcaacgctgatgagaccttctttggagttcagtggatatgcc
1120
mCD70
N L T L P L L P S R N A D E T F F G V Q W I C
347 348 349 350 351 352 353 354 355 356 357 358 359 360 361 362 363 364 365 366 367 368 369

Figure 2. Translated DNA sequence of mCD4-CD70 non-covalent trimer. The translated DNA sequence with single letter amino acid code is illustrated. CD4, linker and CD70 domains are labelled. HindIII and XbaI restriction sites are indicated. The sequence was designed as detailed in section 3.2.5.

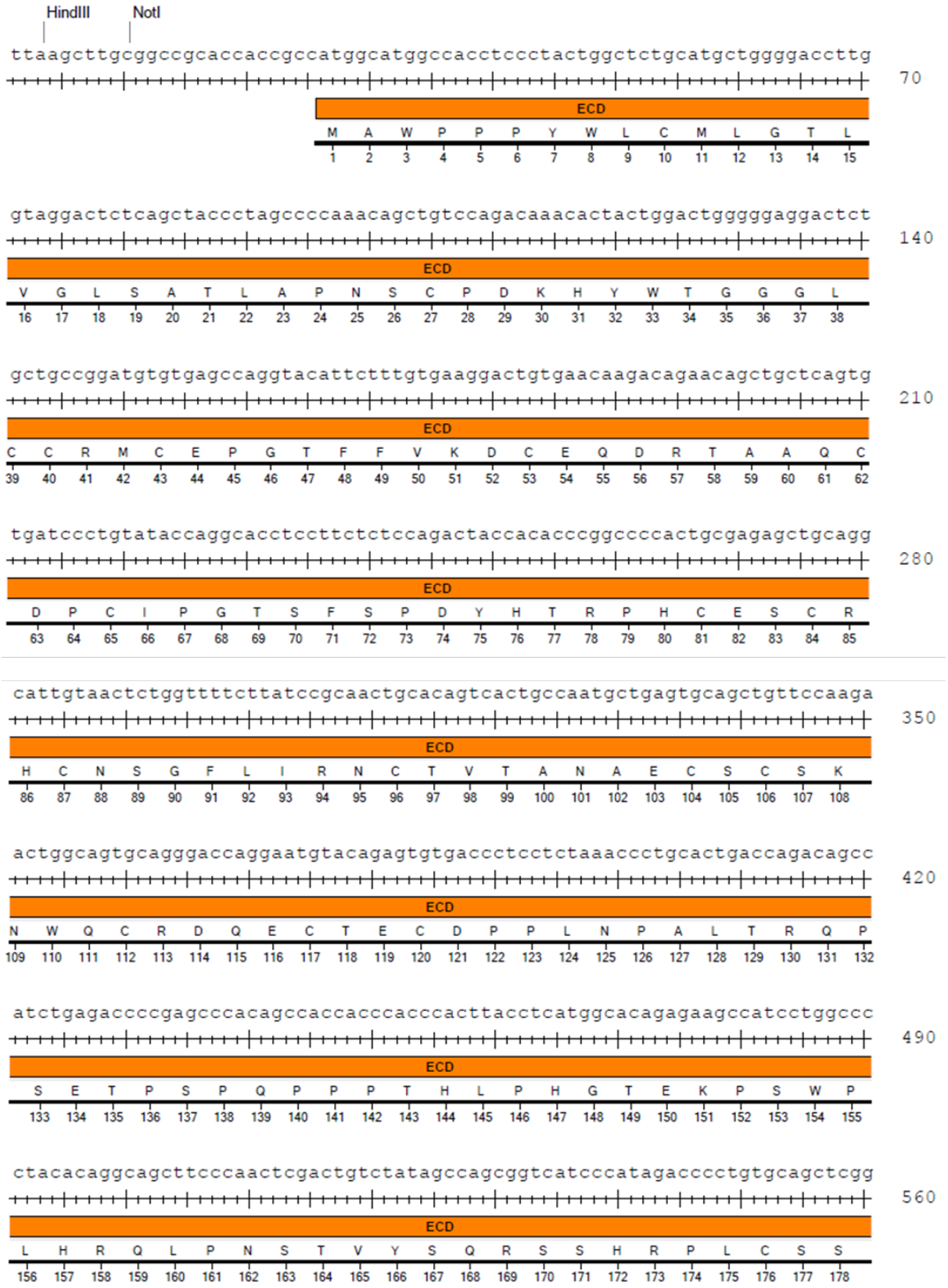
HindIII
NotI
ttaagcttgcggccgcaccaccgccatggcatggccacctccctactggctctgcatgctggggaccttg
70
ECD
M A W P P P Y W L C M L G T L
1 2 3 4 5 6 7 8 9 10 11 12 13 14 15
gtaggactctcagctaccctagccccaaacagctgtccagacaaacactactggactgggggaggactct
140
ECD
V G L S A T L A P N S C P D K H Y W T G G G L
16 17 18 19 20 21 22 23 24 25 26 27 28 29 30 31 32 33 34 35 36 37 38
gctgccggatgtgtgagccaggtacattctttgtgaaggactgtgaacaagacagaacagctgctcagtg
210
ECD
C C R M C E P G T F F V K D C E Q D R T A A Q C
39 40 41 42 43 44 45 46 47 48 49 50 51 52 53 54 55 56 57 58 59 60 61 62
tgatccctgtataccaggcacctccttctctccagactaccacacccggccccactgcgagagctgcagg
280
ECD
D P C I P G T S F S P D Y H T R P H C E S C R
63 64 65 66 67 68 69 70 71 72 73 74 75 76 77 78 79 80 81 82 83 84 85
cattgtaactctggttttcttatccgcaactgcacagtcactgccaatgctgagtgcagctgttccaaga
350
ECD
H C N S G F L I R N C T V T A N A E C S C S K
86 87 88 89 90 91 92 93 94 95 96 97 98 99 100 101 102 103 104 105 106 107 108
actggcagtgcagggaccaggaatgtacagagtgtgaccctcctctaaaccctgcactgaccagacagcc
420
ECD
N W Q C R D Q E C T E C D P P L N P A L T R Q P
109 110 111 112 113 114 115 116 117 118 119 120 121 122 123 124 125 126 127 128 129 130 131 132
atctgagaccccgagcccacagccaccacccacccacttacctcatggcacagagaagccatcctggccc
490
ECD
S E T P S P Q P P P T H L P H G T E K P S W P
133 134 135 136 137 138 139 140 141 142 143 144 145 146 147 148 149 150 151 152 153 154 155
ctacacaggcagcttcccaactcgactgtctatagccagcggtcatcccatagacccctgtgcagctcgg
560
ECD
L H R Q L P N S T V Y S Q R S S H R P L C S S
156 157 158 159 160 161 162 163 164 165 166 167 168 169 170 171 172 173 174 175 176 177 178

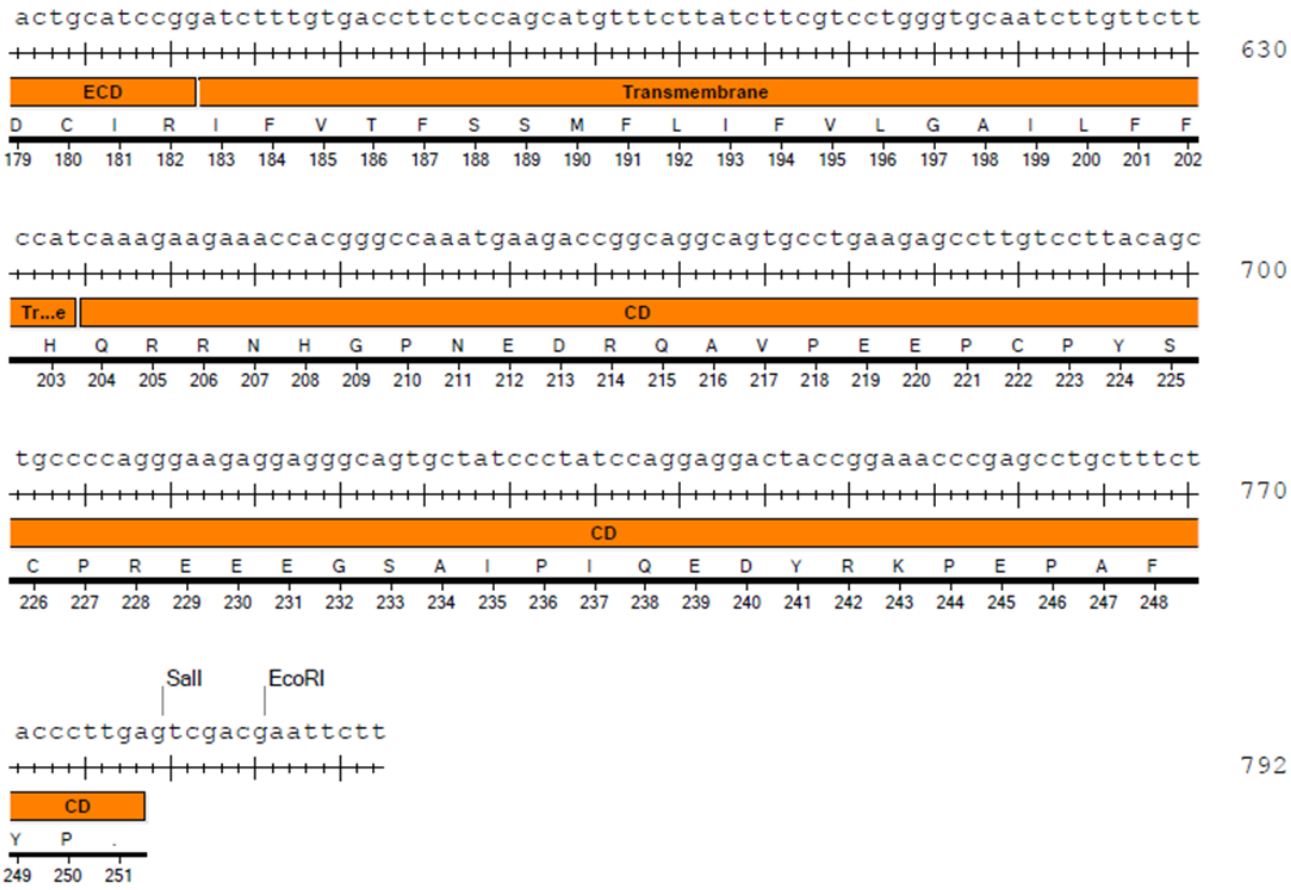

Figure 3. DNA and translated amino acid sequence of WT murine CD27. The translated DNA sequence with single letter amino acid code is illustrated. Extracellular domain (ECD), transmembrane domain and cytoplasmic domain (CD) are labelled. HindIII, NotI, SalI and EcoRI restriction sites are indicated. The sequence was designed as detailed in section 5.2.

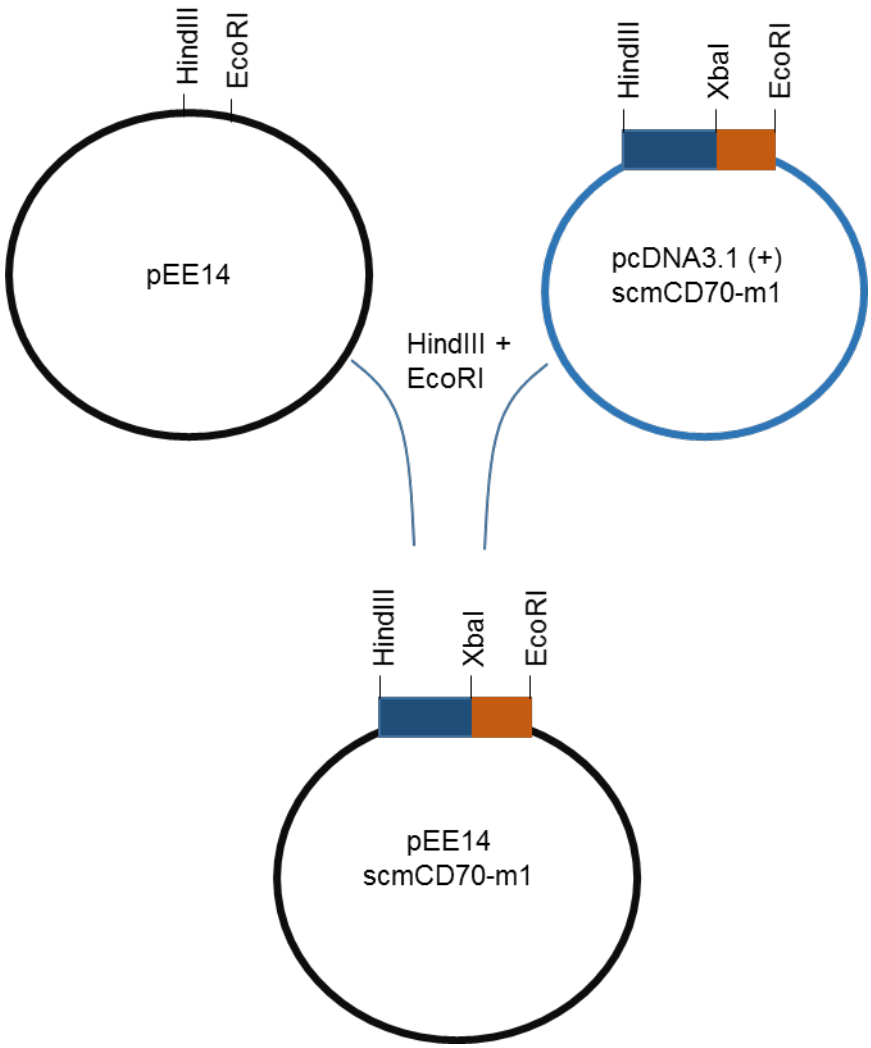

Figure 4. Cloning the scmCD70-m1 insert into pEE14 expression vector. The scmCD70-m1 insert was designed and ordered in pcDNA3.1 (+) vector. In order to clone into pEE14, the vectors were digested with HindIII and EcoRI restriction enzymes. The digested scmCD70-m1 insert was then ligated into pEE14 expression vector as described in detail in section 3.2. The scmCD70-m1 insert is represented as blue (CD70 domain) and orange (Fc domain) rectangles.

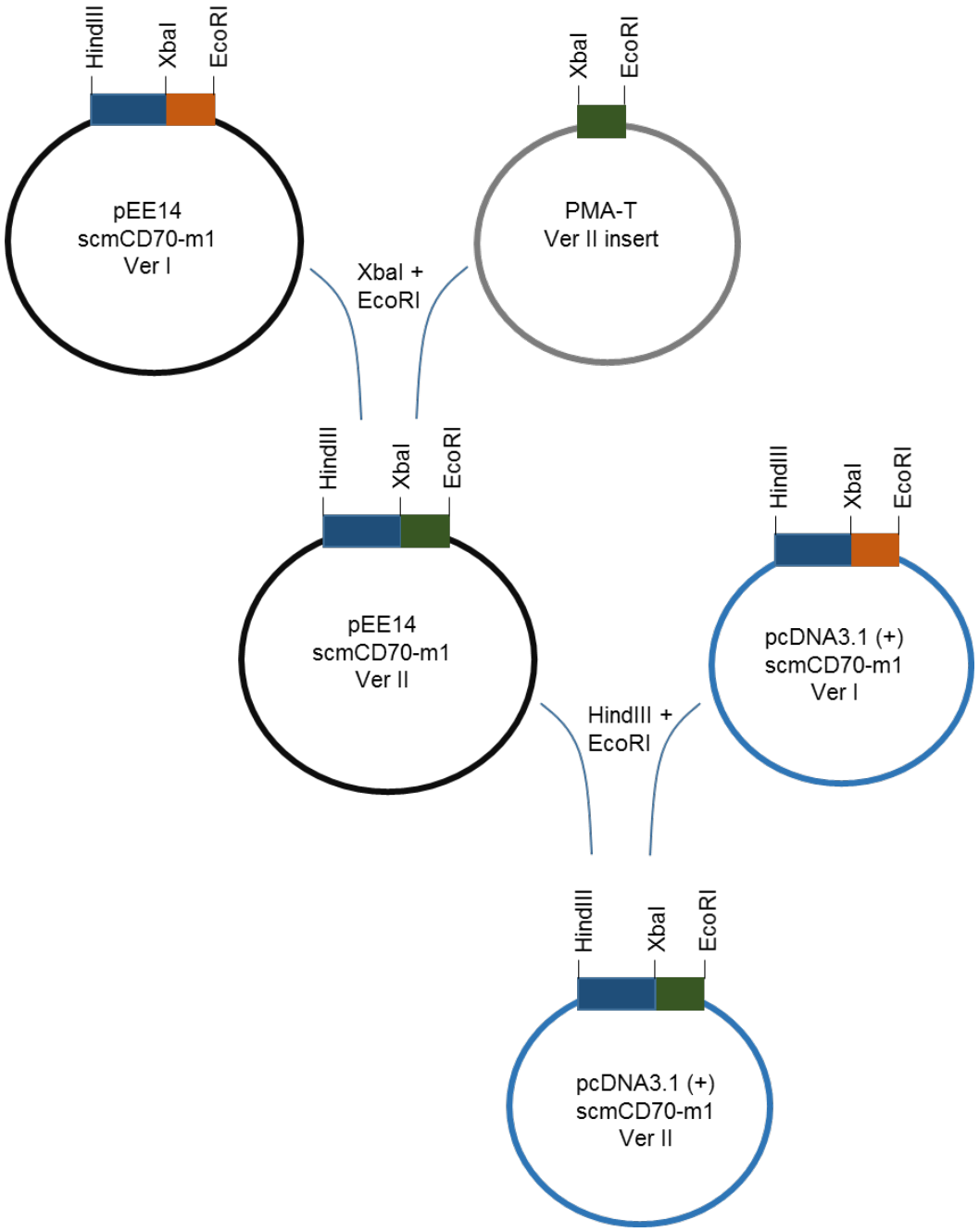

Figure 5. Cloning scmCD70-m1 Ver II into pcDNA3.1 (+) expression vector. The Ver II insert with the mutated hinge region in the Fc domain was ordered in PMA-T vector. The insert was first cloned into pEE14 expression vector. The PMA-T and pEE14 vectors were digested with XbaI and EcoRI restriction enzymes and the insert was ligated into pEE14 expression vector to form the full length scmCD70-m1 Ver II insert. The scmCD70-m1 Ver II insert was then cloned into pcDNA3.1 (+) expression vector. For this, the pcDNA3.1 (+) and pEE14 expression vectors were digested with HindIII and EcoRI restriction enzymes to release the inserts and the scmCD70-m1 Ver II insert was ligated into pcDNA3.1 (+) expression vector as described in detail in section 3.2.4. scmCD70-m1 insert is represented as blue (CD70 domain) and orange (Fc domain) rectangles. The Ver II insert (mutated Fc domain) is represented as green rectangle.

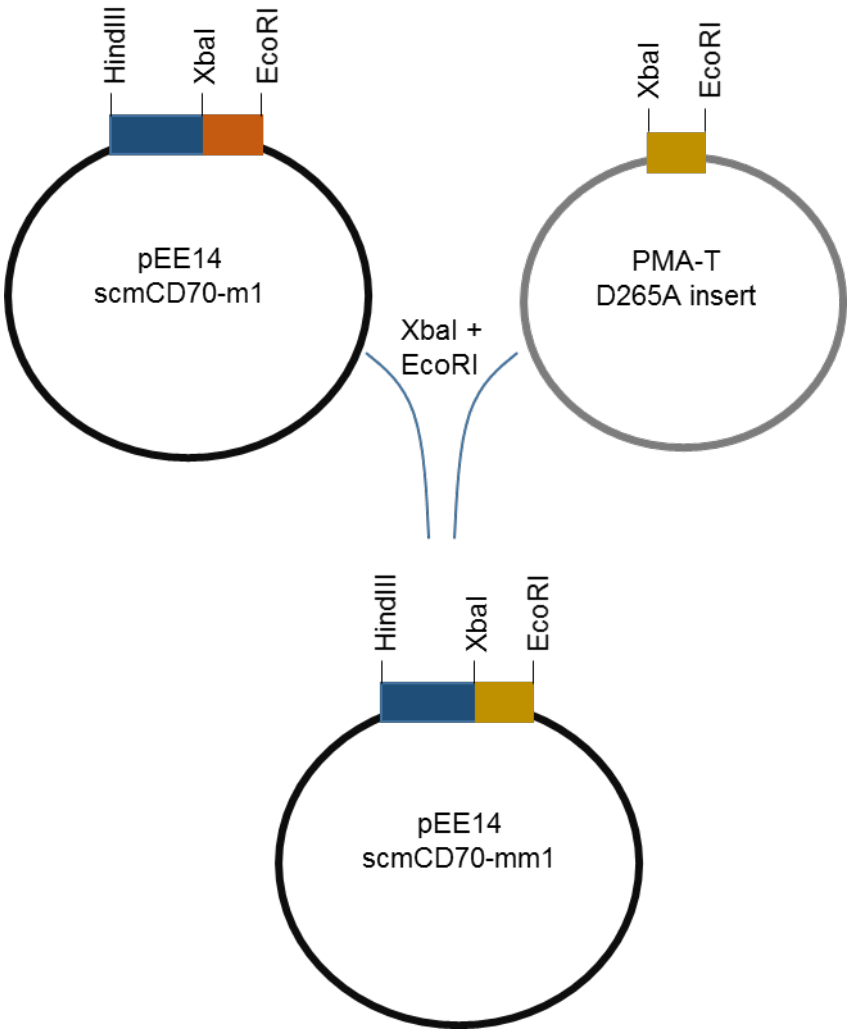

Figure 6. Cloning scmCD70-mm1 insert into pEE14 expression vector. The insert with the mutated Fc domain (D265A) to eliminate FcγR interaction was ordered in PMA-T vector. The insert was cloned into pEE14 vector by digesting both of the vectors with XbaI and EcoRI restriction enzymes. The insert was then ligated into pEE14 vector to form the full length scmCD70-mm1 insert as described in detail in section 4.2.3. scmCD70-m1 insert is represented as blue (CD70 domain) and orange (Fc domain) rectangles. The insert containing the Fc domain with the D265A mutation is represented as gold rectangle.